Year : 2017

Patient and staff dose in fluoroscopically-guided interventions: Exploring new optimisation stratégies

Ryckx Nick

Ryckx Nick, 2017, Patient and staff dose in fluoroscopically-guided interventions: Exploring new optimisation stratégies

Originally published at : Thesis, University of Lausanne

Posted at the University of Lausanne Open Archive http://serval.unil.ch
Document URN : urn:nbn:ch:serval-BIB_659E87FD991D4

UNIL | Université de Lausanne
Faculté de biologie
et de médecine

CHUV – Département de radiologie médicale
Institut de radiophysique

Patient and staff dose in fluoroscopically-guided interventions: Exploring new optimisation strategies

Thèse de doctorat ès sciences de la vie (PhD)

présentée à la

Faculté de biologie et de médecine
de l'Université de Lausanne

par

Nick RYCKX

MSc en physique, Ecole Polytechnique Fédérale de Lausanne

Jury

Prof. Niklaus SCHAEFER	Président (CHUV-UNIL)
Prof. Francis R. VERDUN	Directeur de thèse (CHUV-UNIL)
Dr Juan Fernando IGLESIAS	Expert (CHUV-UNIL)
Dr Wouter J. H. VELDKAMP	Expert (Leiden University Medical Center, NL)
M. Roland SIMMLER	Expert (Hirslanden AG, Zürich)

Lausanne 2017

UNIL | Université de Lausanne
Faculté de biologie
et de médecine

Ecole Doctorale

Doctorat ès sciences de la vie

Imprimatur

Vu le rapport présenté par le jury d'examen, composé de

Président· e	Monsieur	Prof. Niklaus **Schaefer**
Directeur· rice de thèse	Monsieur	Prof. Francis **Verdun**
Experts· es	Monsieur	Dr Wouter J.H. **J.H. Veldkamp**
	Monsieur	M. Roland **Simmler**

le Conseil de Faculté autorise l'impression de la thèse de

Monsieur Nick Ryckx

MSc en physique de l'Ecole Polytechnique Fédérale de Lausanne

intitulée

Patient and staff dose in fluoroscopically-guided interventions : Exploring new optimisation strategies

Lausanne, le 7 août 2017

pour le Doyen
de la Faculté de biologie et de médecine

Prof. Niklaus Schaefer

Remerciements

Je souhaite exprimer toute ma gratitude envers mon directeur de thèse, le Prof. Francis R. Verdun. Il a toujours su orienter ma recherche dans une direction pertinente, en me permettant de ne pas me focaliser sur des détails mais en faisant en sorte de toujours situer mon travail dans un cadre plus global.

Je tiens à remercier les membres de mon jury de thèse, qui ont accepté de dédier une partie de leur temps à sa relecture critique et de s'impliquer dans ses différentes évaluations, en acceptant parfois de se déplacer sur de longues distances.

Je souhaite également remercier le directeur de l'institut, François Bochud, ainsi que l'équipe du secrétariat, en la personne de Nicole Tille, qui m'ont offert un cadre de travail agréable et productif.

Ma gratitude va ensuite vers mes collègues de travail. Les doctorants et collaborateurs du GIM m'ont permis de développer et confronter mes connaissances, ainsi que la pertinence de ma recherche. Les TRM du groupe m'ont permis de garder les pieds dans l'application clinique, permettant à mon message de rester pertinent.

Je salue également tous les co-auteurs de mes différentes publications. La rédaction d'un article scientifique est un exercice difficile, et l'apport de différents regards, parfois éloignés, est toujours une richesse pour le débat scientifique.

Je tiens à remercier tous les TRM, médecins, et personnel infirmier des différentes institutions qui m'ont ouvert leurs portes. Ces échanges réguliers m'ont permis de saisir la portée du paysage radiologique suisse romand.

Je tiens également à remercier mes parents, qui m'ont enseigné de n'accepter un travail que s'il est accompli avec diligence et, avant tout, avec honnêteté. J'espère que cette honnêteté, qui se doit d'être au cœur de la recherche scientifique, transparaîtra au cours du présent manuscrit.

Enfin, et du plus profond de mon cœur, je tiens à exprimer mon éternelle et infinie gratitude à mon épouse Marion, et à ma fille Lucie. Votre soutien a rendu ce travail beaucoup plus facile à aborder.

Résumé

Au cours des dernières décennies, la fluoroscopie est devenue une technique d'imagerie à rayons X diagnostique et thérapeutique largement utilisée pour de nombreuses interventions médicales, grâce à sa capacité à visualiser des phénomènes dynamiques dans le corps humain en temps réel et à un caractère minimalement invasif. En raison de la présence obligatoire de personnel médical dans la proximité immédiate du patient, ces interventions posent un problème unique pour la radioprotection, impliquant que les radiologues et cardiologues interventionnels sont parmi les travailleurs professionnellement exposés aux rayonnements ionisants qui reçoivent les doses efficaces les plus élevées. En outre, de nombreuses autres spécialités médicales ont repris la fluoroscopie comme principal outil de travail. En conséquence, le manque de connaissances et d'une formation spécifique à l'utilisation des rayonnements ionisants est un défi qui peut être difficile à résoudre au niveau institutionnel. En outre, de nombreuses innovations technologiques ont été introduites afin de surveiller les doses délivrées aux patients (p. ex. des logiciels de collecte automatiques des doses), afficher l'exposition du personnel en temps réel, ou encore réduire la dose au patient en appliquant de fortes filtrations du faisceau primaire et en améliorant simultanément la « qualité d'image » en appliquant des traitements d'image en ligne, comme c'est le cas pour la reconstruction itérative des images en tomodensitométrie. Pour la qualité de l'image, il n'y a par conséquent plus de lien direct entre l'exposition du patient et la qualité de l'image – sans parler de l'absence-même de définition adéquate de la qualité d'image. Ainsi, les mesures physiques traditionnellement utilisées pour sa mesure, déjà peu appropriées pour une optimisation clinique pertinente, ne sont plus applicables. Durant cette recherche, nous avons testé plusieurs de ces innovations et tenté d'en déterminer les forces et faiblesses. Tout d'abord, nous avons effectué une revue de la littérature afin de résumer l'actuel état de l'art dans les procédures sous guidage fluoroscopique. Deuxièmement, nous avons décrit les moyens d'évaluer la dose au patient et le risque radiologique associé, ainsi que la façon de corriger les indicateurs dosimétriques en fonction de la corpulence du patient, et avons effectué une analyse spécifique de la prise en charge de la patiente enceinte. Troisièmement, nous avons décrit l'exposition et les risques du personnel médical, principalement en nous concentrant plus avant sur l'irradiation du cristallin et du cerveau (deux organes généralement pas protégés au cours de l'intervention, et pour lesquels plusieurs études récentes ont montré que le risque radiologique avait été sous-estimé), ainsi qu'une description précise de l'efficacité des lunettes plombées. Quatrièmement, nous avons proposé que la qualité d'image devienne la pierre angulaire de l'optimisation clinique. Pour cela, nous avons réalisé une étude de faisabilité de l'utilisation d'un modèle d'observateur mathématique dans des conditions d'acquisition statiques et dynamiques, visant à qualifier la qualité d'image sur la base d'une tâche de détection binaire pertinente d'un point de vue clinique. Enfin, notre conclusion souligne les limites actuelles de notre approche et propose une série de questions à développer, dont la résolution pourrait avoir un impact significatif sur la gestion globale de la dose et de la qualité de l'image.

Summary

Over the last decades, fluoroscopy has become a widely-used diagnostic and therapeutic X-ray imaging technique for numerous medical procedures thanks to its capability of displaying dynamic phenomena in the human body in real time and its minimally-invasive nature. Due to the customary presence of medical staff in the immediate vicinity of the patient, interventional procedures pose a unique radiation protection problem, implying that interventional radiologists and cardiologists are among the professionally-exposed to ionising radiation workers who receive the highest effective doses. In addition, many other medical specialties have taken up fluoroscopy as a central working tool. As a consequence, the lack of radiation awareness and specific training is a challenge that may be difficult to solve at the institutional level. Furthermore, many technical innovations have been introduced to either monitor patient doses (such as automatic dose-collection software solutions), display staff exposure in real time, or reduce patient dose by applying heavy beam filtrations and simultaneously enhancing “image quality” through on-line image post-processing, as is the case for iterative image reconstruction in computed tomography. For image quality, the consequence is that there is no straightforward link anymore between patient exposure and image quality – and not even a proper definition of image quality. Therefore, the physical metrics classically used for quality measurement, already flawed for pertinent clinical optimisation, are no longer applicable. For this research, we tested several of these innovations, and tried to pinpoint their strengths and weaknesses. First, we performed a literature review to summarise the current state-of-the-art in fluoroscopic procedure guidance. Secondly, we described the ways of assessing patient dose and radiological risk, as well as how to correct the dose indicators based on patient body habitus, and performed a dedicated analysis of the management of the pregnant patient. Thirdly, we described the exposure and risks of the medical staff during interventional procedures, mainly by concentrating more thoroughly on eye lens and brain dose (two organs that are usually not protected during interventional procedures, and for which several recent studies have shown that the risk had been previously underestimated), as well as a precise description of the efficiency of leaded glasses. Fourthly, we proposed that the image quality becomes the cornerstone of clinical optimisation. For this purpose, we performed a feasibility study of the use of a mathematical model observer in static and dynamic imaging conditions, aiming at grading image quality on the basis of a clinically relevant binary detection task. Finally, we concluded by pointing out the current limitations of our approach, and proposed a series of follow-up questions whose resolution may have a significant impact on the overall management of patient and staff dose and image quality.

Introduction

Over the last years, fluoroscopy has become a preferred diagnostic and therapeutic imaging technique for numerous minimally-invasive medical procedures. It relies on the real-time visualisation of dynamic phenomena in the human body, such as blood flow restrictions due to an arterial lumen reduction, the position of a needle near a vertebra prior to a vertebral cementoplasty, or the embolisation of a cerebral aneurism, using planar X-ray imaging. Among its advantages are: reduced patient hospitalisation times (only several hours for percutaneous coronary interventions (PCI) against several days for open-heart surgery) and reduced associated costs for the local healthcare reimbursement system; reduced patient septic risk and blood loss; more efficient and flexible clinical workflow. Interventional fluoroscopy poses a unique radiation protection problem, in the sense that the customary presence of medical staff in the immediate vicinity of the patient implies an increased exposure of the operator(s) and mobile staff in angiography suites or operation theatres.

For patients, fluoroscopically-guided interventions are among the medical procedures that yield the highest individual effective doses, and the typical patient exposure for a given medical indication is non predictable. Indeed, interventional radioscopy functions with an automatic exposure control (AEC) system, based on a desired image quality – and thus detector sensitivity. The AEC automatically adjusts the X-ray tube output based on the patient's absorption properties (body size, tissue density, presence of any metallic objects in the patient's body – a prosthesis, bone screws, etc.) and a target detector dose through pre-calibrated voltage – current – exposure time curves, i.e. the imaging parameter space necessary for a pre-desired contrast-to-noise or signal-to-noise ratio, depending on the manufacturer. As such, even for a same diagnostic question, there is no possible way to predict patient dose accurately, and patient effective doses can therefore be consequent, depending on the case complexity. Furthermore, interventional fluoroscopy is a classically diagnostic means of imaging often used for therapeutic purposes. Indeed, the real-time dynamic imaging properties of fluoroscopy have quickly driven it from a pure diagnostic modality towards a tool allowing the guidance of numerous devices intended at curing health conditions previously only reachable by chemicals. For example, the fraction of ST Elevation Myocardial Infarction (STEMI) patients undergoing systemic drug-induced thrombolysis went from 51 % (male) and 39 % (female) in 1997 to less than 1 % for both genders in 2007. Meanwhile, the fraction of the same condition treated by percutaneous coronary intervention (PCI) rose from under 10 % for both genders to 80 % (male) and 70 % (female) in the same decade [Radovanovic 2012]. As a consequence, the exposure burden has the potential to induce severe immediate radiation injuries (mainly skin injuries), in addition to the cumulative

long-term mutagenesis effects such as radiation-induced cancer. Indeed, on the 634 reported radiation-related accidents between 1980 and 2013 (including radiation therapy, industrial imaging, military purposes, orphan sources or other potential causes), 194 (31 %) were due to the use of fluoroscopy [Coeytaux 2015], among which the vast majority of events concerned local skin injuries.

Regarding staff exposure, tissue effects are not to be expected, since only a small fraction of the patient's dose will be scattered to the people positioned next to the patient, especially the main procedure operators. However, cumulative doses may be quite high over one's career, and have become a growing concern over the last few years, since the International Commission on Radiological Protection (ICRP) has stated in 2011 that the threshold of radiation-induced cataract (currently estimated around 0.5 Gy) had been overestimated in the past (i.e. previously thought to be around 5 Gy), thus leading to an overall reduction of the annual eye lens dose limit in national and international regulations to a mere 20 mSv per year [Ciraj-Bjelac 2010, ICRP 2011]. As for the stochastic risk, some publications have recently reported several cases of cardiologists diagnosed with glioblastoma, with an apparent excess of the lesions occurring in the left hemisphere, where the X-ray tube is usually located [Roguin 2013a and b]. Although theses papers are no epidemiological studies but case reports, the mentioned results have brought concern among the interventional cardiology community. But, as a matter of fact, interventional radiologists and cardiologists are among the professionally-exposed to ionising radiation workers who receive the highest effective doses [FOPH 2016]. Classically, fluoroscopically-guided interventions were the "private ground" of radiologists and cardiologists, and the basics of clinical radiation protection and the management of image quality within the ALARA (as low as reasonably achievable) principle is usually taught to those specialists during their training and continuous education. However, many of other medical specialties, traditionally based on more invasive patient treatment techniques, have adopted fluoroscopy as a central working tool. These specialties include – but this list is not restricted to – orthopaedic surgeons, gastroenterologists, urologists, gynaecologists, anaesthesiologists, and vascular surgeons [ICRP 2010]. For example, a questionnaire-based study by S. J. Bordoli et al. showed that, among 311 vascular surgery trainees in the United States in 2012 (with a 14 % response rate), 45 % percent had not followed formal radiation safety training, 74 % did not know the radiation safety policy for pregnant vascular surgeons, 48 % were unable to bring up their radiation safety officer's (RSO) contact information, and 43 % did not even know their yearly acceptable levels of radiation exposure [Bordoli 2014]. This poses a major challenge with respect to patient and staff radiological safety, as well as the technical and scientific knowledge regarding the optimal choice of image acquisition parameters.

Finally, image quality is – and has always been – a key element for an accurate diagnostic and therapeutic efficiency of fluoroscopy. Recent technological innovations have allowed for images to be acquired at much lower doses, thus reducing patient and staff radiation risk, by adapting the AEC systems to spare patient skin dose while aiming at keeping a satisfying image quality. However, this does not prevent potential high exposures, as X-ray tubes become more powerful and can sustain much longer procedure times. Furthermore, as is the case with iterative reconstruction in computed tomography (CT), the link between the classical physical image quality parameters (signal-to-noise ratio SNR, contrast-to-noise ratio CNR, modulation transfer function MTF, etc.) is no longer straightforward. Indeed, the underlying hypotheses for these metrics include noise stationarity and a linear behaviour with respect to detector entrance dose. However, many of these dose-reduction algorithms involve some strength of recursive noise damping, as well as on-line pixel-wise analysis of image content and its subsequent correction based on the statistical knowledge of image noise characteristics and the expected clinical information contained in the images. This implies highly non linear image properties, and thus calls for the need of more reliable – and clinically relevant – tools for assessing image quality, ideally qualifying it on the basis of the capacity of the system to deliver a given diagnostic information, i.e., task based imaging performance. Based on psychophysical formalism [Barrett 2004], the use of model observers can help circumvent the underlying limitations due to non linear image reconstruction algorithms by qualifying image quality based on a clinical task (e.g. signal detection) and the analysis of image background noise properties.

In this work, we will describe our work on the three previously mentioned topics. Firstly, we will perform a short but thorough literature review to pinpoint the current state-of-the-art in fluoroscopic procedure guidance. Secondly, we will describe the ways of assessing patient dose and radiological risk, mainly with respect to skin injuries, as well as how to correct the dose indicators based on patient body habitus, and how the particular condition of the pregnant patient may influence the management of radiation dose. The question of the strengths and weaknesses of automatic patient dose collection software solutions will also be discussed. Thirdly, we will describe the exposure and risks of the medical staff during interventional procedures, as well as a precise description of the efficiency of leaded glasses aiming at reducing eye lens dose. Fourthly, we will describe the decreasing dependency between image dose and image quality, and try circumventing this non-linear behaviour by using a mathematical model observer in static and dynamic imaging conditions. Finally, we will stress out the current limitations of our approach, and propose a series of follow-up questions whose resolution may have a significant impact on the overall management of

patient and staff dose and image quality in a more intricate way as is being carried out currently.

Literature review

This short literature review will summarise the key concepts used within this research. We will first focus on patient exposure and dose management. Next, we will analyse the current state of staff exposure and means of protection available. Then, we will stress out the main challenges of image quality assessment, especially for dynamic imaging tasks. And finally, we will present the main tasks presented to a medical physicist within an interventional radiology suite.

Patient exposure

The quantification of X-ray tube output vs. patient exposure is not straightforward. Ideally, patient dose should be monitored in situ at any moment during a fluoroscopically-guided intervention. The ideal dose measurement for patient deterministic risk assessment would be the peak skin dose (PSD) [Jones 2011], i.e., the highest dose absorbed anywhere by the patient's skin, thus indicating the most likely location for subcutaneous skin injuries, as well as the potential severity of the radiation-induced lesions. A paper by S. Balter et al. [Balter 2010] summarises the potential skin lesions with respect to dose absorbed by the patient's skin, ranging from no early or late effects under 2 Gy, to early transient erythema requiring surgical interventions, and up to long-term telangiectasia or other persistent deeper lesions at doses above 15 Gy. More generally speaking, above 5 Gy, there is a risk for long-term skin affections, and the probability of skin lesion occurrence is close to 100 % at these levels – as a reminder, a dose threshold is defined as the dose necessary for 1 % of the population to develop these effects, with a rapid increase of that proportion with increasing dose. However, the task of accurately measuring patient skin dose, although theoretically feasible by placing adequate radio-transparent dosimeters across the patient's anatomy, is practically impossible to perform on a routine basis. And organ doses – and the subsequent effective dose – cannot be measured directly. Furthermore, the overall absolute number of occurrences remains low, with a further tendency in decrease over the 2000 – 2009 decade [Coeytaux 2015], so risk monitoring should be steadily adapted. This is why the dosimetry evaluation of the patient prior to, during, or after the examination, will rely on pre-defined dose indicators. Indeed, in order to unify dose – as well as risk – management, several easy-to-measure and intuitive patient dose indicators have been established for fluoroscopy by the International Commission on Radiation Units and Measurements (ICRU) [ICRU 2005], of which we will adopt the formalism for dose indicator nomenclature. In addition, a publication by M. S. Stecker et al. [Stecker 2009] summarises the current guidelines on patient radiation dose management, with respect to modern angiography units. We will describe the four most widely used dose indicators.

- Fluoroscopy time (T): The fluoroscopy time (T) is defined as the time during which the pedal is being pressed by the operator. Because of the usual pulsed frame acquisition – rather than continuous exposure – this value is far from being indicative of the actual beam-on time. Indeed, the typical pulse duration is on the order of 10ms. At 8 frames per second [fps], the actual patient exposure time will only be 8 % of the displayed fluoroscopy time. Furthermore, some manufacturers only calculate fluoroscopy time, thus not incrementing the chronometer when proceeding with diagnostic quality imaging. Indeed, there is usually a major distinction between the fluoroscopy and acquisition modes, as stated by the National Council on Radiation Protection and Measurements (NCRP) report 168 [NCRP 2010]:
    - Fluoroscopy: Usually low quality (high noise)/low dose images used for preparatory imaging (catheter positioning, tool guidance). These images are usually not automatically recorded, although some modern units are equipped with RAM allowing for the buffering of the last several seconds of imaging and manual saving if needed – e.g. if their content is sufficient for the diagnosis,
    - Acquisition: High quality/dose images, automatically stored for diagnostic purposes. Typical acquisition series include cineradiography, digital subtraction angiography (DSA) or single-frame digital radiography (DR).

  As a consequence, T is a good indicator of the procedure complexity but is not a reliable patient dose indicator.
- Number of radiographic frames per intervention (N): Like T, N is an indication of the procedure complexity but does not provide an accurate estimation of patient PSD. Indeed, even if much information about the image-wise acquisition parameters (tube voltage and current, pulse duration, focus-to-detector distance, table height, etc.) is stored in their respective DICOM headers, the major part of images are, as mentioned previously, usually not saved, namely the low-quality fluoroscopy frames used solely for positioning or navigation purposes. Nevertheless, it can still serve to optimise image acquisition rate, as identical fluoroscopy times and similar patient body habitus distribution do not necessarily mean an identical number of recorded diagnostic frames.
- Cumulative air kerma-area product (P_{KA}): The cumulative air kerma-area product (P_{KA}) is defined as the integral of the air kerma (K_a) cumulated at a given location over the area exposed by the primary beam at that same location:

$$P_{KA} = \iint_{exposed\ surface} K_a(x,y)dxdy$$

  Conveniently, the P_{KA} does not depend on where it is measured. Indeed, the air kerma rate decreases with the inverse square of the distance to the focal spot,

whereas the exposed area increases with the square of the distance to the focal spot. As a consequence, the product of both is an invariant with respect to the measurement point within the primary beam. A usual application of the P_{KA} is a quick and straightforward – when knowing the beam quality in units of aluminium half-value layers – conversion to patient effective dose using conversion factors determined by extensive Monte-Carlo simulations [Struelens 2009]. Indeed, for a given medical purpose, the X-ray beam will usually be focused on a given anatomical region (head, chest, pelvis, etc.) using beam angles as defined by different medical requirements, and with acquisition parameters determined automatically by the system's AEC. The organs in the primary beam field of view (FOV), along with those exposed by internally scattered X-rays, are thus more or less the same. The P_{KA} is, de facto, an integral value of the number of X-ray photons delivered to the explored patient's anatomy, and effective dose calculated by Monte-Carlo simulations can be normalised by the delivered P_{KA}.

- Cumulative air kerma at a reference point ($K_{a,r}$): Unlike P_{KA}, $K_{a,r}$ has to be expressed relative to at a given location. The International Electrotechnical Commission (IEC) defines the interventional reference point (IRP) as virtually lying at 15 cm from the device's isocenter towards the X-ray tube, along the central beam axis [IEC 2010]. The IRP was designed to be representative of the entrance point of the X-ray beam in the patient, thus used as an estimator of possible patient skin injuries. The Food and Drug Administration (FDA) reference point differs from the IEC reference point by its definition: It is located at 30 cm from the entrance of the imaging device, independently of the focal spot-to-detector distance. According to A. K. Jones et al. [Jones 2011], the $K_{a,r}$ is not equal to the PSD, but is the best dose indicator to perform a quite precise evaluation of PSD, providing the knowledge of beam angle(s), table height and primary beam filtration.

Figure 1 summarises the two latter dose indicators and the location of the IRP. As we see, these indicators remain limited for patient risk assessment, and a solution for this problem could come from a new DICOM object, the Radiation Dose Structured Report (RDSR), recording many operational parameters for all exposure events. It is important to understand that an analogous dose indicator to $K_{a,r}$ used in conventional planar radiography, the entrance surface air kerma (ESAK, measuring the entrance air kerma at the patient's skin) does not imply the same radiological risk. Indeed, for conventional radiography, the usual acquisition parameters (FOV, patient position, beam angle) are quite similar between different radiology centres. As such, the ESAK can be used for patient effective dose estimation, providing a relevant conversion factor. But for fluoroscopy, the P_{KA} is the

preferential choice of effective dose estimator, whereas the $K_{a,r}$ (or ideally PSD), similar to the ESAK, will this time be an indicator of patient tissue effect risks. As we can see, the measurement referential is not the same even if the schematic imaging chain is almost the same between radiography and fluoroscopy.

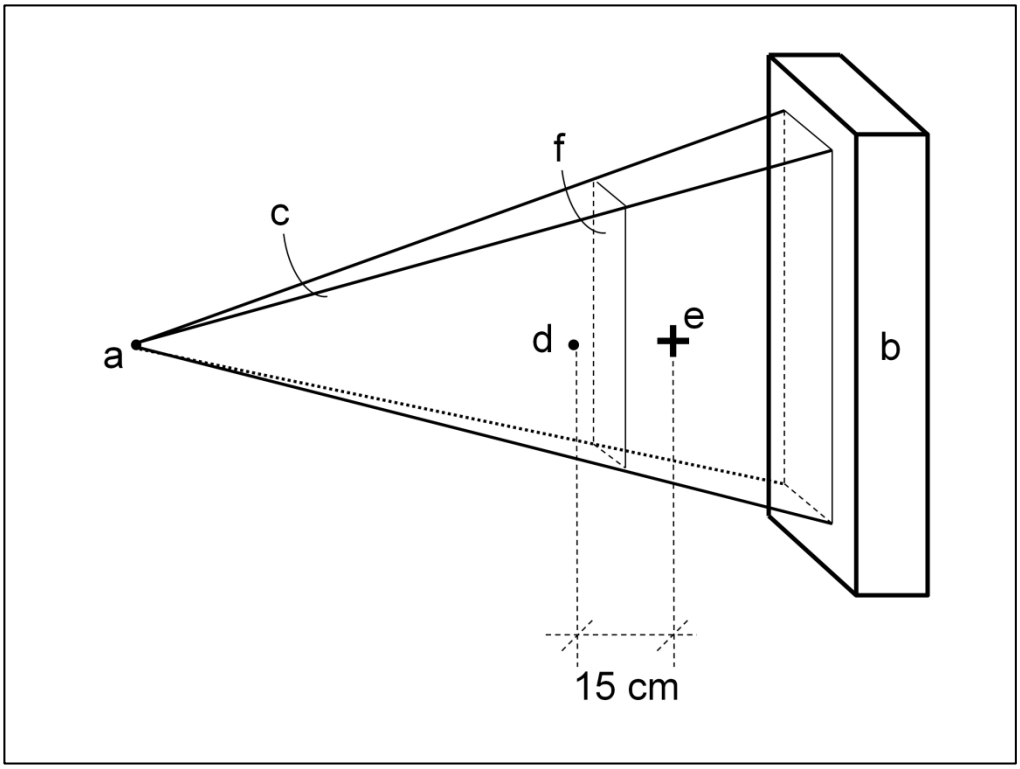

Figure 1: Schematic depiction of the relevant elements defining $K_{a,r}$ and P_{KA}. a: focal spot - b: X-ray detector - c: X-ray primary beam - d: interventional reference point (IRP) - e: isocenter - f: exposed X-ray field at an arbitrary distance from the focal spot.

The patient, by contrast with staff, is not subjected to any dose limitations, the risk of using ionising radiation being, for medical purposes, always considered inferior to the advantage it represents for the well-being of the patient. But the aforementioned dose indicators (T, N, P_{KA} and $K_{a,r}$) are useful to optimise one's practice using diagnostic reference levels (DRL), defined by the ICRP [ICRP 1990]. Usually, DRLs are defined as the third quartile of the distribution of a specific dose indicator (e.g. P_{KA}) for a given medical examination (e.g. coronary angiography) within a single centre. For a whole country, the DRL is calculated as the third quartile of each centre's median dose value. DRLs being defined for a standard patient body habitus, this value can of course be exceeded from time to time if the circumstances require it (large patient, complicated case, unexpected complication, etc.). But if a DRL is regularly exceeded, the operator should take active measures to reduce patient exposure. As we mentioned earlier, fluoroscopy doses being non predictable – and fluoroscopy being also used for therapeutic purposes – we will use the term of reference level (RL) rather than DRL.

Staff exposure

As previously mentioned, staff involved in fluoroscopically-guided procedures is highly exposed to radiation emitted by the patient interacting with the primary beam, mainly by Compton scattering. This implies that the effective doses received by these professionals are among the highest for professionally-exposed radiation workers. For example, in 2015, 93 753 workers were routinely monitored for their exposure to ionising radiation in Switzerland [FOPH 2016]. Out of this population, 68 270 (73 %) were active in medicine (Table 1).

Dose range	**2014**		**2015**	
[mSv / year]	Total	Medicine	Total	Medicine
0-2	89 702	65 888	92 855	68 145
2-4	507	92	594	77
4-6	138	35	203	35
6-8	36	12	75	10
8-10	8	3	21	1
10-12	3	1	3	1
12-14	1	0	1	0
14-16	2	1	1	1
Total	90 397	66 032	93 753	68 270
Total >2 mSv	695	144	898	125
Total person Sv	5.39	1.19	5.88	1.10

Table 1: Number of professionally-exposed workers and subset of medical workers in Switzerland for 2014 and 2015, with respect to their dose ranges. Adapted from [FOPH 2016].

The average dose per medical worker was at 16.1 µSv over the whole year 2015, but the distribution of individual doses was highly asymmetric. Indeed, only 125 (0.2 %) of medical workers had doses between 2 and 16 mSv over the whole year, out of the 898 professionally exposed workers in that same range, representing about 14 % of the workers with effective doses above 2 mSv. Interestingly though, this proportion was higher in 2014 (144 medical workers out of 695 with doses above 2 mSv – about 21 %), for an overall lower number of medical professionals (66 032) for the same year. It is not yet clear if this reduction is due to the technological advancements we will describe later on, or if there is perhaps a reduction in the discipline required to systematically wearing one's dosimeter. Nevertheless, of these several tens of workers with non-zero doses, the majority were interventional radiologists and cardiologists. These doses may, in themselves, be quite low. But due to the high dose rates encountered in angiography suites, interventional staff is required to use high atomic number (Z) protective clothing and leaded means of protection such as glasses or mobile shielding.

The effective dose being measured under the apron, routine dose monitoring may severely underestimate dose scattered to parts of the body not protected by individual clothing.

As mentioned in the literature review on patient dose – and as we will see in the next section on image quality – fluoroscopy units adapt the patient dose rate based on a pre-defined image quality, the patient's body habitus, and the type of tissue that has to be imaged (lung, soft tissue, bone, etc.). It is therefore very difficult to predict an individual operator dose per procedure using routine dosimetry. Indeed, dosimeters used for routine dose monitoring, such as thermoluminescent dosimeters (TLD), are usually read every month, thus displaying an effective or skin dose over a whole month in one reading. Two solutions exist to assess individual procedure doses. The first solution consists of real-time dosimeters, recently brought unto the market, allowing for a real-time visualisation of individual staff dose rates and cumulative doses. The individual solutions, as well as their technical capabilities and limitations, have been thoroughly tested and discussed in the ORAMED report published by the EURADOS in 2012 [Vanhavere 2012]. However, these solutions, although straightforward to implement, are usually very costly, and cannot easily be deployed at a whole hospital level. These solutions are thus used punctually for specific dosimetry studies, or for teaching purposes, usually worn above the apron to assess one's individual radiation protection behaviour. The second solution is the normalisation of cumulative doses by the dose delivered to the patient, usually the P_{KA}. This mathematical tool, usually expressed in [µSv / (Gy cm^2)], is called a *scatter factor*, and allows for a quick estimation of dose scattered around the patient after a specific examination [Schueler 2006]. It is usually expressed at a certain distance from the radiation field centre, or from a pre-defined point on the patient table, when multiple beam angles are used during an intervention. It may be either derived from Monte-Carlo simulations, or following an aforementioned dose assessment campaign using electronic dosimeters. Scatter factors are especially useful for assessing individual radiation protection discipline within a given angiography suite, as different operators may use the available means of protection with different degrees of accuracy.

The risks encountered by medical staff have been recently described in a publication by J. R. Parikh et al. in the American Journal of Roentgenology [Parikh 2017]. The different risks described within this paper are summarised in Table 2. As we can see, the different described health conditions have a very low – yet probably existing – dependence on the long-term exposure to ionising radiation. Particularly brain tumours and radiation-induced cataracts are the recent reasons for concern.

Health condition	Details	Comments
Skin cancer	Basal cell and squamous cell carcinoma No influence on melanoma	Observed in the pre-1950 era, when occupational doses were much higher
Breast cancer	Very low influence	Especially for technologists employed before 1985
Leukaemia	No evidence since the 1970s	-
Thyroid cancer	Very small risk	Radiosensitivity decreases with age
Brain cancer	Case reports on 31 interventional cardiologists deceased from brain tumours	85 % of the malignancies in the left hemisphere
Skin injuries	Permanent depilation of the distal lower extremities	Less frequent than in the past due to lower-hanging draping
Radiation-induced cardiovascular disease	Some strokes or myocardial infarction probably observed	Overall mortality rate from circulatory disease may be in the same order as cancer-induction risk
Radiation-induced cataracts	Tissue effects, threshold around 500 mGy, independent of dose rate (chronic or acute)	ICRP proposed a reduction of the annual equivalent dose limit from 150 mSv to 20 mSv per year

Table 2: Summary of the different health conditions that may be due to long-term exposure to ionising radiation, adapted from [Parikh 2017].

To protect themselves from ionising radiation scattered by the patient, healthcare professionals can use various protective devices in addition to the usually compulsory individual high-Z aprons, such as ceiling-suspended or floor-mounted leaded acrylic shielding, leaded glasses, or highly absorbing high-Z sterile draping to be placed on the patient. These means of protection, although highly efficient in test conditions (incident radiation normal to the protective device, static conditions), may quickly lose their protective efficiency when used with less caution. C. J. Martin analysed the theoretical and effective eye lens dose reduction efficiencies [Martin 2016], and these are synthesised in Table 3. Further means of reducing operator dose by increasing the distance to the patient may also be useful, such as contrast medium injection pumps, rather than the manual injection using a hand-held syringe.

Type of protective device	Lead equivalent thickness [mm Pb]	Dose reduction factor	Comments
Ceiling-suspended or floor-mounted shielding	0.5	In theory: 4 – 33 In practice: 2 – 7	Necessity of high working discipline for accurate device positioning
Sterile patient draping	0.25	2 – 4.5	To be positioned outside the primary X-ray field
Leaded glasses	0.5 – 0.75	In theory: 5 – 7 In practice: 2.5 – 4.5	Less efficient for the less exposed eye (generally right: 1.5 – 2.0)
Integral facial mask	0.1	Unknown	Geometric efficiency probably very high Potential brain dose reduction up to 81 % [Marshall 1992]

Table 3: Summary of the theoretical and practical eye lens dose reduction factors of different means of staff protective devices, adapted from [Martin 2016].

Image exposure and quality

In modern fluoroscopy devices, the X-ray output is automatically adjusted with respect to a pre-required detector entrance dose per acquired frame and a given need of image quality. It is thus highly dependent on patient body habitus and tissue type, as we already stated, but is also vendor-dependant. The current state-of-the-art summary of the different AEC systems has been described in the American Association of Physicists in Medicine (AAPM) task group 125 report, published in 2012 [AAPM 2012]. Twenty-two angiography units were investigated by the different members of the task group and, for each manufacturer (GE Healthcare, Philips Medical Systems, Shimadzu Medical USA, and Siemens Medical Systems – now "Siemens Healthineers"), a representative from the industry was included in the study. Traditional AEC systems are based on three parameters: Tube potential [kV], tube current [mA] and pulse width [ms]. Modern units usually work with two supplementary parameters: Primary X-ray beam filtration [mm Al or mm Cu], and focal spot size (two or three, depending on the manufacturer). These different AEC systems were assessed using PMMA slabs as surrogate for patient attenuation, leaving the respective systems change the exposure parameters. It would be cumbersome to summarise the different vendors, but several elements are quite common between all the systems:

- For increasing patient thickness, the tube potential will steadily increase, while the beam filtration will decrease. This is intended at keeping image contrast as high as possible by adapting the beam effective energy to the patient's body habitus, fine

tuning being performed by the respective power curves for the respective anatomical regions.

- When switching from fluoroscopy to acquisition (diagnostic) series, for a same patient thickness and anatomical region, tube potential will be usually lowered – and tube current increased – while the beam filtration is reduced. This will imply a much lower beam effective energy, and thus a higher contrast. This is because fluoroscopy is usually used during much longer times – for e.g. catheter positioning prior to a diagnostic acquisition or DSA series. This implies that patient skin dose is spared by increasing the effective beam energy for the longer exposure times.

However the current AEC systems are currently aimed at lowering patient skin dose, not all technological innovations have allowed a systematic patient dose reduction. Indeed, E. Vaño et al. [Vaño 2009] showed that, when switching from image intensifiers (II) to flat-panel detectors (FPD), the average patient dose rates for fluoroscopy, as well as the dose per DSA frame do not significantly vary when switching from an older technology (II) to a more modern technology (FPD) (Figure 2). This paradigm shift is similar to the transition from screen-film systems to computed radiography (CR) or digital X-ray imaging (DR): The dynamic range of the imaging systems was increased, thus allowing for much higher patient exposures without the detector saturating, but the payback was a higher flexibility in the acquisition parameters and subsequent possible image post-processing possibilities.

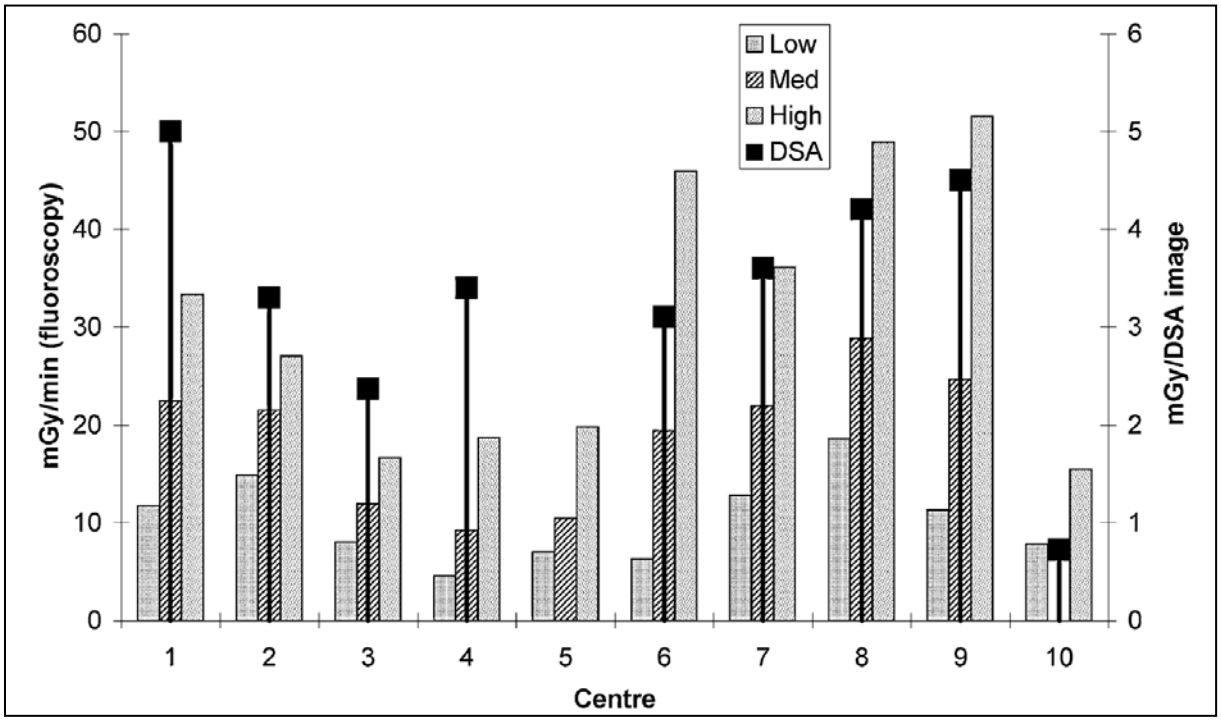

Figure 2: Comparison between II and FPD. Centres 1 to 5 were equipped with II, while centres 6 to 10 were equipped with FPD. The shaded bars show patient dose rates for low, medium and high quality fluoroscopy, while the black squares show the average dose per DSA image. Image from [Vaño 2009].

However, the use of FPD have opened the door to new on-line image post-processing techniques, aiming at reducing patient dose by increasing image quality using new mathematical algorithms for image information maximisation, just like is the case for iterative reconstruction in CT. Furthermore, current norms on fluoroscopic imaging have also required a limitation on patient skin dose rate, as was already the case for detector entrance dose [DIN 2013], as is shown in Figure 3.

Tabelle 4 — Referenzluftkermaleistung für Durchleuchtung im Normal-Mode — Prüfbedingungen und Grenzwerte

Anwendung[a]	Absorberdicke (PMMA) mm	Eingestelltes Format cm	Positionierung des Absorbers	GRENZWERT mGy/min
Herzkatheteruntersuchung	200	≤ 17	Absorbermitte ins Isozentrum	30
	300			60
Angiographie, neuroradiologische Untersuchung	100	≤ 30	Absorbermitte ins Isozentrum	5
	200			20
Untersuchung des Gastrointestinaltraktes	100	≤ 30	Absorber auf Tischplatte	7,5
	200			25
Untersuchungen mit mobilem C-Bogengerät	100	≤ 17	Absorberoberfläche 30 cm vor Bildempfänger	7,5
	200			25

[a] Die Prüfbedingungen (Absorberdicke, eingestelltes Format und Positionierung des Absorbers) repräsentieren für die genannten Anwendungen typische Betriebsbedingungen.

Figure 3: Patient skin dose rate limitations for different fluoroscopic imaging purposes. Table from [DIN 2013].

Image quality is a challenging topic to handle. First, one has to agree on the actual definition of image quality. In 1991, the diagnostic information in an image has been given 6 levels of accuracy [Fryback 1991].The lowest step is probably the easiest to measure, and the higher one aims at increasing the levels of accuracy, the more difficult it becomes to actually quantify the image quality, since it will apply not only on the sole pattern of gray levels in an image, but gradually involve the diagnostic accuracy (level 2), up to the societal efficacy (level 6), thus gradually involving more disciplines, such as psychology, sociology, and even economy. On the first level, image quality relies on well-defined metrics (image noise, CNR, spatial resolution, etc.). These metrics, on their own, have the advantage of being easily reproducible, and can serve to guarantee the technical accuracy of the imaging acquisition and rendering device (quality assurance (QA) of the imaging chain). But it has little to no significance for the end user, i.e., the physician, who has to take a decision on what follow-up to prescribe based on his/her knowledge of the patient's medical status and history and the information extracted from an X-ray image of a possible disease.

The report on objective image quality by M. Tapiovaara [Tapiovaara 2003] describes the first steps of objective image quality assessment. It describes the precise definition of “image”, in this case, the acquired image data, without the actual rendering step; and the definition of “quality”, in this case, the detectability of phantom details that look like diseased structures in actual patients. It therefore concentrates on the second step of Fryback’s scale, and this work will equally concentrate on that same step. Further, it describes the basic (physical) factors of image quality, i.e., the modulation transfer function (MTF), image contrast and the noise power spectrum (NPS), as well as the characterisation of a detector, based on the signal-to-noise ratio (SNR), the noise equivalent quanta (NEQ) and detective quantum efficiency (DQE). Finally, it introduces and describes the tool we are currently working on, which is a *mathematical model observer*, that will us allow to grade image quality based on a clearly defined diagnostic task.

A model observer is a mathematical concept based on statistical decision theory [Barrett 1993 and 2004]. It allows to extract as much information from the imaging chain as possible (ideal linear observer) or to evaluate the entire imaging chain using a model with downgraded performance (anthropomorphic observer). It relies on four cornerstones:

- The choice of a clinically relevant diagnostic task:
    - Classification tasks:
        - Lesion detection (i.e. “do I see what I am looking for?”),
        - Lesion location (i.e. “where is the lesion I am looking for?”),
        - Lesion shape assessment (i.e. “is it spherical or spiculated?”),
    - Estimation tasks:
        - Lesion size change assessment (i.e. “has the lesion grown since last time?”),
- A statistically significant set of images to establish a response curve,
- An observer (ideal or anthropomorphic),
- A figure of merit (FOM) for image quality quantification.

A publication from X. He and S. Park [He 2013] describes the basics of model observer implementation and use in medical imaging, and serves as a concise adaptation of [Barrett 2004] for clinical imaging. Conceptually, model observers can be divided into two categories:

- The ideal observer (IO): It extracts all available statistical information from the image, and is used for unit benchmarking. Ideal does not mean that it always performs right, but that it reflects the technical ability of the imaging unit to acquire and render diseased and healthy structures

- The anthropomorphic observer: Like humans, its performances are below ideal, and it is aimed at qualifying given image acquisition and reconstruction protocols, mimicking the performance and errors a human could do when submitted to a given diagnostic task.

As such, model observers give an image quality grading with respect to a diagnostic task, and are probably the first step for bridging the gap between physics and healthcare. We will further on describe, in the chapter on our work on image quality, how the model was implemented and tested, as well as what is yet to come.

Challenges for the medical physicist

As such, patient and staff dose have become less of a concern, since technological evolution has allowed to drastically – or at least has the potential to – lower patient and therefore staff doses. Of course, long-term exposure to ionising radiation remains a threat for human health, and particular care should be brought to measuring individual doses, as well as offering efficient yet easy-to-use protective solutions. But the key problem resides within the disparity of the users of fluoroscopy devices. Indeed, interventional radiologists and cardiologists are usually pretty-well trained on the risks of ionising radiation and the optimisation of patient dose. But as mentioned by the ICRP [ICRP 2010], a large number of medical specialties outside the imaging department have taken up using fluoroscopy as a primary diagnostic and/or therapeutic tool. Thus, potentially lesser-trained professionals work with units, usually mobile, that are increasingly capable of performing highly irradiating procedures. Furthermore, as stated by that same report, in the absence of proper education or awareness, people might become overconfident – thus exposing themselves and other to increased doses – or, on the contrary, might overestimate the risks, thus potentially underexposing the patient and missing medically relevant lesions.

A publication by M. M. Rehani [Rehani 2015] underlines the current and future challenges in radiation protection in medicine. The first challenge is keeping the current trend in dose lowering reasonably going, especially for paediatric imaging. An examination yielding several mSv of patient dose should not be a cause for over-alarming, and the accent should be put on minimising the risk of radiation-induced skin injuries. With respect to paediatric imaging, several publications are launching controversies on radiation effects in children undergoing CT scans. Indeed, large-cohort studies have potentially statistically shown the carcinogenic effect of low-dose ionising radiation, but these studies are often stained with matters of reversed causality. The risk is avoiding examinations based on hypothetical risks, and potentially creating more harm due to not diagnosing a potentially severe disease.

Furthermore, dose indicators should be refined in order to more precisely assess patient dose and subsequent radiation risk. The AAPM has already introduced a correction faction for $CTDI_{vol}$ based on patient geometry (the size-specific dose estimate or SSDE), and this should also be proposed for interventional fluoroscopy, in order to correct the relevant dose indicators based on patient body habitus. Finally, these procedures will have to be thoroughly documented, within the scope of the upcoming clinical audits, which will be mandatory by 2018. It is also to mention that the big picture of dose optimisation should also not rely on the sole imaging part, but should also include other relevant – and perhaps trickier parameters – such as the volume of injected iodinated contrast media. Indeed, when lowering patient dose, the CNR could become so low that, without the possibility of reducing the image noise, the only solution that remains for the operator is to increase the imaged structure's contrast by injecting more contrast medium, which poses an immediate renal toxicity problem.

Our first publication tried to summarise this approach [Ryckx 2014]. Indeed, since 2008, the implication of medical physicists in medical imaging has been rendered compulsory for CT, interventional fluoroscopy and nuclear medicine in Switzerland. For fluoroscopy, it proposes an evaluation method for patient skin dose due to the AEC system. At that time, no image quality was performed, and the assumption was made that physicians using the devices routinely were judges of image quality suitable for their needs. We noticed a large discrepancy in patient exposure between different manufacturers, and the perspectives of the paper laid the first basis of model observers for objective clinically-relevant image quality optimisation.

Our contributions to the field

Patient exposure

Automatic dose collection and establishment of reference levels

Within the scope of the ICRP recommendation on dose reference levels (RL) [ICRP 1990], implemented in the IAEA basic safety standards (BSS) and the Euratom 2013/59 on the "basic safety standards for protection against the dangers arising from exposure to ionising radiation", the Swiss Federal Office of Public Health (FOPH) is in charge of setting up and updating RL for the different diagnostic procedures using ionising radiation. A call was made to 9 centres to participate in the survey with contribution with data from any interventional cardiology (IC) procedures, both vascular and electrophysiology procedures. Preference was given to centres with high volume of workload and to centres using automatic database generation such as CardioReport™ XP (CVX Medical, France). Data was collected for the period of 2010 – 2013. For each instance, the examination type and the year were required as general data. As dose metrics, the $K_{a,r}$, P_{KA}, T, and the number of sequences (S) were required. As regards the patient, the weight, height, body mass index (BMI), age and catheter access route were requested.

The vascular procedures were: Coronary angiography (CA, 24 261 procedures collected), percutaneous transluminal coronary angioplasty (PTCA, 1 099), CA+PTCA (18 797), shunt closure (SC, 622), transcatheter aortic valve implantation (TAVI, 221) and myocardial biopsy (73). The electrophysiology procedures were: diagnostic procedures (EFO, 210), defibrillator implantation (ICD, 281), pacemaker implantation (PM, 300), radio-frequency ablation (RFA, 720) and alcohol septal ablation (7). The latter was discarded due to an insufficient number of procedures. This list of ten procedures has been an improvement with respect to the previous study, which showed RLs only for CA and PTCA procedures.

Since RLs are established for standard patient body habitus, the collected data could undergo the following correction steps:

- Weight banding, which is the simplest method and consists in the selection of patients within a desired weight range (65 – 75 kg or 60 - 80 kg usually). This method involves a significant loss of data and is therefore not useful for small populations.
- Size correction, which is based on the application of a numerical correction to compensate the deviation in body habitus of those patients outside the mean size in order to compare radiation dose among populations. There are several methods to do so. In the present study we used a correction based on that the method described by

Chapple et al. [Chapple 1995] and Marshall et al. [Marshall 2000], which has been used by other authors, and was also used in the last Swiss survey. The method consists in dividing the P_{KA} by a factor f_{stat} described below:

$$f_{stat} = \frac{P_{KA}(mean\ patient)}{P_{KA}(real\ patient)} = e^{-\mu(d_m - d_r)}$$

where μ is the mean attenuation coefficient, d_m is the diameter of the median patient, and d_r the diameter of the real patient. The original method makes use of a factor k, instead of μ, determined experimentally, that reflects changes in dose for subjects of different sizes owing to changes in kV, mAs and filtration settings. In our method we might use μ instead, which accounts for the primary radiation attenuation. The patient diameters are calculated from the patient height (h) and weight (w), as follows:

$$d = 2\sqrt{\frac{w}{\pi h \rho}}$$

where ρ is the volumetric mass of water (1000 kg m^{-3}). In the last survey a value of 0.3 cm^{-1} was considered for μ. In the present survey we should also consider 0.2 cm^{-1} to take into account the additional Cu filtration of the current machines. These values were calculated for the typical primary beam used in interventional cardiology (75 kVp and 4.5 mm Al with and without Cu filtration). The resulting RLs were calculated using the size correction algorithm and published in June 2016 by the Federal Office of Public Health (FOPH), with the introduction of the $K_{a,r}$ in the FOPH directive, used for tissue reaction risk estimation, in addition to the P_{KA}, T, and N values that were already in the previous revision of the Swiss RLs.

- Linear or polynomial regression. Since the P_{KA} and $K_{a,r}$ correlate with the patient's body-mass index (BMI) and/or weight, an empirical estimation of the aforementioned correction factors might be obtained on a large dataset using basic polynomial fitting. Since the Swiss study collected a large amount of data, the regression has been performed using this method and the applying it to diagnostic CA procedures (about 25 000 examinations collected).

A second order polynomial regression was performed using the R statistical library for the analysis of the P_{KA} as a function of patient weight. This allowed calculating patient-specific RLs (yet to be published, expected to submit by September 2017), of which an excerpt can be seen in Table 4.

As an example, for patients of 90 kg undergoing a percutaneous transluminal coronary angioplasty (PTCA), the specific P_{KA} RL associated to this weight would be 183 Gy cm^2

instead of 130 Gy cm^2. The method yields a P_{KA} RL of 29 Gy cm^2 for patients of 50 kg who undergo a CA, instead of the published value of 50 Gy cm^2.

	Weight-dependent RL [Gy cm^2]		
	CA	**PTCA**	**CA+PTCA**
75 kg patient RL	**50**	**130**	**110**
Patient weight (kg)			
5	2	5	4
10	4	10	8
20	9	22	19
30	14	37	32
40	21	55	47
50	29	75	64
60	38	98	83
70	48	124	105
80	58	152	128
90	70	183	154
100	83	216	183
110	97	252	213
120	112	290	246
130	127	331	280
140	144	375	317
150	162	421	356
160	181	470	398
170	201	522	441
180	221	576	487
190	243	632	535
200	266	692	585

Table 4: Example of patient weight-corrected P_{KA} using statistical analysis, for coronary angiography (CA), standalone percutaneous transluminal coronary angioplasty (PTCA), and the combined procedure (CA+PTCA). The top bold lines show the RLs as published by the FOPH.

On the basis of that same eight-centre dose registry, a paper has been published in Radiation Protection Dosimetry (RPD) [Ryckx 2016] on selective practice optimisation clues based on a large-scale patient dose collection and the cross-comparison to national standards (such as RL) or other large datasets. For this purpose, an in-house software solution (Memoviz, Memoways, Geneva, Switzerland) was elaborated to visualise the data. For each procedure type, T, N, P_{KA} and $K_{a,r}$ could be displayed for each of the eight participating centres. For every dose indicator distribution, the software calculated the first, second and third quartiles of the respective distributions. According to the definition of the RLs, the third quartile was used as the main metric for dose indicator comparison. A visualisation tool could display the respective quartiles of each dose indicator for the ten aforementioned cardiac procedures, as can be seen in Figure 4.

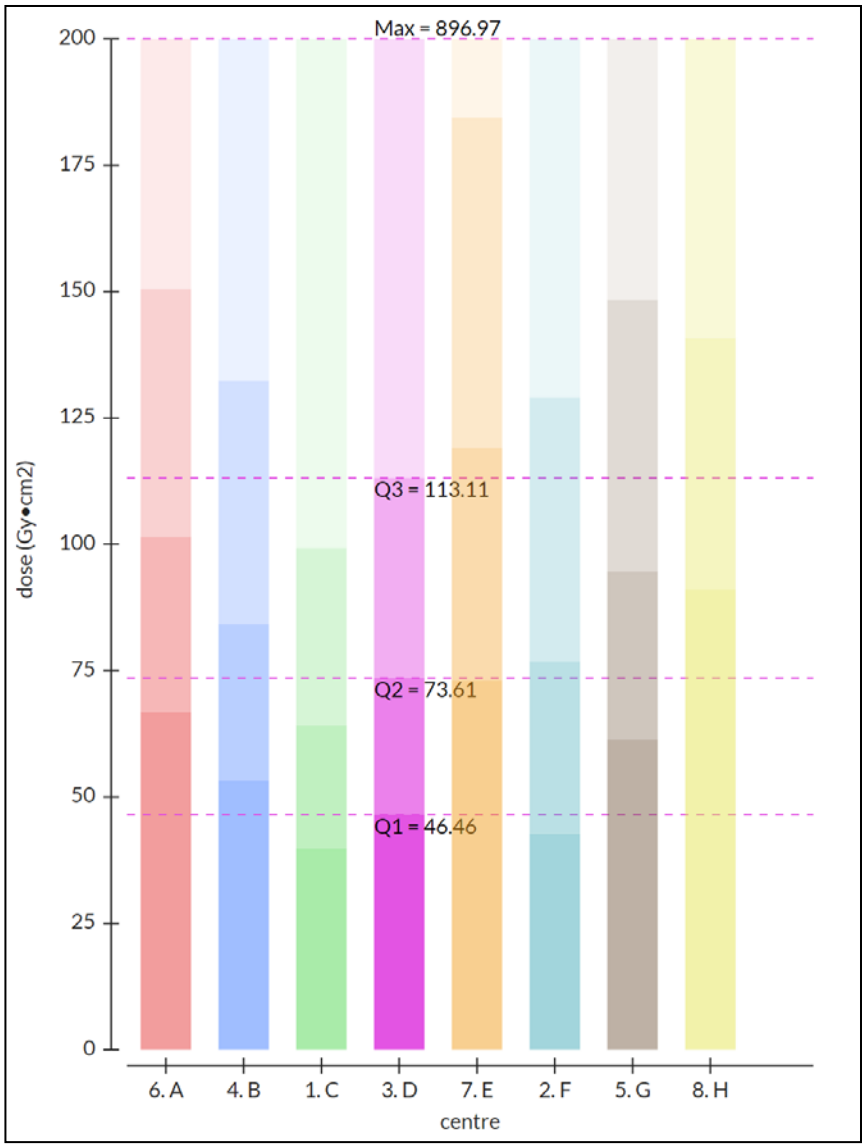

Figure 4: Visualisation of the quartile comparison of P_{KA} (Gy cm²) for CA + PTCA procedures and for all eight cardiology centres. Mouse hover-over allows for an immediate display of the actual quartile values and immediate comparison with the dose levels of the other centres. The numbers are part of the web interface and display the selected dataset. Figure from [Ryckx 2016].

As an example, the third quartiles for CA + PTCA dose indicators for centres B, F and Switzerland (CH) were the following:

- Centre B RL: P_{KA} 132 Gy cm^2, $K_{a,r}$ 2.2 Gy, T 17.9 min, N 1820 images,
- Centre F RL: P_{KA} 129 Gy cm^2, $K_{a,r}$ 1.2 Gy, T 20.5 min, N 2420 images,
- CH RL: P_{KA} 150 Gy cm^2, $K_{a,r}$ 2.0 Gy, T 18.1 min, N 1527 images.

It could be seen that P_{KA} was rather similar for centres B and F, but the $K_{a,r}$ of centre B was roughly twice as high as that of centre F. This could indicate that centre F worked with imaging fields roughly twice as large as B, thus advising for a more thorough use of beam collimation. When comparing the values of centre F with the Swiss values, it could be seen that the number of images (N) at F was much higher for similar fluoroscopy times (T). This

could indicate a higher frame rate (e.g. 30 fps instead of 15 fps, which could still be diagnostically acceptable).

The analysis of the respective distributions could give an indication on where to start the dose optimisation. Indeed, underlining that one single dose indicator out of the four was higher with respect to the other did not necessarily mean that one centre worked 'better' than another. The four dose indicators are, de facto, correlated one to another but are not linearly dependent. This kind of multivariate analysis, based on anonymous centre cross-comparison, could give the respective centres ideas on what to optimise, rather than just telling the operators that their mean doses were higher than pre-existing RLs.

Pregnant patients

A subgroup of patients especially sensitive to ionizing radiation is pregnant patients. In particular, infants, neonates and foetuses are more sensitive to ionizing radiation due to their higher metabolism and rapidly dividing young body cells. However, the mean prevalence of coronary heart disease is only 0.6 % for patients between the ages of 20 and 39 years in the US [Bordoli 2014], making the theoretical and practical skills needed to properly handle these cases quite challenging due to the low volume of clinical opportunities. In this regard, a publication has been co-authored and submitted in the European Journal of Medical Physics (EJMP, Physica Medica), for an upcoming special issue on pregnant patient management. It acts as a literature review on the current status on the management of pregnant patients within cardiac angiography suites, and is currently under review [Kallinikou 2017]. It lists the typical foetal doses, as well as the foetal risks when exposed to alternative procedures, such as drug-induced thrombolysis. Risks due to ionising radiation were weighed against the natural occurrence of peripartum child morbidities. The overall conclusion was that, when care is being taken by the physician, no particular increase in child morbidity risk is to be expected, and the lives of both the mother and child will be preserved when treating acute coronary syndromes properly.

A typical protection of the carrying mother that may be used is placing a lead apron around the lower abdomen to protect the uterus and child from ionising radiation. Although probably relevant before the 1950s and FDA regulations on leakage radiation limitation [FDA 2016], this solution may not be adequate anymore. Therefore, we submitted a paper on the efficiency of patient lead aprons in CT imaging in EJMP for the aforementioned special issue on the pregnant woman [Ryckx 2017], currently under review. First, we performed a literature review, during which we found 11 relevant articles, all of them reporting uterus exposure due to CT imaging performed for exclusion of pulmonary embolism, one of the leading causes of

peripartum deaths in western countries. Our findings of the literature review were that uterus doses – taken as a surrogate for foetal exposure in the early stages of pregnancy – ranged between 60 and 660 µGy per examination, and relative dose reductions to the uterus due to high-Z garments were between 20-56 %. The dose reduction efficiencies of these garments were compared to Monte-Carlo simulations of CT protocols, for which the overall scan length was reduced as a means of patient exposure optimisation (the equivalent way of reducing patient effective dose in fluoroscopy is the reduction of the primary X-ray beam field size by using the collimation system) using the ImPACT Monte-Carlo simulation spreadsheet. shows the ImPACT graphical user interface (GUI). In red are the initial (a) and reduced (b and c) scan lengths.

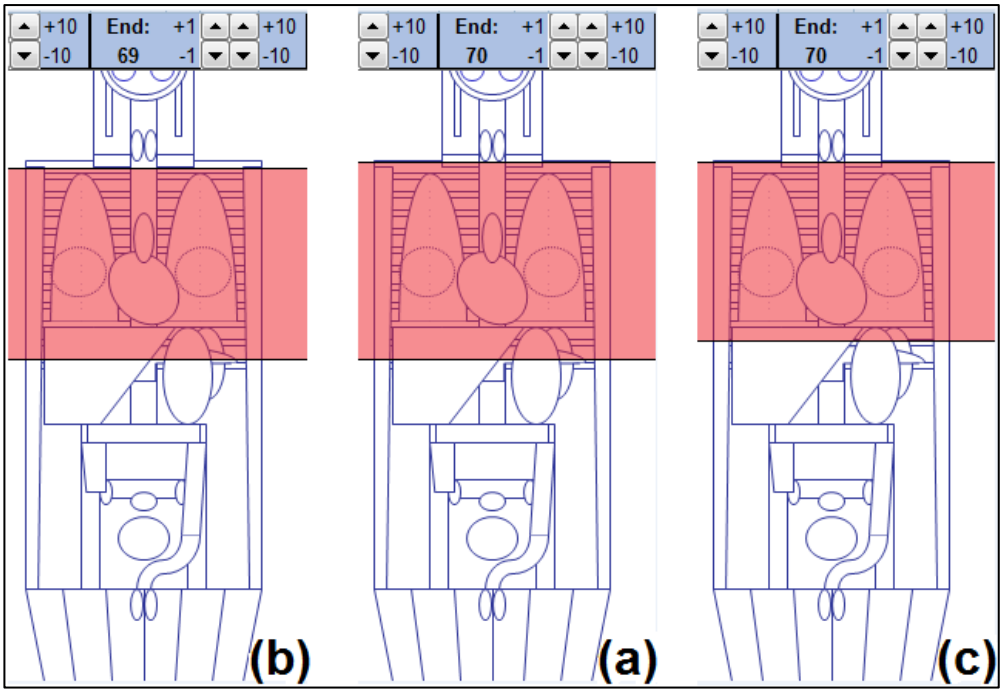

Figure 5: Screenshot of the ImPACT GUI for chest CT. (a) acquisition volume before scan length reduction, (b) acquisition volume after reducing the scan length by 1 cm above the lung apex, (c) acquisition volume after reducing the scan length by 3 cm under the lung base. Figure from [Ryckx 2017] (under review).

Again, uterine doses were taken as surrogate of the foetal doses. Simulations showed that reducing the scan length by one to three centimetres could potentially reduce uterus dose up to 24 % for chest imaging and even 47 % for upper abdominal imaging, thus in the order of the dose savings achieved by high-Z garments. However, using the latter may negatively influence the diagnostic image quality and even interfere with the AEC system. Our conclusions pointed out that efforts should be concentrated on positioning the patient correctly in the gantry and optimising protocol parameters, rather than using high-Z garments for out-of-plane uterus shielding. As no publication on foetal dose reduction in interventional fluoroscopy procedures using lead aprons was found during the preliminary literature review of the publication, we conclude that this practice has been abandoned for fluoroscopically-

guided procedures. And since the apron efficiency in CT is only useful to block radiation back-scattered by the patient table, we assume that the efficiencies of lead garments in CT could be transposed to fluoroscopy.

Staff exposure

Estimation of radiological doses and risks

The current problem with staff exposure is, in contrast to patient exposure, not acute but chronic cumulative doses, be they effective or to certain organs, such as the eye lens or the brain. The error bars of measuring staff dose during a single examination are already quite large, due to measurement uncertainties and variable scattered X-ray spectra around the patient, that degrade electronic or TLD measurement accuracy. As a corollary, the estimation of cumulative doses and risks over a whole career becomes cumbersome. Furthermore, as mentioned earlier, scatter factors are usually given at a specific distance from the patient, as well as for a specific measurement position on the operator, usually at chest level. This implies discrepancies between chest and eye or brain dose due to the distance between the measurement points, as well as the attenuation by the skull and protective devices used by the operator.

To estimate staff risk over a whole career, a website (http://intercardiorisk.creal.cat/) was set up and validated through a publication in the Journal of Radiological Protection in collaboration with a team from the Centre for Research in Environmental Epidemiology (CREAL) in Barcelona [Moriña 2016]. It allows for a staff eye or brain dose and risk estimation based on the following inputs:

- Career span between two dates,
- Number of procedures per working year,
- Operator birth date and gender,
- Protective behaviour according to three working practices:
    - Typical working practice,
    - No radiation protection measure at all,
    - Protective equipment fully employed.
- Operator profile:
    - Interventional cardiologist (vascular procedures),
    - Electrophysiologist.

Doses and risks are displayed as probability distributions of respectively cumulative equivalent dose to the considered organ [mSv], relative risk (RR) for radiation-induced

cataracts and lifetime fractional risk (LFR) for central nervous system tumours. Radiation risks are estimated using the currently accepted linear non-threshold (LNT) model and large-scale published epidemiological data. The eye and brain dose calculations are performed in two consecutive yet conceptually different steps. First, eye lens dose is calculated based on typical patient exposure scenarios and scatter fractions to the eye lens established during the ORAMED study [Vanhavere 2012]. In the second step, brain dose is calculated on the basis of experimentally-determined conversion factors between these two organ doses, which were the part of the study dedicated to our group. For this purpose, we performed phantom simulations of a clinically realistic patient and operator exposure scenario, irradiated in an interventional cardiology suite (Allura Xper FD10, Philips Healthcare) at our hospital. An anthropomorphic adult chest and head phantom (CIRS Inc., Norfolk, USA) representing the operator, was placed next to a stack of PMMA slabs representing the patient, 50 cm laterally from the isocenter and 50 cm at the right of the major patient (and table) axis, as can be seen in Figure 6.

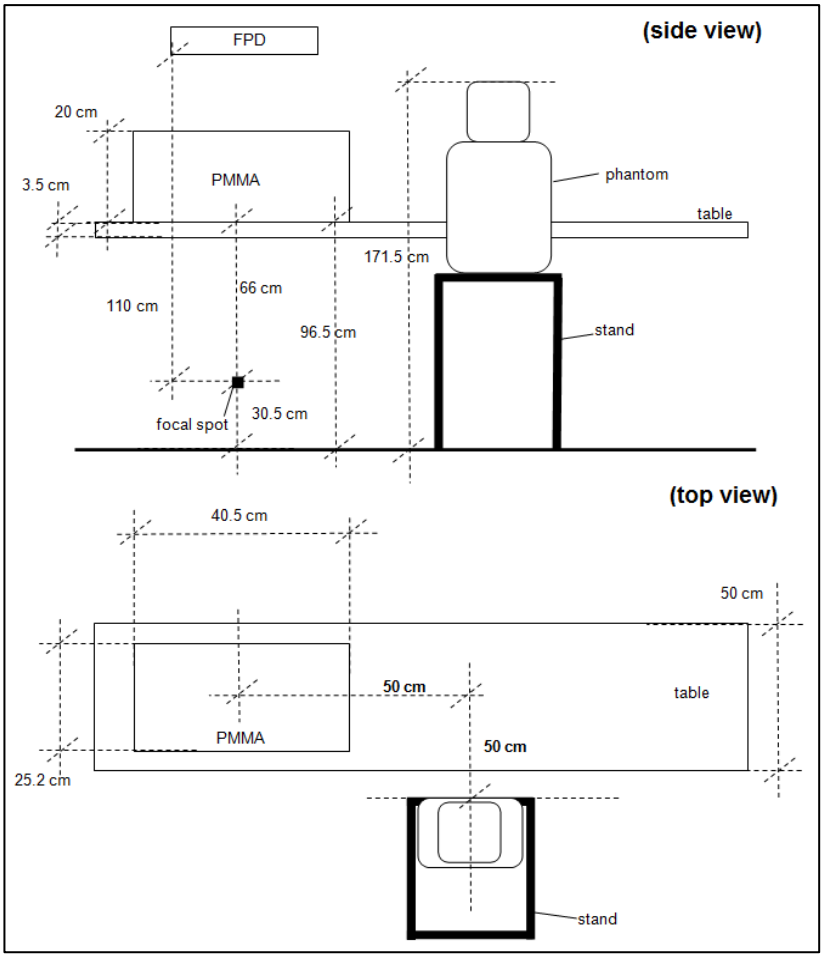

Figure 6: Geometry of the experimental setup aimed at simultaneously measuring eye lens and brain doses using TLDs.

The operator phantom was equipped with a lead apron, and a batch of 13 TLDs was simultaneously used for eye lens- and brain dose assessment, dispatched as following:

- 11 TLDs were used for brain dosimetry,
- 2 TLDs were used for eye dosimetry.

The unit was used with standard clinical AEC settings for both fluoroscopy (low quality) and angiography (high quality). Beam angles were set to the most typical clinical positions, as displayed in Table 5.

Orientation
PA
RAO 30° / CAUD 20°
RAO 30° / CRAN 20°
LAO 20° / CAUD 20°
LAO 20° / CRAN 20°
LAO 50° / CAUD 5°
LLAT

Table 5: Tube angles used for staff dose assessment.

The detail of the individual measurements will not be described here; for each beam angle, the AEC system was allowed to deliver at least 20 Gy cm^2 of P_{KA} to the patient in order to obtain significant amounts of scattered radiation to the operator phantom. No mobile or ceiling-suspended leaded shielding was left in place to attenuate the scattered radiation. The ratios between each measured cumulative eye and a brain doses were then calculated for use as a conversion factor from eye dose to brain dose. The resulting conversion factors ranged from 3.4 (eye furthest from unit) and 8.1 (eye closest to unit). In order to account for uncertainties due to positioning of the interventional cardiologist, the conversion factor was defined as a uniform distribution between 3.4 and 8.1. This project was started in order to give a factual answer possibility to several healthcare professionals claiming to suffer from a radiation-induced cataract, and to show the limitations of current routine under-apron dosimetry.

However, this evaluation may be biased by the underlying hypotheses of practice considered as identical between different interventional angiography suites. Indeed, some procedures are being performed using non-standard approaches (i.e. other than right femoral or right radial punction) like, for example, left radial approach, that forces operators to bend over the patient since they are standing on his/her right side. To assess the exposure differences

between those three approaches, we set up an experimental protocol for a five-manned senior operator team at a local hospital. During seven months, the coronary angiography (CA) and PTCA procedures were monitored using an electronic dosimetry system (DoseAware, Philips Healthcare, The Netherlands). Each procedure cumulative dose (measured above the operator apron) was normalised by patient P_{KA} to evaluate operator exposure by the mean scatter factor per approach. As was expected, the average right femoral approach (RFA) scatter factor was lower than that of the right radial approach (RRA), i.e., 0.06 (0.01-0.18) vs. 0.51 (0.32-0.81) μSv / (Gy cm^2) – values given in parentheses are the 25th and 75th percentile of the individual scatter factor distributions. Surprisingly, the left radial approach (LRA) showed an intermediate value of the scatter factor, i.e., 0.23 (0.10-0.45) μSv / (Gy cm^2). The distribution of the exposure factors are shown in Figure 7.

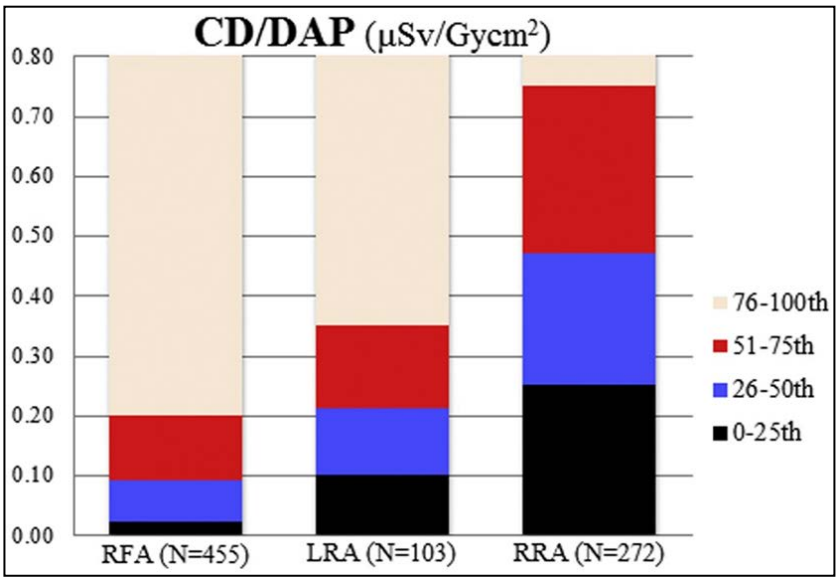

Figure 7: Exposure factors (in the study's nomenclature cumulative dose (CD) divided by dose-area product (DAP) for the RFA, LRA and RRA procedures, shown as the respective quartile distributions, as published in [Kallinikou 2016].

A possible explanation for these findings was that, during RRA procedures, the leaded glass mobile panel is positioned further from the patient in comparison to LRA and RFA, in order to facilitate the right radial access. The gap created between the patient and the leaded shielding was likely to be more pronounced during RRA procedures, thus creating a higher source of radiation exposure to the operator by diminishing the shielding efficiency, as stated by C. J. Martin [Martin 2016]. Second, when using RRA, the operator is de facto positioned closer to the x-ray tube compared with both LRA and RFA procedures. The study's results in terms of respective procedure difficulty (in terms of fluoroscopy and procedural times) and radiation dose of the operator (absolute cumulative dose per procedure) and the patient P_{KA} were in line with published data in the literature. As such, and although not randomised, the study reflected operator exposure in everyday clinical practice, despite a bias in the choice of

vascular access site by the respective operators. These results were subsequently published in the American Journal of Cardiology [Kallinikou 2016].

Efficiency of protective glasses

Currently, effective dose to interventional physicians is not much of a concern, at least for the immense majority of medical radiation-exposed workers. However, as we saw previously, certain organs remain potentially highly exposed, namely the brain and the eye lens. To reduce eye lens dose, physicians may use one or several means of protection, as has been described by C. J. Martin [Martin 2016]. Among these, leaded glasses are a common choice of interventional professionals. As mentioned in the publication by C. J. Martin, the actual protective efficiency of these glasses can vary widely, but the factors influencing the efficiency are not well described. For this purpose, the following radiographer diploma work by C. Bolomey and G. Fasel, whom we followed during approximately one year, addressed this question. In order to determine the factors influencing the efficiency of leaded glasses, measurements were carried out by reproducing the clinical conditions in which these glasses are used. Four pairs of leaded glasses were selected to test the following parameters of influence:

- Equivalent lead thickness: 0.5 or 0.75 mm Pb,
- Surface of the protective glass: 18 or 21 cm^2,
- Presence or not of a lateral protective layer,
- Orientation of the operator's head,
- Use of the frontal or lateral C-arm or both simultaneously.

The orientation of the operator's head is defined as the angle defined by two imaginary lines: the first crosses the centre of the X-ray field at patient level and the operator's forehead; the second crosses the operator's forehead and the diagnostic screens. Depending on the patient size (a child or an adult) or the approach (radial or femoral), the angle may vary between 45° and 90°, as depicted in Figure 8.

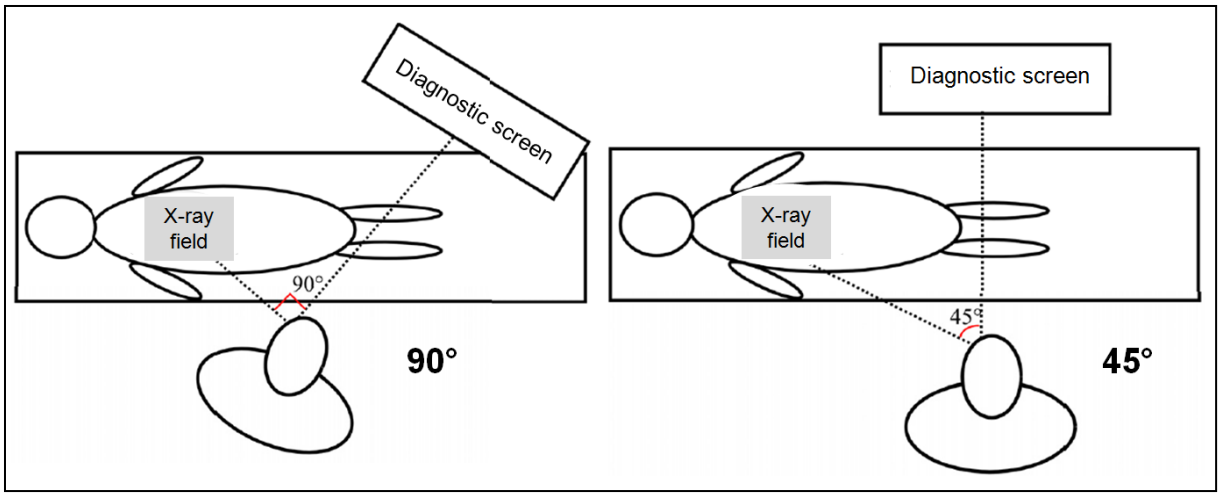

Figure 8: Schematic depiction of the 90° (left) or 45° (right) operator exposure geometry. Figure adapted from [Bolomey 2016].

The respective glasses models tested in this study are shown in Table 6.

Glasses #	Model	Lead equivalent thickness [mm Pb]	Lateral layer	Surface [cm^2]	Image
1	Sports	0.75	Yes	18	
2	Sports	0.75	No	18	
3	Classical	0.5	No	21	
4	Classical	0.75	No	21	

Table 6: Summary of the differences between the different models of glasses. Adapted from [Bolomey 2016].

The different exposure scenarii were simulated by using a solid-state detector (Unfors NED, RaySafe, Sweden) taped against the eye of an anthropomorphic head phantom. The exposure of an anthropomorphic patient head phantom for neuroradiological procedure simulation was performed on a biplane angiography suite (Philips Allura Xper FD20/10). The results of the protective efficiencies, defined as the differences between the scatter factors without and with glasses in front of the solid-state detector, are given in Table 7.

Unit used	Glasses #	Attenuation of the scattered radiation to the eye lens as a function of operator's head orientation			
		Mean attenuation [%]		Standard deviation [%]	
		90°	45°	90°	45°
Frontal	1	8.5	11.8	0.8	0.4
	2	4.0	10.7	2.9	0.6
	3	39.8	23.7	0.2	1.9
	4	53.6	28.4	0.7	1.2
Lateral	1	43.4	61.8	0.1	0.2
	2	31.9	52.1	0.5	0.1
	3	69.0	66.9	0.1	0.3
	4	74.9	67.4	0.1	0.1
Biplane	1	23.5	34.6	0.2	0.6
	2	13.9	23.4	0.9	0.3
	3	52.2	44.8	0.5	0.5
	4	63.1	43.6	0.1	0.6

Table 7: Summary of the measurement results from [Bolomey 2016].

As expected, an increased lead thickness brings a higher attenuation, and is more pronounced for the 90° than the 45° scenario. A larger glass surface also brings a higher protection against scattered radiation, and again this effect is more marked for the 90° scenario. The presence of a 0.5 mm Pb protective layer on the frame side allowed for an increase of the protection efficiency, with no particular difference between 90° and 45°. In summary, the highest protection efficiency is reached by highly covering glasses (large glass area and side protection), the main factor being the glass surface. This may also explain the high reported efficiency for brain dose reduction of leaded acrylic full-face masks of 0.1 mm Pb protective thickness, as has been stated in [Marshall 1992]. Results of this study have been published in Radioprotection [Bolomey 2016].

Image quality: A feasibility study

The ALARA principle states that a diagnostic image – or image series – should be acquired at a dose sufficient for the diagnosis but not more, implying the need of "good" rather than "nice" images. Until recently, image quality relied mainly on the DQE of a detector, thus mainly on the capacity of a detector to detect the maximal amount of impinging photons without adding any further noise, so as to display an image with the maximal amount of statistically significant data, i.e., the lowest possible noise level. Nowadays, detector technology is sufficiently efficient – or does not evolve as quickly as previously – so image reconstruction shifts from a physical – or engineering problem – to a mathematical problem, where acquired data is post-processed in order to enhance image quality by means of step-

wise optimisation processes, as is the case in nuclear medicine or CT, where iterative image reconstruction has been introduced to artificially reduce image noise. Furthermore, a medical physicist usually has no access to the detector raw data, as may be the case for mammography or radiography QA, but only to the unit's user mode. For this purpose, he/she has to propose optimisation possibilities in accordance to the way the fluoroscopy units are used by the physicians.

When these units are upgraded, two alternatives are offered to the users:

- Acquire images at the same dose level as for older reconstruction processes, and using new image reconstruction algorithms to enhance subsequent image quality, namely in terms of image noise,
- Acquire images at lower dose levels, but adapt image quality to reach subjective image quality levels the users' eye is accustomed to.

Both of these paradigms are possible, but only the second one is in phase with the ALARA principle. The most speaking example of such a paradigm shift is the use of iterative image reconstruction in CT. When first and second generation iterative algorithms have been introduced in the past years, the commercial promise of such improvements were in the order of 25 – 40 % dose reduction for first-generation algorithms (mainly based on sinogram de-noising by applying smoothing filters on the data – since CT noise lies mainly in the high frequencies), or even 80 – 90 % dose reduction for model-based algorithms [Image Wisely 2016]. However, due to the reasons we will mention further on, these algorithms were deemed unfit, since the noise texture was too drastically changed for the reader's comfort, and a compromise has been set up by the vendors between the first and second generation, implying 50 – 60 % of potential dose reductions while claiming to maintain a similar image quality when compared to classical filtered back-projection [FBP]. However, the downside of these new image reconstruction algorithms is the fact that they allow dose reductions without assessing the larger picture of clinical tasks whose performances may or may not be deteriorated by this reduction. For example, a recent study by J. Solomon et al. [Solomon 2017] has compared classical FBP to a commercially available state-of-the-art iterative image reconstruction algorithm. They assessed the low contrast detectability (LCD) of subtle hypoattenuating liver lesions using a visual grading analysis (VGA) performed by 16 readers (6 radiologists and 10 medical physicists) grading the diagnostic images. The results showed that, for LCD (one of the most difficult imaging tasks), the dose reduction potential while maintaining the same LCD capacity was merely close to 16 %. On the other hand, a study by B. Pauchard et al. showed that the mean oncologic follow-up CT imaging dose could be reduced by a factor 5 for young patients, using a model-based iterative image reconstruction

technique [Pauchard 2017]. We see that the dose reduction potential is highly dependent on the underlying clinical task. For fluoroscopic imaging, some image post-processing methods have also allowed a potential dose reduction without reducing image quality, as claimed by the respective manufacturers. The potential of these technological improvements could be much different with respect to a clinical task. For example, neuroradiology procedures deal with usually non-moving structures, whereas interventional cardiology procedures have to take into account the rapid motion of the coronary arteries, and the dose reduction possibilities could be different between both specialties, even if they use the same imaging unit.

One of these solutions was evaluated using a similar method as the study by J. Solomon et al. in the following study: Before upgrading the four angiography rooms with a technical and software upgrade (Allura Clarity, Philips Healthcare, The Netherlands), our hospital management asked for an evaluation of the efficiency of this solution. For this purpose, a patient of varying body thickness was simulated using PMMA slabs of 20 by 20 by 5 cm, piled up to obtain thicknesses of 5, 10, 15 and 20 cm, to take into account the behaviour of the AEC system. Entrance air kerma rates were measured using a 6-cc ionisation chamber (RadCal Corp., Monrovia, USA), placed at the entrance of the phantom to asses patient skin dose (and not $K_{a,r}$ per se). At all times, the focus-to-detector distance was kept constant at 110 cm, while the focus-to-ionisation chamber was kept constant at 75 cm, as mentioned in [Ryckx 2014]. For image quality assessment, a standard IQ phantom (TOR CDR, Leeds Test Objects, UK) was placed on top of the first PMMA slab, with additional PMMA slabs subsequently piled on top of the phantom, so as to simulate inner body lesions for different patient morphologies. The 17 low-contrast discs of varying contrast and fixed diameter of 11 mm contained in the phantom were used for LCD assessment, and the phantom's resolution test pattern with 30 line groups of increasing spatial frequency was used to assess perceived spatial resolution. Two units – one upgraded and one before upgrade – were measured using the same experimental setup. The acquired images were displayed on a DICOM 3.14 compliant diagnostic monitor, on which a single observer subjectively assessed image quality of LCD and perceived spatial resolution by noting the disc with lowest detectable contrast – taken as the LCD performance – and line group with highest perceptible frequency as spatial resolution perception.

For fluoroscopy settings, the air kerma rates were systematically lower for the upgraded radiology unit than the reference unit. The average air kerma rate reduction over all PMMA thicknesses was 25.5 % for low fluoroscopy quality, 43.5 % for medium-quality and 34.5 % for high-quality fluoroscopy mode. For DSA, the air kerma per frame reduction was in

average 69.7 % for abdominal angiography and even 84.4 % for lower limb angiography. Subjective static image quality showed no significant decrease for both LCD and perceived spatial resolution. After implementation of this upgrade on our angiography units, a retrospective patient P_{KA} and $K_{a,r}$ assessment for selective neuroangioplasty procedures showed a statistically significant decrease of patient dose by a factor of 3 – 4, with no significant change in fluoroscopy times (T), taken as an indicator of mean case difficulty. These results have been published in RPD [Ryckx 2015]. However, the interventional cardiologists did not find the image quality sufficient, and patient exposure had to be increased after the initial four-fold drop of the aforementioned dose indicators.

Mathematical model observers

Schematically, these new algorithms are based on pixel-wise or neural network image analysis by “black box” hardware and software implementations, and are highly non linear and non stationary, and may see their performances therefore altered for different diagnostic tasks than those the solution was implemented for. Indeed, while interventional neuroradiologists did not perceive any difference in subjective image quality after the units’ upgrade, interventional cardiologists complained of worsened image quality. The main difference between both medical specialties is that neuroradiology concentrates on static structures (the vasculature of the brain), while interventional cardiologists have to follow structures in motion (coronary arteries).

More generally, the necessary hypotheses for the validity of classical image quality metrics based on noise properties (SNR, CNR, NPS) are no longer adequate, as has been re-stated by Verdun et al. in a 2015 review paper [Verdun 2015]. Furthermore, although theses metrics are still useful tools for detector efficiency measurement, clinically relevant image quality and dose optimisation has become very difficult since they are of little use to the end users, who use these images to accomplish certain clinical tasks, as summarised in the present literature review.

In order to circumvent these limitations, the use of mathematical model observers has become of interest to perform clinically relevant image quality assessment. Indeed, state-of-the-art clinical – not technical – image quality assessment is usually performed by defining image quality as how much the desired information can be extracted from an image or a set of images. As performed by J. Solomon et al., VGA studies, based on the response of several observers grading many images (phantom or patient) acquired with precisely known acquisition and reconstruction parameters, allow for a reliable evaluation of clinical image

quality. However, these studies are usually time-consuming, and prone to inter- and intra-observer variability, whatever the sample size.

Studies have shown that using mathematical model observers, such as the channelized Hotelling observer (CHO) [X. He and S. Park], can serve as a surrogate of the human visual system for simple binary tasks, such as signal detection in a given background. However, as will be shown later on, the complete image content analysis using these methods necessitates a tremendous amount of images in order to completely assess the imaging chain, and some preliminary steps will be necessary before grading image quality. We will now describe the overall functioning of model observers, describe the particular case of channelized model observers, and finally describe our proposed solution for fluoroscopic image quality assessment based on a clinical task, i.e., the detection of a high-contrast linear object (a coronary guidewire).

Model observer formalism

Let us summarise the model observer formalism by repeating the four cornerstones of an observer study:

- The choice of a clinically relevant diagnostic task,
- A statistically significant set of images to establish a response curve,
- An observer (human or model),
- A figure of merit (FOM) for image quality quantification.

Mathematical model observers are matrices with dimensions matching the images', as well as matching number of pixels along each dimension. Let us assume that our dataset consists of two-dimensional $n \times m$ images (defining $N = n \cdot m$), designated by $\boldsymbol{g}(x, y)$ as following:

$$\boldsymbol{g} = \boldsymbol{g}(x, y) = \begin{bmatrix} g_{1,1} & \cdots & g_{1,m} \\ \vdots & \ddots & \vdots \\ g_{n,1} & \cdots & g_{n,m} \end{bmatrix}$$

The model observer is defined as a matrix called *template*, designated by $\boldsymbol{w}$, with matching dimensions:

$$\boldsymbol{w} = \boldsymbol{w}(x, y) = \begin{bmatrix} w_{1,1} & \cdots & w_{1,m} \\ \vdots & \ddots & \vdots \\ w_{n,1} & \cdots & w_{n,m} \end{bmatrix}$$

For the sake of mathematical simplicity, both the images and the template are vectorised, i.e., all components are aligned column by column in a single vector form:

$$\boldsymbol{g} = \begin{bmatrix} g_{1,1} \\ g_{2,1} \\ \vdots \\ g_{n,1} \\ g_{2,1} \\ g_{2,2} \\ \vdots \\ g_{n,m} \end{bmatrix} \text{ and } \boldsymbol{w} = \begin{bmatrix} w_{1,1} \\ w_{2,1} \\ \vdots \\ w_{n,1} \\ w_{2,1} \\ w_{2,2} \\ \vdots \\ w_{n,m} \end{bmatrix}$$

Formally, the operation of observing the *i*-th image $\boldsymbol{g}_i$ corresponds to the multiplication of said image $\boldsymbol{g}$ with the transposed observer template $\boldsymbol{w}$:

$$\lambda_i = \boldsymbol{w}^T \boldsymbol{g}_i$$

The subsequent *i*-th λ_i is called a *decision variable* and is analogous to an in-vivo observer grading his/her certainty of perceiving a signal on the image background. Images may either contain a signal (signal-present) or no signal at all (only noise – signal-absent).

The observer template $\boldsymbol{w}$ of the Hotelling observer (HO) is the optimum linear discriminator and is mathematically defined as:

$$\boldsymbol{w}_{opt\ lin} = \boldsymbol{K}_{\boldsymbol{g}}^{-1} \Delta \overline{\boldsymbol{g}}$$

where $\boldsymbol{K}_{\boldsymbol{g}}$ is the image *covariance matrix* of the signal-absent images:

$$\boldsymbol{K}_{\boldsymbol{g}} = \begin{bmatrix} \sigma_{1,1}^2 & \cdots & \sigma_{1,m}^2 \\ \vdots & \ddots & \vdots \\ \sigma_{n,1}^2 & \cdots & \sigma_{n,m}^2 \end{bmatrix}$$

with each $\sigma_{i,j}^2$ being the variance of pixels *i* and *j*. As such, the covariance matrix is the generalisation of the variance to an arbitrary number of dimensions. The application of the covariance matrix allows for noise de-correlation (or *whitening*).

$\Delta \overline{\boldsymbol{g}}$ is defined as the mean difference between the signal-present and signal-absent images (i.e. $\langle \boldsymbol{g}_s - \boldsymbol{g}_n \rangle$), thus representative of the theoretical signal that is being looked after in a given image set.

Channelized model observers

As such, the HO is computationally very expensive, and needs a number of images that is often too large to be acquired within feasible times. Indeed, for an image $\boldsymbol{g}$ with M pixels, the size of the covariance matrix is $M \times M$. Since the application of the HO implies the inversion of the covariance matrix, this means that, in order to obtain an invertible matrix, we will need

at least M^2 images. For example, for a 256×256 image, we will need at least $65\,536$ images, which is usually impossible to obtain on an imaging system.

To reduce the problem dimensionality, the images and the template can be filtered by a given set of *J* channels $\boldsymbol{U}$, with *J* significantly lower than *N*:

$$\boldsymbol{U} = \left[\boldsymbol{u}_1, \boldsymbol{u}_2, \boldsymbol{u}_3, \dots, \boldsymbol{u}_J\right]$$

Each channel $\boldsymbol{u}_i$ has the same dimension of the images. As a consequence, the channel matrix $\boldsymbol{U}$ is a $N \times J$ matrix where each column is an individual channel. The channelization mechanism of an image consists of multiplying the image $\boldsymbol{g}_i$ by the transposed channel matrix $\boldsymbol{U}$, to obtain the channelized image $\boldsymbol{v}_i$:

$$\boldsymbol{v}_i = \begin{bmatrix} v_1 \\ v_2 \\ \vdots \\ v_J \end{bmatrix} = \boldsymbol{U}^T \boldsymbol{g}_i$$

The channels act as a compression mechanism, which selects a certain content of the image information. The channels are chosen depending on the necessary information to be extracted from the images, while eliminating the unnecessary information. As a result, the native images $\boldsymbol{g}_i$ become channelized images $\boldsymbol{v}_i$ of dimension $J \times 1$, of which each component is the results of the *j*-th transposed channel $\boldsymbol{u}_j$ multiplying the image:

$$v_j = (\boldsymbol{u}_j)^T \boldsymbol{g}_i$$

The resulting channelized Hotelling observer (CHO) template $\boldsymbol{w}_{CHO}$ becomes:

$$\boldsymbol{w}_{CHO} = (\boldsymbol{K}_{v/n})^{-1} \langle \boldsymbol{v}_s - \boldsymbol{v}_n \rangle$$

where $\boldsymbol{K}_{v/n} = \boldsymbol{U}^T \boldsymbol{K}_g \boldsymbol{U}$ is the channelized covariance matrix and $\langle \boldsymbol{v}_s - \boldsymbol{v}_n \rangle$ is the mean difference between the channelized signal-present (subscript *s* for *signal*) and signal-absent (subscript *n* for *noise*) images. As a consequence, $\boldsymbol{K}_{v/n}$ is a $J \times J$ matrix. As the current ideal number of channels J is around 10, the resulting channelized covariance matrix is much easier to invert.

The channelized decision variable for the *i*-th channelized image thus becomes:

$$\lambda_{CHO,i} = \boldsymbol{w}_{CHO} \boldsymbol{v}_i$$

The set of images used to set up the template is called the *training set* and the images used for image quality assessment is called the *testing set*.

Model observer analysis workflow

For a set of signal-present and signal-absent images acquired in a given condition, the workflow of image quality grading goes as following:

1. The appropriate set of channels $\boldsymbol{U}$ is created,
2. The CHO template is set up:
    a. The covariance matrix is calculated on the basis of the signal-absent (i.e. noise only) images, channelized using the aforementioned channel matrix, and inverted to achieve the $(\boldsymbol{K}_{v/n})^{-1}$ matrix.
    b. The signal-absent and signal-present images are channelized, and their mean difference $\langle \boldsymbol{v}_s - \boldsymbol{v}_n \rangle$ is calculated, to complete the CHO template $\boldsymbol{w}_{CHO}$,
3. For each channelized image (signal-absent or signal-present) $\boldsymbol{v}_i$, a decision variable λ_i is calculated by applying the CHO template on each individual image,
4. Two distributions are created, as can be seen in Figure 9:
    a. All decision variables corresponding to the signal-present images (red),
    b. All decision variables corresponding to the signal-absent images (blue).

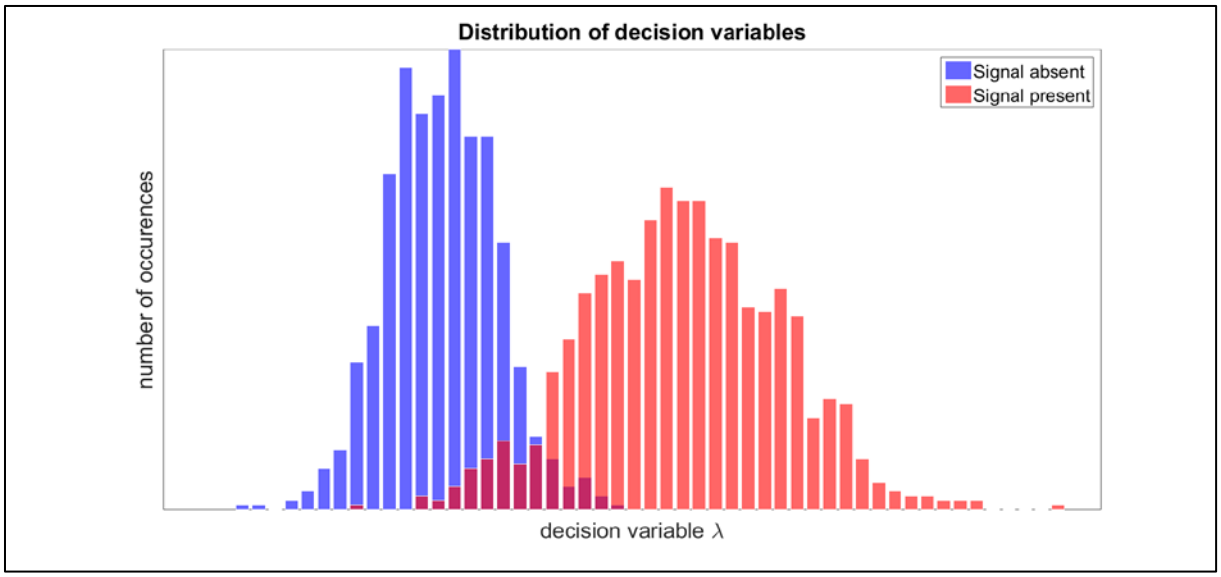

Figure 9: Example of the distributions of signal-present (red) and signal-absent (blue) decision variables for a set of channelized images.

From these distributions, the image quality can be graded using different FOM:

1. The certainty of making the difference between signal-absent and signal-present images is dependent on how much both distribution means lie apart from each other

(difference between both mean values) and how much they overlap (function of the mean difference and both standard deviations). Consequently, a first FOM is known as the signal to noise ratio SNR_λ, defined as:

$$SNR_\lambda = \frac{|\mu_s - \mu_n|}{\sqrt{\frac{1}{2}(\sigma_s^2 - \sigma_n^2)}}$$

where μ_s and μ_n are the respective mean values of the signal-present and signal-absent decision variable distributions, and σ_s and σ_n their respective standard deviations. Per definition, the signal to noise ratio varies between 0 (for the worse possible system) and ∞ (for the best possible system). Caution must be used with this FOM, especially for non-Gaussian distributions with long tails.

2. When an observer has to make a decision on whether an image is apparently containing evidence of pathology, each individual applies a decision threshold to the decision variable distributions, above which the test is deemed positive, and under which it is deemed negative. Based on this assumption, a full description of the system can be performed by establishing a receiver operating characteristic (ROC) curve. For this, an arbitrary decision threshold is "swept" across the entire distribution of both signal-absent and signal-present decision variables. For each position of the threshold, one can extract the true positive fraction (TPF, also called the *sensitivity*), as well as the true negative fraction (TNF, also called the *specificity*). For each threshold position, each $(1 - specificity, sensitivity)$ couple is drawn on a plot, on which both axes are graduated from 0 to 1, as can be seen in Figure 10 (right).

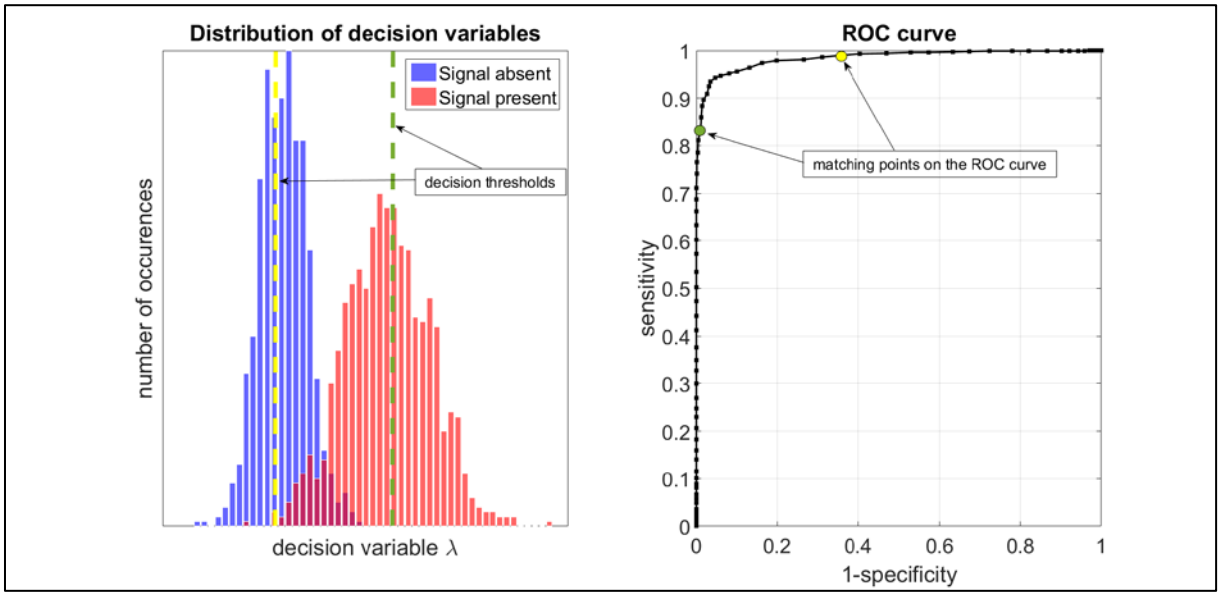

Figure 10: Schematic illustration of the calculation of a ROC curve for a binary observation strategy by "sweeping" a decision threshold across the decision variable space.

The second FOM that can be derived from this result is the area under the ROC curve (AUC). By construction of the sensitivity and specificity, the worst system is not better than randomly assigning a “lesion present” or “lesion absent” decision to each image, so every point of the ROC curve will be on the first diagonal (intersecting the origin). The consecutive AUC has a value of 0.5. On the contrary, the perfect system will have an AUC of 1.0.

3. When both signal-present and signal-absent distributions are Gaussian with equal variance, the ROC curve becomes symmetric with respect to the second diagonal. A third FOM may be derived from this particular distribution, and is called the detectability index $d' = SNR_{\lambda}$. By definition, d' will have a value of 0 for the worst system and a value of ∞ for the perfect system.

Detectability of a coronary guidewire

The choice of the clinical task and specific channel matrix depends on the underlying diagnosis. For example, focal liver lesion detection in CT imaging relies on the capability of detecting low-contrast lesions, as has been described in [Racine 2016a], [Racine 2016b] and [Ott 2016]. For these studies, the diagnostic task was the detection of a low-contrast sphere in a homogenous background; the set of images consisted of at least 40 signals of the same size and contrast for each acquisition and reconstruction protocol; the observer was the CHO with dense difference of Gaussian channels (D-DOG); and the FOM was the AUC under the ROC curve.

For this work, we decided to develop the following model:

- Clinical task: The detectability of a high contrast thin linear object with a periodic motion, i.e. a coronary guidewire;
- Image set: A series of images of a home-made phantom, which we will describe later on;
- Observer: CHO with Gabor channels;
- FOM: The SNR_{λ}.

Gabor channels G are described using the following formula:

$$G(x,y) = exp\left(-\frac{(x-x_0)^2 + (y-y_0)^2}{2\sigma^2}\right) \cdot \cos\left[2\pi f \cdot \left((x-x_0)\cdot\cos(\theta) + (y-y_0)\cdot\sin(\theta) + \beta\right)\right]$$

where x and y are the spatial coordinates, x_0 and y_0 the centre of the specific channel, θ the channel orientation, β the phase of the channel, f the selected spatial frequency and $\sigma = 0.56/f$, as described in [Favazza 2015].

When analysing the expression of a Gabor channel, we see two components: The first is the definition of a two-dimensional Gaussian curve of variance σ^2 and means x_0 and y_0; the second is a cosine function with frequency f, orientation θ, and phase β. This indicates that Gabor channels are selective to the spatial orientation and the size of the signal, making them appropriate for linear signal selection. An example of a Gabor channel is given in Figure 11.

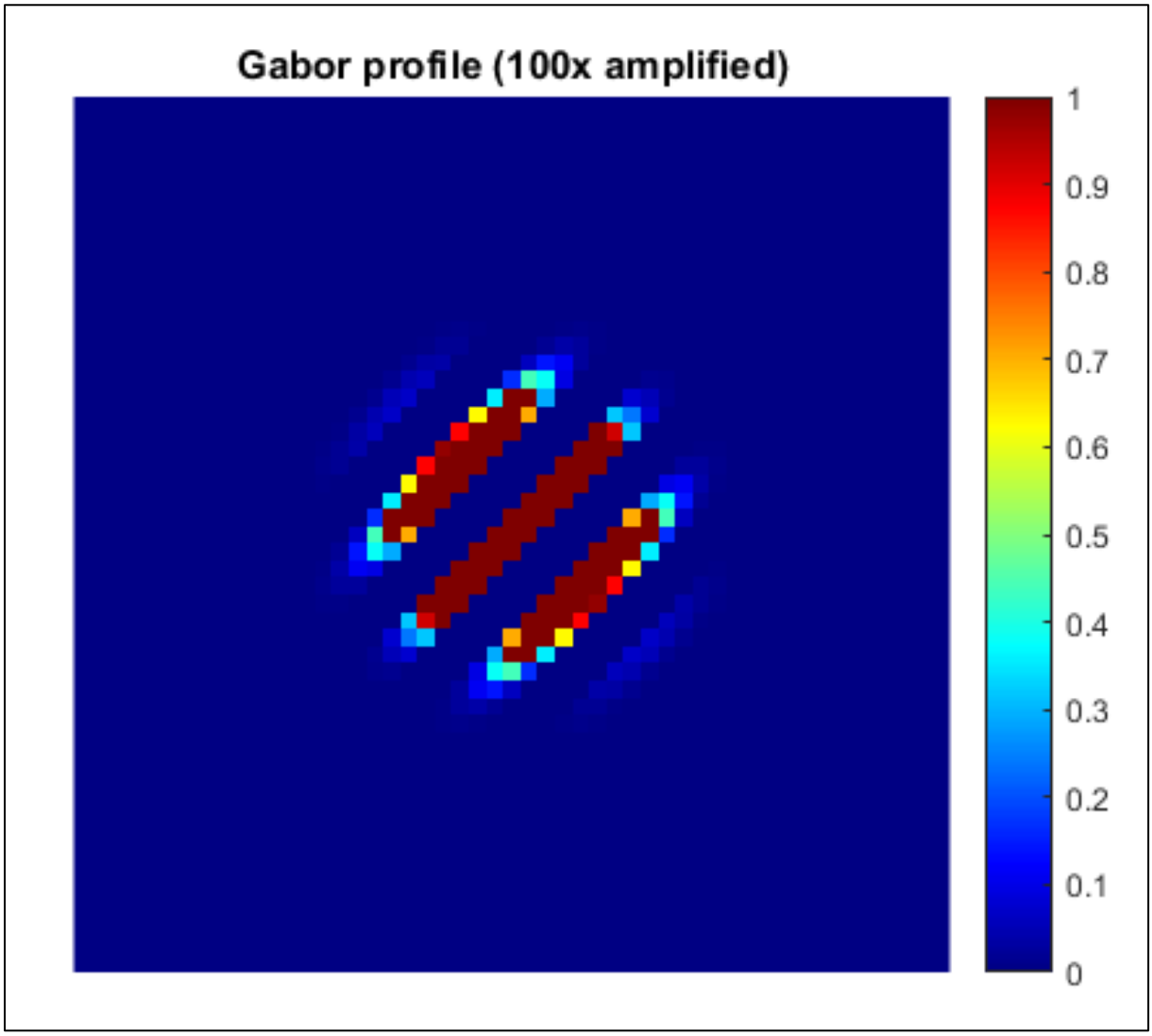

Figure 11: Example of a Gabor channel profile (100x amplified for better visualisation), with frequency 1.1 mm^{-1}, phase 0 rad and orientation $3\pi/4$ rad.

The experimental setup consists of a 3 mm thick PMMA plate (lateral dimensions 25 x 25 cm), engraved with a 1 mm deep and 1 mm wide grove with 45° edges along one of the diagonals. The grove is intended at receiving a 0.014" coronary guidewire. This metallic thread is designed to allow coronary angioplasty material (such as balloons and stents) to be guided, as though they were on a rail, to the lesion to be dilated. Symmetrically to the plate's centre, two 3 mm diameter lead cylinders of 3 mm thickness, 10 cm apart from each other,

serve as imaging fiducials, marking the position of the guidewire with absolute certainty. These fiducials will serve as a non-ambiguous target for the extraction of the regions of interest (ROI) required by the program.

The plate is placed parallel to the patient table, and the guidewire is positioned at the isocenter by tethering two magnets on both sides of the plate on its geometric middle, allowing the gantry to fully rotate around the plate, and setting the table position until the visualisation of the magnets remains in the middle of the field of view, thus indicating that the guidewire centre is at the unit's isocenter.

2.5 and 5.0 cm PMMA slabs (lateral dimensions of 30 x 30 cm) are placed above and under the guidewire holder plate, to ensure that the signal we want to acquire is in the middle of our surrogate PMMA patient. PMMA thicknesses (without the 3 mm wire holder) range from 5 to 20 cm, by steps of 5 cm. A set of LEGO blocks allow to separate the plates, so the wire holder can freely move between the PMMA slabs. The 3 mm wire holder plate is suspended to a little lever, itself attached to an electrical motor allowing the wire holder to move parallel to the table with pre-selected motion profiles (QRM-Sim2D, QRM, Germany). A photograph of the experimental setup can be seen in Figure 12.

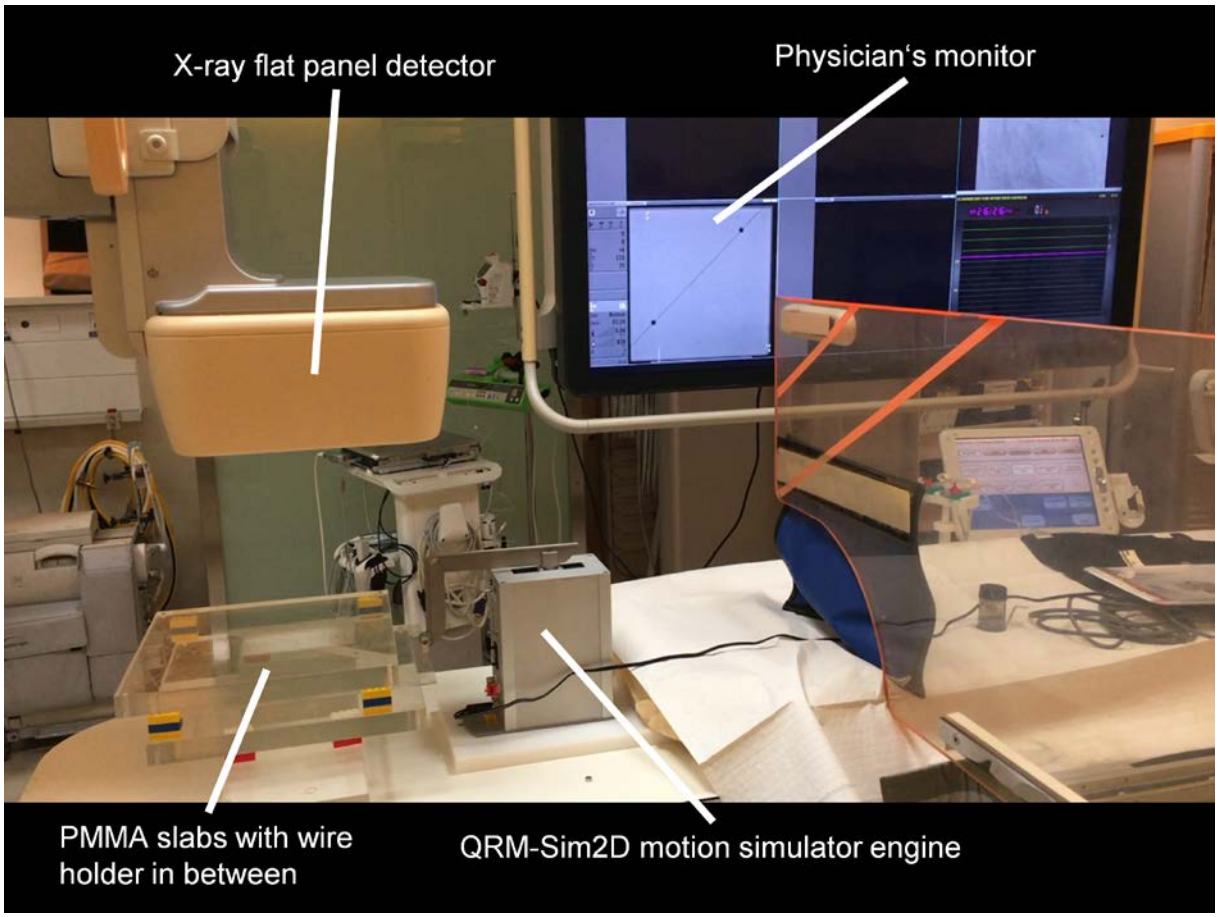

Figure 12: Photography of the experimental setup.

Using the previously described experimental setup, two series of images are acquired for each PMMA thickness and AEC setting (fluoroscopy or image acquisition):

- One series with the motor switched off: This first series will allow us to create the model template. Indeed, as mentioned previously, the AEC system adapts the dose rates by changing up to five parameters at the same time, including the focal spot size. This last parameter will have an influence on the spatial resolution of the images, thus influencing the apparent size of the signal. For this reason, the training set consists of static images, and we will hypothesise that the noise characteristics are identical between the training and the testing set;
- One series with the motor switched on: When switching on the QRM-Sim2D engine, the lever follows a back-and-forth motion based on a pre-implemented profile. We used the 75 bpm pre-recorded motion, as the writing rights on the engine did not allow us to implement a motion with both steps of one stroke defined as a uniformly rectilinear motion with known velocity.

The recorded images look like the one represented in Figure 13.

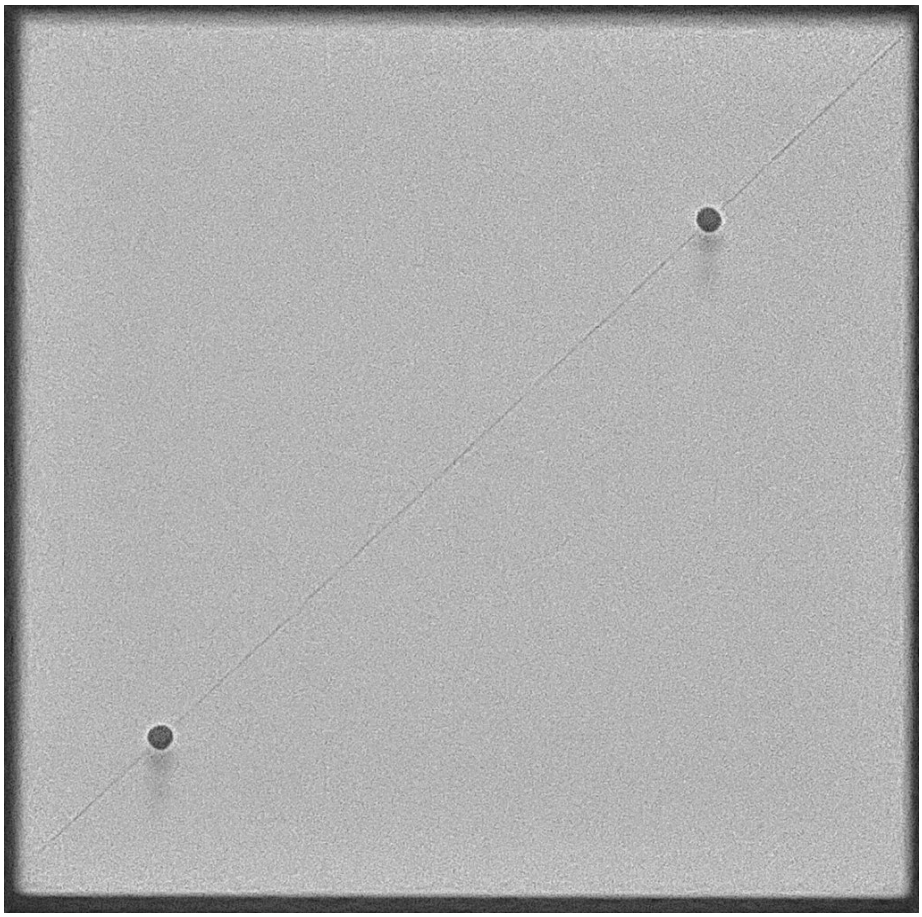

Figure 13: Example of a fluoroscopy image (20 cm PMMA, medium quality AEC setting). Note the trail left by the lead fiducials.

The first set of channels consists of four frequencies (the same as [Favazza 2015]) and two orientations ($\pi/4$ and $3\pi/4$). The phase was left at zero.

At first, the AUC was chosen as the FOM. However, it turned out that, even for the most difficult conditions (20 cm PMMA, low quality fluoroscopy), the AUC was close to 1.0, with little variation between the different conditions, as can be seen in Table 8. Furthermore, for a purely static image (no cardiac motion), the detection assessment is trivial, as a motionless high contrast target is very easy to detect, whatever the viewing conditions. The assessment of dynamic image quality is less trivial, although the system we tested our model on (Philips Allura Xper FD10 with AlluraClarity) performs well even for the theoretically most difficult conditions, because angiography units are dedicated to detecting these kinds of rectilinear signals in moving conditions.

Fluoroscopy setting	**Static conditions**		**Dynamic conditions**	
FOM	SNR_λ	AUC	SNR_λ	AUC
Low quality	5.40	0.99997	3.45	0.9931
Medium quality	6.95	1.0	4.12	0.99914
High quality	11.32	1.0	4.90	0.99919

Table 8: AUC and SNR results for static (left) and dynamic (right) acquisition conditions. We see that the AUC rapidly "saturates", rendering it useless as a FOM. But the SNR being not limited, it serves as a more pertinent FOM.

Since the AUC is no longer a pertinent FOM, we decided to use the SNR_λ as the FOM. The aim of the present model will thus be to serve as an objective quality indicator when fine-tuning the AEC system or other dose-reduction solutions, such as recursive filters, that may blur even high-contrast objects.

Conclusion

Throughout this research project, we have discussed the three main aspects of fluoroscopically-guided procedures: Patient exposure, staff exposure, and image quality.

For patient exposure optimisation for IC procedures, the data we collected in eight interventional cardiology centres using CardioReport has been analysed using the R software, and the results have allowed to establish a set of corrective factors for the P_{KA} and $K_{a,r}$, allowing a physician to compare a specific procedure – on a patient of arbitrary body habitus – to the dose that would have been delivered to a standard body-sized patient. The corresponding paper is still in the writing process, and we expect to have it submitted to a peer-review journal by the end of the third trimester. Furthermore, a literature review on the exposure of the pregnant woman during IC procedures, as well as on the current low pertinence of patient high-Z protective garments, have been performed and are currently under review for a special issue on the management of the pregnant patient in radiology in EJMP.

For staff dose, the last epidemiological studies have shown that the risks for radiation-exposed medical staff have been underestimated, especially for eye lens and brain exposure, and that there is a need for a good quantification of the exposure of these organs, that are not protected by lead aprons. Throughout this research, we have gained a better knowledge of their exposure, and the efficiencies of the protective devices that can be used to reduce scattered dose. We have seen that, nowadays, staff effective dose is no longer a concern, since technological advances have allowed or a drastic reduction for patient and subsequent staff effective doses. However, routine dosimeters should always be worn to continuously monitor medical radiation workers, as this working category remains a special topic in the management of professional health questions. The main concern now comes from eye lens and brain dose, as cumulative doses to both these organs can grow quite high over a whole career, and their radiosensitivity has been underestimated [ICRP 2011].

Finally, and this was probably the most innovative part of this research, for image quality, we have seen that there is a need for clinically-relevant image quality assessment. This may be either performed by VGA studies by several human observers, but this method is time-consuming and prone to inter- and intra-observer variability. Also, the non linearity of current image reconstruction processes has rendered previously used physical metrics (such as CNR or MTF) non applicable for objective image quality assessment. For this purpose, the use of mathematical model observers could be a solution for clinically relevant objective image quality qualification. These models are based on statistical decision theory, and can

be either used to assess a detector performance by extracting all available information from a dataset (i.e. the ideal observer), or its performance could be degraded to match that of humans (i.e. an anthropomorphic observer) to assess local acquisition and reconstruction protocols. Model observers necessitate the clear definition of four cornerstones:

- A clinical task,
- A statistically relevant set of images,
- An observer (ideal or anthropomorphic),
- A figure of merit (FOM).

For this purpose, we decided to qualify the detectability (binary detection task) of high-contrast thin linear objects (i.e. a coronary guidewire) in moving imaging conditions using an anthropomorphic channelized Hotelling observer (CHO). The test object we designed is a thin PMMA wire support plate, set in motion by a dedicated electrical motor applying a motion pattern similar to the heart strokes in a patient. The acquired images consist of a set of regions of interest (ROI) of the guidewire (signal-present images) and ROI of only noise in a homogenous background (signal-absent images). The application of the HO consists of multiplying the acquired images by a template, that consists of the average difference between both signal-present and signal-absent images and the covariance matrix of the signal-absent images for noise de-correlation. Since the calculation of the covariance necessitates a very large amount of images, and the inversion of large matrices being computationally expensive, we applied a set of Gabor channels to the template and the images, so as to extract the useful image information and to reduce the problem's dimensionality. Gabor channels are fit for this imaging purpose, as they are sensitive to the orientation and size of the signal. A fine tuning of the number and parameters of the channels remains to be done in order to make the model more anthropomorphic, but we have already seen that the relative responses for different image qualities (low, medium and high fluoroscopy) and static vs. dynamic imaging conditions show the right trend. The FOM we decided to use is the signal-to-noise ration SNR_{λ} of the decision variables' distributions, as the area under the ROC curve (AUC) quickly reaches its maximal value of 1.0 without bringing any extra information on image quality.

Perspectives

As we have seen, all three aspects we covered (patient dose, staff exposure, and image quality) are all intrinsically linked, as is schematically depicted in Figure 14. Indeed, changing one of the three summits of the represented schematic triangle often impacts the two remaining aspects. For example, reducing staff dose by increasing the detector sensitivity may alter the subsequent image quality, increasing the risk of under-diagnosing or missing a lesion. To continue the optimisation steps opened by this research, we propose several research themes in the field of fluoroscopically-guided procedures. But first, we would like to propose a paradigm shift. Indeed, until now, dose optimisation relied on the collection and analysis of patient doses, and practice optimisation using trial and error, with the physician's opinion as FOM for image quality assessment. However, we propose to place image quality as the beginning step of clinical practice optimisation, and adapt patient exposure – and subsequent staff exposure – in adequacy to a precisely defined clinical task. The first step of this process will consist on the actual definition of the respective tasks for the different medical specialties.

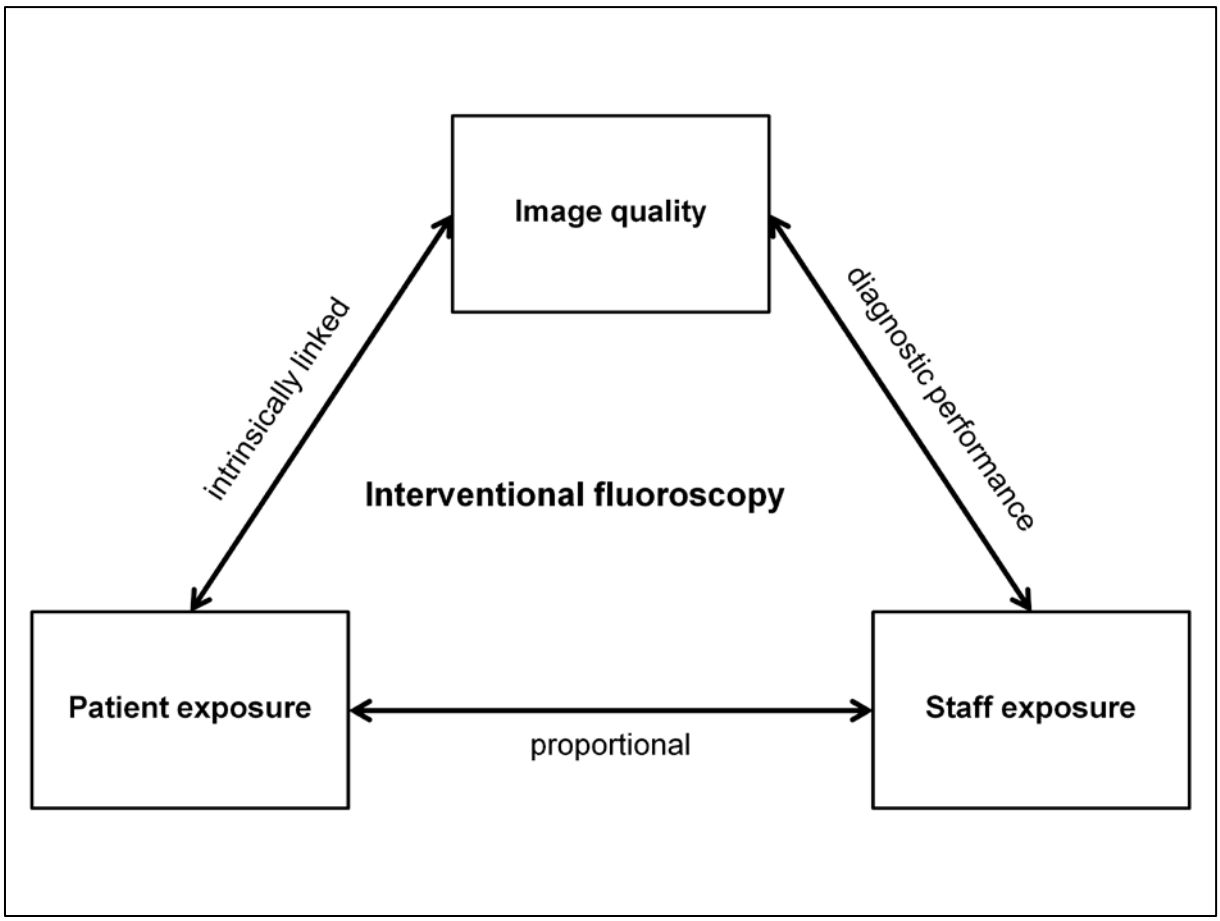

Figure 14: Schematic representation of the three-pronged problematic of fluoroscopic imaging.

By the end of 2013, automatic dose collection software (DoseWatch, GE Healthcare) was installed at our hospital, as in many other centres. It performs a direct query on the devices linked to the system, and extracts many technical and clinical parameters from the Radiation Dose Structured Report (RDSR), an object recently introduced in the DICOM standard, that records all technical parameters for every irradiation sequence. The software was configured to collect all dose indicators for the five CT and seven angiography units from CHUV. Of these seven angiography units, three are dedicated to interventional cardiology (one single-plane and one dual-plane room), three to interventional radiology (same configuration), and one is used in the operation theatre, mainly for vascular surgery procedures. Although convenient, these software solutions usually perform their statistical classification based on the local protocol name, and our local solution is unfortunately highly sensitive to the actual spelling of the protocol name. For CT imaging, this implies that the current number of "different" protocols listed in our database is equal to 148, although a multi-disciplinary task force, consisting of radiologists, technologists and physicists decided on a 46 entry list for protocol nomenclature. As such, much valuable information is potentially diluted in useless entries.

For interventional radiology and cardiology, the problem is more subtle. Indeed, although it would be difficult, the task of converging to a similar protocol description nomenclature is theoretically feasible. However, many examinations starting as a diagnostic procedure (e.g. a CA) may be immediately followed by a therapeutic procedure (e.g. a PTCA, when a coronary stenosis has been diagnosed). Since standalone therapeutic procedures are quite rare, many therapeutic procedures will thus be recorded as diagnostic procedures, with which they usually start. This may be problematic for establishing RLs, as the information on the actual procedure is lost. Overall, software aiming at only collecting patient doses rather than the whole procedural informational contents is at high risk of losing valuable information. In opposition to this, a dedicated global structured reporting and billing solution such as CardioReport is much less prone to miss-classification of procedures. One research perspective could consist on finding a better procedure classification algorithm, based not only on the entries on the respective radiological units, but also procedural data such as the treatment used or a special diagnostic tool that was used for a specific medical indication. The establishment of IC RLs for the FOPH was possible since the habit in the field of IC is a thorough open reporting of the procedures performed in Switzerland. An illustrative example of this paradigm is the AMIS Plus initiative, which is a national registry of acute myocardial infarction in Switzerland (http://www.amis-plus.ch/). Other fields using fluoroscopy as a diagnostic and therapeutic tool, such as interventional radiology or vascular surgery, could benefit from a more pragmatic and structured practice reporting. Only a correct classification

of the procedures will allow for a pertinent setup of the respective imaging tasks that will serve as the starting point for practice optimisation.

On the subject of patient dose and risk estimation, the P_{KA}, although derived from air kerma, does not benefit from a primary metrology standard, and is therefore subject to large error margins. For example, in Swiss law, the tolerated error margin for the measurement of P_{KA} is of ±30 %. This implies that two examinations performed on two separate units, although physically delivering the same dose to two patients, may display doses showing up to 60 % difference. For this purpose, the AAPM task group 190 has issued a report on the accuracy of P_{KA} and $K_{a,r}$ evaluation, precisely describing a measurement methodology to verify the accuracy of both dose indicators [AAPM 2015]. For $K_{a,r}$ measurement, this method relies on the punctual measurement of air kerma at the isocenter, and correcting it by the inverse square of the distance for the IRP. It also discusses the sources and estimation methods for the uncertainties. As for the P_{KA}, the measured $K_{a,r}$ is multiplied by the exposed surface, measured using an object of known dimensions at the same location, such as a metallic grid or a radio-opaque ruler. However straightforward, this method does not take into account the correction for beam filtration – especially when using solid-state chambers – or the heel effect of the anode, since the kerma is only measured at the field centre. Some large ionisation chambers, or arrays of diodes (like the electronic portal imaging device (EPID) for megavolt (MV) imaging in radiotherapy gantries) do exist for direct P_{KA} measurement, but they do not benefit from a metrological attachment, at least not in Switzerland. We are convinced that, if P_{KA} measurements were traceable back to the French Bureau International des Poids et Mesures (BIPM), both patient stochastic and deterministic risks could be better estimated on the basis of the values measured and displayed by the fluoroscopy units.

For staff exposure, as routine effective dose monitoring has shown to be efficient, the physical measurement of eye lens dose, rather than the correction of the usual dosimetry worn at the chest level, would probably be the best solution to assess the risk of developing radiation-induced cataract. This dosimeter could also be used, provided good correction factors, to estimate brain dose. However, no dose indicator is yet sufficiently well-defined for the measurement of eye lens dose. Indeed, routine chest dosimeters are usually calibrated on the basis of depth dose (i.e. the absorbed dose under 10 mm of soft tissue – Hp(10)) surface dose (i.e. the absorbed dose under 0.07 mm of soft tissue – Hp(0.07)). A proposed intermediate calibration (Hp(3)) is probably the best compromise, and is currently being tested by the French IRSN (Dosiris).

To sum up, perhaps the most challenging task for the medical physicist is the understanding of the needs of the different fluoroscopy units' users (in terms of diagnostic quality and

availability of protective devices), while assuring and maintaining a proper education of the workers involved in interventional procedures. For this purpose, the combined use of electronic dosimetry during actual clinical procedures, along with the fine-tuning of image quality using clinically relevant model observers, will benefit the entire medical team. It would allow the physicians to express and define their respective diagnostic needs and how to quantify their outcome on a diagnostic image, as well as to optimise staff exposure by actively defining the proper radiation protection measures to be implemented at a local or institutional level, with respect to the needed image quality – and subsequent exposure. Furthermore, as patient dose benefits from a legal framework (local or national RLs), so may image quality, if an objective measurement standard were introduced along the average patient exposure for a given procedure. The final aim is to set up a metrological attachment of the model observer measurement method, as is the case for most of the dose measurements, be it routine monitoring or device dose indicators. The centre of gravity of practice optimisation will have to be shifted from dose optimisation to objective image quality assessment.

References

[AAPM 2012] Functionality and Operation of Fluoroscopic Automatic Brightness Control/Automatic Dose Rate Control Logic in Modern Cardiovascular and Interventional Angiography Systems: A Report of AAPM Task Group 125 Radiography/Fluoroscopy Subcommittee, Imaging Physics Committee, Science Council, June 2012.

[AAPM 2015] Accuracy and calibration of integrated radiation output indicators in diagnostic radiology: A report of the AAPM Imaging Physics Committee Task Group 190, P. J. Lin, B. A. Schueler, S. Balter, K. J. Strauss, K. A. Wunderle, M. T. LaFrance, D. S. Kim, R. H. Behrman, S. J. Shepard, I. H. Bercha, Med Phys. 2015 Dec;42(12):6815-29.

[Balter 2010] Fluoroscopically guided interventional procedures: a review of radiation effects on patients' skin and hair, S. Balter, J. W. Hopewell, D. L. Miller, L. K. Wagner, M. J. Zelefsky, Radiology. 2010 Feb; 254(2):326-41.

[Barrett 1993] Model observers for assessment of image quality, H. H. Barrett, J. Yao, J. P. Rolland, K. J. Myers, Proc Natl Acad Sci U S A. 1993 Nov 1; 90(21): 9758–9765.

[Barrett 2004] Foundations of Image Science, H. H. Barrett, K. J. Myers, Wiley, Hoboken, NJ, 2004.

[Bordoli 2014] Radiation safety education in vascular surgery training, S. J. Bordoli, C. G. Carsten III, D. L. Cull, B. L. Johnson, S. M. Taylor, J Vasc Surg 59 (2014), pp. 860 – 864.e1.

[Chapple 1995] A phantom based method for deriving typical patient doses from measurements of dose-area product on populations of patients, C. L. Chapple, D. A. Broadhead, K. Faulkner, Br J Radiol 68:1083-1086 (1995).

[Ciraj-Bjelac 2010] Risk for Radiation-Induced Cataract for Staff in Interventional Cardiology: Is There Reason for Concern?, O. Ciraj-Bjelac, M. M. Rehani, K. H. Sim, H. B. Liew, E. Vaño, N. J. Kleiman, Catheterization and Cardiovascular Interventions, 2010, 76(6), pp. 826 – 834.

[Coeytaux 2015] Reported Radiation Overexposure Accidents Worldwide, 1980- 2013: A Systematic Review, K. Coeytaux, E. Bey, D. Christensen, E. S. Glassman, B. Murdock, C. Doucet, (2015). Plops ONE 10(3): e0118709. doi:10.1371/journal.pone.0118709

[DIN 2013] DIN 6868-150 (2013-06): Image Quality Assurance In Diagnostic X-ray Departments - Part 150: Rv Acceptance Test Of Medical Radiographic And Fluoroscopic X-ray Equipment, German Institute for Standardisation (Deutsches Institut für Normung).

[Favazza 2015] Implementation of a channelized Hotelling observer model to assess image quality of x-ray angiography systems. C. P. Favazza, K. A. Fetterly, N. J. Hangiandreou, S. Leng, B. Schueler. J. Med. Imaging. 2015 Jan; 2(1).

[FDA 2016] FDA regulation on X-ray devices, accessed online on 19.04.2017, https://www.accessdata.fda.gov/scripts/cdrh/cfdocs/cfcfr/CFRSearch.cfm?FR=1020.30

[FOPH 2016] Rapport annuel 2015 : Dosimétrie des personnes exposées aux radiations dans l'exercice de leur profession en Suisse, Office Fédéral de la Santé Publique (OFSP), Division radioprotection, July 2016.

[Fryback 1991] The efficacy of diagnostic imaging, D. G. Fryback, J. R. Thornbury, Med Decis Making. 1991 Apr-Jun; 11(2):88-94.

[IEC 2010] International Electrotechnical Commission. Medical electrical equipment - Part 2-43: Particular requirements for the basic safety and essential performance of X-ray equipment for interventional procedures. Publication IEC 60601-2-43. Geneva.

[ICRP 1990] ICRP, 1991. 1990 Recommendations of the International Commission on Radiological Protection. ICRP Publication 60. Ann. ICRP 21 (1-3).

[ICRP 2010] Radiological Protection in Fluoroscopically Guided Procedures outside the Imaging Department, ICRP Publication 117, M. M. Rehani, O. Ciraj-Bjelac, E. Vaño, D. L. Miller, S. Walsh, B.D. Giordano, J. Persliden Ann. ICRP 40(6), 2010.

[ICRP 2011] Statement on Tissue Reactions. ICRP ref 4825-3093-1464.

[ICRU 2005] International Commission on Radiation Units and Measurements – Patient Dosimetry for X rays used in medical imaging, Report 74, J. ICRU, 2005, 5(2), University Press Oxford.

[Image Wisely 2016] http://www.imagewisely.org/imaging-modalities/computed-tomography/imaging-physicians/articles/adaptive-iterative-reconstruction-in-ct

[Jones 2011] Calculating the peak skin dose resulting from fluoroscopically guided interventions. Part I: Methods, A. K. Jones, A. S. Pasciak. Journal of Applied Clinical Medical Physics, Vol. 12(4).

[Marshall 1992] An investigation into the effect of protective devices on the dose to radiosensitive organs in the head and neck, N. W. Marshall, K. Faulkner, P. Clarke, Br J Radiol. 1992 Sep; 65(777):799-802.

[Marshall 2000] Reference levels in interventional radiology, N. W. Marshall, C. L. Chapple, C. J. Kotre, Phys Med Biol 45:3833-3846 (2000).

[Martin 2016] Eye lens dosimetry for fluoroscopically guided clinical procedures: Practical approaches to protection and dose monitoring, C. J. Martin, Radiat Prot Dosimetry. 2016 Jun; 169(1-4):286-91.9.

[NCRP 2010] National Council on Radiation Protection and Measurements (NCRP) Report No. 168 - Radiation Dose Management for Fluoroscopically-Guided Interventional Medical Procedures (2010)

[Parikh 2017] Potential Radiation-Related Effects on Radiologists, J. R. Parikh, R. A. Geise, E. I. Bluth, C. E. Bender, G. Sze, A. K. Jones, Human Resources Commission of the American College of Radiology, AJR Am J Roentgenol. 2017 Mar; 208(3):595-602.

[Pauchard 2017] Iterative Reconstructions in Reduced-Dose CT: Which Type Ensures Diagnostic Image Quality in Young Oncology Patients? B. Pauchard, K. Higashigaito, A. Lamri-Senouci, J.-F. Knebel, D. Berthold, F. R. Verdun, H. Alkadhi, S. Schmidt, Acad Radiol. 2017 Mar 29.

[Radovanovic 2012] Temporal trends in treatment of ST-elevation myocardial infarction among men and women in Switzerland between 1997 and 2011, D. Radovanovic, B. K. Nallamothu, B. Seifert, O. Bertel, F. Eberli, P. Urban, G. Pedrazzini, H. Rickli, J.-C. Stauffer, S. Windecker, P. Erne. European Heart Journal: Acute Cardiovascular Care 1(3) 183-191.

[Rehani 2015] Looking into future: Challenges in radiation protection in medicine, M. M. Rehani, Radiation Protection Dosimetry (2015), Vol. 165, No. 1–4, pp. 3–6.

[Roguin 2013a] Brain and neck tumors among physicians performing interventional procedures, A. Roguin, J. Goldstein, O. Bar, J. A. Goldstein, Am J Cardiol. 2013 May 1; 111(9): pp. 1368 – 1372.

[Roguin 2013b] Brain tumours among interventional cardiologists: a cause for alarm? Report of four new cases from two cities and a review of the literature, A. Roguin, J. Goldstein, O. Bar, EuroIntervention, 2013, 7, pp. 1081 – 1086.

[Schueler 2006] An Investigation of Operator Exposure in Interventional Radiology. B. A. Schueler, T. J. Vrieze, H. Bjarnason, A. W. Stanson. Radiographics 26: 1533-1541.

[Solomon 2017] Effect of Radiation Dose Reduction and Reconstruction Algorithm on Image Noise, Contrast, Resolution, and Detectability of Subtle Hypoattenuating Liver Lesions at Multidetector CT: Filtered Back Projection versus a Commercial Model–based Iterative Reconstruction Algorithm, J. Solomon, D. Marin, K. R. Choudhury, B. Patel, E. Samei, Radiology. 2017 Feb 7:161736.

[Stecker 2009] Guidelines for patient radiation dose management, M. S. Stecker, S. Balter, R. B. Towbin, D. L. Miller, E. Vañó, G. Bartal, J. F. Angle, C. P. Chao, A. M. Cohen, R. G. Dixon, K. Gross, G. G. Hartnell, B. Schueler, J. D. Statler, T. de Baère, J. F. Cardella, SIR Safety and Health Committee, CIRSE Standards of Practice Committee, J Vasc Interv Radiol. 2009 Jul; 20(7 Suppl):S263-73.

[Struelens 2009] DAP to effective dose conversion in cardiology and vascular/interventional radiology, L. Struelens. F. Vanhavere. K. Bacher. H. Thierens, FANC/SCK/UGent, 2009.

[Tapiovaara 2003] Objective measurement of image quality in fluoroscopic X-ray equipment: FluoroQuality, M. Tapiovaara, STUK-A196 / May 2003.

[Vanhavere 2012] ORAMED: Optimization of Radiation Protection of Medical Staff, F. Vanhavere, E. Carinou, G. Gualdrini, I. Clairand, M. Sans-Merce, M. Ginjaume, D. Nikodemova, J. Jankowski, J.-M. Bordy, A. Rimpler, S. Wach, P. Martin, L. Struelens, S. Krim, C. Koukorava, P. Ferrari, F. Mariotti, E. Fantuzzi, L. Donadille, C. Itié, N. Ruiz, A. Carnicer, M. Fulop, J. Domienik, M. Brodecki, J. Daures, I. Barth, P. Bilski, EURADOS Report 2012-02, Braunschweig, April 2012.

[Vaño 2009] Importance of Dose Settings in the X-Ray Systems Used for Interventional Radiology: A National Survey. E. Vaño, R. Sanchez, J. M. Fernandez, F. Rosales, M. A. Garcia, J. Sotil, J. Hernandez, F. Carrera, J. Ciudad, M. M. Soler, T. Ballester. J. Cardivasc. Interv. Radiol. 2009; 32:121–126.

[Verdun 2015] Image quality in CT: From physical measurements to model observers, F. R. Verdun, D. Racine, J. G. Ott, M. J. Tapiovaara, P. Toroi, F. O. Bochud, W. J. H. Veldkamp, A. Schegerer, R. W. Bouwman, I. Hernandez Giron, N. W. Marshall, S. Edyvean, Physica Medica 31 (2015) 823–843.

Articles

[Ryckx 2014] Medical physicists' implication in radiological diagnostic procedures: results after 1 y of experience, N. Ryckx, S. Gnesin, R. Meuli, C. Elandoy, F. R. Verdun, Radiat Prot Dosimetry. 2015 Apr; 164(1-2):120 – 125.

[Ryckx 2015] System upgrade on Philips Allura FD20 angiography systems: Effects on patient skin dose and static image quality, N. Ryckx, M. Sans-Merce, R. Meuli, J.-B. Zerlauth, F. R. Verdun, Radiat Prot Dosimetry. 2016 Jun; 169(1-4): pp. 313 - 318.

[Ryckx 2016] Patient dose assessment after interventional cardiology procedures: A multi-centric approach to trigger optimisation, N. Ryckx, J.-J. Goy, J.-C. Stauffer, F. R. Verdun, Radiat Prot Dosimetry. 2016 Jun; 169(1-4): pp. 249 - 252.

[Ryckx 2017] The use of out-of-plane high Z patient shielding for foetal dose reduction in computed tomography: Literature review and comparison with Monte-Carlo simulations of an alternative optimisation technique, N. Ryckx, M. Sans-Merce, S. Schmidt, P.-A. Poletti, F. R. Verdun, EJMP (under review).

[Bolomey 2016] Irradiation du personnel en neuroradiologie interventionnelle pédiatrique : focus sur le cristallin de l'opérateur, C. Bolomey, G. Fasel, N. Ryckx, R. Le Coultre, Radioprotection 51(3), pp. 163 – 170 (2016). (and its erratum).

[Kallinikou 2016] Radiation Exposure of the Operator During Coronary Interventions (from the RADIO Study), Z. Kallinikou, S. G. Puricel, N. Ryckx, M. Togni, G. Baeriswyl, J.-C. Stauffer, S. Cook, F. R. Verdun, J.-J. Goy, Am J Cardiol. 2016 Jul 15; 118(2): pp. 188 – 194.

[Kallinikou 2017] Coronary angiography and percutaneous intervention during pregnancy: What practical measures can be taken by interventional cardiologists?, Z. Kallinikou, N. Ryckx, F. R. Verdun, J.-C. Stauffer, J.-J. Goy, EJMP (under review).

[Moriña 2016] InterCardioRisk: a novel online tool for estimating doses of ionising radiation to occupationally-exposed medical staff and their associated health risks, D. Moriña, J. Grellier, A. Carnicer, E. Pernot, N. Ryckx, E. Cardis, J Radiol Prot. 2016 Sep;36(3): pp. 561 - 578.

[Ott 2016] Patient exposure optimisation through task-based assessment of a new model-based iterative reconstruction technique, J. G. Ott, A. Ba, D. Racine, N. Ryckx, F. O. Bochud, H. Alkadhi, F. R. Verdun, Radiation Protection Dosimetry (2016), Vol. 169, No. 1–4, pp. 68–72.

[Racine 2016a] Benchmarking of CT for patient exposure optimisation, D. Racine, N. Ryckx, A. Ba, J. G. Ott, F. O. Bochud, F. R. Verdun, Radiat Prot Dosimetry. 2016 Jun; 169(1-4): pp. 78-83.

[Racine 2016b] Objective task-based assessment of low-contrast detectability in iterative reconstruction, D. Racine, J. G. Ott, A. Ba, N. Ryckx, F. O. Bochud, F. R. Verdun, Radiation Protection Dosimetry (2016), Vol. 169, No. 1–4, pp. 73–77.

Radiation Protection Dosimetry (2014), pp. 1–6 doi:10.1093/rpd/ncu356

MEDICAL PHYSICISTS' IMPLICATION IN RADIOLOGICAL DIAGNOSTIC PROCEDURES: RESULTS AFTER 1 Y OF EXPERIENCE

Nick Ryckx*, Silvano Gnesin, Reto Meuli, Christel Elandoy and Francis R. Verdun
Institute of Radiation Physics, Lausanne University Hospital, Rue du Grand-Pré 1, Lausanne CH-1007, Switzerland

*Corresponding author: nick.ryckx@chuv.ch

Since January 2008—*de facto* 2012—medical physics experts (MPEs) are, by law, to be involved in the optimisation process of radiological diagnostic procedures in Switzerland. Computed tomography, fluoroscopy and nuclear medicine imaging units have been assessed for patient exposure and image quality. Large spreads in clinical practice have been observed. For example, the number of scans per abdominal CT examination went from 1 to 9. Fluoroscopy units showed, for the same device settings, dose rate variations up to a factor of 3 to 7. Quantitative image quality for positron emission tomography (PET)/CT examinations varied significantly depending on the local image reconstruction algorithms. Future work will be focused on promoting team co-operation between MPEs, radiologists and radiographers and on implementing task-oriented objective image quality indicators.

In 1997, the European Council Directive 97/43/EURATOM introduced the implication of medical physics experts (MPEs) in the optimisation process of radiological diagnostic procedures. That recommendation has been translated into the Swiss Radiological Protection Ordinance (RO[(1)]) and applied officially in 2008, *de facto* in 2012. This contribution summarises the application methodology, as well as the results, after 1 y of experience. (NB: The Radiological Protection Ordinance is usually abbreviated using RPO, but RO will be used in this text to avoid any confusion with 'Radiation Protection Officer'.)

INTRODUCTION

In Switzerland, the Federal Office of Public Health (FOPH) legally authorises the manufacturer for performing quality control tests of their radiological devices. The minimal frequency, as well as the contents of those periodical controls, is set by the FOPH.

The manufacturer ensures that the device runs in accordance with the norms and criteria established by the International Electrotechnical Commission (IEC) standards. As a consequence, until now, the tasks of the manufacturer were completely separated from those of the users (physicians and radiographers).

In addition to these tests, the FOPH audits the different radiological centres on a regular basis, in order to ensure compliance with the national and international safety and quality standards.

Until now, no MPE was involved in the optimisation process in diagnostic and therapeutic radiological procedures. As such, the manufacturer is judge and jury of the implemented clinical protocols. The authors' aim is to provide objective image quality assessment tools in order to use the devices to their full potential in dose optimisation while remaining clinically relevant. As such:

- The manufacturer will continue to maintain the technical integrity of the device, ensuring the link between detector dose and image quality.
- The radiation protection expert is in charge of the operational safety of the staff using the device.
- The MPE, in close collaboration with the physicians and radiographers, will make sure that the device is being properly used on patients, ensuring the link between patient dose and image quality (or, more specifically, diagnostic quality).

In opposition to several countries where MPEs are already in place, a lot had to be done to rethink the role of the MPE. The MPEs' work had to yield added value to the clinical practice without substituting the manufacturer for the periodical technical controls.

The major part of the authors' effort was put in the field of computed tomography (CT), since it is the most common diagnostic device in the vast majority of private and public radiology practices. Furthermore, the radiation protection requirements in interventional radiology and nuclear medicine (NM) being more obvious, the involvement of an MPE was much easier in these fields.

OBJECTIVES AND METHODOLOGY

The authors will now describe the approach used for the implementation of Article 74, Paragraph 7, of the RO. The description, as well as the rest of this contribution, will be separated into three imaging fields: CT, fluoroscopy and NM.

A common objective for those three fields was to make an inventory of the different devices and

technologies used by the centres in the authors' database, as well as gaining acceptance within the different radiology institutes.

Computed tomography

The approach used for CT was focused on three axes:

- verification of the main dose indicators, since they are used as the primary tools for protocol optimisation,
- benchmarking of the institutions' image quality using a pre-defined acquisition and reconstruction protocol on a QA phantom,
- dosimetry assessment of the clinical use of the devices.

Machine output

First: control of the main output parameters of the device itself:

- volumetric computed tomography dose index ($CTDI_{vol}$), using a standard IEC 16-cm-diameter head phantom and a 100-mm pencil ion chamber (Radcal Corporation, Monrovia, California),
- beam collimation and penumbra, using self-developing Gafchromic XR-CT strips,
- Hounsfield unit (HU) calibration in water at the available X-ray tube voltages,
- laser alignment using a Catphan® 600 aligned on the lasers, later on compared with the projection image (topogram).

Local abdomen protocol qualification and unit benchmarking for a given $CTDI_{vol}$ condition

Second: qualification of the local abdomen acquisition and image reconstruction protocols using a standard QA phantom (Catphan® 600, The Phantom Laboratory, Salem, New York). Furthermore, a standard acquisition and reconstruction protocol was elaborated in order to enable device benchmarking. Standard test parameters were as follows:

- $CTDI_{vol}$ of 15 mGy, corresponding to the Swiss diagnostic reference level (DRL) for an abdominal examination,
- gantry rotation time of 1 s,
- reconstructed slice thickness of 2.5 mm (or 2 mm, depending on the CT manufacturer and/or software version), with contiguous slices,
- standard (soft tissue) reconstruction kernel,
- filtered back-projection, no iterative reconstruction,
- field of view (FOV) of 220 mm.

As body examinations yield the largest effective doses[2] with the largest spread in clinical practice[3], one of the critical aspects in diagnosis is the low-contrast detectability (LCD). This depends strongly on the used dose, the reconstruction convolution kernel, the slice thickness and the detector performance. The three first parameters being equal, the latter could be benchmarked. For this purpose, three observers have looked at the images on a diagnostic screen and estimated subjectively the diameter of the smallest rod they could distinguish for a given contrast.

Clinical use of the device

Third: dosimetry analysis of a sample of clinical examinations sent by the different institutions. The requested examinations concerned standard head, chest, abdomen, paediatric, upper- and lower-limb and cardiac acquisitions. The analysed parameters were as follows:

- $CTDI_{vol}$ per scan,
- cumulated dose–length product (DLP), as well as DLP per scan,
- examination effective dose E[2],
- number of scans per examination,
- measurement of the antero–posterior and lateral (LAT) patient dimensions, to calculate the size-specific dose estimate[4],
- used slice thicknesses,
- noise in a homogeneous zone for a given slice thickness,
- assessment of the use of the automatic exposure control system,
- positioning of the patient in the gantry,
- visibility check of a given list of organs by review of the diagnostic images by an experienced radiographer.

Fluoroscopy

Fluoroscopy units were characterised using the locally implemented clinical parameters. The characterisation was done using PMMA slabs of different thicknesses, thus simulating patients of different sizes (Figure 1). Dose rates measured in different sites and units were collected and compared.

Since the dose rates of different units can differ significantly[5], the aim was to provide the users of the unit with a framework that showed the orders of magnitude of their patients' exposure by their most commonly used clinical protocols.

No image quality measurements were performed. However, clinical image quality requirements were apparently satisfied for all systems since physicians use those units without any preference.

Nuclear medicine

Quantitative imaging is of prime importance in NM. Indeed, the estimation of the volumetric activity in a lesion will yield precious information about its metabolism and will influence the subsequent clinical decisions. This is why these aspects have to be assessed correctly.

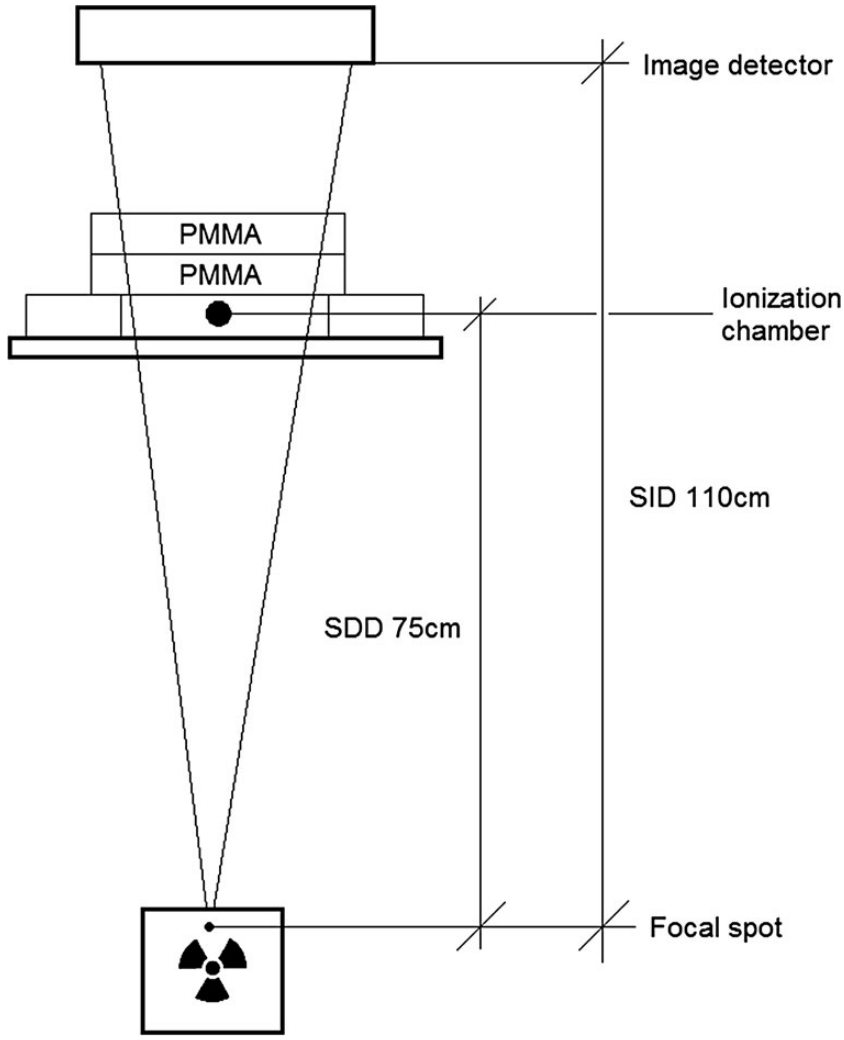

Figure 1. Schematic figure of the fluoroscopy characterisation geometry: PMMA in the primary beam, ion chamber at the entrance point of the beam. Source-to-imaging device distance (SID): 110 cm, source-to-detector distance (SDD): 75 cm.

Single photon emission computed tomography

For single photon emission computed tomography (SPECT), the use of the Jaszczak (Deluxe) phantom for overall system performance assessment is recommended by the European Association of Nuclear Medicine (EANM)[6], but also by the American Association of Physicists in Medicine (AAPM) and the American College of Radiology.

In this protocol, the phantom was filled with 400 MBq of ^{99m}Tc. Uniformity of the reconstructed slices, cold sphere contrast and spatial resolution based on the visualisation of cold rods were evaluated. The presence of macroscopic artefacts was also checked by visual inspection of the reconstructed images.

Positron emission tomography

For quantitative PET performance assessment, the EANM promoted EARL protocol (http://earl.eanm.org/cms/website.php?id=/en/projects/fdg_pet_ct_accreditation.htm) was adopted as a reference. This protocol is based on a PET/CT acquisition of the NEMA-IEC body phantom filled with an ^{18}F-FDG activity concentration ratio of 10 : 1 between the hot spheres and the background, respectively. However, differently from the EARL protocol, the two largest

spheres were filled with plain water (no activity) to test cold contrast and, indirectly, the performance of scatter and attenuation corrections.

CT use in NM and feedback

Since there are currently no DRLs for the CT units used in SPECT/CT and PET/CT, the use of CT has to be evaluated in the scope of the different imaging purposes. Indeed, the dose requirements are not the same for a diagnostic scan than for the creation of a correction attenuation map. Furthermore, the technology employed in NM can differ from state of the art radiologic CT (e.g. cone-beam CT or a pseudo-CT with common gantry with the cameras). Therefore, CT imaging in NM examinations has to be correctly assessed based on the specific tasks to be accomplished.

For both imaging modalities (SPECT/CT and PET/CT), the local acquisition protocols were tested, results were discussed and a specific advice was given in order to optimise the image acquisition and/or reconstruction protocols to improve both qualitative and quantitative outcomes.

Continuous education

The collected data were summarised and shared with the users during continuous education (CE) sessions. The aim was to update the users' knowledge in radiation protection, optimise the clinical use of the devices, as well as to promote a team collaboration spirit.

RESULTS

Computed tomography

Forty-five CT units were tested in 2013 (~18 % of all CT units in the country). Several elements were noticed.

Machine output

Four devices evidenced patient positioning laser alignment off by as much as 10 mm, possibly resulting in an increase in patient dose of 6 %[7].

Nine of 45 CT units (20 %) presented a beam collimation that was widely different from the value stated by the device, e.g. 4 mm measured for 1 mm nominal. These units took this parameter into account into their beam efficiency calculation. For example, for a 1-mm single-slice acquisition protocol (e.g. examination of the posterior fossa or the petrous bone), one unit displayed an efficiency of 14 %, thus resulting in a $CTDI_{vol}$ of 299 mGy, whereas a same-generation CT unit with a beam collimation of 1.25 mm with the exact same parameters displayed a $CTDI_{vol}$ of 41.5 mGy for a beam efficiency of 55 %. Radiographers were not aware of the importance of their choice of collimator settings.

Twenty-one of 45 CT units had HU in water that were not within the legal tolerance (0 $\pm$ 4 HU) for tube voltages different from 120 or 140 kV. This was mainly due to a lack of calibration because the tensions were not used in routine. Surprisingly, even then, an acquisition at a non-calibrated tension was still available in user mode, thus potentially leading to a completely erroneous examination if, for example, a newly engaged radiologist were to perform an examination at a lower tube voltage.

Abdomen protocol qualification

The subjective estimation of the LCD performance yielded some interesting results. For 2-mm slices, 4 of 16 CT units showed a lower detection performance, whereas for the 2.5-mm slices, 3 of 27 CT units showed LCD performance under the mean value. The mean values are given in Table 1. Without clearly setting one manufacturer apart from the others, it reminded the users that, for the same acquisition parameters, an increase in the slice thickness could lead to an increased LCD.

However, one of the main limitations of the authors' approach was that this was subjectively assessed, without taking into account the spatial frequency of the noise.

Clinical use of the device

The clinical use of the devices showed a large variability, especially for the abdominal examinations. Tables 2 and 3 and Figure 2 give an overview of this dispersion. For example, the ratio of the 75th and 25th percentile of the mean $CTDI_{vol}$ was 1.9, whereas the effective dose showed a dispersion factor of 3.0. This shows that the number of scans per examination is not uniform.

In 2008, the FOPH estimated the mean effective dose for abdominal examinations at ~9 mSv. The current analysis shows a value of 18.7 $\pm$ 12.7 mSv, more than twice the last value (Figure 2 and Table 2). Reasons for this could be a miscalculation of the 2008 value, a quick increase in the number of scans per examination during this period or a biased selection of the examinations.

One critical aspect is that, among CT users—and MPEs—the concept of DRL is not clear, especially since the number of scans is not standardised. The current approach allowed for a clarification of the

Table 1. LCD performance for the unit benchmarking protocol.

Slice thickness [mm]	LCD@0.5 % [mm]	LCD@0.3 % [mm]
2	9.6 $\pm$ 2.8	14.5 $\pm$ 1.7
2.5	8.0 $\pm$ 0.6	14.0 $\pm$ 2.3

LCD performance is given in terms of the average smallest low-contrast insert detected, for a given native contrast (0.5 or 0.3 %).

Table 2. Mean values of the main dose indicators for clinical use of CT units, along with the measured ranges.

Protocol	Mean $CTDI_{vol}$ [mGy]	Mean DLP [mGy cm]	No. of phases	E [mSv]
Head	51.2 ± 13.9 22.1–84.2	905 ± 275 286–1812	1.7 ± 0.7 1–4	3.2 ± 1.3 1.0–6.6
Chest	8.5 ± 5.5 2.6–31.8	310 ± 165 96–816	1.4 ± 0.5 1–3	6.2 ± 3.5 1.4–20.3
Abdomen	12.2 ± 7.0 2.6–48.8	535 ± 320 96–2085	2.4 ± 1.3 1–9	18.7 ± 12.7 2.0–112.0

Mean $CTDI_{vol}$ and DLP are given per scan, whereas the effective dose and number of scans are given per examination.

Table 3. Dispersion of the clinical use in terms of the percentile of abdomen dose indicators.

Percentile	Mean $CTDI_{vol}$ [mGy]	Mean DLP [mGy cm]	Cumulated DLP [mGy cm]	No. of phases	E [mSv]
25th	8.0	320	550	1	8.4
75th	14.8	665	1655	3	25.4
75th/25th	1.9	2.1	3.0	3	3.0

The dispersion of the practice is given by the ratio between the 75th percentile and the 25th percentile of the distribution, thus ignoring the extreme values.

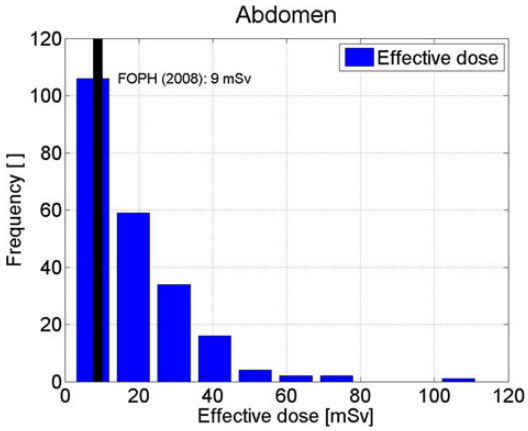

Figure 2. Dispersion of the clinical use of CT for abdominal examinations in terms of effective dose per examination. The 2008 value from the FOPH dose estimation is given as a comparison.

actual patient exposure, thus triggering discussions among radiologists in order to limit the dispersion of the practice.

A further limitation was the collection of clinical cases on the basis of anatomical regions. Thus, a bias was introduced by comparing examinations for obviously different clinical demands. An effort will be placed upon analysing clinical practice with respect to demand in the coming years.

Fluoroscopy

For approximately the same clinical settings, the dose rates showed large variations. For example, when putting 20 cm of PMMA in the primary beam, acquisitions at 15 frames per second (typical for interventional cardiology procedures) had differences up to a factor 3 (Figure 3). Measurements made with diagnostic settings (cineradiography or digital subtraction angiography) even yielded differences up to a factor 7.

Nuclear medicine

The analysis of early results obtained from a few tested devices showed heterogeneous PET performance. The main factor for differences was the availability or not of time-of-flight and point spread function corrections that strongly impact both overall image noise and activity recovery in small-sized lesions.

Furthermore, although the radiographers practising SPECT/CT and/or PET/CT examinations were fairly aware of the principles of radiation protection when manipulating radioactive sources, they were not comfortable with the interpretation of the CT dose indicators, as there are still no existing DRLs specifically for transmission imaging in NM.

Continuous education

Approximately 150 radiographers have participated into 7 CE sessions organised throughout the year. The lecture's themes were a description of the methodology

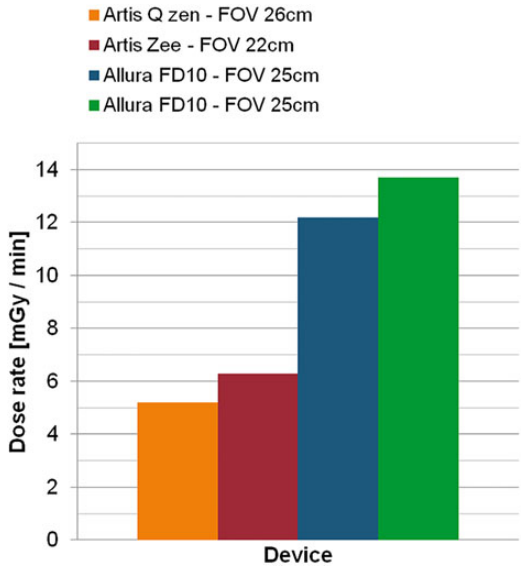

Figure 3. Discrepancy in the dose rates for different fluoroscopy units with the same acquisition settings (fluoroscopy, medium quality, 15 frames per second, 20 cm of PMMA in the primary beam, comparable FOV).

used in CT qualification within the new legal framework and a reminder of the dose indicators as well as the metrics of image quality with respect to dose. One important aspect was the gain of confidence between the radiographers and the MPE.

PERSPECTIVES

For CT, the future tasks are divided into two subsets. First, there is a strong need for an objective qualification of LCD, so the user is aware of the potential loss in LCD performance when using low-dose protocols along with iterative image reconstruction algorithms. Second, the sampling of examinations is to become task-oriented rather than relative to a given anatomical region. The ultimate goal would be to have one (or several) objective image quality indicator(s) for a given clinical demand. For example, the search of kidney stones (high contrast) does not need the same dose level than a suspected liver carcinoma. For this, the implementation of model observers on anthropomorphic systems is a promising tool towards this solution.

For fluoroscopy, a great deal of effort has been put into the establishment of new reference levels in interventional cardiology. For this purpose, automated dose collection software will become of prime importance. Nonetheless, a crucial point that has yet not been investigated thoroughly is the reliability of the dose indicators of the devices, such as cumulative dose or cumulative dose–area product. Indeed, the former is defined at two different locations in the beam (FDA or IEC reference points); the latter, especially since diagnostic beams are heavily filtered using copper, is, based on preliminary measurements, potentially off by a factor of 2. A new investigation protocol to address this problem is currently being set up by the AAPM task group 190, and their final report is due in December 2014. As a consequence, the traceability of the testing instruments will be even more important, and the tolerance on dose indicators will have to be lowered. Furthermore, the nomenclature of the specific diagnostic and/or therapeutic interventions is not unified, thus making a proper large-scale dose collection tedious. Interventional cardiology, for which soon-to-be published DRL have been established (as cited previously), could serve as a role model for this task. An effort will also be taken on the establishment of a database of objective image quality indicators for parameters deemed acceptable by physicians after optimisation.

Finally, for NM, two aspects seem to emerge from the first results. First, a great deal of effort has to be put into the calibration of the individual activity meters of the different institutions, by using a solid $^{68}Ga/^{68}Ge$ phantom for PET and the Jaszczak phantom for SPECT. Second, the use of CT for attenuation correction will, as for conventional CT, benefit of the model observer routines to tackle objective image quality.

The CE sessions have allowed the MPE to gain knowledge of the devices across the country and confidence with respect to their clinical applications. The next step will be to establish partnerships with radiologists.

REFERENCES

1. Swiss Federal Council. *Radiological Protection Ordinance (RPO) of 22 June 1994, classified compilation 814.501*. Swiss Federal (2008).
2. Deak, P. D. *et al. Multisection CT protocols: Sex- and age-specific conversion factors used to determine effective dose from dose-length product*. Radiology **257**, 1 (2010).
3. Paolicchi, F. *et al. Real practice radiation dose and dosimetric impact of radiological staff training in body CT examinations*. Insights Imaging, **4**(2), 239–2441 (2013).
4. *AAPM Report 204, Size-Specific Dose Estimates (SSDE) in pediatric and adult CT examinations*. ISBN: 978-1-936366-08-8, AAPM (2011).
5. Mesbahi, A. *et al. Comparison of radiation dose to patient and staff for two interventional cardiology units: a phantom study*. Radiat. Prot. Dosim. **131**(3), 399–403 (2008).
6. *Routine quality control recommended for nuclear medicine instrumentation*. Eur. J. Nucl. Med. Mol. Imaging **37**, 662–671 (2010).
7. Habibzaden, M. A. *et al. Impact of miscentering on patient dose and image noise in x-ray CT imaging: phantom and clinical studies*. Physica. Medica. **28**, 191–199 (2012).

Radiation Protection Dosimetry (2015), pp. 1–6 doi:10.1093/rpd/ncv484

SYSTEM UPGRADE ON PHILIPS ALLURA FD20 ANGIOGRAPHY SYSTEMS: EFFECTS ON PATIENT SKIN DOSE AND STATIC IMAGE QUALITY

Nick Ryckx[1,*], Marta Sans-Merce[1,2], Reto Meuli[3], Jean-Baptiste Zerlauth[3] and Francis R. Verdun[1]
[1]Lausanne University Hospital, Institute of radiation physics, Rue du Grand-Pré 1, CH-1007 Lausanne, Switzerland
[2]Geneva University Hospital, Geneva, Switzerland
[3]Radiodiagnostic and Interventional Radiology Service, Lausanne University Hospital, Rue du Bugnon 21, CH-1011 Lausanne, Switzerland

*Corresponding author: nick.ryckx@chuv.ch

Fluoroscopically guided procedures might be highly irradiating for patients, possibly leading to skin injuries. In such a context, every effort should be done to lower patient exposure as much as possible. Moreover, patient dose reduction does not only benefit to the patient but also allows reducing staff exposure. In this framework, Philips Healthcare recently introduced a system upgrade for their angiography units, called 'AlluraClarity'. The authors performed air kerma rate measurements for all available fluoroscopy modes and air kerma per frame measurements for the digital subtraction angiography protocols, along with subjective spatial resolution and low-contrast detectability assessments using a standard QA phantom. Air kerma reductions ranging from 25.5 to 84.4 % were found, with no significant change in image quality when switching from a standard operating mode to an upgraded version. These results are confirmed by the comparison of actual patient exposures for similar procedures.

INTRODUCTION

Fluoroscopically guided interventions are among the most highly irradiating diagnostic and/or therapeutic procedures, both for the patient and the operating staff. Therefore, according to the as low as reasonably achievable principle, all available measures should be taken to optimise the use of ionising radiation.

One way to proceed is the use of technological improvements. In this scope, Philips Healthcare (Best, The Netherlands) has issued an upgrade for their Allura angiography units called AlluraClarity. This technology makes use of both particular X-ray tube and filter settings [especially additional Cu-filtration and smaller focal spot[1]] and image processing that are, unfortunately, not fully described in the literature. The final result is an overall reduction in the image noise level, allowing for a subsequent patient dose reduction, up to 75 % according to the literature[1].

This drastic dose reduction is associated with the production of images that remain fully satisfying for the users as mentioned by Söderman *et al.*[1,2]

The authors' aim is to assess the variability of air kerma reduction and image quality (IQ) preservation using controlled exposure conditions and an IQ phantom when going from the standard Philips Allura system to the AlluraClarity upgraded system.

MATERIALS AND METHODS

The patient was simulated using PMMA slabs of 20 by 20 by 5 cm, piled up to obtain thicknesses of 5, 10, 15 and 20 cm, in order to study the behaviour of the automatic exposure control system. The air kerma rates were measured using a 6-cc ionisation chamber (10 × 5–6, RadCal Corp., Monrovia, CA, USA) and a readout unit/power supply (9015, RadCal Corp.). All measurements are traceable to the Swiss Federal Office of Metrology (METAS).

Two sets of measurements were taken in two slightly different geometric set-ups, one for the air kerma rate measurements and one for the IQ. At all times, the focus-to-detector distance was kept constant at 110 cm, while the focus-to-ionisation chamber was kept constant at 75 cm. This geometry has been chosen to reproduce typical clinical acquisition geometry[3].

The set-up used for dosimetry consisted in placing the ionisation chamber in the middle of the entrance surface of the X-ray field, close to the phantom (Figure 1). It is worth mentioning that the ionisation chamber was not localised at the interventional reference point since the choice made was to be as close as possible to clinical conditions.

Concerning the set-up used for the IQ measurements, and as previously mentioned, the focus-to-detector and focus-to-PMMA have been kept constant. A standard IQ phantom (TOR CDR, Leeds Test Objects, Boroughbridge, UK) was placed on top of the first PMMA slab (Figure 2). The additional PMMA slabs were subsequently piled on top of the phantom, so as to simulate inner body lesions for different patient morphologies, following a standard

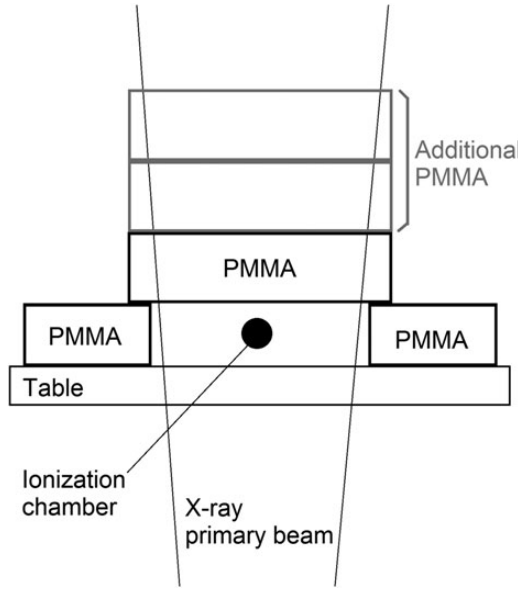

Figure 1. Schematic figure of the dosimetry set-up geometry: PMMA in the primary beam, ion chamber at the entrance point of the beam. The additional 5-cm PMMA slabs are represented in grey.

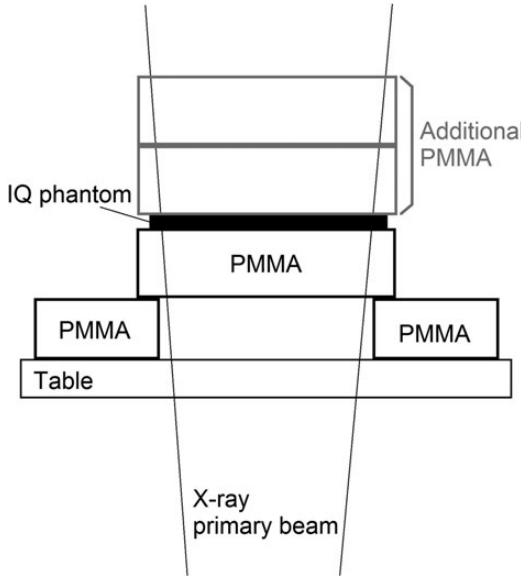

Figure 2. Schematic figure of the IQ set-up geometry: PMMA in the primary beam, TOR CDR IQ phantom on top of the first PMMA slab. The additional 5-cm PMMA slabs, piled up on the IQ phantom, are represented in grey.

internal procedure. The total patient thickness was of 5-, 10- and 15-cm PMMA + the extra 1 cm of the phantom.

Table 1. Air kerma rates for fluoroscopy setting II (medium quality).

PMMA [cm]	FOV [cm]	Air kerma rate [mGy min^{-1}]		Difference [%]
		Upgraded	Reference	
5	42	0.650	1.305	−50.2
	27	0.920	1.640	−43.9
	15	1.255	2.200	−43.0
10	42	2.00	3.67	−45.5
	27	2.80	4.63	−39.5
	15	3.70	6.20	−40.3
15	42	4.75	9.00	−47.2
	27	6.55	11.50	−43.0
	15	9.00	16.00	−43.8
20	42	11.5	20.0	−42.5
	27	14.5	24.0	−39.6
	15	19.5	34.5	−43.5

PMMA thickness ranges from 5 through 20 cm, whereas the FOV are 42, 27 and 15 cm, respectively.

Table 2. Air kerma rates for fluoroscopy setting I (low quality) and III (high quality).

PMMA [cm]	FOV [cm]	Air kerma rate [mGy min^{-1}]		Difference [%]
		Upgraded	Reference	
10	42	1.40	1.80	−22.2
		3.30	5.20	−36.5
	27	1.95	2.35	−17.0
		4.40	6.55	−32.8
	15	2.55	2.89	−11.8
		6.30	8.90	−29.2
20	42	6.7	10.1	−33.7
		21.0	31.2	−32.7
	27	8.7	13.0	−33.1
		27.5	40.5	−32.1
	15	11.5	17.5	−34.3
		36.0	50.5	−28.7

PMMA thicknesses are of 10 and 20 cm, whereas the FOV are 42, 27 and 15 cm, respectively.

The phantom consists of a solid polymer disc embedded with four groups of test objects:

- 17 high-contrast discs of varying contrast and fixed diameter of 0.5 mm,
- 10 discs, fixed diameter of 5.6 mm, used for grey-scale calibration,
- 17 low-contrast discs of varying contrast and fixed diameter of 11 mm,
- A resolution test pattern with 30 line groups of increasing spatial frequency.

The two latter elements were used for IQ assessment in terms of, respectively, low-contrast detectability (LCD) and spatial resolution. The acquired images were displayed on a DICOM 3.14 compliant diagnostic monitor (RadiForce MX 210, Eizo Nanao Corp., Hakusan, Japan). An observer subjectively assessed IQ by noting the disc with lowest detectable contrast (thus defining LCD performance, see Table 4) and the line

Table 3. Air kerma per image for lower limb DSA (PMMA thickness of 5 and 10 cm) and abdominal DSA (PMMA thickness of 15 and 20 cm).

	PMMA [cm]	FOV [cm]	Air kerma per image [mGy]		Difference [%]
			Upgraded	Reference	
Lower limb DSA	5	42	0.032	0.160	−80.0
		27	0.032	0.219	−85.4
		15	0.047	0.320	−85.2
	10	42	0.076	0.538	−85.9
		27	0.106	0.749	−85.8
		15	0.159	1.109	−85.7
Abdominal DSA	15	42	0.288	1.046	−72.5
		27	0.414	1.521	−72.8
		15	0.648	1.918	−66.2
	20	42	0.827	3.061	−73.0
		27	1.229	4.286	−71.3
		15	1.889	4.573	−58.7

The FOV are 42, 27 and 15 cm, respectively, for both anatomical regions.

Table 4. Subjective IQ assessment, in terms of spatial resolution and LCD.

PMMA [cm]	FOV [cm]	Mode	Resolution [lp mm^{-1}]		LCD [%]	
			Upgraded	Reference	Upgraded	Reference
5	42	DR	2.24	2.24	1.3	1.3
		DSA	2.24	2.24	1.3	1.3
		Sc. II	2.00	1.60	1.7	2.2
	31	DR	2.80	2.80	1.3	1.3
		DSA	2.80	2.50	1.3	1.5
		Sc. II	2.50	2.24	1.7	2.2
10	42	DR	2.24	2.24	2.2	2.2
		DSA	2.24	2.24	1.5	2.2
		Sc. II	1.80	1.80	2.7	2.7
	31	DR	2.80	2.80	1.5	1.5
		DSA	2.80	2.50	1.5	1.5
		Sc. II	2.24	2.24	1.7	2.7
15	42	DR	2.24	2.24	2.2	2.2
		DSA	2.24	2.24	2.2	2.2
		Sc. I	1.60	1.60	3.2	3.2
		Sc. II	1.60	1.60	2.7	2.7
		Sc. III	1.60	1.60	2.7	2.2
	31	DR	2.50	2.80	2.2	1.7
		DSA	2.50	2.80	1.7	1.5
		Sc. I	2.24	2.00	2.7	2.2
		Sc. II	2.24	2.24	2.7	2.2
		Sc. III	2.24	2.24	2.7	2.2

PMMA thickness ranges from 5 through 15 cm, whereas the FOV are 42 and 31 cm, respectively. Imaging modes were fluoroscopy (Sc.) of medium (II) quality, single exposure (DR) and abdominal DSA. For 15 cm of PMMA, the results are also given for low (I)- and high (III)-quality fluoroscopy. The LCD percentage is the native contrast of the perceived disc as defined by the manufacturer (70 kVp tube voltage and 1-mm additional copper on the X-Ray tube, ranging from 0.2 to 7.5 %).

group with highest distinguishable spatial frequency. Measurements were performed on the same day, in the same viewing conditions, by the same person (N. R.).

The same measurements were done for two separated angiography units in two different hospitals, both used mainly for pelvic and lower limb percutaneous blood vessel interventions. Both rooms were equipped with an Allura Xper FD20 flat-panel detector fluoroscopy unit, one equipped with the AlluraClarity upgrade, the other not. From this point on, they will be respectively designated as 'upgraded' and 'reference'.

For the dosimetry assessment, the following protocols were used:

- Fluoroscopy (used for positioning, images not recorded, only last image hold recorded), with three quality settings (I, II and III), 15 fps, all available fields of view (FOV),
- Abdomen digital subtraction angiography (DSA), varying frame rate, 3 FOV (15, 27 and 42 cm),
- Lower limb DSA, varying frame rate, 3 FOV (idem).

For the fluoroscopy settings, the frame rate was high enough in order to measure an air kerma rate at all quality settings, all FOVs and all PMMA thicknesses.

For the DSA runs, since the frame rate varied during the acquisition process and was quite low ($\leq$3 fps), the dosemeter was switched to 'air kerma integration' mode and the cumulated air kerma was divided by the resulting number of acquired frames. The authors thus obtained an average air kerma per frame, as is customary for DSA[4].

For the IQ assessment, the following protocols were used:

- Fluoroscopy, with three quality settings (I, II and III), 15 fps,
- Abdomen DSA, varying frame rate, raw images displayed (no subtraction of the mask),
- Single exposure (DR).

Finally, a statistical analysis of actual patient exposures before and after the upgrade of a further unit was performed using dose-collection software (DoseWatch, GE Healthcare, Little Chalfont, UK).

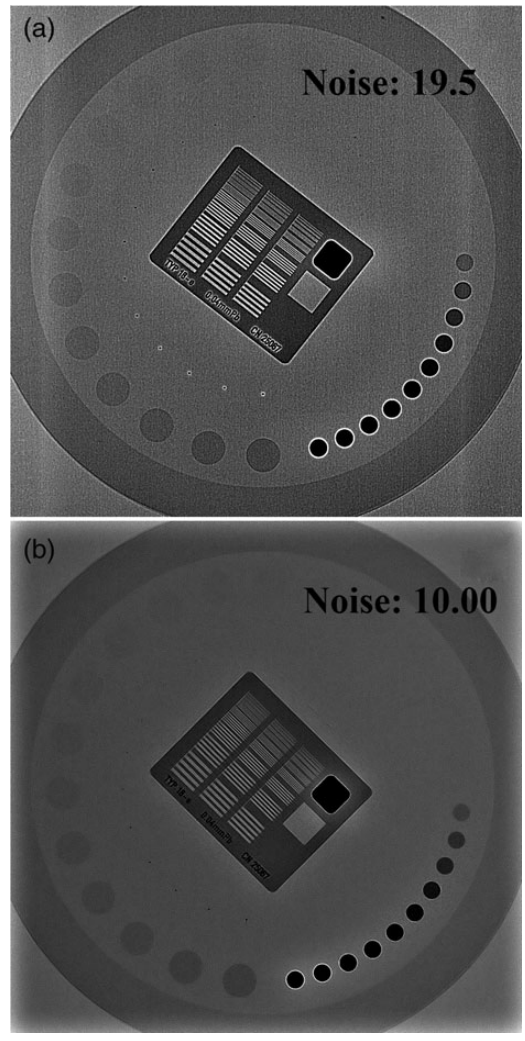

Figure 3. Images of the IQ phantom taken in the same acquisition and viewing conditions [i.e. same grey window width (300) and level (400)]: 10-cm PMMA, FOV 31 cm, single exposure (DR) for the (**a**) reference unit and (**b**) the upgraded.

RESULTS

Dosimetry

Tables 1–3 show examples of the effect of the upgrade on air kerma and air kerma per image, respectively. For fluoroscopy settings, the air kerma rates were systematically lower for the upgraded radiology unit than the reference unit. The average air kerma rate reduction over all PMMA thicknesses was 25.5 % for low-quality, 43.5 % for medium-quality and 34.5 % for high-quality fluoroscopy mode. The reduction was higher for larger FOV (e.g. lesser magnification).

For DSA, the air kerma reduction was in average 69.7 % for abdominal angiography and even 84.4 % for lower limb angiography. Again, the effect was more prominent for larger FOV, and no clear effect is shown with respect to the PMMA thickness.

Image quality

Table 4 shows the results of the IQ assessment. Only two FOV (31 and 42 cm) were studied, since the 15-cm FOV did not allow for the low-contrast targets to remain into the primary beam. Overall, there was no significant change in IQ. The mean spatial resolution

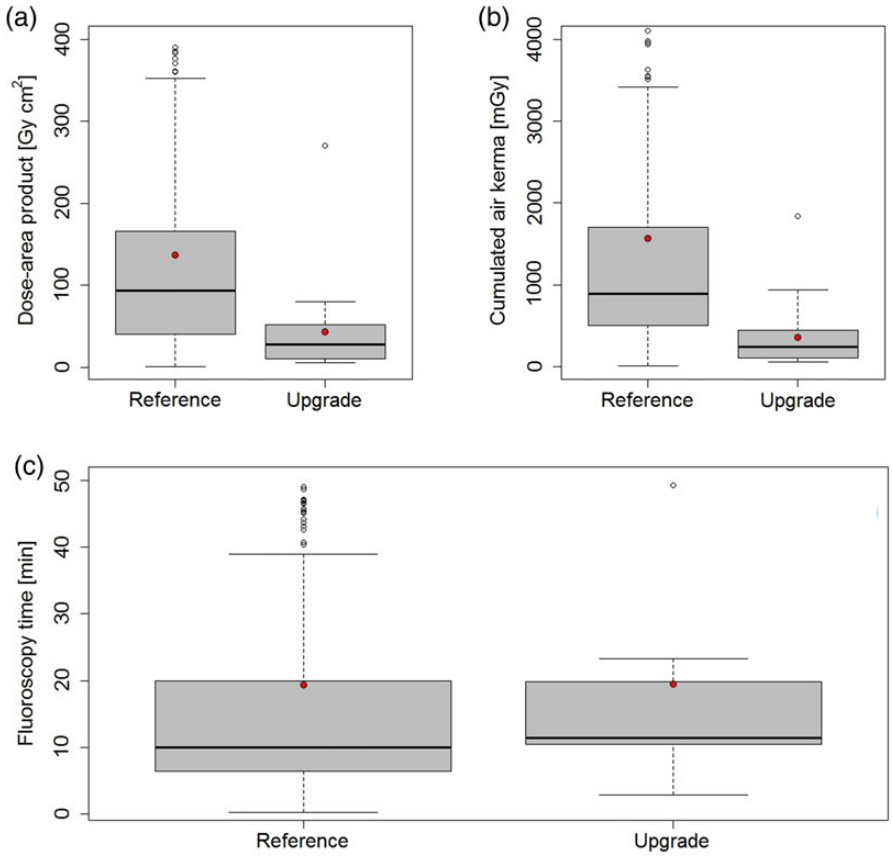

Figure 4. Box plots showing the DAP (**a**), AK (**b**) and FT (**c**) distributions. The bold bar shows the median, the filled point the mean, box hinges show the first and third quartiles, whereas the whisker ends extend to the 5th and 95th percentiles. The topmost rings show the outliers. Results are systematically shown for the reference (left) and upgraded (right) systems.

performance showed a slight but non-significant increase for the upgraded system (two-sample *t*-test, *p*-value 0.55). The same could be said for the mean LCD (*p*-value 0.15).

Figure 3 shows an example of two images taken exactly in the same conditions [10-cm PMMA, single exposure (DR), FOV 31 cm, grey window width of 300 and level of 400]. The topmost (a) was made on the reference angiography unit, whereas the second (b) was taken on the upgraded unit. Respective standard deviations (noise) measured in an 18 × 18 mm square region of interest were 19.5 and 10.0, showing a noise reduction of a factor ~2 for the present conditions when using the upgraded unit.

Clinical dosimetry

A preliminary data collection (Figure 4) was performed by N. R. for a further unit recently upgraded, using automated dose-collection software.

Data consisted of neurological angiography and angioplasty procedures, 388 performed with the reference unit and 22 with the upgraded unit. Statistical analysis showed a significant decrease in the mean dose–area product (DAP) and cumulated air kerma (AK) of respectively 63 and 72 % (*p*-values <0.01). The mean fluoroscopy time (FT) showed a slight but non-significant increase of 5 % (*p*-value 0.96). Those values are comparable to the results of phantom measurements presented in this study, showing a reduction in patient air kerma rate between 25.5 % for low-quality fluoroscopy and 84.4 % for lower limb DSA.

DISCUSSION AND PERSPECTIVES

The AlluraClarity upgrade for Allura angiography units allows for a significant reduction in patient dose. Although this has not been measured here, the consequence is also a reduction in staff dose.

One major drawback in these measurements is the subjectivity of the assessment, since the performance characterisation was carried out by a single human observer, prone to intra-subject variability. At the time of the measurements, the observer was the only familiar with the actual procedure and present at the place where the measurements were performed. Furthermore, the measurements were carried out solely in static imaging conditions, whereas these units are used to visualise dynamic phenomena, such as contrast medium wash through or coronary angiography.

A solution for both these problems would be to use model observers, such as the channelised Hotelling observer, as proposed by Favazza *et al.*[5], or to use several experienced radiologists to grade the phantom images.

Finally, the thickness of 15 cm of PMMA for IQ assessment, although compliant with the internal procedure used, is not representative of patient with a larger body habitus. This peculiar aspect will have to be modified so as to correspond to the evolution of the morphologies in Western countries.

CONCLUSION

A set of measurements carried out in controlled conditions showed that the AlluraClarity for Allura angiography rooms is able to significantly reduce patient dose with no significant change in IQ. However, several limitations, such as a single human observer, as well as conditions that do not include larger patient habitus, will have to be taken into account for further investigations. The use of model observers seems to be a good solution to reduce inter- and/or intra-observer variability, as well as to take into account the assessment of dynamic phenomena.

REFERENCES

1. Söderman, M., Holmin, S., Andersson, T., Palmgren, C., Babi, D. and Hoornaert, B. *Image noise reduction algorithm for digital subtraction angiography: clinical results.* Radiology **269**, 553–560 (2013).
2. Söderman, M., Mauti, M., Boon, S., Omar, A., Marteinsdóttir, M., Andersson, T., Holmind, S. and Hoornaert, B. *Radiation dose in neuroangiography using image noise reduction technology: a population study based on 614 patients.* Neuroradiology **1023**, 1365–1372 (2013).
3. Ryckx, N., Gnesin, S., Meuli, R., Elandoy, C. and Verdun, F. R. *Medical physicists' implication in radiological diagnostic procedures: results after 1 y of experience.* Radiat. Prot. Dosim. **164**, 120–125 (2014).
4. Kotre, C. J. and Marshall, N. W. *A review of image quality and dose issues in digital fluorography and digital subtraction angiography.* Radiat. Prot. Dosim. **94**, 73–76 (2001).
5. Favazza, C. P., Fetterly, K. A., Hangiandreou, N. J., Leng, S. and Schueler, B. A. *Implementation of a channelized Hotelling observer model to assess image quality of X-ray angiography systems.* J. Med. Imag. **2**, 015503 (2015).

Radiation Protection Dosimetry (2016), pp. 1–4 doi:10.1093/rpd/ncv525

PATIENT DOSE ASSESSMENT AFTER INTERVENTIONAL CARDIOLOGY PROCEDURES: A MULTI-CENTRIC APPROACH TO TRIGGER OPTIMISATION

Nick Ryckx[1,*], Jean-Jacques Goy[2], Jean-Christophe Stauffer[2] and Francis R. Verdun[1]
[1]Lausanne University Hospital, Institute of Radiation Physics, Rue du Grand-Pré 1, Lausanne CH-1007, Switzerland
[2]Cardiology Department, Fribourg Hospital, Fribourg CH-1708, Switzerland

*Corresponding author: nick.ryckx@chuv.ch

As the number and complexity of fluoroscopically guided interventions increase, a serious effort has to be put on the optimisation of the X-ray dose delivered to the patient. In order to set up this optimisation process, the clinical practice for a given cardiology centre has to be analysed with relevant statistical power and compared with the data at local or national level. Data from 8 Swiss cardiology centres for 10 different vascular and heart rhythm procedures have been collected. The collected dose indicators were, when available, cumulated air kerma, cumulated dose-area product, fluoroscopy time and the number of images per procedure. Data analysis was performed using an in-house software solution in terms of the first, second and third quartiles. This kind of large-scale analysis could yield some onsets towards local practice optimisation based on anonymous dose indicator cross-comparison. Further effort should nevertheless be made in order to proceed towards an operator-based data analysis, thus allowing for an individual practice optimisation.

INTRODUCTION

Interventional cardiology (IC) procedures are among the most dose-intensive for patients. Nevertheless, they are performed in increasing numbers because of their minimally invasive nature, which reduces septic risks and patient hospitalisation time. In Switzerland, the frequency of fluoroscopically guided diagnostic and therapeutic procedures accounts for 0.8 % of all X-ray examinations, whereas their dose contribution is 20.7 % of the collective dose from X-rays to the Swiss population[(1)].

The European Council Directive 2013/59/EURATOM[(2)] underlines the importance of a regular review of patient dose levels in order to optimise medical practice. A major problem in dose optimisation for fluoroscopically guided interventions is the non-predictability of the four main dose indicators, which are fluoroscopy time, the number of frames, cumulated dose-area product and cumulated air kerma. For example, for a computed tomography (CT) examination, the volume CT dose index ($CTDI_{vol}$) and dose length product (DLP) are known after performing the scanogram, used for automatic X-ray tube current modulation and anatomic volume planning, thus before the actual procedure. In fluoroscopy, the resulting dose levels depend on numerous factors, many of which are not known before performing the examination: patient body habitus, lesion complexity, operator experience, image acquisition pre-settings, beam collimation and filtration, etc.

Unfortunately, some of those parameters are the ones an operator will have to monitor in order to lower the value of a given dose indicator. Since the main dose indicators used in fluoroscopy are strongly correlated one to another, the optimisation process has to start after a statistical analysis of a substantial number of procedures, for which the dose indicators have been collected, analysed and cross-compared. The aim of this study was to show the main cues on patient dose optimisation based on a statistical analysis of a large number of procedures.

MATERIALS AND METHODS

In the framework of updating the Swiss national diagnostic reference levels (DRLs) for IC, eight cardiology centres reported their data, mainly through the use of an automatic dose collection software (CardioReport, CVX Medical, Croissy-Beaubourg, France). A total number of 46 591 interventions have been collected for the following 10 procedures:

- Coronary angiography (CA),
- Percutaneous transluminal coronary angioplasty (PTCA),
- CA + PTCA,
- Shunt closure,
- Transcatheter aortic valve implantation (TAVI),
- Myocardial biopsy,
- Diagnostic electrophysiology procedures (EFO),
- Defibrillator implantation (ICD),
- Pacemaker implantation (PM),
- Radio-frequency ablation (RFA).

Table 1 shows the respective numbers for each intervention.

Table 1. Distribution of the data collected in the eight participating cardiology centres.

Intervention	Number recorded
CA	24 261
Coronary angioplasty (PTCA)	1099
CA + PTCA	18 797
TAVI	221
Shunt closure	622
Myocardial biopsy	73
Diagnostic electrophysiology (EFO)	210
ICD	281
PM	300
RFA	720
Alcohol septal ablation	7[a]

[a]Data discarded due to a too low number of cases.

An in-house software solution (Memoviz, Memoways, Geneva, Switzerland) was elaborated to visualise the data. For each procedure type, the following dose indicators could be displayed:

- Fluoroscopy time (FT),
- Number of acquired images (N),
- Cumulative dose-area product (P_{KA}),
- Cumulative reference air kerma ($K_{a,r}$).

Up to eight sets of data, i.e. all eight centres or seven centres and the Swiss mean values, could be displayed alongside. This allowed for an immediate cross-comparison of the dose values of a given centre with the Swiss values or between different centres. All data have been displayed anonymously, all centres being designated with a character between A and H.

For each dose indicator distribution, the software calculated the first, second and third quartiles (Q1, Q2 and Q3). According to the definition of the DRLs, Q3 was used as the main metric for dose indicator comparison. The data analysis has been performed for the 10 types of IC interventions.

RESULTS

Figure 1 shows, as an example, the quartiles of P_{KA} for CA + PTCA procedures. Hovering over a given bar displays the numeric values of the respective centres, thus permitting an immediate comparison of the selected dose indicator.

Tables 2–5 show the results for, respectively, CA, CA + PTCA, TAVI and myocardial biopsy, as produced by the software. The analysis of the tables could give an indication on where to start the dose optimisation. Indeed, underlining that one single dose indicator out of the four was higher with respect to the other does not necessarily mean that one centre worked 'better' than another. The four dose indicators are correlated one to another but are not linearly dependent.

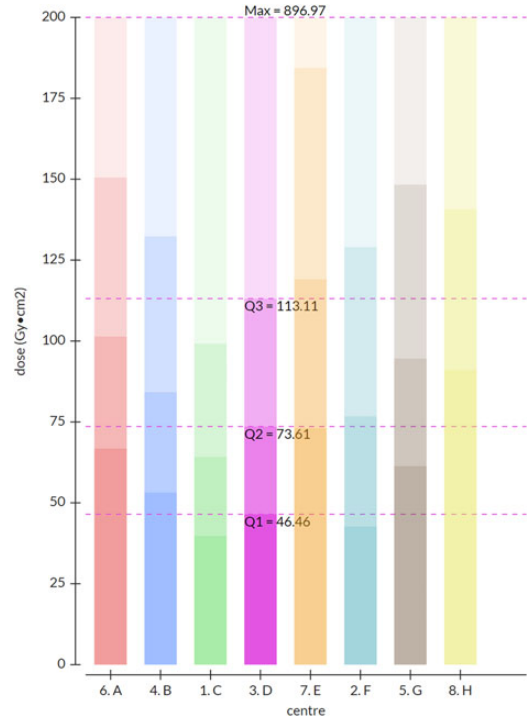

Figure 1. Quartile comparison of P_{KA} (Gy cm^2) for CA + PTCA procedures and for all eight cardiology centres. Mouse hover-over allows for an immediate display of the actual quartile values and immediate comparison with the dose levels of the other centres. The numbers are part of the web interface and display the selected dataset.

Table 2. Third quartiles (Q3) for CA for all eight cardiology centres and all dose indicators.

CA: Third quartile (Q3)

Centre	P_{KA} (Gy cm^2)	$K_{a,r}$ (mGy)	FT (min)	N
A	72	960	6.6	749
B	60	812	8.9	1006
C	51	752	6.0	850
D	65	857	12.3	N/A
E	81	N/A	8.3	887
F	50	329	8.9	1070
G	66	N/A	7.7	N/A
H	90	1146	9.6	1389
Switzerland	**69**	**841**	**8.9**	**877**

Centres E and G did not record $K_{a,r}$, and Centres D and G did not record N.

Table 3. Third quartiles (Q3) for CA + PTCA for all eight cardiology centres and all dose indicators.

CA + PTCA: Third quartile (Q3)				
Centre	P_{KA} (Gy cm^2)	$K_{a,r}$ (mGy)	FT (min)	N
A	150	2300	13.5	1170
B	132	2170	17.9	1820
C	99	1660	12.3	1390
D	113	N/A	23.4	N/A
E	184	N/A	19.3	1930
F	129	1230	20.5	2420
G	148	N/A	16.3	N/A
H	213	N/A	20.8	3530
Switzerland	150	2014	18.1	1527

Centres D, E, G and H did not record $K_{a,r}$, and Centres D and G did not record N.

Table 4. Third quartiles (Q3) for TAVI for all seven cardiology centres (Centre H did not perform any TAVI) and all dose indicators.

TAVI: Third quartile (Q3)				
Centre	P_{KA} (Gy cm^2)	$K_{a,r}$ (mGy)	FT (min)	N
A	114	934	12.1	625
B	128	1337	23.8	1216
C	73	933	8.7	1714
D	153	N/A	29.9	N/A
E	198	N/A	24.0	N/A
F	201	N/A	32.8	N/A
G	153	N/A	15.5	N/A
Switzerland	**141**	**1189**	**28.4**	**1011**

Centres D through G did not record $K_{a,r}$ and N.

As an example, the third quartiles (Q3) for CA + PTCA (Table 3) for Centres B, F and Switzerland (CH) are the following:

- Centre B: 132 Gy cm^2, 2.2 Gy, 17.9 min, 1820 images,
- Centre F: 129 Gy cm^2, 1.2 Gy, 20.5 min, 2420 images,
- CH: 150 Gy cm^2, 2.0 Gy, 18.1 min, 1527 images.

It can be seen that P_{KA} was rather similar for Centres B and F, but the $K_{a,r}$ of Centre B was roughly twice as high as the $K_{a,r}$ of Centre F. This could indicate that Centre F worked with imaging fields roughly twice as large as B, thus advising for a more thorough use of beam collimation. When comparing the values of Centre F with the Swiss values, it can be seen that the number of images at F was much higher for similar fluoroscopy times. This could indicate a higher frame rate (e.g. 30 fps instead of 15 fps, which could still be diagnostically acceptable).

Table 5. Third quartiles (Q3) for myocardial biopsies for four cardiology centres (B, D, F and H).

Myocardial biopsy: Third quartile (Q3)				
Centre	P_{KA} (Gy cm^2)	$K_{a,r}$ (mGy)	FT (min)	N
B	13	146	5.2	81
D	9	N/A	5.5	N/A
F	12	106	20.5	6
H	9	N/A	3.4	N/A
Switzerland	**12**	**146**	**5.9**	**81**

Centres D and H did not record $K_{a,r}$ nor N.

For the sake of clarity, another example, also related to CA + PTCA, is taken to illustrate the use of data cross-comparison, in the same table, but this time Q3 values for Centres A and B:

- Centre A: 150 Gy cm^2, 2.3 Gy, 13.5 min, 1170 images,
- Centre B: 132 Gy cm^2, 2.2 Gy, 17.9 min, 1820 images,
- CH: 150 Gy cm^2, 2.0 Gy, 18.1 min, 1527 images.

It can be seen that the P_{KA} and the $K_{a,r}$ were rather similar but that Centre B had longer times and a higher N. This could mean that Centre A worked with a higher image quality, since a lower N resulted in the 'same' patient dose. Thus, Centre A could potentially lower their image quality (e.g. by increasing the image noise), thus reducing the dose per frame and the resulting patient dose.

DISCUSSION AND PERSPECTIVES

This kind of multivariate analysis, based on anonymous centre cross-comparison, could give the respective centres ideas on what to optimise, rather than just telling the operators that their mean doses are higher. However, several limitations arise for this study.

Firstly, the heart rhythm procedures (EFO, RFA, PM and ICD) were given only for one centre. Cross-comparison was thus not possible. The values for this centre might also underestimate the mean exposure, since that centre is equipped with an electroanatomic mapping system—based on the position of markers on a catheter in a local magnetic field—designed to enhance the 3D representation of the heart chambers and main vessels, thus reducing the radiation burden.

Secondly, the quartile analysis was done for individual centres. Since the dose values are very much operator dependant, a finer analysis per centre and per operator would yield a more detailed set of recommendations for patient dose optimisation. Unfortunately, some procedures, especially the ones with a heavier physiological

burden, such as TAVI, were much less than the vascular interventions. As a consequence, splitting a lower number into a higher number of fractions will strongly reduce the statistical power of the analysis.

Finally, extra care has to be taken on the reliability of the respective dose indicators, thus implying extra efforts by medical physicists in the characterisation of the dose monitors of the respective imaging units.

An interesting solution for the sometimes low number of interventions might come from local dose collection software, such as DoseWatch (GE Healthcare, Little Chalfont, UK), Radimetrics (Bayer Healthcare, Berlin, Germany) or even open-source software such as OpenREM (Ed McDonagh, UK). Indeed, this software allows an all-time full access to the dose information and a per-operator dose analysis. Although still expensive, these systems tend to be more and more used in healthcare facilities.

REFERENCES

1. Gremion, I. and Stoll, B. *Les doses d'irradiation médicale diagnostique à la population*. Bull. Méd. Suisses **11**, 449–451 (2014).
2. European Council Directive 2013/59/EURATOM, http://eur-lex.europa.eu/, last accessed 19 May 2015.

Elsevier Editorial System(tm) for Physica Medica: European Journal of Medical Physics
Manuscript Draft

Manuscript Number:

Title: The use of out-of-plane high Z patient shielding for foetal dose reduction in computed tomography: Literature review and comparison with Monte-Carlo simulations of an alternative optimisation technique

Article Type: SI: Fetal Dose

Keywords: pregnant patient; uterus dose; computed tomography; high Z garments; protocol optimisation

Corresponding Author: Mr. Nick Ryckx, MSc in physics

Corresponding Author's Institution: Lausanne University Hospital (CHUV)

First Author: Nick Ryckx, MSc in physics

Order of Authors: Nick Ryckx, MSc in physics; Marta Sans-Merce; Sabine Schmidt; Pierre-Alexandre Poletti; Francis R Verdun

Abstract: When performing CT examinations on pregnant patients, great effort should be dedicated towards optimising the exposure of the mother and the conceptus. For this purpose, many radiology departments use high-Z garments to be wrapped around the patient's lower abdomen for out-of-plane organ shielding to protect the foetus. To assess their current protection efficiency, we performed a literature review and compared the efficiencies mentioned in the literature to Monte-Carlo simulations of CT protocols, for which the overall scan length was reduced. We found 11 relevant articles, all of them reporting uterus exposure due to CT imaging performed for exclusion of pulmonary embolism, one of the leading causes of peripartum deaths in western countries. Uterus doses ranged between 60 and 660 µGy per examination, and relative dose reductions to the uterus due to high-Z garments were between 20-56%. Simulations showed that reducing the scan length by one to three centimetres could potentially reduce uterus dose up to 24 % for chest imaging and even 47 % for upper abdominal imaging. These dose reductions were in the order of those achieved by high-Z garments. However, using the latter may negatively influence the diagnostic image quality and even interfere with the automatic exposure control system thus increasing patient dose if positioned in the primary beam, for example in the overranging length in helical acquisition. We conclude that efforts should be concentrated on positioning the patient correctly in the gantry and optimising protocol parameters, rather than using high-Z garments for out-of-plane uterus shielding.

Cover Letter

Nick Ryckx
Institute of radiation physics
Lausanne University Hospital
Rue du Grand-Pré 1
CH - 1007 Lausanne

Lausanne, the 16th February 2017

Object: Submission of a paper for the special issue on fetal dose

Dear Editor,

On behalf of my colleagues, I wish to submit a new manuscript entitled “The use of out-of-plane high Z patient shielding for foetal dose reduction in computed tomography: Literature review and comparison with Monte-Carlo simulations of an alternative optimisation technique” for consideration by the European Journal of Medical Physics, in its special issue on fetal dose.

We confirm that this work is original and has not been published elsewhere nor is it currently under consideration for publication elsewhere.

In this paper, we report on a literature review on uterus dose reduction due to out-of-plane high Z protective garments, and compare the reported dose reduction efficiencies to Monte-Carlo simulations performed using the ImPACT simulation spreadsheet for computed tomography. The main results show that, with regard to the current technical capabilities of modern CT units, such garments have been rendered obsolete. The paper should be of interest to readers in the area of clinical radiation protection, especially radiation safety officers seeking a solid study on which to base their decision in using or not aforementioned garments.

Please address all correspondence concerning this manuscript to me at Nick.Ryckx@chuv.ch.

Thank you for your consideration of this manuscript.

Yours sincerely,

Nick RYCKX

***Highlights (for review)**

- A literature review on patient uterus dose reduction by high Z drapes was performed.
- MC simulations for optimised protocols were proposed for efficiency comparison.
- Current CT technical have rendered the need for high Z garments obsolete.

The use of out-of-plane high Z patient shielding for foetal dose reduction in computed tomography: Literature review and comparison with Monte-Carlo simulations of an alternative optimisation technique

Nick Ryckx (1), Marta Sans-Merce (1, 2), Sabine Schmidt (3), Pierre-Alexandre Poletti (2), Francis R. Verdun (1)

1) Institute of radiation physics, Lausanne University Hospital, Switzerland

2) Radiology department, Geneva University Hospital, Switzerland

3) Department of Radiology, Lausanne University Hospital, Switzerland

Abstract

When performing CT examinations on pregnant patients, great effort should be dedicated towards optimising the exposure of the mother and the conceptus. For this purpose, many radiology departments use high-Z garments to be wrapped around the patient's lower abdomen for out-of-plane organ shielding to protect the foetus. To assess their current protection efficiency, we performed a literature review and compared the efficiencies mentioned in the literature to Monte-Carlo simulations of CT protocols, for which the overall scan length was reduced. We found 11 relevant articles, all of them reporting uterus exposure due to CT imaging performed for exclusion of pulmonary embolism, one of the leading causes of peripartum deaths in western countries. Uterus doses ranged between 60 and 660 µGy per examination, and relative dose reductions to the uterus due to high-Z garments were between 20-56%. Simulations showed that reducing the scan length by one to three centimetres could potentially reduce uterus dose up to 24 % for chest imaging and even 47 % for upper abdominal imaging. These dose reductions were in the order of those achieved by high-Z garments. However, using the latter may negatively influence the diagnostic image quality and even interfere with the automatic exposure control system thus

increasing patient dose if positioned in the primary beam, for example in the overranging length in helical acquisition. We conclude that efforts should be concentrated on positioning the patient correctly in the gantry and optimising protocol parameters, rather than using high-Z garments for out-of-plane uterus shielding.

1. Introduction

Over the 20th century, X-ray imaging has become an extremely useful diagnostic tool in medicine. Since its introduction in the 1970s, computed tomography (CT) has become an indispensable imaging tool within numerous clinical facilities. Recently, due to several technical and software innovations, the use of CT imaging has increased to represent a non-negligible proportion of diagnostic examinations using ionising radiation. For example, in 2013, it represented roughly 10% of all X-ray examinations, for a mean collective dose contribution of 70% due to X-ray medical imaging in Switzerland [1].

For any X-ray imaging modality, apart from the primary beam, several other sources of radiation can expose the patient: tube leakage and patient-induced scattered radiation (see **Error! Reference source not found.**). However, the tube leakage is limited by the International Electro-technical Commission (IEC) to a maximum dose rate of 0.1 mGy/h at 1 m from the patient, and will be substantially lower than the patient scatter [2]. Several lead and non-lead (high Z) based protective garments have been proposed to reduce scattered radiation: aprons, skirts and wrap-around drapes. The latter is the most commonly used within radiology suites. Currently, high Z garments used on patients for organ shielding outside the primary field are often proposed to provide some protection from radiation scattered by the table. Indeed, a study by Weber et al., decomposing the different components of scattered radiation in CT, found out that the main component of scatter irradiating the patient is internally-produced scatter, and that high Z garments are only efficient against radiation back-scattered from the table [3]. This implies that the proper use of these drapes is not to wrap it around the patient but merely to place it between the table and the patient, although many practitioners prefer wrapping the drape around the patient's lower abdomen.

Infants are highly sensitive to ionising radiation [4]. It is therefore of current practice to perform the imaging of pregnant women with more consideration. However, the use of out-of-plane high Z garments in the clinical routine gives rise to many questions within the radiology practice, and its application is quite heterogeneous. For example, the mean European usage rate of high Z garments for pregnant patients was 46.3%, whereas it rose to 94.5% in North America [5]. Furthermore, 25% of practitioners handling high Z garments complained about the weight of these garments, with approximately 20% experiencing occupationally-related back pain [5]. Within the current legal framework of all European countries, it is of interest to wonder whether these protection tools are still of any interest, or if they ought to be safely discarded with respect to alternative technical patient protection methods.

The two purposes of this paper were the following: First, we sought to establish a literature review of high Z out-of-plane patient shielding efficiency for uterus dose reduction in CT. Then, we compared the respective efficiencies of the shielding items to simple examination optimisation techniques using a dedicated Monte-Carlo simulation. We will not discuss in-plane garments, as these impair the diagnostic quality, as well as the functioning of the AEC system, as we will detail further on.

2. Materials and methods

2.1. Literature review

We performed a literature search using the PubMed search engine. Search words were: shielding, radiology, computed tomography, uterus, and pregnant patient. Papers published before 2006 (older than 10 years) were discarded, to take into account the recent evolution of CT imaging, mainly automatic tube current modulation and iterative image reconstruction. Papers not citing uterus dose were rejected.

2.2. Monte-Carlo simulations

We performed Monte-Carlo simulations to compare the efficiency of dose reduction when using high Z garments from data gathered from the literature to the dose sparing to the

uterus when optimising the CT examinations by reducing the acquired scan length. We used the ImPACT dose calculation spreadsheet [6], version 1.0 (28.08.2009), to simulate standard single-phase CT examinations of the upper abdomen (**Error! Reference source not found.**) and the chest (**Error! Reference source not found.**). Since image quality at a given location is intrinsically linked to $CTDI_{vol}$ [7], to optimize the dose while keeping the image quality constant we reduced the respective scan lengths by several cm in steps of one cm, while maintaining the coverage of the organs of interest. The subsequent absorbed uterus doses for each protocol was calculated. The $CTDI_{vol}$ was set to correspond to approximately 10 mGy, which is the diagnostic reference level (DRL) for a standard chest CT in Switzerland [8].

3. Results

3.1. Literature review

We found 11 relevant articles, listed in **Error! Reference source not found.** [3, 9-18]. All of them reported uterus exposure due to CT imaging performed for exclusion of pulmonary embolism (PE). Indeed, the risk of venous thromboembolism (VTE) is increased by the haemodynamic changes during pregnancy, with a rate of 1.72 per 1000 deliveries [19], and is the sixth leading cause of maternal mortality in the US, with 20 to 30% of peripartum deaths due to PE [20]. It is thus the main indication of chest CT for pregnant women. Uterus doses, taken as a surrogate for foetal exposure, ranged between 60 and 660 µGy per examination. High Z garments, wrapped around the waist of the woman, allowed for a relative absorbed dose reduction between 20 and 56% to the uterus.

3.2. Monte-Carlo simulations

Error! Reference source not found. and **Error! Reference source not found.** show the results obtained by our Monte Carlo simulations for the dose sparing to the uterus for upper abdomen and chest CT respectively. Reducing the scan length by one to three centimetres can potentially reduce uterus dose up to 24 % for chest imaging and even 47 % for upper

abdomen imaging. These dose sparings are in the order of those achieved by high Z garments wrapped around the patient (between 20% and 56% dose sparing). Reducing the scan length by 1, 2 or 3 cm allows for an absolute uterus dose reduction of respectively 400, 700 and 900 µGy for upper abdomen CT imaging, while a 3 cm length reduction in a chest examination will reduce the uterus dose by about 17 µGy (**Error! Reference source not found.** and **Error! Reference source not found.**).

4. Discussion

The efficiency of high Z garments to protect the uterus of pregnant patients is highly sensitive to its actual positioning. According to the extensive modelling study by G. Iball et al. [10], there seems to be a linear relationship between the uterus-to-garment edge distance and the uterine dose. As such, when the garment edge is placed at the same position as the uterus along the main patient axis, the dose reduction is about 10%, whereas it linearly increases when sliding the garment closer to the scanned volume (60% decrease with garment edge 22.5 cm above the uterus), with a uterus dose of 63.3 µGy without any high Z garment. This seems to be in correspondence to a further measurement in that same study, where it is shown that the uterine dose increases exponentially with scan edge being moved closer to the edge of the garment, kept constant at 15 cm above the uterus with respect to the main patient axis.

However, both experiments resulted in a partial irradiation of the anatomy covered by the garment. This presents several negative consequences. First, as is shown in a study by Dauer et al. [21], a high Z garment (in the present case a male gonadal shield in the primary beam) leads to massive photon starvation artefact, that render the images generated at those locations hardly useful for any diagnosis. Furthermore, the vast majority of adult CT protocols are based on automatic exposure control (AEC). Schematically, the information obtained by the scanned projection radiography (SPR) performed before the data acquisition is used for the scanned volume planning. It uses the information of patient's attenuation along the main table axis and/or in both postero-anterior and lateral directions, and plans the

X-ray tube current accordingly to achieve a pre-defined noise level across the subsequently reconstructed images, independently of tissue absorption [22]. This implies that such high Z garments, when used, have to be kept outside the primary field, to guarantee images of good diagnostic quality, but also avoid a steep increase in patient dose rate when the highly absorbing garment is found to be in the primary field. Finally, even if the garment is left outside the scanned volume, scan lengths (in helical acquisition) are extended on both ends due to over-ranging, a side effect of data interpolation for image reconstruction in helical acquisition, which is the case for practically all scans nowadays [23]. This implies that organs right next to the planned acquisition volume might be irradiated by the primary beam, even if this exposure will not lead to any reconstructed images. This holds true if the protective garment is placed right next to the planned volume. Unfortunately, some CT manufacturers have recently introduced, a top of SPR-based AEC, 'on-the-fly' dose rate correction based on the actual dose rates measured directly on the CT detectors during the acquisition [24]. Due to this added feature, the dose rate might be unknowingly increased locally, thus increasing scattered radiation inside the patient and annihilating the desired effect of the garment.

Additionally, the efficiency of increasing high Z thickness seems to quickly 'saturate'. Indeed, as described by Iball et al. [10], efficiency rapidly increases between 0 and 3.5 mmPb, and seems to remain constant above these values. As such, too heavy garments may be detrimental to patient comfort and operator back constraints [16, 18], with no significant gain in dose reduction efficiency.

Furthermore, the increase in the hypothetic lifetime risk of cancer or leukaemia induction in the child is in the order of 1 in 170 after a 100 mGy exposure (which is between two and three orders of magnitude above the mentioned dose sparing), whereas the overall risk of contracting cancer during a lifetime is about 1 in 3, 1 in 5 being the risk for a fatal malignancy [25]. Caution may be taken when reducing the scan length for a suspicion of PE, as sudden onset of lower chest pain may also be caused, although rarely, by adrenal haemorrhage, which can even become life-threatening [26]. As adrenal spontaneous haemorrhage has

been recorded as a complication during pregnancy, which can mimic PE symptoms, the spearing of few centimetres in the scanned volume could be dangerous.

Finally, since the demand in CT examinations is steadily increasing, there is a growing pressure on medical staff to optimise the time the patient spends within the radiology department. In opposition to MRI imaging, the acquisition time of a single – or multiple – CT phase(s) is a mere matter of seconds [27]. As such, there is often limited time dedicated per CT procedure, implying a pertinent choice among the means of optimisation at the disposal of the medical staff. Thus, a proper positioning of the high Z garments for an efficient protection will consume time that could be spent to guarantee the overall patient care.

One limitation of our study is not addressing the topic of in-plane bismuth protections. But, as for iterative reconstruction, organ-based modulation is sufficiently widespread in current CT imaging that those devices, prone to inducing photon starvation artefacts, are no longer deemed relevant for the protection of in-plane anatomy [28, 29].

5. Conclusion

The expected dose savings from the use of high Z garments may be counterbalanced by the optimisation of scan lengths, a parameter immediately accessible by the operator of the unit. Although dose savings from high Z garments might seem high (up to 56%), the absolute uterine doses delivered outside the primary field are already quite low (a few hundred µGy) per examination. In comparison, the efficiency in terms of dose reduction by correctly selecting the scan length is similar to the exposure reduction due to high Z garments, without the potential adverse effects, especially when using on-line dose rate adjustment.

To summarise, a thorough justification of the examination [30], optimal patient positioning to fully take advantage of the bow tie filter and AEC, the choice of an appropriate clinically relevant image quality level and the strict limitation of the scan range will yield uterine dose sparing in the order of those expected for well-placed high Z garments, without the latter's downsides. Patient exposure savings by means of optimising the examination length and

dose are probably much less time- and energy-consuming. The current main optimisation paradigm is adapting the acquisition parameters to the actual clinical demand and clinical task [7], that allows for an objective quantification of image quality gain (or loss) with respect to patient exposure, especially when using low-dose protocols. Dose sparing by high Z garments, albeit coming ‘free of charge’, is only to be expected if no other relevant technical or clinical parameter might be optimised, and if no garment is ever placed in the primary field of view, including the over-ranging in CT imaging. The current status of CT technology allows for drastic dose reductions by correctly using the AEC systems and/or increasing the level of iterative reconstruction. For the latter, one should take care as to not finally lose any diagnostic information, especially for low contrast detectability [7]. High Z garments may be used for psychological protection, even if their absolute efficiencies are quite low [31].

References

[1] *Exposure of the Swiss population by radiodiagnostics: 2013 review*, R. Le Coultre, J. Bize, M. Champendal, D. Wittwer, N. Ryckx, A. Aroua, P. Trueb, F. R. Verdun, Radiat Prot Dosimetry. 2016 Jun;169(1-4):221-4.

[2] *Radiation shielding for diagnostic radiology*, C. J. Martin, Radiat Prot Dosimetry. 2015 Jul;165(1-4):376-81.

[3] A model-based approach of scatter dose contributions and efficiency of lead shielding for radiation protection in CT, N. Weber, P. Monnin, C. Elandoy, S. Ding, Phys Med. 2015 Dec;31(8):889-96.

[4] The 2007 Recommendations of the International Commission on Radiological Protection, ICRP Publication 103, March 2007.

[5] *Use of lead shielding on pregnant patients undergoing CT scans: Results of an international survey*, G. R. Iball, D. S. Brettle, Radiography 17 (2011) 102-108.

[6] http://www.impactscan.org/, accessed on 26 Jan. 2017.

[7] *Image quality in CT: From physical measurements to model observers*, F. R. Verdun, D. Racine, J. G. Ott, M. J. Tapiovaara, P. Toroi, F. O. Bochud, W. J. Veldkamp, A. Schegerer, R. W. Bouwman, I. H. Giron, N. W. Marshall, S. Edyvean, Phys Med. 2015 Dec;31(8):823-43.

[8] *Patient doses in CT examinations in Switzerland: implementation of national diagnostic reference levels*, R. Treier, A. Aroua, F. R. Verdun, E. Samara, A. Stuessi, P. R. Trueb, Radiat Prot Dosimetry. 2010 Dec;142(2-4):244-54.

[9] *Radiation Dose to the Fetus from Body MDCT During Early Gestation*, L. M. Hurwitz, T. Yoshizumi, R. E. Reiman, P. C. Goodman, E. K. Paulson, D. P. Frush, G. Toncheva, G. Nguyen, L. Barnes, AJR:186, March 2006.

[10] *Investigation into the effects of lead shielding for fetal dose reduction in CT pulmonary angiography*, G. R. Iball, E. V. Kennedy, D. S. Brettle, Br J Radiol. 2007 Aug; 80(956):631-8.

[11] *Modelling the effect of lead and other materials for shielding of the fetus in CT pulmonary angiography*, G. R. Iball, E. V. Kennedy, D. S. Brettle, Br J Radiol. 2008 Jun;81(966):499-503.

[12] *Lead Apron Shielding for Fetal Dose Reduction during CT Pulmonary Angiography*, J. Palmer, A dissertation submitted to the Department of Physics, University of Surrey, in partial fulfilment of the degree of Master of Science in Radiation and Environmental Protection, September 2008.

[13] *Fetal radiation dose from CT pulmonary angiography in late pregnancy: a phantom study*, S. K. Doshi, I. S. Negus, J. M. Oduko, Br J Radiol. 2008 Aug; 81(968):653-8.

[14] *Imaging for suspected pulmonary embolism in pregnancy—what about the fetal dose? A comprehensive review of the literature*, T. Niemann, G. Nicolas, H. W. Roser, J. Müller-Brand, G. Bongartz, Insights Imaging. 2010 Nov; 1(5-6):361-372.

[15] *Reduction Of Uterus Dose In Clinical Thoracic Computed Tomography*, D. Danova, B. Keil, B. Kästner, J. Wulff, M. Fiebich, K. Zink, K. J. Klose, J. T. Heverhagen, Rofo. 2010 Dec; 182(12):1091-6.

[16] *Use of lead shielding on pregnant patients undergoing CT scans: Results of an international survey*, G. R. Iball, D. S. Brettle, Radiography, May 2011, Volume 17, Issue 2, Pages 102–108.

[17] *Organ and effective dose reduction in adult chest CT using abdominal lead shielding*, G. R. Iball, D. S. Brettle, Br J Radiol. 2011 Nov;84(1007):1020-6.

[18] *Patient and radiographer perspectives of two lead shielding devices for fœtal dose reduction in CT scanning*, G. R. Iball, D. S. Brettle, Radiography, November 2011, Volume 17, Issue 4, Pages 297–303.

[19] *Venous thromboembolism during pregnancy and the postpartum period: incidence, risk factors, and mortality*, A. H. James, M. G. Jamison, L. R. Brancazio, E. R. Myers, Am J Obstet Gynecol. 2006 May;194(5):1311-5.

[20] *Changes in pregnancy mortality ascertainment: United States, 1999-2005*, A. P. MacKay, C. J. Berg, X. Liu, C. Duran, D. L. Hoyert, Obstet Gynecol. 2011 Jul;118(1):104-10.

[21] *Radiation dose reduction at a price: the effectiveness of a male gonadal shield during helical CT scans*, L. T. Dauer, K. A. Casciotta, Y. E. Erdi, L. N. Rothenberg, BMC Med Imaging. 2007 Mar 16; 7:5.

[22] *Radiation dose modulation techniques in the multidetector CT era: from basics to practice*, C. H. Lee, J. M. Goo, H. J. Ye, S. J. Ye, C. M. Park, E. J. Chun, J. G. Im, Radiographics. 2008 Sep-Oct; 28(5):1451-9.

[23] *Overranging at multisection CT: an underestimated source of excess radiation exposure*, A. Schilham, A. J. van der Molen, M. Prokop, H. W. de Jong, Radiographics. 2010 Jul-Aug; 30(4):1057-67.

[24] *Overview, practical tips and potential pitfalls of using automatic exposure control in CT: Siemens Care Dose 4D*, M. Söderberg, Radiat Prot Dosimetry. 2016 Jun; 169(1-4):84-91. doi: 10.1093/rpd/ncv459.

[25] ICRP, 2000. Pregnancy and Medical Radiation. ICRP Publication 84. Ann. ICRP 30.

[26] *Spontaneous adrenal haemorrhage in pregnancy,* A. Anagnostopoulos, S Sharma, BMJ Case Rep 2011 Sep 13; 2011. pii: bcr0720114496. doi: 10.1136/bcr.07.2011.4496.

[27] *MRI: Time Is Dose—and Money and Versatility*, W. A. Edelstein, M. Mahesh, J. A. Carrino, J Am Coll Radiol. 2010 Aug; 7(8): 650–652.

[28] *AAPM Position Statement on the Use of Bismuth Shielding for the Purpose of Dose Reduction in CT scanning*, https://www.aapm.org/publicgeneral/BismuthShielding.pdf, accessed on 07.02.2017.

[29] *Lead versus Bismuth-Antimony Shield for Fetal Dose Reduction at Different Gestational Ages at CT Pulmonary Angiography*, L. C. Chatterson, D. A. Leswick, D. A. Fladeland, M. M. Hunt, S. T. Webster, Radiology: Volume 260: Number 2—August 2011.

[30] *Imaging in Pregnant Patients: Examination Appropriateness*, K. M. Wieseler, P. Bhargava, K. M. Kanal, S. Vaidya, B. K. Stewart, M. K. Dighe, RadioGraphics 2010; 30:1215–1233.

[31] ACR practice guideline for imaging pregnant or potentially pregnant adolescents and women with ionizing radiation, available at

http://www.who.int/tb/advisory_bodies/impact_measurement_taskforce/meetings/prevalence_survey/imaging_pregnant_arc.pdf, accessed on 07.02.2017

Table 1

Authors	Year	Type of examination	Type of study	Type of dosimeter	Comments	Reference uterus/foetal dose	Efficiency
Hurwitz et al.	2006	PA, appendicitis, renal stones	Anthropomorphic phantom	TLD + MOSFET	Uterus dose, no use of garments	Between 240 and 660 µGy	N/A
Iball et al.	2007	PA	Anthropomorphic phantom	Ionisation chamber	Systematic testing of acquisition parameters (kV, mA, scan length, garment position)	Between 60 and 500 µGy	Average: -39.7% kVp: [-33% -47%] (0.7 mmPb) Pitch: [-41% -45%] (0.7 mmPb) Garment posterior: -20% Garment around: -40% mAs: linear dose variation Rotation time: no sign. change Collimation: no sign. change
Iball et al.	2008	PA	Anthropomorphic phantom	Ionisation chamber	Testing of different garment materials, proposal of a predictive irradiation model	Between 30 and 190 µGy	Between -40% and -55%
Palmer	2008	PA	Anthropomorphic phantom	TLD	MSc thesis	~210 µGy	-56% (0.7 mmPb)
Doshi et al.	2008	PA	Anthropomorphic phantom	unknown	-	Between 60 and 230 µGy	mA modulation: -10% High Z garment: -35% 5cm shorter scan length: -56%
Niemann et al.	2010	PA	Literature review	N/A	Uterus dose due to CT and nuclear medicine for pulmonary embolism	Between 13 and 26 µGy (early pregnancy) Between 60 and 100 µGy (late pregnancy)	N/A
Danova et al.	2010	Chest CT	Anthropomorphic phantom	TLD	-	~65 µGy	High Z garment posterior: -26% High Z garment around: -34%
Iball et al.	2010	CT	Worldwide survey	N/A	Questionnaire for radiographers	N/A	N/A
Iball et al.	2011	Chest CT	Anthropomorphic phantom	TLD	Estimated dose savings for multiple organs	N/A	-35%
Iball et al.	2011	Chest CT	Local survey	N/A	Radiographers alternatively playing the role of the patient	N/A	N/A
Weber et al.	2015	CT	CTDI phantom	TLD	Decomposition of the scatter components	N/A	N/A

Table 2

Parameters	Length [cm]	Uterus dose [µGy]	Dose reduction	Dose reduction in literature due to high Z garment
$CTDI_{vol}$: 10.4 mGy Tension: 120 kV Current: 200 mA Pitch: 1.375 Rotation: 0.75 s Collimation: 40 mm	32	39	-	Between -20% and -56%
	31 (top)	39	0 %	
	29 (bottom)	22	-24 %	

Table 3

Parameters	Length [cm]	Uterus dose [mGy]	Dose reduction	Dose reduction in literature due to high Z garment
$CTDI_{vol}$: 10.4 mGy Tension: 120 kV Current: 200 mA Pitch: 1.375 Rotation: 0.75 s Collimation: 40 mm	24.5	1.9	-	N/A
	23.5	1.5	-21 %	
	22.5	1.2	-37 %	
	21.5	1.0	-47 %	

Figure 1

Click here to download high resolution image

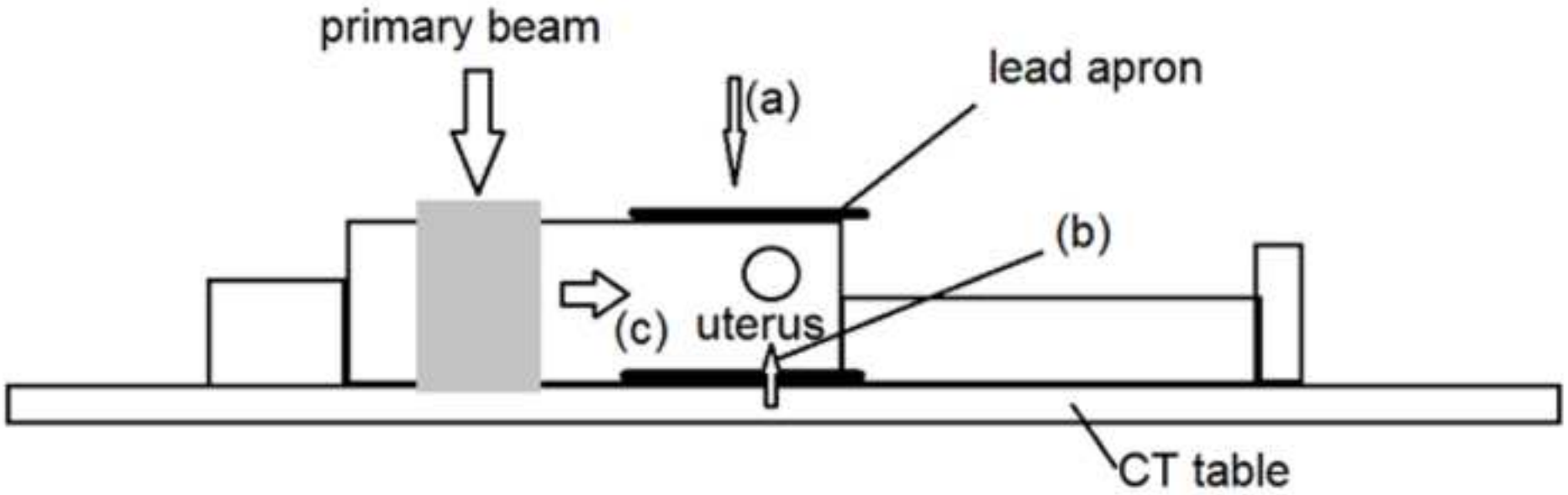

Figure 2

Click here to download high resolution image

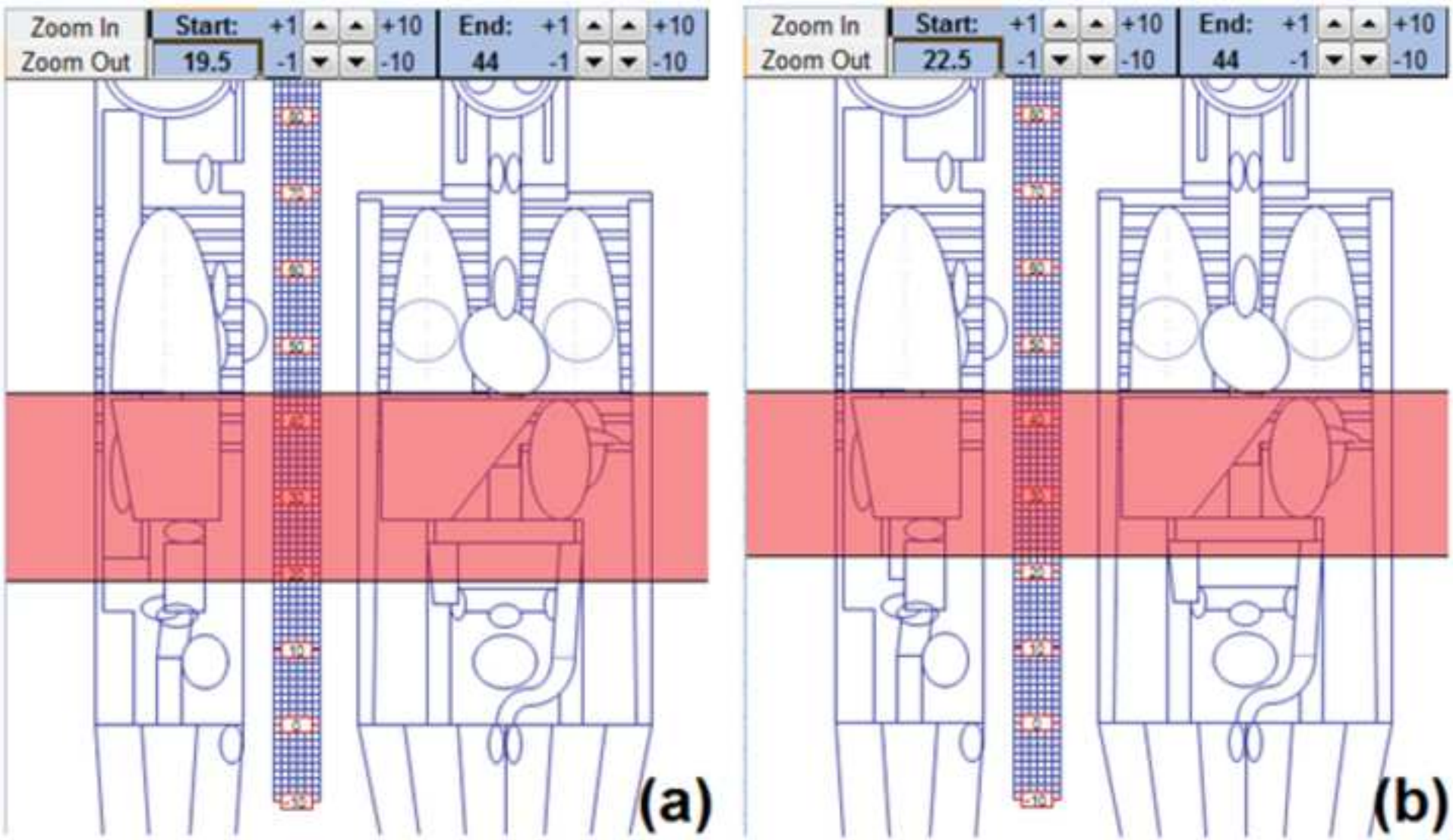

Figure 3

Click here to download high resolution image

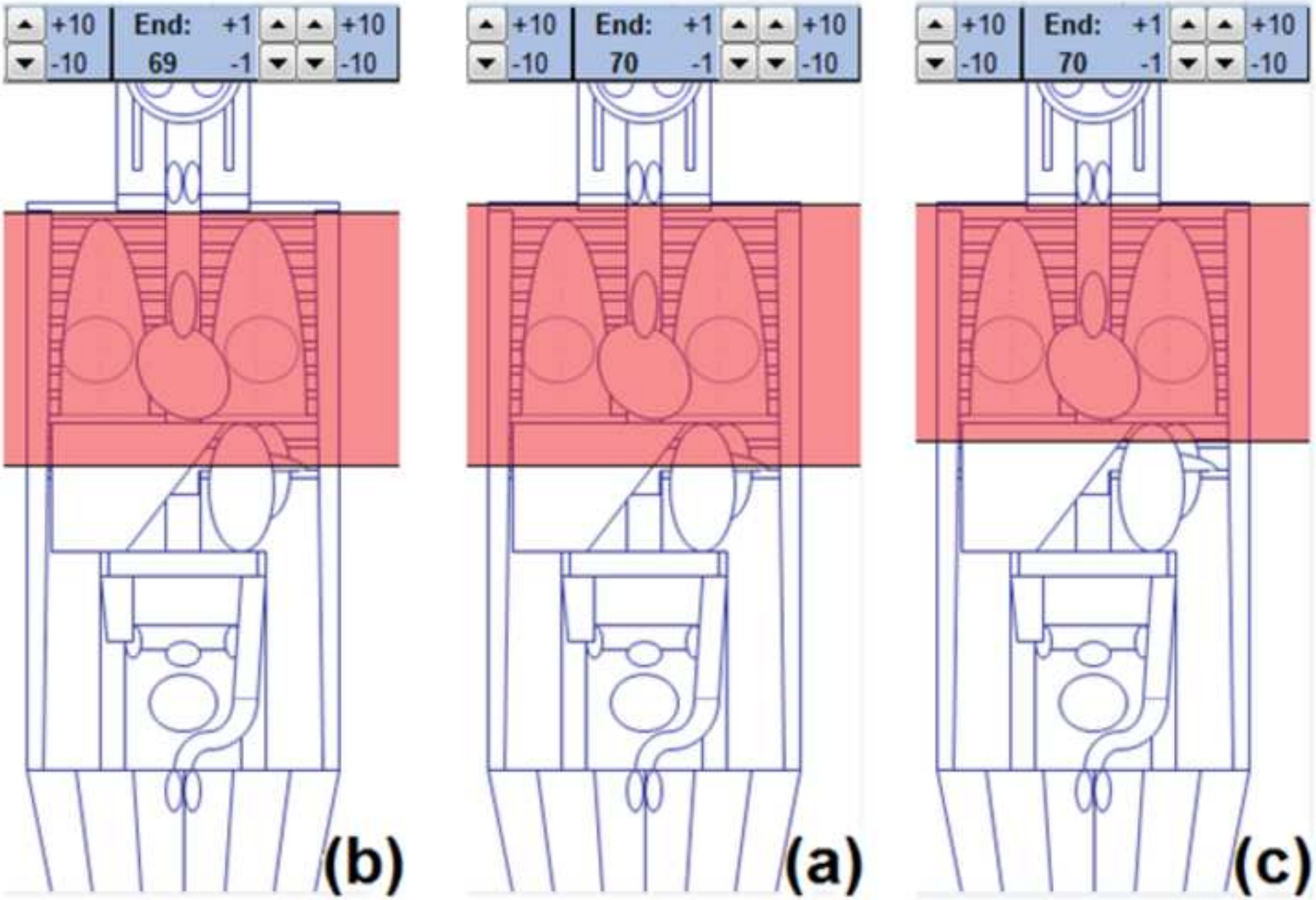

Table and figure captions

Table 1: Papers published in the literature, addressing the potential uterine doses and dose reductions due to CT examinations.

Table 2: Technical parameters simulated for the chest CT examination.

Table 3: Technical parameters simulated for the upper abdomen CT examination.

Figure 1: Schematic depiction of the components of scatter for a chest CT examination using a high Z garment wrapped around the patient's waist. a) External scatter/leakage radiation, b) backscatter from the x-ray table, c) internal scatter.

Figure 2: Screenshot of the ImPACT GUI for upper abdomen CT. (a) acquisition volume before scan length reduction, (b) acquisition volume after reducing the scan length by 3 cm under the liver.

Figure 3: Screenshot of the ImPACT GUI for chest CT. (a) acquisition volume before scan length reduction, (b) acquisition volume after reducing the scan length by 1 cm above the lung apex, (c) acquisition volume after reducing the scan length by 3 cm under the lung base.

Radioprotection
© EDP Sciences 2016
DOI: 10.1051/radiopro/2016024

Disponible en ligne :
www.radioprotection.org

ARTICLE

Irradiation du personnel en neuroradiologie interventionnelle pédiatrique : focus sur le cristallin de l'opérateur

C. Bolomey[1], G. Fasel[1], N. Ryckx[2] et R. Le Coultre[1]*

[1] Haute École de Santé Vaud (HESAV), Haute École Spécialisée de Suisse Occidentale (HES-SO), Lausanne, Suisse.
[2] Institut de Radiophysique (IRA), Centre Hospitalier Universitaire Vaudois (CHUV), Lausanne, Suisse.

Reçu le 30 décembre 2015 – Accepté le 7 juin 2016

Résumé – Précédemment fixée à 150 mSv an^{-1}, la CIPR recommande dorénavant de limiter la dose équivalente au cristallin à 20 mSv an^{-1}. En neuroradiologie interventionnelle pédiatrique, l'irradiation du cristallin de l'opérateur peut être majorée par l'utilisation d'un système de radioscopie biplan et par la plus grande proximité du médecin avec le patient. En pratique, l'efficacité des lunettes plombées dépend de nombreux facteurs. La présente étude traite ces deux aspects. Premièrement, la dose au cristallin d'un neuroradiologue a été mesurée, durant 12 interventions, à l'aide de 36 TLD placés sur son bonnet chirurgical. Dans un deuxième temps, en vue de déterminer l'efficacité des lunettes plombées, des mesures ont été effectuées en reproduisant les conditions cliniques. Un détecteur a été placé sur l'œil gauche d'un fantôme représentant l'opérateur. Quatre paires de lunettes plombées ont été sélectionnées en vue de tester différents paramètres. Pour les 12 interventions, un équivalent de dose individuel Hp(0,07) de 457 μSv pour le cristallin côté tube a été obtenu. Cette étude démontre un ratio dose au cristallin / PDS 5 fois plus élevé que lors d'interventions réalisées chez des patients adultes. La dose au cristallin peut être réduite d'environ un facteur 3 avec l'utilisation de lunettes plombées adaptées. Le modèle de lunettes le plus couvrant atténue jusqu'à 50 % de plus qu'un modèle moins couvrant. L'ajout d'une protection latérale permet d'augmenter l'atténuation jusqu'à 13 % comparé au même modèle sans protection latérale.

Abstract – Staff exposure in pediatric interventional neuroradiology: focus on the operator's eye lens. Previously at 150 mSv year^{-1}, the ICRP now recommends limiting the equivalent dose to the eye lens to 20 mSv year^{-1}. For pediatric interventional neuroradiology, the exposure of the operator's eye lens may be increased by the use of a biplane fluoroscopy system and by the proximity of the physician to the patient. In practice, the efficiency of leaded glasses depends on many factors. This study addresses both aspects. First, the eye lens dose of a neuroradiologist was measured during 12 procedures using 36 TLDs placed on his surgical cap. Secondly, in order to determine the efficiency of leaded glasses, measurements were carried out by reproducing the clinical conditions. A detector was placed on the left eye of a phantom representing the operator. Four pairs of leaded glasses were selected to test various parameters. During the 12 procedures, an individual dose equivalent Hp(0.07) of 457 μSv was obtained for the eye lens closest to the tube. This study shows an eye lens dose to DAP ratio 5 times higher than for procedures performed on adult patients. The eye lens dose might be reduced by a factor of approximately 3 with the use of appropriate leaded glasses. The eyewear model with the most coverage reduces the dose by up to 50% more than the model with the least coverage. The addition of lateral protection increases the attenuation by up to 13% compared with the same model without side protection.

Keywords: radiation protection / leaded glasses / radioscopy / eye lens dose / neuroradiology / pediatrics

1 Introduction

Anciennement de 150 mSv an^{-1}, la Commission internationale de protection radiologique (CIPR) recommande dorénavant de limiter la dose équivalente au cristallin à 20 mSv an^{-1}. Cette modification conduit à de nombreuses préoccupations concernant l'irradiation du cristallin du personnel médical. Alors que leur efficacité est clairement démontrée, le port de lunettes plombées n'est pourtant pas suffisamment appliqué en routine. L'étude ORAMED met ainsi en évidence que 24 % des opérateurs considérés sont susceptibles de dépasser la nouvelle limite de 20 mSv an^{-1}. De plus, seuls 31 %

* regis.lecoultre@hesav.ch

des opérateurs en radiologie interventionnelle portent systématiquement des lunettes de protection (Vanhavere *et al.*, 2012).

En radiologie interventionnelle pédiatrique, l'exposition de l'opérateur peut être d'autant plus conséquente du fait de l'utilisation fréquente d'un système de radioscopie biplan et de la plus grande proximité du médecin avec le patient (Vaño *et al.*, 2009).

En radioprotection, l'efficacité des différents moyens de protection dépend de nombreux paramètres. Pour l'exposition du cristallin, le choix du modèle de lunettes plombées utilisées influence grandement sa protection et devrait être effectué de manière éclairée.

Cette étude porte sur ces deux thématiques intrinsèquement liées. Tout d'abord, la dose au cristallin d'un neuroradiologue exerçant en pédiatrie a été mesurée au moyen de dosimètres thermoluminescents (TLD) placés à différents endroits sur un bonnet chirurgical, mesurant ainsi l'exposition du cristallin en l'absence de lunettes de protection. Ce praticien utilisant systématiquement des lunettes plombées, il a également été choisi de se pencher sur l'efficacité de ces dernières ainsi que les différents paramètres d'influence. Pour ce faire, quatre paires différentes ont été évaluées en reproduisant les conditions cliniques observées durant la première partie de l'étude.

L'apport aux travaux existants de cette étude est l'articulation dans un contexte clinque bien délimité de la problématique de l'évaluation de la dose au cristallin conjuguée avec la problématique de l'efficacité des lunettes plombée portées en pratique. Les résultats présentés ne remettent nullement en cause les connaissances amenées par les travaux existants, mais vise à apporter un éclairage du terrain, une étude de cas, de la complexité inhérente aux situations de travail rencontrées en radiologie interventionnelle.

2 Matériel et méthode

2.1 Mesure de la dose au cristallin

Pour ces mesures, 36 détecteurs thermo-luminescentes (TLD) de type LiF :Mg,Cu,P (MCP-N, TLD Poland, Pologne, http://www.tld.com.pl/tld/mcpns.html) ont été répartis sur un bonnet chirurgical. Ils ont été placés à raison de 12 dosimètres positionnés respectivement au niveau de l'œil gauche, au centre et au niveau de l'œil droit de l'opérateur (Figure 1). Ce dernier a porté le bonnet muni des détecteurs pendant 12 interventions de neuroradiologie pédiatrique.

Sur les 12 interventions, 10 ont été réalisées sur un système biplan et 2 sur un système monoplan. Le produit dose-surface (PDS) de chaque intervention a été relevé directement sur l'installation de radioscopie. L'installation a été utilisée selon les réglages standards utilisés en neuroradiologie interventionnelle pédiatrique dans l'institution. La modulation automatique de dose (AEC, automatic exposure control) contrôlait le débit au patient – et ainsi le PDS – tout au long de la procédure. Les PDS ont été relevés tels qu'indiqué par l'installation de radioscopie. L'étalonnage du système de mesure du PDS de l'installation a été effectué conformément à la législation en vigueur.

Les TLD nécessitant d'être lus relativement rapidement après la première irradiation, les 12 interventions ont été fractionnées en 3 mesures, comprenant chacune 4 interventions. Les dosimètres ont été utilisés sur une période maximale de 6 semaines entre l'étalonnage et la lecture. La lecture des dosimètres par l'Institut de Radiophysique de Lausanne sur un lecteur Harshaw s'est effectuée au moins 24 h après la dernière irradiation, mais dans le mois qui l'a suivie, permettant ainsi à la réponse de se stabiliser ainsi qu'il est d'usage pour la dosimétrie TLD. Il faut noter qu'il est également important de procéder à une lecture rapide des TLD MCP suite à leur « mise à zéro » afin d'éviter que les faibles doses mesurées ne soient cachées par l'incertitude sur le bruit de fond. L'étalonnage de la chaîne de lecture des TLD est traçable à un étalon primaire selon la législation suisse en vigueur. La réponse des TLD est exprimée en termes de Hp(0,07), leur étalonnage initial effectué au Co-60 étant corrigé par un facteur correspondant à un champ de rayonnement X d'énergie moyenne inférieure à 100 keV. Un étalonnage en termes de Hp(3) plutôt que Hp(0,07) aurait probablement été plus adéquat, mais l'institut en question n'offre pour l'heure pas encore cette possibilité. L'utilisation du Hp(0,07) à la place du Hp(3) reste toutefois acceptable dans les conditions de mesure de la radiologie interventionnelle comme démontré dans l'étude ORAMED (Vanhavere *et al.*, 2012).

Dans la suite de l'article, la dénomination suivante est utilisée : mesure 1 = interventions 1–4 ; mesure 2 = interventions 5–8 ; mesure 3 = interventions 9–12.

2.2 Efficacité des lunettes plombées

Les mesures d'efficacité des lunettes plombées ont été réalisées en reproduisant les conditions cliniques observées durant la mesure de la dose au cristallin. À partir de données relevées durant les interventions, la position et l'angulation des tubes, la hauteur de la table d'examen ainsi que les différents paramètres d'acquisitions ont alors été déterminés. Un dosimètre électronique (Unfors NED, http://www.rosalina.in/Unfors/ned_sensorchar.pdf) étalonné en termes de Hp(0,07), deux fantômes anthropomorphes adultes représentant respectivement le patient et l'opérateur ainsi que quatre différentes paires de lunettes plombées ont été utilisés. Afin d'être conservatif, c'est donc un fantôme de tête anthropomorphe adulte qui a été utilisé pour simuler le diffusé généré par un patient pédiatrique, le crâne atteignant assez rapidement son diamètre de l'âge adulte. Le dosimètre Unfors NED n'était, lui, pas rattaché à une chaîne métrologique conformément à la législation en vigueur. Néanmoins, un étalonnage en conditions contrôlées par le même institut ayant fourni les TLD a permis de vérifier la stabilité ainsi que la reproductibilité des mesures. Les résultats étant indiqués en valeurs relatives, les facteurs d'étalonnage se simplifient dans les équations.

Les lunettes ont été choisies afin de tester différents paramètres pouvant influencer leur efficacité. Il a été montré que la surface couverte par les lunettes plombées jouait un rôle important dans la protection du cristallin. De même, l'efficacité des lunettes plombées est fortement influencée par l'orientation de la tête de l'opérateur par rapport à la source de rayonnement diffusé. En effet, l'angle entre l'opérateur et la source

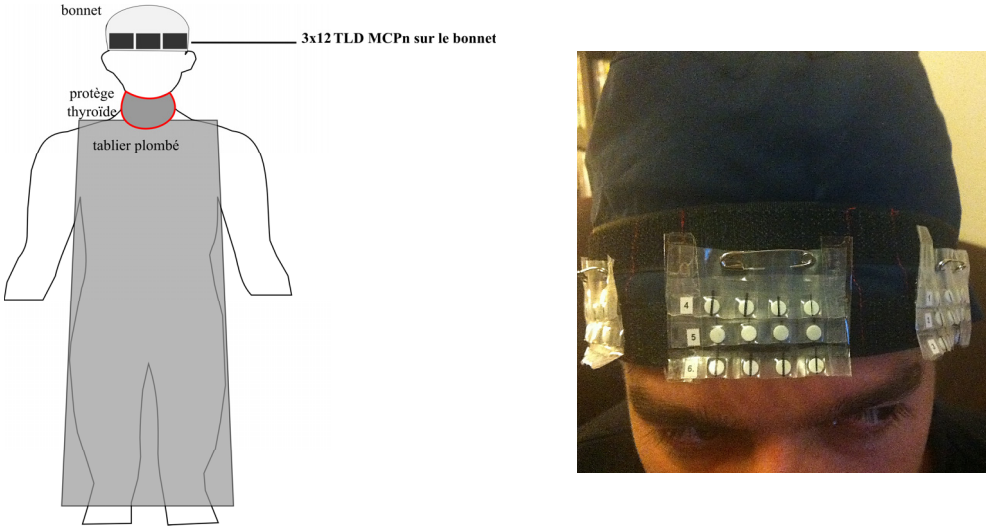

Figure 1. Répartition et disposition des différents dosimètres.
Distribution and position of different dosimeters.

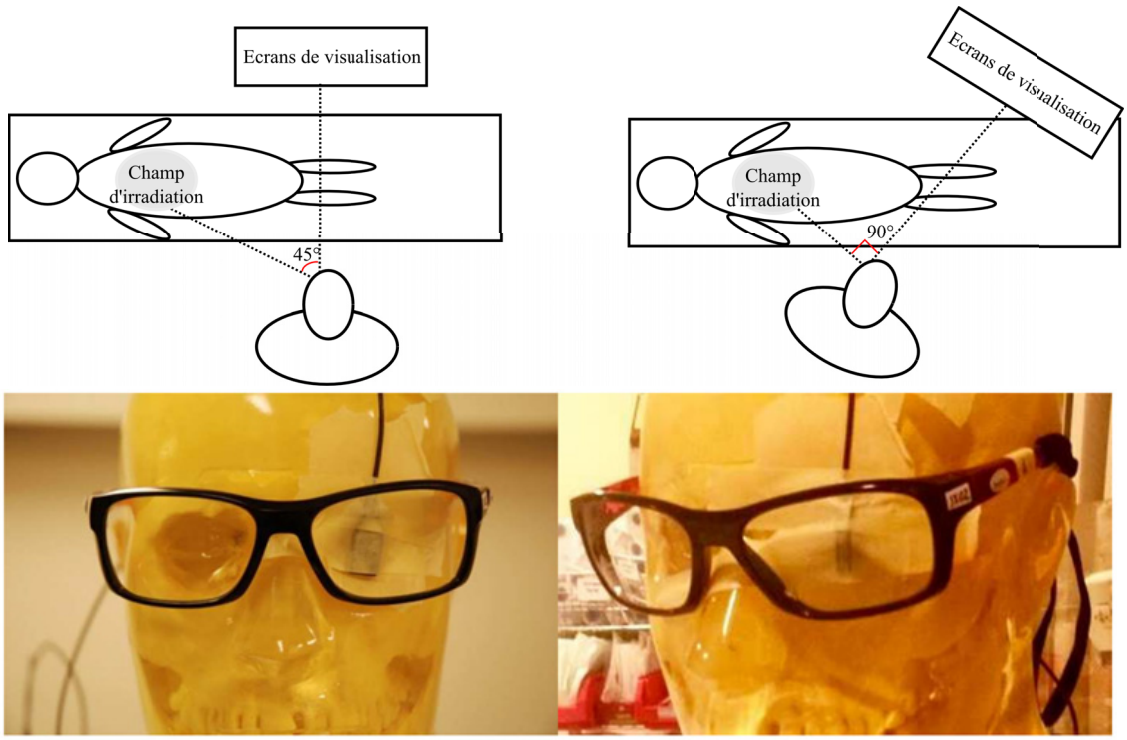

Figure 2. Orientation de l'opérateur par rapport à la source de rayonnement diffusé.
Operator orientation with respect to the source of scattered radiation.

de rayonnement diffusé peut varier de 45° à 90° en fonction du type d'intervention ou de la taille du patient (Figure 2). À 90°, le modèle le moins couvrant présente un facteur d'atténuation du rayonnement diffusé de 1,4 par rapport aux deux autres modèles testés, qui présentent respectivement des facteurs de 2,6 et 3,9 selon les paires de lunettes (Sturchio *et al.*, 2013).

L'Agence Internationale de l'Énergie Atomique mentionne également que la surface couverte par les lunettes plombées est un facteur important et que les conditions d'irradiation, ainsi que l'orientation par rapport à l'opérateur, doivent être prises en compte dans le choix des lunettes de protection (IAEA, 2013).

À partir de ces données, il a été choisi de comparer un modèle standard avec un modèle plus couvrant afin de mettre en évidence la contribution de la surface des verres dans la protection du cristallin.

Afin de connaître l'apport réel d'une protection latérale, deux lunettes d'un même modèle ont été testées, équipées ou non d'une protection latérale de 0,5 mm d'équivalent de plomb (mmEqPb).

Tableau 1. Caractéristiques des lunettes sélectionnées.
Characteristics of the selected glasses.

Lunettes n°	Modèle	Épaisseur EqPb [mmEqPb]	Protection latérale	Surface max. du verre [cm^2]	Image
1	Sport	0,75	Oui (05 mmPb)	18	
2	Sport	0,75	Non	18	
3	Classique	0,5	Non	21	
4	Classique	0,75	Non	21	

Tableau 2. PDS et Kerma air cumulé des 12 interventions.
DAP and cumulative air Kerma of 12 procedures.

Intervention	PDS cumulé [mGy cm^2]	Kerma air cumulé tube frontal [mGy]	Kerma air cumulé tube latéral [mGy]	Kerma air cumulé [mGy] *Système monoplan*
1	27 964			331,7
2	21 787	258,3	71,7	
3	22 288	236,6	98,2	
4	18 367	250,2	78,5	
5	50 641			482,8
6	15 673	191,3	76,8	
7	52 290	351,2	151,8	
8	42 675	477,8	125,3	
9	70 122	512,7	261,6	
10	26 282	222,8	114,0	
11	26 805	101,7	111,4	
12	24 987	222,7	134,3	

En effet, l'épaisseur d'équivalent de plomb n'est pas un paramètre fiable à des fins d'estimation d'efficacité des lunettes plombées, notamment à cause de l'importante contribution du rétrodiffusé ainsi que des potentiels rayons non atténués arrivant par le côté participant à l'irradiation du cristallin (Sturchio *et al.*, 2013). De ce fait, il a été décidé de tester ce paramètre en utilisant deux paires de lunettes similaires, mais présentant une fois 0,5 mmEqPb et une fois 0,75 mmEqPb. Le choix des lunettes s'est donc effectué selon plusieurs critères distincts : l'influence de la surface protectrice, la contribution d'une protection latérale et l'influence de l'épaisseur d'équivalent de plomb des verres.

Les 4 paires de lunettes choisies ont été fournies par la société Scanflex-SIRAD :

- 2 paires de lunettes du modèle « spor » Ultralite 9941 (Protech, USA) avec et sans protection latérale. La protection latérale est composée 'une petite plaque 'une épaisseur de 0,5 mmEqPb.
- 2 autres paires de lunettes du modèle « classiqu » Sx-0.5 et Sx-0.75 (APX, France) avec 0,5 et 0,75 mmEqPb.

Le Tableau 1 liste les différentes paires lunettes utilisées pour cette étude, les numéros par lesquelles elles sont identifiées dans la suite du document ainsi que leurs caractéristiques.

Pour commencer, la paire de lunettes n° 1 a été placée sur le fantôme anthropomorphe représentant l'opérateur. Le patient simulé a été irradié, en mode graphie, jusqu'à obtenir 450 μSv au niveau de l'œil gauche de l'opérateur. Le temps d'exposition nécessaire a été relevé, puis l'opération a été répétée avec les 3 autres paires de lunettes, en utilisant strictement les mêmes conditions d'irradiation. C'est le temps d'irradiation qui a servi de référence.

L'efficacité des lunettes plombées a été testée pour des acquisitions avec le tube frontal et latéral séparément, ainsi que pour une acquisition réalisée en biplan. Chaque mesure a été réalisée pour les deux orientations de la tête de l'opérateur, à 45° et 90° par rapport à la source.

Chaque mesure a été réalisée deux fois et l'atténuation des lunettes plombées a été calculée par le rapport des doses avec et sans protection plombée. Le résultat final a été déterminé par les valeurs obtenues moyennées sur les deux mesures. L'exposition du cristallin est exprimée en normalisant la dose cumulée par le PDS du patient et exprimé en μSv/(Gy cm^2), un rapport utilisé de manière standard en radiologie interventionnelle et nommé facteur d'exposition (Schueler *et al.*, 2006).

3 Résultats

3.1 Mesure de la dose au cristallin

La moyenne des résultats des trois différentes mesures a premièrement été effectuée. Le PDS cumulé des différentes interventions est résumé dans le Tableau 2. Le Tableau 3 présente les moyennes des équivalents de dose individuelle Hp(0,07) des différentes mesures des yeux en fonction de leur localisation ainsi que les facteurs d'exposition obtenus en divisant

Tableau 3. Moyenne des équivalents de dose individuel Hp(0,07) au niveau des yeux en fonction de la localisation des TLD, ainsi que les facteurs d'exposition du cristallin obtenus en divisant le cumul de dose TLD par le cumul de PDS des trois groupes d'interventions tels que listés dans le Tableau 2. L'incertitude élargie ($k = 2$) liée au TLD s'élève à 11 %.
Average individual dose equivalents Hp(0.07) of the eyes as a function of the location of the TLDs, and the eye lens exposure factors obtained by dividing the cumulative TLD doses by the respective cumulative DAP of the three groups of procedures, as listed in Table 2. The expanded uncertainty ($k = 2$) related to the TLD is 11%.

Emplacement des TLD	Mesure n°	Moyenne Hp(0,07) [μSv] (CI 95 %)	Facteur d'exposition [μSv/(Gy cm^2)]
Gauche	1	141 ± 7 (136, 146)	12
	2	134 ± 8 (129, 139)	12
	3	218 ± 10 (212, 224)	19
Centre	1	127 ± 7 (123, 131)	0,8
	2	115 ± 9 (109, 121)	0,7
	3	178 ± 12 (171, 185)	11
Droite	1	51 ± 16 (41, 61)	0,3
	2	28 ± 9 (22, 34)	0,2
	3	37 ± 8 (32, 42)	0,2
Moy. gauche		457 ± 27	12
Moy. droite		268 ± 30	0,6

le cumul de Hp(0,07) des trois groupes d'interventions par le cumul des PDS des interventions résumées dans le Tableau 2.

En vue d'estimer la dose reçue par le cristallin de l'œil gauche, une moyenne des valeurs des TLD placés sur la gauche avec ceux placés au centre a été effectuée. Pour le cristallin de l'œil droit, c'est la moyenne des TLD placés à droite avec ceux du centre qui a été effectuée.

La dose totale au cristallin a ensuite été déterminée par la somme des moyennes des trois mesures. L'équivalent de dose individuelle Hp(0,07) obtenu est de 457 ± 27 μSv pour l'œil gauche et de 268 ± 30 μSv pour l'œil droit.

3.2 Efficacité des lunettes plombées

Afin de pallier une exposition du cristallin potentiellement élevée au cours d'une carrière, la protection offerte par des lunettes plombées est un atout non négligeable en neuroradiologie interventionnelle. Ainsi, les résultats des mesures concernant l'évaluation de l'efficacité des différentes paires de lunettes plombées sont indiqués dans le Tableau 4 selon l'orientation de la tête de l'opérateur, pour chaque paire de lunettes ainsi que vous chaque tube utilisé (tube frontal, latéral et biplan).

4 Discussion

4.1 Mesure de la dose au cristallin

4.1.1 Dose par intervention et « spécificité » des interventions pédiatriques

Il a été obtenu respectivement 38 ± 2 μSv par procédure pour l'œil côté tube et 22 ± 3 μSv par procédure pour l'œil opposé. Ces valeurs représentent une irradiation du cristallin sans lunettes plombées mais avec l'utilisation de moyens de protection structurels (écran mobile 0,5 mmEqPb, tablier0,5 mmEqPb et protège thyroïde 0,5 mmEqPb). Sur un total de 104 procédures pédiatriques effectuées en 2014 sur cette installation, cela équivaudrait à un total théorique de 4,0 mSv an^{-1} pour l'œil côté tube et 2,3 mSv an^{-1} pour l'œil opposé pour la seule neuroradiologie pédiatrique.

Les interventions pédiatriques peuvent être considérées comme étant plus irradiantes que les interventions chez les adultes, notamment à cause de l'utilisation d'une installation de radioscopie biplan et de la proximité de l'opérateur vis-à-vis de la source, la moyenne d'âge des patients étant de 3 ans pour cette étude (*i.e.* le patient). Cependant, la procédure étudiée requérait une durée d'irradiation relativement faible, s'expliquant par le fait qu'elle est réalisée fréquemment dans cet établissement hospitalier et que les patients ne présentent pas, en règle générale, de comorbidité associée.

Pour une procédure pédiatrique fréquente, l'opérateur reçoit 38 μSv à son œil situé du côté tube, ce qui correspond aux résultats délivrés dans l'étude ORAMED, réalisée chez des patients adultes (40 μSv pour des procédures de type angiographie cérébrale).

Le PDS de chaque intervention a été relevé durant la récolte de données. Une comparaison entre le PDS moyen des interventions pédiatriques avec les valeurs publiées dans le rapport ORAMED montre que la dose au cristallin côté tube est similaire alors que le PDS des interventions pédiatriques est 5 fois plus faible. En effet, pour les angiographies cérébrales, le PDS moyen mesuré durant l'étude ORAMED est de 126 Gy cm^2 (Vanhavere *et al.*, 2012) alors que, dans cette étude, le PDS moyen de l'ensemble des interventions pédiatriques d'une année s'élève à 29 Gy cm^2 par procédure.

4.1.2 Différence entre les deux yeux

Dans cette situation, qui est similaire à ce qui peut se retrouver dans la littérature, les tubes RX se trouvent sur la gauche de l'opérateur. Une différence importante est constatée entre la dose mesurée à l'œil côté tube (œil gauche) par rapport à l'autre œil.

Tableau 4. Atténuation des lunettes plombées en fonction de l'orientation de l'opérateur et du tube utilisé.
Attenuation of the leaded glasses as a function of the operator's orientation and the tube used.

Atténuation en fonction de l'orientation de la tête de l'opérateur					
Tube utilisé	**Lunettes n°**	**Moyenne [%]**		**Écart type [%]**	
		90°	**45°**	**90°**	**45°**
Frontal	1	85	118	0,8	0,4
	2	4,0	107	29	0,6
	3	398	237	0,2	19
	4	536	284	0,7	12
Latéral	1	434	618	0,1	0,2
	2	319	521	0,5	0,1
	3	69,0	669	0,1	0,3
	4	749	674	0,1	0,1
Biplan	1	235	346	0,2	0,6
	2	139	234	0,9	0,3
	3	522	448	0,5	0,5
	4	631	436	0,1	0,6

Selon Chong *et al.* (2000), la raison d'une telle différence réside dans l'orientation de la tête de l'opérateur selon la disposition des écrans de visualisations.

Il est intéressant de noter que la différence entre les deux yeux mériterait d'être prise en compte dans l'estimation de la dose reçue par le cristallin. Il serait alors conservatif de considérer prioritairement l'œil côté tube.

4.1.3 Facteurs d'exposition Hp(0,07)/PDS

Le calcul des facteurs d'exposition (rapport entre Hp(0,07) mesurée au niveau du cristallin [μSv] et le PDS de l'intervention [Gy cm^2], Schueler *et al.*, 2006) met également en évidence une différence entre l'œil côté tube (gauche) et l'œil opposé, qui est due à la différence de dose mesurée au niveau des deux yeux. Le facteur pour l'œil gauche s'élève à 1,2 μSv/(Gy cm^2) contre 0,7 μSv/(Gy cm^2) pour l'œil droit. Rappelons que ces facteurs d'exposition sont représentatifs d'une situation dans laquelle l'opérateur ne porte pas de lunettes plombées mais utilise un écran de protection latéral. En multipliant ces facteurs d'exposition par le PDS moyen de 29 Gy cm^2 par intervention pour les 104 interventions pédiatriques en 2014, nous obtenons respectivement 3,6 et 1,8 mSv an^{-1} pour l'œil gauche et droite, donc à peu près les mêmes résultats qu'à la Section 4.1.1.

Ces résultats sont corroborés par ceux utilisés par l'IAEA. En effet, cette dernière préconise un facteur de conversion de 1 μSv/(Gy cm^2) dans une situation similaire à cette étude (avec écran latéral et sans lunettes plombées). Sans moyen de protection, l'IAEA préconise un facteur de 10 μSv/(Gy cm^2), ce qui démontre l'importance de l'utilisation de l'ensemble des moyens de protection.

4.2 Efficacité des lunettes plombées

Après avoir mesuré la dose au cristallin durant les interventions, il est intéressant de se pencher sur l'efficacité des lunettes plombées. L'étude ORAMED souligne que seuls 31 % des opérateurs en radiologie interventionnelle portent systématiquement des lunettes de protection. De ce fait, il est important de pouvoir quantifier leur efficacité. Un équivalent de dose au cristallin de 4 mSv an^{-1} est certes faible, mais elle ne résulte que des examens pédiatriques, qui représentent seulement une faible proportion de l'activité habituelle d'un clinicien.

Dans les chapitres précédents, une variabilité de dose relativement importante est constatée entre les deux yeux. Notons ici que, pour l'évaluation de l'efficacité des lunettes plombées, le détecteur a été placé sur l'œil du fantôme anthropomorphe côté tube. Les conclusions développées dans les chapitres suivants sont donc conservatives et valables uniquement pour l'œil côté tube. Il est toutefois probable que l'efficacité des lunettes plombées ne sera pas identique entre l'œil côté tube et l'œil opposé. Afin de diminuer le temps d'exposition nécessaire pour les mesures, l'écran de protection latéral n'a pas été utilisé.

4.2.1 Contribution de l'épaisseur d'équivalent de plomb

Afin d'évaluer la contribution de l'épaisseur d'équivalent de plomb, la comparaison de l'efficacité a été effectuée avec les lunettes n° 2, modèle sport possédant 0,75 mmEqPb et n° 3, modèle classique possédant 0,5 mmEqPb. Les résultats démontrent que la paire de lunettes n° 3 (modèle classique) est plus efficace que la n° 2 (modèle sport), alors qu'elle possède une plus faible épaisseur d'équivalent de plomb. En effet, pour le tube frontal, la paire n° 3 atténue le rayonnement incident de 39,8 ± 2 % (tête à 90°) contre 4,0 ± 2,9 %. Pour le tube latéral et les deux tubes en simultané, c'est respectivement 69,0 ± 0.1 % (contre 31,9 ± 0,5 % pour la paire n° 2) et 52,2 ± 0,5 % (contre 13,9 ± 0,9 %) de réduction en dose. La tendance est similaire, quoique moins marquée, pour la tête orientée à 45°. Ceci confirme l'hypothèse stipulant que l'épaisseur d'équivalent de plomb n'est pas considérée comme un bon indicateur en vue de déterminer l'efficacité d'un modèle de lunettes plombées (Figure 3).

Dès lors, il s'avérait intéressant de savoir si augmenter l'épaisseur d'équivalent de plomb dans un même modèle de lunettes augmenterait leur efficacité. Pour ce faire, une comparaison a été faite avec les lunettes n° 3 et 4, toutes deux

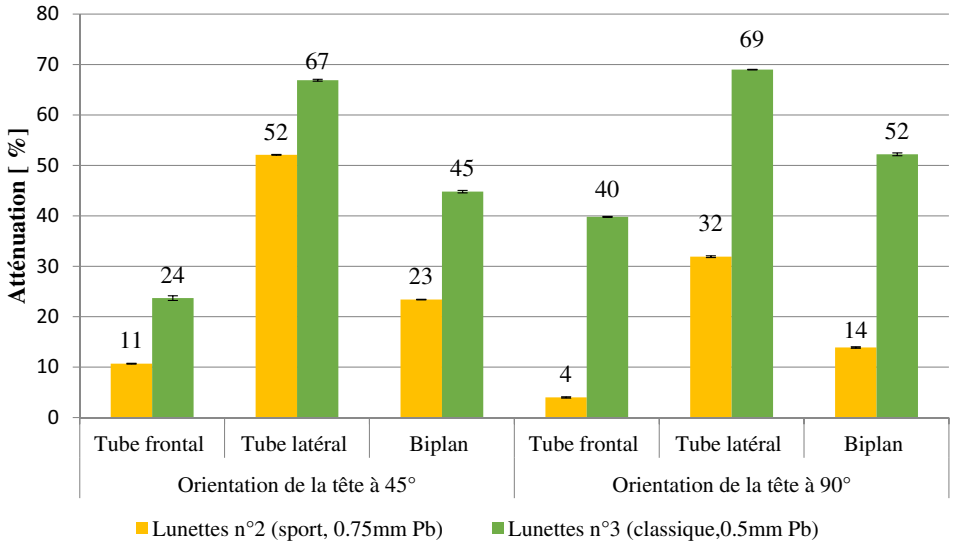

Figure 3. Influence de la différence des épaisseurs d'équivalent de plomb.
Influence of the different lead equivalent thicknesses.

du modèle classique mais possédant respectivement 0,5 et 0,75 mmEqPb. Les résultats démontrent que les lunettes possédant 0,75 mmEqPb protègent davantage le cristallin lorsque la tête de l'opérateur est positionnée à 90° , orientation prépondérante pour les interventions pédiatriques, notamment à cause de la proximité de l'opérateur avec le patient. En effet, pour les tubes frontal, latéral et pour les deux tubes combinés, la protection offerte par la paire n° 4 est de respectivement 53,6 ± 0,7 % (contre 39,8 ± 0,2 % pour la paire n° 3), 74,9 ± 0,1 % (contre 69,0 ± 0,1 %) et 63,1 ± 0,1 % (contre 52,2 ± 0,5 %). À 45°, l'épaisseur d'équivalent de plomb n'a par contre pas d'influence majeure sur l'efficacité des lunettes.

4.2.2 Contribution de la protection latérale

Les deux paires de lunettes du modèle sport (lunettes n° 1 et 2) ont été testées, mais une seule possédait une protection latérale (lunettes n° 1). La contribution de cette dernière est clairement démontrée. En effet, la protection offerte pour la tête à 90° et les tube frontal, latéral et les deux tubes combinées, est de respectivement 8,5 ± 0,5 % pour la paire n° 1 (contre 4,0 ± 2,9 % pour la paire n° 2), 43,4 ± 0,1 % (contre 31,9 ± 0,5 %) et 23,5 ± 0,2 % (contre 13,9 ± 0,9 %). Lorsque le tube frontal est utilisé, la différence d'efficacité est plus marquée à 90° qu'à 45° . La lunette munie d'une protection latérale est ainsi plus efficace dans toutes les situations. Ces résultats démontrent que l'ajout d'une protection latérale sur la monture est bénéfique. En effet, le gain d'atténuation peut aller jusqu'à 13 % pour le modèle possédant une protection latérale.

4.2.3 Contribution de la surface couverte

Formellement, c'est davantage l'angle solide couvert entre le centre du cristallin et les bords du verre qui joue un grand rôle dans la radioprotection. Nous ferons cependant l'hypothèse que la distance entre les verres et le cristallin est identique entre les différents modèles. C'est donc la surface du verre qui sera déterminante pour la suite de l'évaluation. Les deux modèles qui ont été testés présentent une légère différence au niveau de la surface maximale du verre. En effet, le modèle sport possède des verres de 18 cm^2 alors que ceux du modèle classique sont de 21 cm^2. Notons tout de même que ces valeurs sont approximatives les verres ayant été considérés comme rectangulaires pour simplifier l'estimation de leur surface. Par conséquent, le modèle « classique » (lunettes n° 3 et 4) couvre d'avantage l'œil que le modèle « sport » (lunettes n° 1 et 2). L'importance de la surface couverte est bien démontrée. Les lunettes les plus couvrantes sont plus efficaces dans toutes les situations. La Figure 4 compare le modèle sans protection latérale avec le modèle plus couvrant possédant la même épaisseur d'équivalent de plomb. Il est possible de constater que la différence d'efficacité est beaucoup plus marquée à 90° (54 % contre 4 %, 75 % contre 32 % et 63 % contre 14 % de réduction de dose pour les tubes frontal, latéral et la combinaison des deux tubes) qu'à 45° (28 % contre 11 %, 67 % contre 52 % et 44 % contre 23 % pour ces mêmes tubes). Ceci est probablement dû au fait qu'à 90°, l'irradiation du cristallin par la partie latérale de l'œil est majorée, le plan d'incidence des rayons X diffusés étant quasiment tangent au verre principal. Il est donc extrêmement important d'opter pour une paire de lunettes minimisant au maximum l'espace « libre » entre l'opérateur et la lunette, et particulièrement lorsque ce dernier est amené à détourner la tête (tête à 90°).

Sturchio *et al.* (2013) ont eux aussi comparé un modèle « sport » avec un modèle « classique » plus couvrant, et démontrent également qu'une paire de lunettes plus couvrante possède une meilleure efficacité. Ceci permet non seulement de soutenir l'hypothèse de cette étude, mais aussi de penser que ces résultats sont transposables à des modèles différents de ceux que testé dans cette étude (Sturchio *et al.*, 2013).

5 Conclusion

La radiologie interventionnelle pédiatrique est un domaine particulièrement irradiant pour l'opérateur, avec un ratio dose

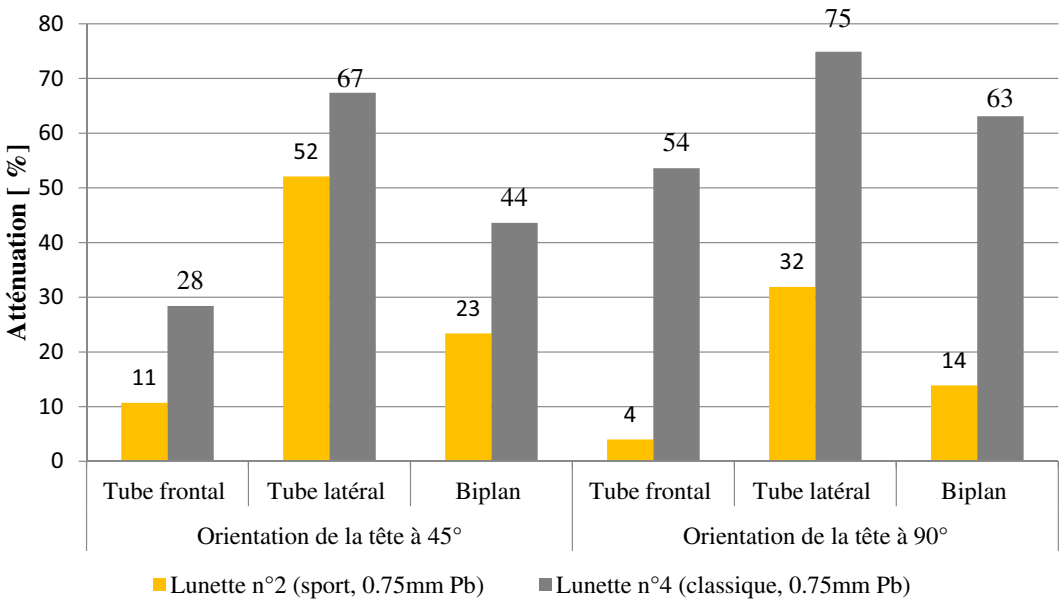

Figure 4. Influence de la surface couverte.
Influence of the covered area.

au cristallin / PDS 5 fois plus élevé que lors d'interventions réalisées chez des patients adultes (McVey *et al.*, 2013). Bien que la pédiatrie représente généralement une faible partie de la charge de travail globale des neuroradiologues interventionnistes, cette dernière nécessite néanmoins d'être prise sérieusement en compte, compte tenu de son caractère particulièrement irradiant.

Un moyen efficace pour réduire la dose au cristallin réside dans l'utilisation adéquate de moyens de radioprotection. Parmi ceux-ci, les lunettes plombées permettent d'atténuer jusqu'à 75 % de la dose au cristallin. Il a été mis en évidence que l'efficacité de ces dernières était grandement tributaire de certains paramètres, le plus important étant la surface couvrante, dont l'effet est plus marqué que la simple équivalence d'épaisseur de plomb dans le verre à géométrie égale. De plus, l'ajout d'une protection latérale sur la monture des lunettes est bénéfique pour réduire l'irradiation du cristallin en augmentant simultanément la surface couvrante ainsi qu'en réduisant le rayonnement avec un grand angle d'incidence.

Le positionnement des écrans de visualisation joue également un rôle important dans la protection du cristallin. En effet, l'angle entre la tête de l'opérateur et la source de rayonnement diffusé influence grandement la dose au cristallin, principalement celle de l'œil côté tube.

Références

Chong N., Yin W., Chan P., Cheng M., Ko H., Jeng S., Lee J. (2000) Evaluation of Absorbed Radiation Dose to Working Staff During Cardiac Catheterization Procedures, *Chinese Medical Journal* **63**, 816-821.

IAEA (2013) Implications for Occupational Radiation Protection of the New Dose Limit for the Lens of the Eye, TECDOC No. 1731.

McVey S., Sandison A., Sutton D.G. (2013) An assessment of lead eyewear in interventional radiology, *J. Radiol. Prot*. **33**, 647.

Schueler B.A., Vrieze T.J., Bjarnason H., Stanson A.W. (2006) An investigation of operator exposure in interventional radiology, *Radiographics* **26**, 1533-1541.

Sturchio G., Newcomb R., Molella R., Varkey P., Hagen P., Schueler B. (2013) Protective Eyewear Selection for Interventional Fluoroscopy, *The Radiation Safety Journal* **104**, 11-16.

Vanhavere F., Carinou E., Gualdrini G., Clairand I., Sans Merce M., Ginjaume M., Nikodemova D., Jankowski J., Bordy J-M., Rimpler A., Wach S., Martin P., Struelens L., Krim S., Koukorava C., Ferrari P., Mariotti F., Fantuzzi E., Donadille L., Itié C., Ruiz N., Carnicer A., Fulop M., Domienik J., Brodecki M., Daures J., Barth I., Bilski P. (2012). ORAMED : Optimization of Radiation Protection of Medical Staf, EURADOS Report 2012-02.

Vaño E., Ubeda C., Leyton F., Miranda P., Gonzalez L. (2009). Staff Radiation Doses in Interventional Cardiology : Correlation With Patient Exposure, *Pediatr. Cardiol.* **30**, 409-413.

Cite this article as: C. Bolomey, G. Fasel, N. Ryckx, R. Le Coultre. Irradiation du personnel en neuroradiologie interventionnelle pédiatrique : focus sur le cristallin de l'opérateur. Radioprotection, DOI: 10.1051/radiopro/2016024.

Radioprotection 51(4), 293 (2016)

DOI: 10.1051/radiopro/2016081

Available online at:
www.radioprotection.org

ERRATUM

Erratum de : Irradiation du personnel en neuroradiologie interventionnelle pédiatrique : focus sur le cristallin de l'opérateur

C. Bolomey[1], G. Fasel[1], N. Ryckx[2] and R. Le Coultre[1]*

[1] Haute École de Santé Vaud (HESAV), Haute École Spécialisée de Suisse Occidentale (HES-SO), Lausanne, Suisse.
[2] Institut de Radiophysique (IRA), Centre Hospitalier Universitaire Vaudois (CHUV), Lausanne, Suisse.

Radioprotection 51(3), 163–170 (2016), **DOI: 10.1051/radiopro/2016024**

Received 4 November 2016

Des erreurs se sont glissées lors de la mise en page des Tableaux 3 et 4. Les valeurs sont corrigées dans cet erratum.

Table 3. Moyenne des équivalents de dose individuel Hp(0,07) au niveau des yeux en fonction de la localisation des TLD, ainsi que les facteurs d'exposition du cristallin obtenus en divisant le cumul de dose TLD par le cumul de PDS des trois groupes d'interventions tels que listés dans le Tableau 2. L'incertitude élargie ($k = 2$) liée au TLD s'élève à 11 %.

Average individual dose equivalents Hp(0.07) of the eyes as a function of the location of the TLDs, and the eye lens exposure factors obtained by dividing the cumulative TLD doses by the respective cumulative DAP of the three groups of procedures, as listed in Table 2. The expanded uncertainty ($k = 2$) related to the TLD is 11%.

Emplacement des TLD	Mesure n°	Moyenne Hp(0,07) [μSv] (CI 95 %)	Facteur d'exposition [μSv] Sv/(Gy cm^2)]
Gauche	1	141 ± 7 (136, 146)	1,2
	2	134 ± 8 (129, 139)	1,2
	3	218 ± 10 (212, 224	1,9
Centre	1	127 ± 7 (123, 131)	0,8
	2	115 ± 9 (109, 121)	0,7
	3	178 ± 12 (171, 185	1,1
Droite	1	51 ± 16 (41, 61)	0,3
	2	28 ± 9 (22, 34	0,2
	3	37 ± 8 (32, 42	0,2
Moy. gauche		457 ± 27	1,2
Moy. droite		268 ± 30	0,6

Table 4. Atténuation des lunettes plombées en fonction de l'orientation de l'opérateur et du tube utilisé.

Attenuation of the leaded glasses as a function of the operator's orientation and the tube used.

		Atténuation en fonction de l'orientation de la tête de l'opérateur			
		Moyenne [%]		Écart type [%]	
Tube utilisé	Lunettes n°	90°	45°	90°	45°
Frontal	1	8,5	11,8	0,8	0,4
	2	4,0	10,7	2,9	0,6
	3	39,8	23,7	0,2	1,9
	4	53,6	28,4	0,7	1,2
Latéral	1	43,4	61,8	0,1	0,2
	2	31,9	52,1	0,5	0,1
	3	69,0	66,9	0,1	0,3
	4	74,9	67,4	0,1	0,1
Biplan	1	23,5	34,6	0,2	0,6
	2	13,9	23,4	0,9	0,3
	3	52,2	44,8	0,5	0,5
	4	63,1	43,6	0,1	0,6

* regis.lecoultre@hesav.ch

Radiation Exposure of the Operator During Coronary Interventions (from the RADIO Study)

Zacharenia Kallinikou, MD[a], Serban G. Puricel, MD[a], Nick Ryckx, MSc[b], Mario Togni, MD[a], Gerard Baeriswyl, MD[a], Jean-Christophe Stauffer, MD[a], Stephane Cook, MD[a], Francis R. Verdun, PhD[b], and Jean-Jacques Goy, MD[a,*]

We sought to compare operator radiation exposure during procedures using right femoral access (RFA), right radial access (RRA), and left radial access (LRA) during coronary angiography (CA) and percutaneous coronary intervention (PCI). Because of an increased incidence of long-term malignancy in interventional cardiologists, operator radiation exposure is of rising concern. This prospective study included all consecutive patients who underwent elective or emergency CA ± PCI from September 2014 to March 2015. The primary end point was operator radiation exposure, quantified as the ratio of operator cumulative dose (CD) and patient radiation reported as dose-area product (DAP) (CD/DAP). Secondary end points included CD, DAP, and fluoroscopy time (FT). Overall 830 procedures (457 CA [55%] and 373 PCI [45%]) were performed, 455 (55%) through RFA, 272 (33%) through RRA, and 103 (12%) through LRA. The CD/DAP was lower in RFA (0.09 μSv/Gycm^2 [0.02 to 0.20]) compared with RRA (0.47 μSv/Gycm^2 [0.25 to 0.75], p <0.001). The LRA showed lower CD/DAP compared with RRA (p <0.001). CD was significantly lower in RFA (3 μSv [1 to 7]) compared with RRA (12 μSv [6 to 29], p <0.001). The LRA showed lower CD compared with RRA (p <0.001). There were no significant differences in DAP among the 3 access sites. FT was similar for the 3 groups (RFA 7 ± 7, RRA 5 ± 5, LRA 6 ± 5 minutes, RFA vs RRA: p = 1, RFA vs LRA: p = 0.16, RRA vs LRA: p = 0.52). In conclusion, the use of RFA during CA ± PCI is associated with significantly lower operator radiation exposure compared with RRA. LRA is associated with significantly lower operator radiation exposure compared with RRA. **(Am J Cardiol 2016;■:■−■)**

Because of a presumably increased stochastic risk of cancer induction among interventional cardiologists, especially neoplasms of the unprotected brain, nasopharyngeal tract, and upper extremities, operator radiation exposure during coronary angiography (CA) and/or percutaneous coronary intervention (PCI) is of rising concern.[1,2] Therefore, we undertook a comparison of operator radiation exposure during right femoral access (RFA), left radial access (LRA), and right radial access (RRA) during CA and CA followed by ad hoc PCI in a real-world population.

Methods

From September 2014 to March 2015 at the University and Hospital Fribourg, all consecutive procedures of elective or emergency CA and CA followed by ad hoc PCI were prospectively considered for operator radiation exposure measurements. Procedures were performed by 5 senior interventional cardiologists with significant experience (>3,000 PCI each) in both femoral and radial access routes. Selection of the percutaneous access site was left to the discretion of the operator. Crossover access site procedures were excluded. This study was part of the Catheterization Registry Fribourg (CardioFR), which was approved by the Ethics Committee of Canton Vaud (protocol no: 339/14).

The primary end point of the study was operator radiation exposure, expressed as the cumulative equivalent dose (in μSv) over the lead apron at chest level, normalized for the patient radiation exposure (dose-area product [DAP] in Gycm^2). Secondary end points included cumulative dose (CD), DAP, and fluoroscopy time (FT).

Procedures were performed on a digital single-plane cineangiography unit (Allura FD10; Philips Medical Systems, Hamburg, Germany) with an undertable x-ray tube MRC20025 with a magnification factor leading to a field of view of 21 cm and an acquisition frequency of 15 frames/s. All procedures were performed with respect to current guidelines using either 5Fr or 6Fr hydrophilic sheaths. Conventional diagnostic and guiding catheters were used.

The femoral access was achieved, under local anesthesia with 2% rapidocain, through the anterior wall puncture of the artery; 5Fr or 6Fr Terumo (Pinnacle; Terumo Medical, Tokyo, Japan) introducer was placed in the femoral artery. CA and PCI were performed according to standard practice using catheter and drugs left to the discretion of the operator. Hemostasis was achieved using closure devices

[a]Department of Cardiology, Hospital and University of Fribourg, Fribourg, Switzerland; and [b]Department of Radiology, Institute of Radiophysics, Centre Hospitalier Universitaire Vaudois, Lausanne, Switzerland. Manuscript received January 5, 2016; revised manuscript received and accepted April 26, 2016.

See page 7 for disclosure information.

*Corresponding author: Tel: (+41) 26 426 7285; fax: (+41) 26 426 8135.

E-mail address: jjgoy@goyman.com (J.-J. Goy).

0002-9149/16/$ - see front matter
http://dx.doi.org/10.1016/j.amjcard.2016.04.045

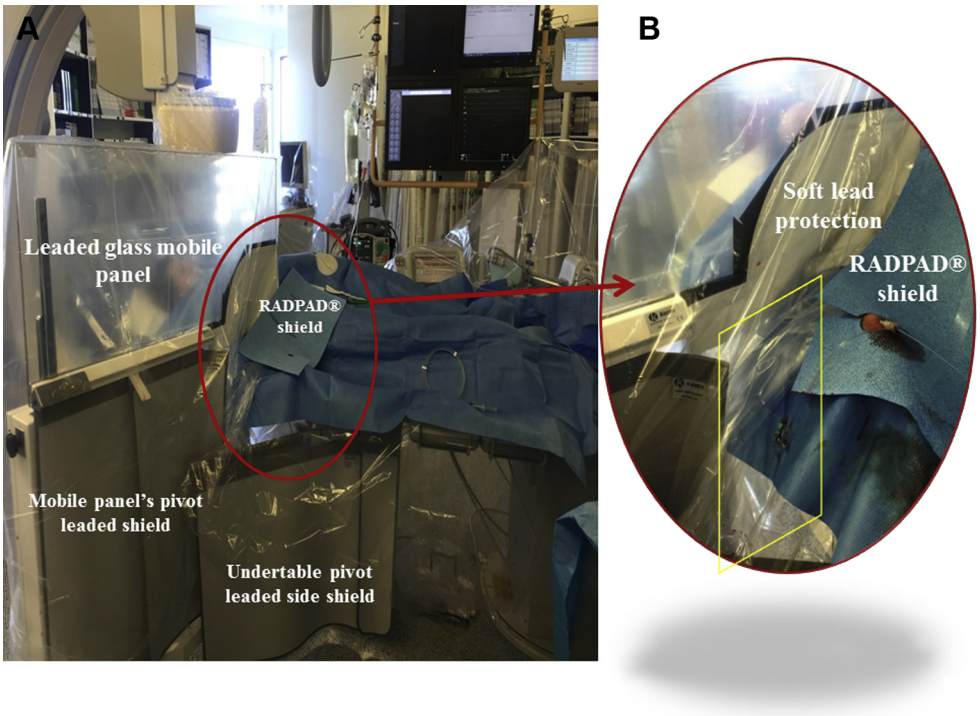

Figure 1. *(A)* Radioprotection equipment and materials. Image acquisition during a right radial case. *(B)* Although the shields are approximated as closely as possible to minimize operator irradiation, there is still a radioprotection gap *(yellow box)*, which is inevitably more important during right radial procedures.

Table 1
Baseline patient and procedural characteristics

	RFA (N=455)	LRA (N=103)	RRA (N=272)	p-values		
				RFA vs. LRA	RFA vs. RRA	LRA vs. RRA
Patients						
Age (years±SD)	68±12	69±10	65±12	1.00	0.02	0.05
Male	310 (68%)	71 (69%)	181 (67%)	1.00	1.00	1.00
Weight (kg±SD)	80±16	80±18	81±16	1.00	1.00	1.00
Height (m±SD)	1.70±0.09	1.70±0.09	1.70±0.09	1.00	1.00	1.00
BMI (kg/m^2±SD)	27±5	27±5	28±5	1.00	1.00	1.00
Procedure						
CA	216 (47%)	65 (63%)	176 (65%)	0.01	<0.01	1.00
CA followed by ad hoc PCI	239 (53%)	38 (37%)	96 (35%)	0.01	<0.01	1.00
Procedural time (min±SD)	20±19	15±11	18±12	0.05	1.00	0.08
Fluroscopy time (min±SD)	7±7	5±5	6±5	0.16	1.00	0.52
Nb of cine-angiograms (n±SD)	954±520	659±351	727±300	<0.001	<0.01	<0.001

Variables are reported in numbers (%) or mean ± SD.

BMI = body mass index; CA = coronary angiography; DAP = dose area product; LRA = left radial access; PCI = percutaneous coronary intervention; RFA = right femoral access; RRA = right radial access; SD = standard deviation.

(Femoseal; St. Jude Medical, St. Paul, Minnesota) or external mechanical compression (Femostop; St. Jude Medical).

After sterile preparation and anesthesia with 2% rapidocain infiltration, radial artery was punctured with a 20-gauge needle. A 0.021 Teflon-sheathed short guidewire was inserted in the needle. A 3.2-section BD Venflon was then inserted in the artery. A Terumo (Pinnacle; Terumo Medical) 0.021 hydrophilic guidewire was advanced through the radial and brachial artery. A 5Fr introducer was then inserted in the radial artery. Vasodilator cocktail consisting of verapamil 3 mg and enoxaparin 3,400 units was administered after sheath insertion. Specific catheters were used for CA and PCI. Exchange to a 6Fr sheath was possible when technically necessary. At the end of the procedure, the sheath was removed and an inflatable pressure band placed to the access site. All radial accesses were performed at the right side of the patient.

Operator protection was ensured with the same equipment for all procedures. A leaded glass mobile panel with a

Table 2
Radiation exposure of the operator and patient

	RFA	LRA	RRA	RFA vs. LRA			RFA vs. RRA			LRA vs. RRA		
				p-value	Adjusted difference (95%CI)	Adjusted p-value	p-value	Adjusted difference (95%CI)	Adjusted p-value	p-value	Adjusted difference (95%CI)	Adjusted p-value
CA and CA followed by ad hoc PCI	N=455	N=103	N=272									
DAP ($Gycm^2$)	36 (22-63)	30 (18-47)	32 (19-52)	0.01	+4 (-11 to 20)	0.57	0.02	+6 (-3 to 15)	0.2	0.84	-1 (-9 to 6)	0.73
CD (μSv)	3 (1-7)	6 (3-11)	12 (6-29)	<0.001	+1 (-3 to 5)	0.63	<0.001	-16 (-22 to 11)	<0.001	<0.001	-20 (-30 to -10)	<0.001
CD/DAP (μSv/$Gycm^2$)	0.09 (0.02-0.20)	0.21 (0.10-0.35)	0.47 (0.25-0.75)	<0.001	-0.01 (-0.06 to 0.05)	0.79	<0.001	-0.36 (-0.43 to 0.28)	<0.001	<0.001	-0.39 (-0.54 to -0.26)	<0.001
CA alone	N=216	N=65	N=176									
DAP ($Gycm^2$)	24 (16-39)	24 (15-35)	27 (17-42)	1.00	-2 (-15 to 12)	0.81	0.81	-6 (-14-2)	0.12	0.67	-4 (-11-3)	0.27
CD (μSv)	2.5 (1-6)	5 (2-10)	10 (6-19)	<0.001	1 (-2 to 4)	0.45	<0.001	-14 (-21 to -8)	<0.001	<0.001	-10 (-18 to -2)	0.01
CD/DAP (μSv/$Gycm^2$)	0.10 (0.03-0.22)	0.21 (0.11-0.38)	0.44 (0.24-0.71)	<0.001	-0.01 (-0.01 to 0.07)	0.91	<0.001	-0.30 (-0.37 to -0.23)	<0.001	<0.001	-0.25 (-0.36 to -0.14)	<0.001
CA followed by ad hoc PCI	N=239	N=38	N=96									
DAP ($Gycm^2$)	54 (34-90)	45 (29-62)	49 (26-71)	0.16	2 (-25 to 30)	0.87	0.07	7 (-10 to 24)	0.42	1.00	3 (-11 to 18)	0.65
CD (μSv)	4 (1-10)	6.5 (3-13)	24 (9.5-45.5)	0.21	-1 (-8 to 6)	0.83	<0.001	-23 (-33 to -13)	<0.001	<0.001	-30 (-53 to -7)	0.01
CD/DAP (μSv/$Gycm^2$)	0.07 (0.02-0.18)	0.19 (0.10-0.34)	0.54 (0.27-0.87)	<0.001	-0.01 (-0.01 to 0.09)	0.86	<0.001	-0.47 (-0.61 to -0.34)	<0.001	<0.001	-0.55 (-0.87 to 0.25)	0.001

Values are reported in medians (interquartile range: P25 to P75).
CA = coronary angiography; CD = cumulative dose; DAP = dose area product; LRA = left radial access; PCI = percutaneous coronary intervention; RFA = right femoral access; RRA = right radial access; SD = standard deviation.

patient contour cutout (0.5 lead equivalent; MAVIG, Munich, Germany) was positioned at the left side of the operator. An undertable pivot-leaded side shield (0.5-mm lead equivalent) was mounted to the side of the table. An additional soft lead shield was adjusted in the contour cut of the leaded glass mobile panel to minimize radiation exposure. The 37 × 42 cm upper-shield flap (RADPAD, Worldwide Innovations & Technologies, Inc, Kansas City, USA) was placed over the access site in each procedure to reduce scatter radiation (Figure 1). Additional radiation protection materials were standardized for all operators and included a lead apron, thyroid lead collar, and leaded glasses. All procedures were performed from the patients' anatomical right side.

Operator radiation was measured using individual electronic dosimeters (DoseAware; Philips Healthcare, Best, The Netherlands) positioned on the sternum, outside the lead apron. The dosimeters are silicon-based semiconductor detectors with a dose-response between 1 μSv and 10 Sv, in steps of 1 μSv (calibrated in ambient equivalent dose Hp(10)) and a temporal resolution of 1 second. The following parameters were recorded for each procedure: (1) operator CD through the use of dedicated readout software (DoseView), measured by the individual dosimeters; (2) FT; (3) number of cine angiograms (NC); and (4) the DAP-normalized CD defined as the dose (μSv) received by the operator with each $Gycm^2$ applied to the patient (known as the exposure factor) has been advocated[3] and applied to our study as it isolates differences in patient radiation among the 3 vascular access sites. Patient radiation dose was expressed as DAP. Furthermore, radiation exposure of the assistant nurse, the first nurse on the operator's right side, was assessed using similar dosimeters, in a subgroup of consecutive procedures, with the aim to compare radiation exposure of the operator versus assistant nurse.

All statistical analyses were performed using dedicated software (Stata, version 13; StataCorp LP, College Station, Texas) at a 2-tailed significance level of alpha <0.05. Baseline patient and procedural characteristics, and variables assessing radiation exposure of the operator, were compared among the 3 vascular access sites. Categorical variables are reported as counts and percentages; continuous variables are reported as mean and SD or as median with 25% to 75% interquartile range according to their distribution. Normality was assessed by visual inspection of histograms, the computation of Q-Q plots and the Shapiro-Wilk test. Categorical variables were compared using the chi-square or Fisher's exact test as appropriate. Continuous variables were analyzed using the 1-way ANOVA or the Wilcoxon rank-sum test according to their distribution. To account for differences of the individual operators on radiation exposure according to access site, we computed a generalized linear model including the individual operators as potential confounders of the overall treatment effect. To account for multiple comparisons, p values are Bonferroni adjusted, that is, multiplied by the number of comparisons. Comparison of radiation exposure between the operator and the first assistant was assessed using the paired student's *t* test or the signed-rank Wilcoxon test according to distribution.

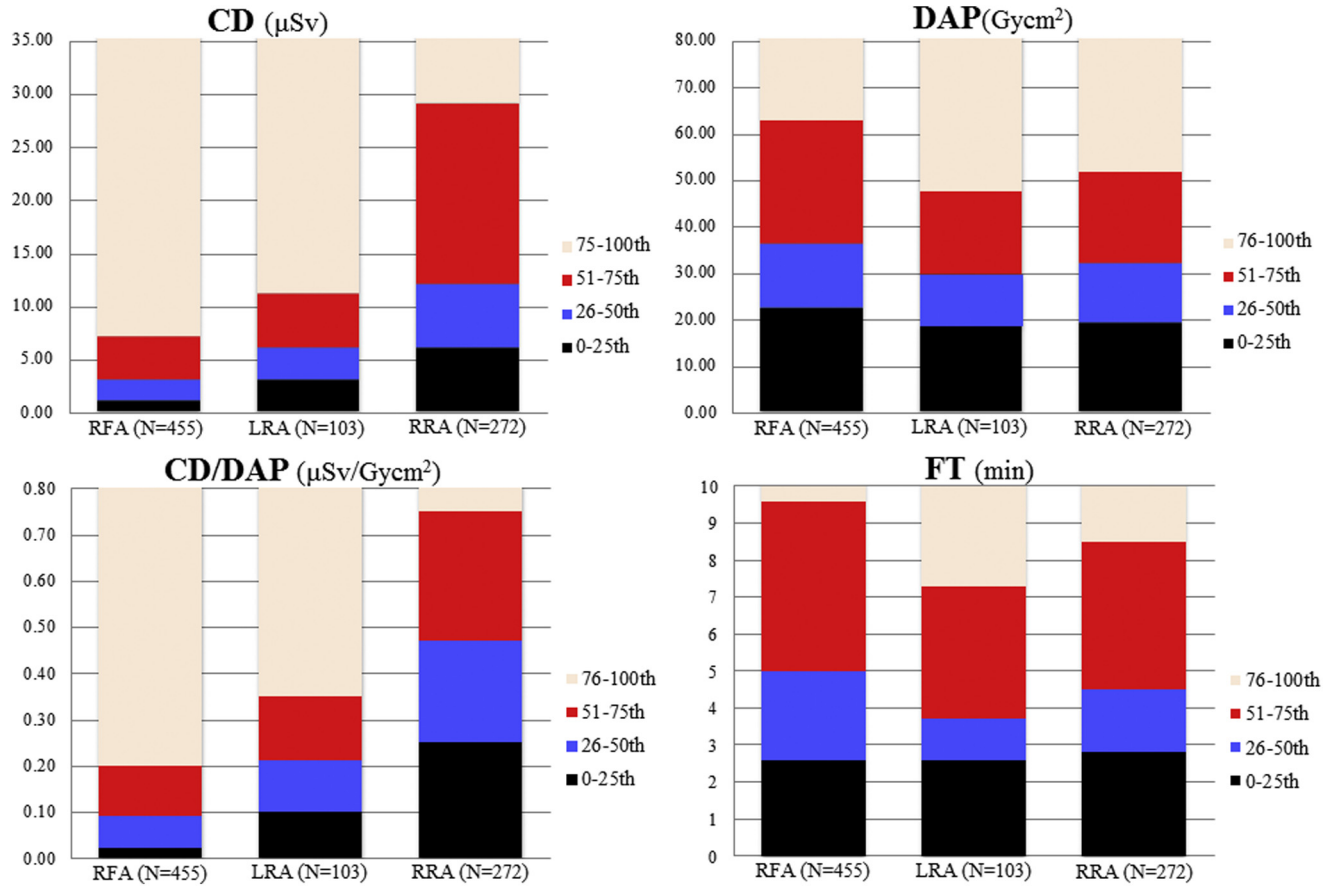

Figure 2. Operator CD, patient radiation dose (DAP), operator radiation exposure (CD/DAP), and FT for all procedures: CA and CA followed by ad hoc PCI. Columns: 3 vascular access sites in percentiles (colors): black: 0 to 25th, blue: 26 to 50th, red: 51 to 75th, and beige: 76 to 100th, median values on the board of blue and red columns.

Results

During September 2014 and March 2015, 849 consecutive procedures for elective or emergency CA and CA followed by ad hoc PCI were performed in our catheterization laboratory with a dedicated dosimeter for radiation evaluation. Nineteen procedures (1.8%) were excluded because of a crossover in access sites. No patient was excluded because of lesion or procedural complexity. Finally, 830 consecutive procedures were included in the trial, 457 CA alone (55%) and 373 CA followed by ad hoc PCI (45%). With regard to vascular site, 455 procedures (55%) were carried out using the RFA, 103 (12%) using the LRA, and 272 (33%) using the RRA. Baseline patient characteristics were generally well balanced and depicted in Table 1. Analysis of procedural characteristics as listed in Table 1 revealed no difference in FT among the groups and showed a significantly greater NC in RFA compared with LRA and RRA group and in RRA compared with the LRA group, probably reflecting higher procedural complexity.

The radiation exposure of the assistant nurse standing at the operator's right side was also assessed in a subgroup of first 293 consecutive procedures, 152 CA alone (52%) and 141 CA followed by ad hoc PCI (48%), 164 (56%) through RFA, 49 (17%) through LRA, and 80 (27%) through RRA.

Table 2 and Figure 2 list patient and operator radiation exposure. Adjusted CD was significantly lower in RFA compared with RRA but not to LRA. CD was lower for procedures using LRA than RRA. Patient radiation dose expressed by DAP did not significantly vary among the 3 access sites. Operator radiation dose reported as the DAP-normalized CD was significantly higher in the RRA compared with the RFA and LRA group for all procedures, procedures with CA alone, and procedures with CA followed by ad hoc PCI. There were no significant differences between the RFA and the LRA for any kind of procedure. Table 3 indicates DAP, CD, and DAP-normalized CD for the individual operators. A significantly higher radiation exposure comparing the RRA with the RFA was consistently found for all operators. Significant differences in radiation exposure between RFA and LRA and RRA and LRA were found only for 2 of the 5 operators. Radiation exposure for elective and urgent procedures is provided in Table 4. During elective procedures, radiation exposure was lower for RFA compared with RRA, but not to LRA. However, LRA showed a lower DAP-normalized CD compared with RRA ($p < 0.001$). In addition to the aforementioned differences, LRA was associated with a higher radiation exposure than RFA, when only urgent procedures were considered

Table 3
Radiation exposure according to the individual operator

	RFA	LRA	RRA	p-values		
				RFA vs. LRA	RFA vs. RRA	LRA vs. RRA
CA andCA followed by ad hoc PCI						
Operator 1	N=39	N=77	N=88			
DAP ($Gycm^2$)	31 (20-59)	28 (17-41)	32 (19-55)	0.28	1.00	0.16
CD (μSv)	9 (4-15)	6 (4-11)	15.5 (8-33)	0.08	<0.01	<0.001
CD/DAP (μSv/$Gycm^2$)	0.28 (0.16-0.44)	0.23 (0.14-0.35)	0.51 (0.37-0.84)	0.33	<0.001	<0.001
Operator 2	N=132	N=3	N=28			
DAP ($Gycm^2$)	44 (31-90)	67 (37-90)	36 (18-56)	1.00	0.07	0.20
CD (μSv)	1 (0-2)	1 (0-3)	1 (0.5-7.5)	1.00	<0.01	1.00
CD/DAP (μSv/$Gycm^2$)	0.01 (0-0.04)	0.01 (0.00-0.04)	0.05 (0.00-0.17)	1.00	<0.01	0.53
Operator 3	N=98	N=1	N=3			
DAP ($Gycm^2$)	36 (21-67)	73	135 (14-166)	0.73	0.60	1.00
CD (μSv)	4 (2-10)	7	87 (25-484)	1.00	<0.01	0.02
CD/DAP (μSv/$Gycm^2$)	0.10 (0.05-0.19)	0.09	1.78 (0.64-2.90)	1.00	<0.01	0.36
Operator 4	N=139	N=12	N=69			
DAP ($Gycm^2$)	30 (17-54)	36 (24-128)	33 (22-50)	0.23	0.49	0.82
CD (μSv)	4 (1-6)	1.5 (1-3.5)	12 (7-36)	0.16	<0.001	<0.001
CD/DAP (μSv/$Gycm^2$)	0.10 (0.05-0.18)	0.05 (0.01-0.08)	0.45 (0.24-0.78)	<0.01	<0.001	<0.001
Operator 5	N=47	N=10	N=84			
DAP ($Gycm^2$)	35 (21-51)	27 (14-49)	30 (17-47)	0.92	0.40	1.00
CD (μSv)	7 (4-13)	12 (11-37)	12 (8-28)	0.04	<0.001	0.81
CD/DAP (μSv/$Gycm^2$)	0.21 (0.12-0.35)	0.59 (0.44-1.43)	0.48 (0.32-0.72)	<0.01	<0.001	0.55

Values are reported in medians (interquartile range: P25 to P75).

CA = coronary angiography; CD = cumulative dose; DAP = dose area product; LRA = left radial access; PCI = percutaneous coronary intervention; RFA = right femoral access; RRA = right radial access; SD = standard deviation.

Table 4
Radiation exposure of the operator and patient stratified by operator

	RFA	LRA	RRA	Crude p-values			Adjusted p-values		
				RFA vs. LRA	RFA vs. RRA	LRA vs. RRA	RFA vs. LRA	RFA vs. RRA	LRA vs. RRA
CA and CA followed by ad hoc PCI									
Elective	N=285	N=90	N=206						
DAP ($Gycm^2$)	34 (21-57)	32 (19-48)	31 (19-50)	0.37	0.41	1.00	0.77	0.35	0.72
CD (μSv)	3 (1-6)	6 (3-12)	11 (6-25)	<0.001	<0.001	<0.001	0.36	<0.001	<0.01
CD/DAP (μSv/$Gycm^2$)	0.09 (0.03-0.20)	0.22 (0.12-0.35)	0.43 (0.23-0.72)	<0.001	<0.001	<0.001	0.13	<0.001	<0.001
Urgent	N=170	N=13	N=66						
DAP ($Gycm^2$)	41 (25-84)	25 (12-44)	38 (21-57)	0.02	0.11	0.29	0.69	0.62	0.16
CD (μSv)	3 (1-10)	4 (1-6)	17.5 (8-41)	1.00	<0.001	<0.001	<0.01	<0.001	0.001
CD/DAP (μSv/$Gycm^2$)	0.08 (0.02-0.19)	0.15 (0.10-0.21)	0.55 (0.37-0.85)	0.16	<0.001	<0.001	<0.01	<0.001	<0.001

Values are reported in medians (interquartile range: P25 to P75).

CA = coronary angiography; CD = cumulative dose; DAP = dose area product; LRA = left radial access; PCI = percutaneous coronary intervention; RFA = right femoral access; RRA = right radial access; SD = standard deviation.

($p < 0.01$). In the subgroup of the first consecutive 293 procedures, operator exposure was significantly higher compared with the assistant nurse's as listed in Table 5 for all procedures and by access site.

Discussion

The main findings of the current prospective trial are the following: (1) interventional Cardiologists are exposed to a lower degree of radiation when performing CA or CA followed by ad hoc PCI through the RFA rather than the RRA; (2) interventional cardiologists are exposed to a lower degree of radiation when performing CA or CA followed by ad hoc PCI using the LRA rather than the RRA; and (3) the operator is more exposed to radiation compared with the assistant nurse standing at his right side during the procedures.

Transradial cardiac catheterization is known to be associated with an increased operator radiation dose even for highly experienced interventional cardiologists and despite the use of radioprotection optimization techniques.[4–9] Data are limited with regard to operator radiation exposure when right and left radial accesses are compared,[10–13] with most investigators reporting lower radiation levels for LRA, alike

Table 5
Comparison of radiation exposure between operator and assistant nurse

CA and CA followed by ad hoc PCI (N=293)	Operator	Assisstant nurse	p-value
DAP (Gycm^2)	32 (20-53)	32 (20-53)	1.00
CD (μSv)	5 (1-13)	2 (1-5)	<0.001
CD/DAP (μSv/Gycm^2)	0.16 (0.04-0.46)	0.07 (0.03-0.13)	<0.001
RFA (N=164)			
CD/DAP (μSv/Gycm^2)	0.06 (0.01-0.18)	0.06 (0.03-0.11)	<0.05
LRA (N=49)			
CD/DAP (μSv/Gycm^2)	0.23 (0.10-0.45)	0.06 (0.04-0.10)	<0.001
RRA (N=80)			
CD/DAP (μSv/Gycm^2)	0.51 (0.32-0.81)	0.10 (0.06-0.17)	<0.001

Values are reported in medians (interquartile range: P25 to P75).

CA = coronary angiography; CD = cumulative dose; DAP = dose area product; LRA = left radial access; PCI = percutaneous coronary intervention; RFA = right femoral access; RRA = right radial access; SD = standard deviation.

to initial scientific concerns and despite the operator's inconvenience when leaning over to reach the patient's left side. To our knowledge, this is the first single-center trial to compare operator radiation exposure among these 3 vascular access sites for CA and CA followed by ad hoc PCI. Recently, the Randomized Evaluation of Vascular Entry Site and Radiation Exposure trial[14] evaluated patient and operator radiation exposure among the 3 access sites RFA, LRA, and RRA and included only CA procedures without CA followed by ad hoc PCI procedures. It reported higher operator radiation for LRA using air kerma as primary end point, which is not the ideal patient exposure metric, although also analyzing DAP as a secondary end point and found an FT much shorter than our study's, presumably because PCIs were excluded. Furthermore, the population included in the Randomized Evaluation of Vascular Entry Site and Radiation Exposure trial shows a median weight and height of 64 to 65 kg and 163 to 164 cm, respectively, resulting subsequently in lower DAP values (in the order of 26 Gycm^2 per procedure).

Both procedure-related and operator-related factors appear responsible for the differences in operator radiation exposure per vascular access site. It has been reported that increased operator radiation exposure during radial access, as opposed to femoral access, is related to increase in FT, reflecting technical difficulties and to the slightly closer operator's position to the x-ray tube and to the patient, compared with femoral access.[5,15,16] In contrast, decreased operator radiation dose and shorter FT have been reported when using LRA compared with RRA.[10,11,17–20] In our study, there are some details in radiation protection techniques that should be taken into consideration: First, during RRA procedures, the leaded glass mobile panel is positioned less proximally to the table compared with LRA and RFA to facilitate the right radial access. The radioprotection gap which is inevitably created between the leaded glass mobile panel and the patient table is more pronounced during RRA procedures, thus creating a considerable source of radiation exposure to the operator (Figure 1). Second, when using RRA, the operator is positioned closer to the x-ray tube and closer to the patient compared with both LRA and RFA procedures, increasing the effect of the patient as the main source of scatter radiation to the operator. Furthermore, technical challenges in maneuvering catheters into the coronary vessels can lead in longer FT. In particular, the vascular anatomy associated with the right radial artery, including the right subclavian artery-common brachiocephalic trunk bifurcation and the common brachiocephalic trunk-aorta bifurcation, could account for tortuosity and calcifications that could impair procedural success. In considering the left radial artery, the left subclavian artery stems directly from the aortic arch, thus reducing the technical challenges in catheter manipulation, whereas in the right femoral artery there is no such issue at all. Finally, further technical difficulties associated with radial artery access include spasm or tortuosity of the radial artery, which could increase fluoroscopy and procedure times. Nonetheless, in our study, FT did not differ significantly among the 3 access sites, suggesting a high level of operator experience across the 3 groups. On the contrary, the longer procedural times and the greater NC in the femoral group reflect a higher complexity of procedures being performed through this access, while still benefitting from decreased operator radiation exposure compared with the 2 radial groups.

The present study confirms the greater radiation exposure of the operator compared with the first assistant who is standing at his right side, regardless of the vascular access site. This is expected because of the nurse's greater distance from the source of radiation and from the patient. Most authors studying operator radiation dose issues report results normalized per procedure and not per-patient radiation dose measured as DAP. This means that whether the dose is higher for femoral or radial approach will be a result of both the higher or lower DAP (and FT), the distance effect, and radiation protection aspects. If the dose is normalized per DAP, one can isolate, to a certain extent, the first 2 issues, and the results will then be mostly related to the radiation protection level and the distance between operator and patient.[21] Our results in terms of procedure (fluoroscopy and procedural times) and radiation dose of the operator (CD) and the patient (DAP) are in line with published data in the literature. Although not randomized, the present study reflects operator radiation exposure in a real-world population in everyday clinical practice, despite a bias in the choice of vascular access site by the operator. Furthermore, the 3 groups were homogenous with regard to characteristics that influence operator and patient irradiation such as patients' body mass index and procedural and FTs, thus reflecting a representative sample of a real-world population without exclusion of emergent or complex procedures. The greater NC in the RFA group compared with the LRA and RRA groups and in the RRA compared with the LRA group probably suggests increased procedural complexity and could be reflected in the higher patient irradiation (DAP) in the RFA group compared with the 2 radial groups. The normalization, however, of the operator irradiation for patient irradiation takes into consideration such parameters as procedural complexity and patient corpulence, thus accurately reflecting the actual operator radiation dose, and is dependent only on the following 2 parameters: (1) the degree of radioprotection itself and (2) the distance between patient and operator. Therefore, interpretation of results using the DAP-normalized operator radiation

dose allows for isolation and meaningful evaluation of technical differences among the 3 vascular access sites based on the positioning of radioprotection equipment, the operator's position, and his distance from the patient and the x-ray tube.

This was a nonrandomized, single-center study. Therefore, these results have to be interpreted with caution for other catheterization laboratories because of possible differences in operator experience, training and techniques, radioprotection materials, and devices. Furthermore, procedures were performed by 5 different, although highly experienced, interventional cardiologists implicating differences in catheterization techniques, procedural and FTs, NC, and thus effecting individual radiation dose. Finally, in our study, operator dose was measured by 1 single dosimeter positioned externally to the sternum, with no possibility to measure and compare radiation exposure of other corporal areas.

Disclosures

The authors have no conflicts of interest to disclose.

1. Bashore TM. Radiation safety in the cardiac catheterization laboratory. *Am Heart J* 2004;147:375−378.
2. von Boetticher H, Lachmund J, Hoffmann W. An analytic approach to double dosimetry algorithms in occupational dosimetry using energy dependent organ dose conversion coefficients. *Health Phys* 2010;99:800−805.
3. Kuon E. Radiation exposure in invasive cardiology. *Heart* 2008;94:667−674.
4. Lange HW, von Boetticher H. Randomized comparison of operator radiation exposure during coronary angiography and intervention by radial or femoral approach. *Catheter Cardiovasc Interv* 2006;67:12−16.
5. Brasselet C, Blanpain T, Tassan-Mangina S, Deschildre A, Duval S, Vitry F, Gaillot-Petit N, Clement JP, Metz D. Comparison of operator radiation exposure with optimized radiation protection devices during coronary angiograms and ad hoc percutaneous coronary interventions by radial and femoral routes. *Eur Heart J* 2008;29:63−70.
6. Lange HW, von Boetticher H. Reduction of operator radiation dose by a pelvic lead shield during cardiac catheterization by radial access: comparison with femoral access. *JACC Cardiovasc Interv* 2012;5:445−449.
7. Michael TT, Alomar M, Papayannis A, Mogabgab O, Patel VG, Rangan BV, Luna M, Hastings JL, Grodin J, Abdullah S, Banerjee S, Brilakis ES. A randomized comparison of the transradial and transfemoral approaches for coronary artery bypass graft angiography and intervention: the RADIAL-CABG Trial (RADIAL versus Femoral Access for Coronary Artery Bypass Graft Angiography and Intervention). *JACC Cardiovasc Interv* 2013;6:1138−1144.
8. Neill J, Douglas H, Richardson G, Chew EW, Walsh S, Hanratty C, Herity N. Comparison of radiation dose and the effect of operator experience in femoral and radial arterial access for coronary procedures. *Am J Cardiol* 2010;106:936−940.
9. Mercuri M, Mehta S, Xie C, Valettas N, Velianou JL, Natarajan MK. Radial artery access as a predictor of increased radiation exposure during a diagnostic cardiac catheterization procedure. *JACC Cardiovasc Interv* 2011;4:347−352.
10. Kado H, Patel AM, Suryadevara S, Zenni MM, Box LC, Angiolillo DJ, Bass TA, Guzman LA. Operator radiation exposure and physical discomfort during a right versus left radial approach for coronary interventions: a randomized evaluation. *JACC Cardiovasc Interv* 2014;7:810−816.
11. Dominici M, Diletti R, Milici C, Bock C, Placanica A, D'Alessandro G, Arrivi A, Italiani M, Buono E, Boschetti E. Operator exposure to x-ray in left and right radial access during percutaneous coronary procedures: OPERA randomised study. *Heart* 2013;99:480−484.
12. Sciahbasi A, Romagnoli E, Trani C, Burzotta F, Sarandrea A, Summaria F, Patrizi R, Rao S, Lioy E. Operator radiation exposure during percutaneous coronary procedures through the left or right radial approach: the TALENT dosimetric substudy. *Circ Cardiovasc Interv* 2011;4:226−231.
13. Kanei Y, Nakra NC, Liou M, Vales LL, Gowda R, Rosero H, Kwan T, Fox JT. Randomized comparison of transradial coronary angiography via right or left radial artery approaches. *Am J Cardiol* 2011;107:195−197.
14. Pancholy SB, Joshi P, Shah S, Rao SV, Bertrand OF, Patel TM. Effect of vascular access site choice on radiation exposure during coronary angiography: the REVERE trial (Randomized Evaluation of Vascular Entry Site and Radiation Exposure). *JACC Cardiovasc Interv* 2015;8:1189−1196.
15. Kiemeneij F, Laarman GJ, Odekerken D, Slagboom T, van der Wieken R. A randomized comparison of percutaneous transluminal coronary angioplasty by the radial, brachial and femoral approaches: the access study. *J Am Coll Cardiol* 1997;29:1269−1275.
16. Vano E. Radiation exposure to cardiologists: how it could be reduced. *Heart* 2003;89:1123−1124.
17. Pelliccia F, Trani C, Biondi-Zoccai GG, Nazzaro M, Berni A, Patti G, Patrizi R, Pironi B, Mazzarotto P, Gioffre G, Speciale G, Pristipino C; Prospective Registry of Vascular Access in Interventions in Lazio Region Study Group. Comparison of the feasibility and effectiveness of transradial coronary angiography via right versus left radial artery approaches (from the PREVAIL Study). *Am J Cardiol* 2012;110:771−775.
18. Freixa X, Trilla M, Feldman M, Jimenez M, Betriu A, Masotti M. Right versus left transradial approach for coronary catheterization in octogenarian patients. *Catheter Cardiovasc Interv* 2012;80:267−272.
19. Larsen P, Shah S, Waxman S, Freilich M, Riskalla N, Piemonte T, Jeon C, Pyne C. Comparison of procedural times, success rates, and safety between left versus right radial arterial access in primary percutaneous coronary intervention for acute ST-segment elevation myocardial infarction. *Catheter Cardiovasc Interv* 2011;78:38−44.
20. Biondi-Zoccai G, Sciahbasi A, Bodi V, Fernandez-Portales J, Kanei Y, Romagnoli E, Agostoni P, Sangiorgi G, Lotrionte M, Modena MG. Right versus left radial artery access for coronary procedures: an international collaborative systematic review and meta-analysis including 5 randomized trials and 3210 patients. *Int J Cardiol* 2013;166:621−626.
21. Carnicer A, Baechler S, Canetti L, Verdun FR. Staff exposure in interventional cardiology for the Swiss Federal Office of Public Health, 2014.

Elsevier Editorial System(tm) for Physica Medica: European Journal of Medical Physics
Manuscript Draft

Manuscript Number: EJMP-D-17-00128

Title: Coronary angiography and percutaneous intervention during pregnancy: What practical measures can be taken by interventional cardiologists?

Article Type: SI: Fetal Dose

Keywords: percutaneous coronary intervention; pregnant patient; ionizing radiation; interventional cardiology

Corresponding Author: Mr. Nick Ryckx, MSc in physics

Corresponding Author's Institution: Lausanne University Hospital (CHUV)

First Author: Zacharenia Kallinikou, MD

Order of Authors: Zacharenia Kallinikou, MD; Nick Ryckx, MSc in physics; Francis R Verdun; Jean-Christophe Stauffer; Jean-Jacques Goy

Abstract: Percutaneous coronary interventions have become one of the leading medical techniques for managing acute or chronic coronary artery diseases thanks to reduced septic risks, higher rates of success and lower hospitalization times. This implies a higher radiation burden on patients undergoing such procedures. An especially sensitive subgroup of patients is pregnant women, because of the higher radiation sensitivity of the fetus. However, the mean prevalence of coronary heart disease in this population is low, so theoretical and practical skills needed to properly handle these cases can be challenging due to the low volume of clinical cases. Nevertheless, some guidelines on the management of pregnant patients have been published by several medical societies. In this article, we will first summarize fetal risks due to ionizing radiation and the injection of iodinated contrast media. Then, we will detail the management of patients with positive pregnancy status known before the intervention. In this part, we will focus on the typical fetal doses, as well as the fetal risks when exposed to alternative procedures, such as drug-induced thrombolysis. Finally, we will address the actions to be taken when discovering pregnancy after the performed procedure. Especially, the risks due to ionizing radiation will be weighed against the natural occurrence of peripartum child morbidities. The overall conclusion is that, when care is being taken by the physician, no particular increase in child morbidity risk is to be expected, and the lives of both the mother and child will be preserved when treating acute coronary syndromes properly.

Cover Letter

Nick Ryckx
Institute of radiation physics
Lausanne University Hospital
Rue du Grand-Pré 1
CH - 1007 Lausanne

Lausanne, the 20th February 2017

Object: Submission of a paper for the special issue on fetal dose

Dear Editor,

On behalf of my colleagues, I wish to submit a new manuscript entitled “Coronary angiography and percutaneous intervention during pregnancy: What practical measures can be taken by interventional cardiologists?” for consideration by the European Journal of Medical Physics, in its special issue on fetal dose.

We confirm that this work is original and has not been published elsewhere nor is it currently under consideration for publication elsewhere.

In this paper, we report on the risks to the conceptus during percutaneous coronary interventions (PCI), reporting not only radiation risks but also those due to some of the medication used in interventional cardiology, that may be sometimes more harmful than ionising radiation. We focus on the strategies when pregnancy status is known before or after the procedure. The paper should be of interest to readers in the area of clinical radiation protection, especially medical physicists involved in staff training, or interventional cardiologists looking for a solid summary of the rationale behind the management of pregnant patients in angiography suites.

Please address all correspondence concerning this manuscript to me at Nick.Ryckx@chuv.ch.

Thank you for your consideration of this manuscript.

Yours sincerely,

Nick RYCKX

***Highlights (for review)**

- Summary of the management of the pregnant woman in interventional cardiology.
- Radiation risk compared against the effects of iodine and thrombolysis on the child.
- Methodologies when positive pregnancy status known before or after the procedure.

Coronary angiography and percutaneous intervention during pregnancy: What practical measures can be taken by interventional cardiologists?

Zacharenia Kallinikou (1), Nick Ryckx (2), Francis R. Verdun (2), Jean-Christophe Stauffer (3), Jean-Jacques Goy (3)

1) Cardiology department, Inselspital, Switzerland

2) Institute of radiation physics, Lausanne University Hospital, Switzerland

3) Cardiology department, Hôpital Fribourgeois, Switzerland

Abstract

Percutaneous coronary interventions have become one of the leading medical techniques for managing acute or chronic coronary artery diseases thanks to reduced septic risks, higher rates of success and lower hospitalization times. This implies a higher radiation burden on patients undergoing such procedures. An especially sensitive subgroup of patients is pregnant women, because of the higher radiation sensitivity of the fetus. However, the mean prevalence of coronary heart disease in this population is low, so theoretical and practical skills needed to properly handle these cases can be challenging due to the low volume of clinical cases. Nevertheless, some guidelines on the management of pregnant patients have been published by several medical societies. In this article, we will first summarize fetal risks due to ionizing radiation and the injection of iodinated contrast media. Then, we will detail the management of patients with positive pregnancy status known before the intervention. In this part, we will focus on the typical fetal doses, as well as the fetal risks when exposed to alternative procedures, such as drug-induced thrombolysis. Finally, we will address the actions to be taken when discovering pregnancy after the performed procedure. Especially, the risks due to ionizing radiation will be weighed against the natural occurrence of peripartum child morbidities. The overall conclusion is that, when care is being taken by the physician, no particular increase in child morbidity risk is to be expected, and the lives of both the mother and child will be preserved when treating acute coronary syndromes properly.

Introduction

Percutaneous coronary interventions (PCI) have become increasingly popular due, in part, to their minimally-invasive nature and reduced septic risks. Advantages of fluoroscopically-guided interventions include a high rate of success as well as shortened in-hospital stays when compared to open heart surgery. Accordingly, the proportion of ST-Elevation Myocardial Infarction (STEMI) patients undergoing systemic drug-induced thrombolysis went from 51% (male) and 39% (female) in 1997 to less than 1% for both genders in 2007, while the proportion of direct PCI rose from 10% to 80% [1]. However, a significant downside to this treatment paradigm shift is an increased exposure to ionizing radiation. Indeed, fluoroscopy times for these patients may range from a few seconds for simple diagnostic cases to a few hours of beam-on time, depending on numerous factors, such as vascular abnormalities, procedure complexity, procedure-related complications, patient health condition and operator experience. This may potentially lead to excessive skin radiation doses and high patient total radiation exposure.

A subgroup of patients who are especially sensitive to ionizing radiation is pregnant patients. In particular, infants, neonates and fetuses are more sensitive to ionizing radiation due to their higher metabolism and rapidly dividing young body cells [2]. These cases are somewhat rare as the mean prevalence of coronary heart disease is only 0.6% for patients between the ages of 20 and 39 years in the US [3]. Simultaneously, the pregnancy rate in the U.S. in 2010 was slightly under 10% (98.7 per 1000) for women between the ages of 15 and 44 years [4]. This implies a minimal cohort of female patients at risk of undergoing PCI during pregnancy. Consequently, the theoretical and practical skills needed to properly handle these cases can be challenging due to the low volume of clinical opportunities. However, due to significant hemodynamic changes in the maternal cardiovascular system (increase in circulating volume and cardiac output, decrease in vascular resistance and hypercoagulation), as much as 0.2 to 4.0 % of all pregnancies could be complicated by cardiovascular disease [3]. Also, the number of pregnant women with coronary disease is expected to grow due to advanced pregnancy-maternal age, the development of reproductive techniques and increased cardiovascular risk factors in women, making heart disease an increasingly important cause of maternal morbidity and

mortality during pregnancy [3]. Most cardiac problems arising in pregnant women with heart disease can be managed without interventional procedures; however, hemodynamic changes during pregnancy may sometimes lead to deterioration in previously stable patients. Maternal mortality after acute coronary syndromes (ACS) (myocardial infarction, unstable angina) is estimated at 5–10% and is highest during the peripartum period. Survival has improved with primary percutaneous coronary intervention [5-7].

We address here the main elements that should be considered before, during and after performing interventional cardiology (IC) procedures on pregnant patients. These procedures include cardiac catheterization, coronary angiography and/or percutaneous coronary interventions. First, we summarize the risks for the fetus when the mother undergoes an IC procedure. Next, we describe management of the patient when pregnancy status is known prior to intervention. And finally, we describe management of the patient after intervention or when pregnancy is discovered post-procedure.

Fetal risk during IC procedures

During IC procedures, the embryo or fetus is exposed to two different risk classes: Ionizing radiation exposure and contrast agent injection [8]. Risk to the embryo or fetus depends on the amount and type of radiation delivered and the gestational age at the time of irradiation. Concerns related to ionizing radiation include radiation-induced teratogenesis, malignancy in childhood and mutagenesis.

Ionizing radiation exposure

Effects of radiation on the fetus have been derived from animal studies, human exposures to diagnostic and therapeutic radiation, atomic bomb radiation at Hiroshima and Nagasaki in 1945, and to fallout of the Chernobyl nuclear power plant explosion in April 1986. The currently accepted maximum limit of ionizing radiation exposure to the fetus during pregnancy is a cumulative dose of 50 mSv (or 50 mGy) [9-12]. Importantly, no single diagnostic study typically approaches this cautionary dose of 50 mSv. Cardiac catheterizations, coronary angiography, electrophysiology procedures, and even more complex interventions are unlikely to exceed the

50 mGy threshold. The amount of radiation exposure to the fetus during a fluoroscopic study is typically in the range of 0.01 to 0.5 mSv, depending on duration of fluoroscopic time and operator technique [13].

Teratogenesis or malformations are typically associated with central nervous system problems, particularly microcephaly and mental retardation, and have a threshold of 100 to 200 mGy or higher. Fetal doses of 100 mGy are not reached with 3 pelvic computed tomography (CT) scans, 20 conventional diagnostic x-ray examinations or even complex fluoroscopic cardiac interventions. These levels can be reached however, with fluoroscopically guided interventional procedures of the pelvis and with radiotherapy. After Hiroshima, many victims exposed in utero to doses greater than 100 to 150 mSv developed microcephaly [14]. A linear, dose-related association between radiation dose and severe mental retardation was also found [15, 16]. Exposure to as little as 10 to 20 mSv has been associated with an increase in childhood malignancies, especially leukemia, as a stochastic effect [17]. The general background rate of leukemia in children is about 3.6 per 10,000. Exposure to 10 to 20 mSv increases this rate to 5 per 10,000 which equates to a small absolute increase of ~ 1 in 10,000 [9, 18].

Germ-line mutations potentially affecting future generations are another stochastic effect of radiation. Although radiation is commonly believed to create bizarre new mutations, data show that it usually increases the frequency of mutations occurring naturally in the general population [19]. The dosage required to double this baseline mutation rate is between 500 and 1000 mSv [20]. Common cardiovascular fluoroscopy studies do not reach these levels. The risks of ionizing radiation are more significant during organogenesis and in the early fetal period, somewhat less in the second trimester, and least in the third trimester. Interestingly, in most cases of Hiroshima victims with severe mental retardation, exposure was during weeks 8 to 15 of gestation [15, 16]. The least harmful period to perform invasive procedures is the beginning of the second trimester when organogenesis is complete but the uterus is still small [8].

Contrast medium injection

Intravenous iodinated contrast media likely cross the placenta by simple diffusion and are evenly distributed in fetal tissues [21]. Substances such as iohexol, iopamidol, iothalamate,

ioversol, ioxaglate and metrizamide have been studied in animals and do not appear to be associated with teratogenic effects [22]. However, iodinated contrast media can cause neonatal hypothyroidism [23]. Bourjeily et al. studied the effect of in utero exposure to a single high dose of iodinated contrast material on neonatal thyroid function and identified no serious risks [24]. The currently used low-osmolality iodinated contrast agents are classified in pregnancy category B [25].

Patient management when pregnancy status is known prior to intervention

The most frequently performed cardiac percutaneous interventions during pregnancy are mitral balloon valvuloplasty, coronary angiography and coronary angioplasty. Radiation doses to the mother for such procedures are usually lower than 20 mSv and even lower for the fetus because it is outside the primary field during cardiac procedures.

In emergency cases of ACS, coronary angiography with the possibility of PCI is preferred to thrombolysis as it will also diagnose coronary artery dissection. Although recombinant tissue plasminogen activator does not cross the placenta, it may induce bleeding complications (sub placental bleeding); therefore, thrombolytic therapy should be reserved for life-threatening ACS when there is no access to PCI [26]. All reported stenting to manage ST-elevation myocardial infarction during pregnancy utilized bare metal stents. The safety of drug-eluting stents in pregnant woman is therefore still unknown; furthermore, these require prolonged dual antiplatelet therapy and should thus be avoided [8]. In women with intermediate or high risk non ST-elevation myocardial infarction, an invasive approach is indicated. In stable conditions with exertional symptoms, watchful waiting and conservative medical therapy is the treatment of choice [27]. In the case of recurrent coronary dissections, pre-term delivery may be considered according to fetal viability. Data on emergency coronary artery bypass graft surgery during pregnancy is rare, with a potentially high mortality rate [5, 6].

Radiation protection optimization methods for the management of the pregnant patient during invasive cardiology procedures include thoughtful operator technique, as well as radioprotective aprons. However, efficiency of the latter is not well established. In addition, there is a risk that part of the apron is in the primary X-ray field of view, thus triggering the automatic exposure

control (AEC) system of the radioscopy unit to increase radiation dose, as is also the case when using leaded gloves in the primary beam [29].

Radiation exposure to the fetus predominantly arises from scattered radiation within the patient [9, 30]. Procedures should be performed by well experienced invasive cardiologists for attainment of the lowest radiation rates by minimizing radiation time.

A vascular access choice via the upper extremities could avoid direct fetal irradiation during catheter passage in many cases. Use of a lead apron on the table to shield the primary X-ray beam from reaching the fetus may be an option, as well as external shielding of the maternal pelvis; although radiation dose absorbed by the fetus without shielding was found to be only 3% higher than that with external shielding for all periods of gestation [30]. As mentioned previously, lead shielding in the primary field can potentially lead to a large increase in primary beam dose rate due to the response of the AEC system.

Consideration of the following additional radioprotection measures may further significantly reduce radiation exposure of the patient and fetus: i) Minimization of fluoroscopy time and the number of fluorographic images; ii) avoiding direct radiation of the abdominal region; iii) using available patient dose reduction technologies such as low-fluoroscopy-dose-rate settings, low-frame-rate pulsed fluoroscopy, removal of the anti-scatter grid, spectral beam filtration and use of increased X-ray beam energy; iv) positioning the patient as far distant from the X-ray tube as possible, placing the image receptor as close as possible to the patient and directing the primary beam as far away from the fetus as possible; v) adjusting collimator blades tightly to the area of interest, thus reducing patient dose and improving image quality by reducing scatter; vi) calculating the dose in concert with a knowledgeable medical physicist, if necessary; and vii) minimization of total administered contrast agent volume. Finally, medical physicists and radiologists may be consulted to evaluate such cases and consult with pregnant patients before or after a planned or unplanned examination with radiation.

Patient management when pregnancy status is determined after the intervention.

Cardiac diagnostic and therapeutic fluoroscopy procedures may be performed inadvertently on patients with unsuspected pregnancies. This would most often occur early in pregnancy,

perhaps after only a few weeks of gestation, when results of routine urine pregnancy tests are less reliable. Occasionally, human error or miscommunication is responsible for such events.

As previously mentioned, even the most complicated cardiac interventions are unlikely to exceed the fetal radiation dose cautionary threshold of 50 mGy. To our knowledge, there are no case data directly linking diagnostic imaging to fetal harm. In 1999, Brent et al. projected a general population total risk of spontaneous abortion, major malformations, mental retardation and childhood malignancy of approximately 286 per 1000 deliveries (28.6%). Exposing the fetus to 5 mSv may add approximately 0.17 cases per 1000 deliveries to this baseline rate, or about one additional case in 6000 [31]. It is generally not possible to convincingly differentiate between radiation-induced or spontaneous adverse fetal consequences. In cases where a positive pregnancy status is discovered after the IC procedure, proper interdisciplinary consultation and advising the patient regarding fetal risks associated with radiation exposure are important. In general, termination of pregnancy is not recommended unless there is reasonable documentation that an estimated fetal dose greater than 150 mGy has occurred. If doses between 100 and 150 mGy are suspected, individual circumstances should be considered to determine an appropriate course. Termination of gestation is generally not justified when fetal doses are below 100 mGy [11, 32-34].

Conclusion

The number of percutaneous cardiac interventions performed on pregnant women, although relatively low, is likely to increase due to rising maternal age and other factors. A main fetal concern when performing PCI during patient pregnancy is managing the volume of iodinated contrast medium, which can cause neonatal hypothyroidism. Fetal exposure to ionizing radiation is a second, but lesser risk. For pregnant patients with ACS, percutaneous coronary intervention is preferable to drug-induced thrombolysis due to a decreased risk of mortality. Further, the risk of sub placental bleeding associated with thrombolysis is increased and is life threatening to the conceptus. For women in stable condition with exertional symptoms, watchful waiting and conservative medical therapy is the preferred treatment. In the case of recurrent coronary dissections, pre-term delivery may be considered after assessing fetal viability.

References

[1] *Temporal trends in treatment of ST-elevation myocardial infarction among men and women in Switzerland between 1997 and 2011*. D. Radovanovic, B. K. Nallamothu, B. Seifert, O. Bertel, F. Eberli, P. Urban, G. Pedrazzini, H. Rickli, J.-C. Stauffer, S. Windecker, P. Erne. European Heart Journal: Acute Cardiovascular Care 1(3) 183-191.

[2] *ICRP publication 84: pregnancy and medical radiation,* R. Brent, F. Mettler, L. Wagner, Streffer, M. Berry, S. He, T. Kusama, ICRP (2001) 30/1.

[3] *Heart disease and stroke statistics – 2015 update: A report from the American Heart Association, D.* Mozaffarian, E. J. Benjamin, A. S. Go, D. K. Arnett, M. J. Blaha, M. Cushman, S. de Ferranti, J. P. Després, H. J. Fullerton, V. J. Howard, M. D. Huffman, S. E. Judd, B. M. Kissela, D. T. Lackland, J. H. Lichtman, L. D. Lisabeth, S. Liu, R. H. Mackey, D. B. Matchar, D. K. McGuire, E. R. Mohler 3rd, C. S. Moy, P. Muntner, M. E. Mussolino, K. Nasir, R. W. Neumar, G. Nichol, L. Palaniappan, D. K. Pandey, M. J. Reeves, C. J. Rodriguez, P. D. Sorlie, J. Stein, A. Towfighi, T. N. Turan, S. S. Virani, J. Z. Willey, D. Woo, R. W. Yeh, M. B. Turner; American Heart Association Statistics Committee and Stroke Statistics Subcommittee, Circulation. 2015 Jan 27; 131(4):e29-322.

[4] *2010 Pregnancy Rates Among U.S. Women*, S. C. Curtin, J. C. Abma, Division of Vital Statistics, NCHS; K. Kost, Guttmacher Institute, Centers for Disease Control and Prevention (CDC).

[5] *Acute myocardial infarction in pregnancy: a United States population-based study*, M. G. Jamison, M. S. Biswas, L. R. Brancazio, G. K. Swamy, E. R. Myers, Circulation 113, 1564–71 (2006).

[6] *Acute myocardial infarction in pregnancy and the puerperium: a population-based study*, H. E. Ladner, B. Danielsen, W. M. Gilber, Obstet Gynecol 105, 480–4 (2005).

[7] *Acute myocardial infarction associated with pregnancy, A.* Roth, U. Elkayam, *J. Am. Coll. Cardiol.* 52, 171–80 (2008).

[8] *ESC Guidelines on the management of cardiovascular diseases during pregnancy: the Task Force on the Management of Cardiovascular Diseases during Pregnancy of the European*

Society of Cardiology (ESC), European Society of Gynecology (ESG), Association for European Paediatric Cardiology (AEPC), German Society for Gender Medicine (DGesGM) et al., Eur. Heart J. 32(24), 3147–3197 (2011).

[9] *Cardiovascular imaging of the pregnant patient,* P. M. Colletti, K. H. Lee, U. Elkayam, *AJR Am J Roentgenol* 200, 515–21 (2013).

[10] *Utilization of developmental basic science principles in the evaluation of reproductive risks from pre- and postconception environmental radiation exposures,* R. L. Brent, Teratology 59, 182–204 (1999).

[11] *Radiation exposure and pregnancy: when should we be concerned?* C. H. McCollough, B. A. Schueler, T. D. Atwell, N. N. Braun, D. M. Regner, D. L. Brown, A. J. LeRoy. Radiographics 27, 909–17; discussion 917–8 (2007).

[12] *The effects of embryonic and fetal exposure to ionizing radiation: counseling the patient and worker about these risks*, Brent RL, in: Mossman KL, Mill WA (eds), The Biological Basis of Radiation Protection Practice. Baltimore (MD): Williams & Wilkins, 1992: 3.

[13] *Radiation absorbed dose to the embryo/fetus from radiopharmaceuticals*, J. R. Russell, M. G. Stabin, R. B. Sparks, E. Watson, Health Phys 73, 756–69 (1997).

[14] *Mental retardation following in utero exposure to the atomic bombs of Hiroshima and Nagasaki,* W. J. Blot, R. W. Miller, Radiology 106, 617–9 (1973).

[15] *Perinatal loss and neurological abnormalities among children of the atomic bomb. Nagasaki and Hiroshima revisited, 1949 to 1989,* J. N. Yamazaki, W. J. Schull, JAMA 264, 605–9 (1990).

[16] *In utero exposure to A-bomb radiation and mental retardation; a reassessment*, M. Otake, W. J. Schull, Br J Radiol 57, 409–14 (1984).

[17] *Radiation exposure from CT scans in childhood and subsequent risk of leukaemia and brain tumours: a retrospective cohort study*, M. S. Pearce, J. A. Salotti, M. P. Little, K. McHugh, C. Lee, K. P. Kim, N. L. Howe, C. M. Ronckers, P. Rajaraman, A. W. Craft, L. Parker, A. Berrington de González, The Lancet, Volume 380, No. 9840, p499–505, 4 August 2012.

[18] *A new calculation of the carcinogenic risk of obstetric X-raying*, J. F. Bithell, C. A. Stiller, Stat Med 7, 857–64 (1988).

[19] *Cognitive function and prenatal exposure to ionizing radiation*, W. J. Schull, M. Otake, Teratology 59, 222–6 (1999).

[20] Committee on Biological Effects of Ionizing Radiation, Board on Radiation Effects Research, Commission on Life Sciences, National Research Council. Health effects of exposure to low levels of ionizing radiation. In: Beir V (ed). Washington, DC: National Academy Press, 1990.

[21] *The use of iodinated and gadolinium contrast media during pregnancy and lactation,* J. A. Webb, H. S. Thomsen, S. K. Morcos, Eur Radiol 15, 1234–40 (2005).

[22] *Reproductive, developmental, and genetic toxicology of ioversol,* W. H. Ralston, M. S. Robbins, P. James, Invest Radiol 24 Suppl 1, S16–22 (1989).

[23] *Guidelines for diagnostic imaging during pregnancy*, ACOG Committee Opinion, Obstet Gynecol, Number 299, September 2004 (replaces No. 158, September 1995), 104, 647–51 (2004).

[24] *Neonatal thyroid function: effect of a single exposure to iodinated contrast medium in utero,* G. Bourjeily, M. Chalhoub, C. Phornphutkul, T. C. Alleyne, C. A. Woodfield, K. K. Chen, Radiology 256, 744–50 (2010).

[25] *Imaging-related medications: a class overview*, J. M. Widmark, Proc (Bayl Univ Med Cent) 20, 408–17 (2007).

[26] *Thrombolytic therapy in pregnancy, G.* Leonhardt, C. Gaul, H. H. Nietsch, M. Buerke, E. Schleussner, J. Thromb. Thrombolysis 21, 271–6 (2006).

[27] *Early invasive vs conservative treatment strategies in women and men with unstable angina and non-ST-segment elevation myocardial infarction: a meta-analysis,* M. O'Donoghue, W. E. Boden, E. Braunwald, C. P. Cannon, T. C. Clayton, R. J. de Winter, K. A. Fox, B. Lagerqvist, P. A. McCullough, S. A. Murphy, R. Spacek, E. Swahn, L. Wallentin, F. Windhausen, M.S. Sabatine, JAMA 300, 71–80 (2008).

[29] IAEA Radiation Protection of Patients (RPOP) webpage, available at https://rpop.iaea.org/RPOP/RPoP/Content/InformationFor/HealthProfessionals/4_InterventionalRadiology/fluoroscopy-operating-theatres/fluoroscopy-staff-protection.htm, accessed on 17.02.2017

[30] *Conceptus radiation dose and risk from cardiac catheter ablation procedures*, J. Damilakis, N. Theocharopoulos, K. Perisinakis, E. Manios, P. Dimitriou, P. Vardas, N. Gourtsoyiannis, Circulation 104, 893–7 (2001).

[31] *The effect of embryonic and fetal exposure to x-ray, microwaves, and ultrasound: counseling the pregnant and nonpregnant patient about these risks,* R. L. Brent, Semin. Oncol. 16, 347–68 (1989).

[32] *Imaging in pregnant patients: examination appropriateness,* K. M. Wieseler, P. Bhargava, K. M. Kanal, S. Vaidya, B. K. Stewart, M. K. Dighe, Radiographics 30, 1215–29; discussion 1230–3 (2010).

[33] *Diagnostic medical exposures: advice on exposure to ionizing radiation during pregnancy,* C. Sharp, J. A. Shrimpton, R. F. Bury, Oxon, UK: National Radiological Protection Board, 1998

[34] *ACR practice guideline for imaging pregnant or potentially pregnant adolescents and women with ionizing radiation*, V. A. Reston, American College of Radiology, 2008, available at http://www.who.int/tb/advisory_bodies/impact_measurement_taskforce/meetings/prevalence_survey/imaging_pregnant_arc.pdf, accessed on 17.02.2017

IOP Publishing | Society for Radiological Protection Journal of Radiological Protection

J. Radiol. Prot. **36** (2016) 561–578 doi:10.1088/0952-4746/36/3/561

InterCardioRisk: a novel online tool for estimating doses of ionising radiation to occupationally-exposed medical staff and their associated health risks

David Moriña[1,2,3,4,5], James Grellier[1,2,3,6], Adela Carnicer[7], Eileen Pernot[2,3,4], Nick Ryckx[7] and Elisabeth Cardis[2,3,4]

[1] ISGlobal, Centre for Research in Environmental Epidemiology (CREAL), Barcelona, Spain
[2] Universitat Pompeu Fabra (UPF), Barcelona, Spain
[3] CIBER Epidemiología y Salud Pública (CIBERESP), Barcelona, Spain
[4] Unit of Infections and Cancer (UNIC), Cancer Epidemiology Research Program (CERP), Catalan Institute of Oncology (ICO)-IDIBELL, L'Hospitalet de Llobregat, Barcelona, Spain
[5] Grups de Recerca d'Àfrica i Amèrica Llatines (GRAAL)—Unitat de Bioestadística, Facultat de Medicina, Universitat Autònoma de Barcelona, Bellaterra 08193, Spain
[6] Department of Epidemiology and Biostatistics, Imperial College, London, UK
[7] Institute of Radiation Physics (IRA), Department of Radiology, Centre Hospitalier Universitaire Vaudois (CHUV), Lausanne, Switzerland

E-mail: dmorina@iconcologia.net

Received 23 October 2015, revised 30 May 2016
Accepted for publication 14 June 2016
Published 27 July 2016

Abstract

Those working in interventional cardiology and related medical procedures are potentially subject to considerable exposure to x-rays. Two types of tissue of particular concern that may receive considerable doses during such procedures are the lens of the eye and the brain. Ocular radiation exposure results in lens changes that, with time, may progress to partial or total lens opacification (cataracts). In the early stages, such opacities do not result in visual disability; the severity of such changes tends to increase progressively with dose and time until vision is impaired and cataract surgery is required. Scattered radiation doses to the eye lens of an interventional cardiologist in typical working conditions can exceed 34 μGy min^{-1} in high-dose fluoroscopy modes and 3 μGy per image during image acquisition (instantaneous rate values) when radiation protection tools are not used. A causal relation between exposure to ionising radiation and increased risk of brain and central nervous system tumours has been shown in a number of studies. Although

absorbed doses to the brain in interventional cardiology procedures are lower than those to the eye lens by a factor between 3.40 and 8.08 according to our simulations, doses to both tissues are among the highest occupational radiation doses documented for medical staff whose work involves exposures to x-rays. We present *InterCardioRisk*, a tool featuring an easy-to-use web interface that provides a general estimation of both cumulated absorbed doses experienced by medical staff exposed in the interventional cardiology setting and their estimated associated health risks. The tool is available at http://intercardiorisk.creal.cat.

Keywords: fluoroscopy, dosimetry, brain tumour risk, cataracts risk, occupational exposure

S Online supplementary data available from stacks.iop.org/JRP/36/561/mmedia

(Some figures may appear in colour only in the online journal)

1. Introduction

Interventional cardiology (IC) comprises a variety of minimally-invasive procedures used in the diagnosis and treatment of cardiovascular disease. In fluoroscopy, a key technology used in this work, hard x-rays (photon energies typically above 5–10 keV) are passed through a patient onto a detector; catheters and contrast agents are used thereby allowing real-time visualisation of internal structures, processes and activities [1]. Since interventional cardiologists and electrophysiologists carry out their work in close proximity to the patient on whom the imaging is being carried out, they are exposed occupationally to ionising radiation (IR) under normal working conditions.

Used appropriately to support a variety of procedures, IC provides enormous clinical benefits over other surgical procedures, including minimal invasiveness, reduced pain and risk of complications, shorter hospital stays, and lower costs [2, 3]. The benefits of catheterisation over open surgery have resulted in a considerable increase in workloads for IC staff over the past two decades and, although concomitant improvements in technology and radiation protection (RP) measures have reduced doses per procedure, there is concern that higher cumulated doses result in increased risks to IC staff (particularly surgeons) of cataracts and may increase the risk of brain tumours [4]. Effective use of RP measures can reduce doses to exposed organs and thereby lower the magnitude of associated health risks. Doses to both the patient and IC staff can be lowered via configuration of the fluoroscope. Doses to IC staff are typically reduced through personal use of lead (or lead equivalent) aprons and thyroid shields. International best practice recommendations state that physicians involved in interventional procedures should wear such an apron, a thyroid shield and leaded eyewear as a minimum set of RP measures [5], and these are currently used routinely in most IC procedures. A number of additional protection measures may, however, be employed to further reduce operator doses. As well as personal protective equipment such as lead caps, several radiation shielding devices may be employed, including flexible blanket-type shields laid over the patient during interventions to reduce operator exposure to scattered radiation, table skirts (screens suspended between the operating table and the floor), RP cabins (several screens assembled so as to surround the operator, with apertures for the hands), and ceiling-suspended screens (manoeuverable screens that can be pulled down in front of the operator's face) [6]. The degree to

which such measures are employed vary by procedure, specialisation, experience, individual, hospital and country. There are differences in their availability as well: while table skirts and ceiling-suspended screens are available in most IC environments, flexible blanket-type shields are not commonly available and RP cabins are very seldom installed. It has been suggested that such measures are not employed in all catheterisation laboratories, possibly due, in part, to the lack of available information and training in RP [7]. This is especially true for those protection measures that are widely available such as table skirts and ceiling-suspended screens. The latter is probably the most important item of protection for the head. In some cases, impracticability, discomfort and occupational back pain may also play a role in IC staff not employing certain measures. Recent substitution of lightweight high atomic number materials for the heavier lead used in protective clothing has reduced discomfort for personnel and increased compliance [8]. Given typical RP practices at the present time, the organs of operators that remain chiefly exposed are those in the head, including the eyes and the brain. This gives cause for concern, since IR is known to have the potential for causing damage to these tissues.

Scattered radiation doses to the eye lens of an interventional cardiologist in typical working conditions can exceed 34 μGy min^{-1} in high-dose fluoroscopy modes and 3 μGy per image during image acquisition (instantaneous rate values) when radiation protection tools are not used [9]. Radiation-induced cataract has been recognised as a highly relevant non-cancer endpoint among those exposed to IR since the 1930s [10]. Radiation-induced cataracts typically develop as central opacities in the subcapsular posterior region of the lens, and consist of small granules and vacuoles that form a roughly circular opacity. Defects in lens transparency cause little or no visual impairment in the early stages of the disease, but eventually cause distortion and clouding. The reaction of the lens to radiation is partly attributable to lifelong continued differentiation of the epithelial cells that make up the lens (fibrogenesis); aberrant differentiation of cells due to exposure to radiation results in their accretion to the superficial posterior cortex [11].

Primary tumours of the central nervous system (CNS) include tumours, both malignant and benign, of the brain, brain stem and spinal cord. The epidemiological literature provides clear evidence for a causal association between brain tumours and exposures to IR [12, 13]. Although some of the available literature supporting this association relate to childhood exposures to low linear energy transfer (LET) radiation (such as x-rays) [14], studies of the Japanese atomic bomb survivors indicate increased risks of various CNS tumours (mainly brain tumours) characterised by linear dose-response in adults [15].

Accurate estimation of health impacts to medical staff from IR under a variety of operational and RP scenarios is increasingly important as use of IC procedures continues to grow. Of the existing online radiation risk assessment tools, the majority are focused on radiation exposures to the general population or to medical patients undergoing specific diagnostic or radiotherapeutic procedures, and tend to provide estimates of cancer risk only [16, 17]. Our primary objective was to produce a tool that estimates the most relevant organ doses in IC staff occupationally exposed to radiation, and to estimate the associated health impacts due to these exposures taking into account all sources of uncertainty, specifically in terms of the risk of cataracts and brain tumours. All the abbreviations used throughout the paper are available as supplementary material (stacks.iop.org/JRP/36/561/mmedia).

2. Methods

We designed a tool that produces distributions of annual and total cumulated absorbed doses to the brain and eye lens by employing robust estimators of parameters [18] based on a multiple

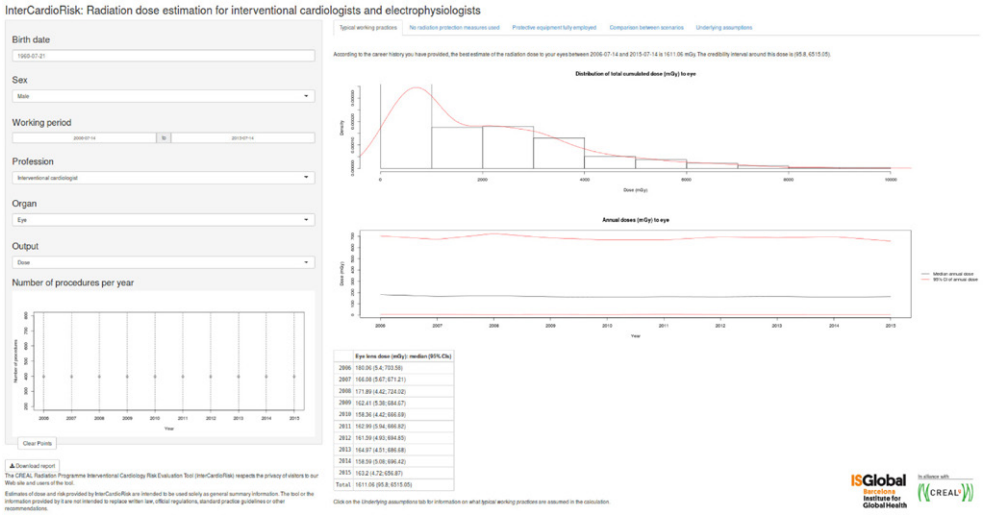

Figure 1. Screenshot of the web-based tool, showing the estimated absorbed dose (in mGy) to the eye lens for an interventional cardiologist, under the 'typical working practices' scenario.

linear regression of predictors of dose, and subsequently estimates risk based on published epidemiological data.

We developed the tool in **R** [19] using the `shiny` package [20], which allows construction of interactive web applications from **R** and provides an easy-to-use web front-end. The user interface (figure 1) comprises two panels, positioned side by side. In the left-hand 'input' panel, the users can introduce specific data concerning their career (profession, work period and annual numbers of procedures), the target organ of interest (brain or eye lens), and the required output in terms of either absorbed dose (in mGy) or associated health risk. Results are automatically generated and presented in the right-hand 'output' panel.

The output panel is further divided into five tabs, the first three presenting the user with organ-specific absorbed doses to the eye lens or brain (in mGy), and the associated risk of cataracts and CNS tumours, respectively. These tabs correspond to dose and risk estimates under different RP scenarios, namely (a) 'typical working practices'; (b) 'no radiation protection measures used'; and (c) 'protective equipment fully employed'—a career during which all RP measures typically available throughout that time period were used. Absorbed doses are presented both annually and cumulated across the whole career, together with 95% credibility intervals. The fourth tab presents the cumulated doses and risk estimates for each of the three scenarios side by side, thereby facilitating comparison of the potential impacts on dose and risk of employing RP measures. The last tab presents a summary of the underlying assumptions employed by the tool in its calculations. In addition to the web version of the results, the user can download a summary report in PDF format that includes all input data and results.

An eye lens dose prediction model was built using data collected in the ORAMED (Optimization of RAdiation protection for MEDical staff) project—described in section 2.1—and from the literature, together with the user-defined occupational history. The potential predictors of absorbed dose to the eye lens included the usage of RP measures, catheterisation access route, tube configuration and operator experience. It was considered

unduly cumbersome to input precise details of every cardiological procedure carried out over a career. Instead, the tool was designed so that the user is required to specify only annual numbers of interventions carried out during their career (via a graphical interface), and an occupational history is reconstructed using the proportion of procedures reported as typical for France across each decade between 1970 and 2010 [21], in the absence of country-specific data. For the 'typical working practices' career scenario, the occupational history is reconstructed also assuming the RP practices typical amongst French cardiologists over the same time period. For the other two scenarios, the amount of RP practices incorporated into dose calculations is altered accordingly. Changes in dose area product (DAP) typically available to interventional cardiologists over the past four decades were taken into account by fitting a metaregression model using results from the literature [22–34], and subsequently adjusting the computed doses using these values. Probability distributions of measures of risk under each scenario are calculated on the basis of the resulting cumulated absorbed doses, using estimates of dose-response and related uncertainties derived from the epidemiological literature (described in section 2.3). Various sources of uncertainty are taken into account by means of Monte Carlo simulation, which allows uncertainties in several model inputs to be propagated through to results, and thereby expressed as 95% credibility intervals on estimates of dose and risk.

2.1. Data

The data used for fitting the dose prediction model were collected previously within the framework of the ORAMED project, a collaborative project funded in 2008 by the European Union under its 7th Framework Programme. Its remit included the development of methodologies for better assessing and reducing exposures to medical staff from procedures that potentially result in large radiation doses or are associated with complex radiation fields, such as those used in fluoroscopically guided procedures and nuclear medicine. The project collected information on the doses incurred to the eyes and the extremities of operators during IC and electrophysiology procedures in seven European countries (Belgium, Greece, France, Italy, Poland, Slovakia and Switzerland) through a measurement campaign. In total, 381 such procedures were monitored, including coronary angiography (CA) and percutaneous transluminal coronary angioplasty (PTCA), radiofrequency (RF) ablations and pacemakers and cardiac defibrillator implantations (PM/ICD). For each type of procedure, detailed data were collected on the configuration of the x-ray tube employed, the degree of usage of RP measures, and operator experience. These data are the most extensive data (in terms of number of monitored procedures and countries included) so far collected through measurements following a common protocol [35].

2.2. Dose estimation

Doses to the eye lens were estimated by means of a robust linear regression model on the basis of ORAMED data (dose per unit DAP considering the most exposed eye), including usage of table skirt, cabin and ceiling screen, on the type of procedure, on tube configuration, and on operator experience (defined as high after 4 years of working in IC or electrophysiology) as predictors of the absorbed dose. The obtained estimates are shown in table 1.

For instance, the dose estimated by the model for an interventionalist with relatively little work experience, using a biplane tube configuration and conducting a CA intervention, protected only by screen and table is $\exp(1.031 + 0.057 - 1.183 - 0.486 - 0.011) = 0.55\ \mu\text{Sv Gy} \cdot \text{cm}^{-2}$. The corresponding average dose in the ORAMED database is $0.52\ \mu\text{Sv Gy} \cdot \text{cm}^{-2}$.

Table 1. Parameter estimates and confidence intervals.

	$\hat{\beta}_0$ **(95% CI)**
Intercept	1.031 (0.56; 1.51)
Protection method	$\hat{\beta}$ **(95% CI)**
Table	−0.011 (−0.369; 0.346)
Screen	−0.486 (−0.788; −0.184)
Cabin	−0.648 (−1.118; −0.177)
Procedure	$\hat{\beta}$ **(95% CI)**
CA PTCA	Reference
PM/ICD	0.610 (0.225; 0.995)
RF ablation	−0.025 (−0.355; 0.305)
Tube configuration	$\hat{\beta}$ **(95% CI)**
Above	Reference
Below	−0.869 (−1.249; −0.489)
Biplane	−1.183 (−1.681; −0.684)
Experience	$\hat{\beta}$ **(95% CI)**
High	Reference
Low	0.057 (-0.178; 0.293)

In theory, dose to the eye lens is typically reduced by a factor of around 30 when 0.5 mm lead-equivalent eyewear are used, but this degree of attenuation is only achieved under frontal exposure to non-scattered radiation. In reality, interventionalists tend to position themselves sideways to the primary beam, are also subjected to scattered radiation emitted from the patient, and coverage of the eye may be reduced due to poor eyewear fit [36]. The reduction factor of absorbed dose to the eye lens due to the usage of protective eyewear was therefore assumed to follow a project evaluation and review techniques (PERT) distribution [37] with minimal, modal and maximal values of 1, 3 and 10 respectively, based on expert opinion and a review of the literature [8, 38–40]. The PERT distribution is a particular case of the Beta distribution, characterized by the density function

$$f(x) = \begin{cases} \dfrac{x^{\alpha-1}(1-x)^{\beta-1}}{B(\alpha,\beta)} & : 0 \leqslant x \leqslant 1 \\ 0 & : \text{Otherwise} \end{cases}$$

where $B(\alpha, \beta)$ is the beta function, defined by

$$B(\alpha,\beta) = \int_0^1 y^{\alpha-1}(1-y)^{\beta-1}\mathrm{d}y. \tag{1}$$

Sampling from the beta distribution requires minimum and maximum values (scale) and two shape parameters, α and β. The PERT distribution uses the mode or most likely parameter to generate the shape parameters α and β. An additional scale parameter λ scales the height of the distribution; the default value for this parameter is 4. In the PERT distribution, the mean μ is calculated as

$$\mu = \frac{\min + \max + \lambda \cdot \text{mode}}{\lambda + 2} \tag{2}$$

And it can be used to compute the Beta distribution parameters α and β:

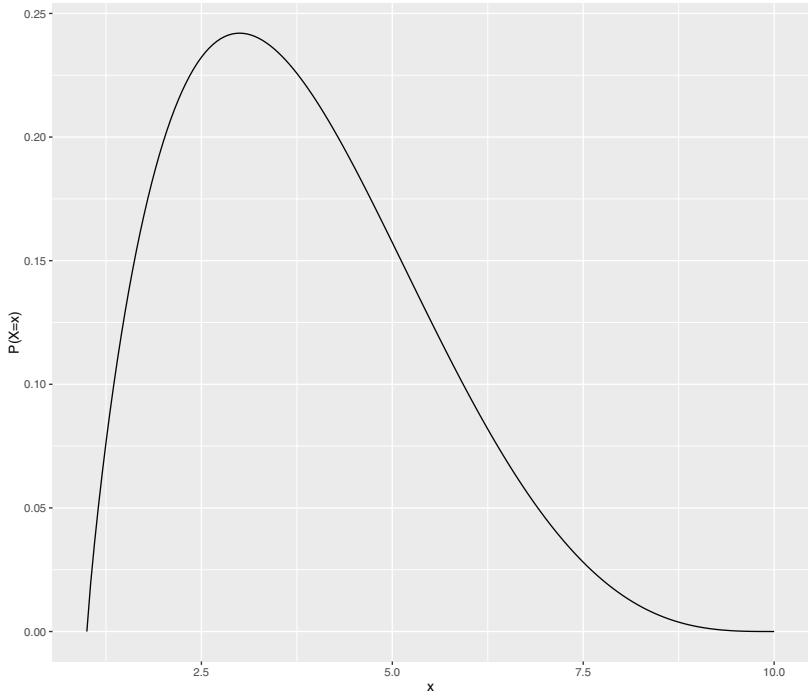

Figure 2. Profile of a PERT distribution with minimum 1, maximum 10 and mode 3.

$$\alpha = \frac{(\mu - \min) \cdot (2\text{mode} - \min - \max)}{(\text{mode} - \mu) \cdot (\max - \min)}$$
$$\beta = \frac{\alpha \cdot (\max - \mu)}{\mu - \min} \tag{3}$$

The PERT distribution was preferred over the triangular distribution, which is commonly used to model data elicited from experts or assembled from a variety of published courses, as it does not suffer the same potential for systematic bias [37]. Like the triangular distribution, the PERT distribution emphasizes the 'most likely' value over the minimum and maximum estimates. However, unlike the triangular distribution the PERT distribution constructs a smooth curve which places progressively more emphasis on values around (near) the most likely value, rather than on values around the edges.

The considered PERT distribution profile is shown in figure 2.

The metaregression model fitted to incorporate the changes in DAP over time was $893.34–0.43 \cdot \text{year}$. Therefore, the estimated dose in μSv Gy $\cdot$ cm^{-2} is multiplied by the corresponding factor taking into account the year to obtain an estimated dose per procedure (in μSv). This dose is finally multiplied by the number of procedures carried out that year by the user and converted into mGy to be reported by the tool.

Doses to the brain were estimated as a function of modelled eye lens dose assuming a linear relationship. This function was estimated by way of carrying out measurements in a typical angiography room. Doses were measured using thermoluminescent dosimeters (TLD) in a CIRS 702-D anthropomorphic female phantom, which was draped with a lead apron and a thyroid shield, and positioned laterally to a single flat panel detector (Philips Allura XPer

Figure 3. Set-up of anthropomorphic phantom in angiography room.

FD10) (figure 3). The patient was simulated with polymethyl methacrylate (PMMA) slabs assembled as a rectangular cuboid of dimensions 25.2 cm × 20 cm × 40.5 cm. Eleven TLDs were used for brain dosimetry (distributed across four 2.5 cm slabs), and 2 TLDs were used to measure doses to the eye lens. Absorbed doses were measured for the eyes and for the brain (those parts considered most relevant in terms of tumours). The ratios between each measured eye dose and a brain dose weighted on the volumes of individual anatomical regions in which the TLDs were placed, were calculated for use as a conversion factor from eye dose to brain dose. This conversion factor was found to be between 3.40 (eye furthest from fluoroscope) and 8.08 (eye closest to fluoroscope). Operators increasingly work from both sides of the patient during procedures [1]. In order to account for uncertainties due to positioning of the interventionalist in our estimation of brain dose, the conversion factor was defined as a uniform distribution between 3.40 and 8.08.

2.3. Risk estimation

In addition to providing estimates of dose to the eye lens and to the brain, the tool also provides the user with estimates of the magnitude of health impacts associated with cumulated doses of IR, specifically in terms of the relative risk (RR) of radiation-related cataracts and the lifetime fractional risk (LFR) of CNS tumours, a measure that scales the lifetime attributable risk (LAR) to the lifetime spontaneous cancer incidence or mortality [41]. For the sake of internal consistency and to ease comparisons to other studies, RR of CNS tumours are also shown.

In the case of the eye lens, we calculated a dose-response coefficient for stage 1 to 5 cataracts, by scaling summary risk estimates at 1 Gy derived from the epidemiological literature [11] (Odds Ratio: 1.70; 95% confidence intervals: 1.22, 1.38). Using the published 95% confidence intervals for the summary risk estimates it was possible to calculate the standard error (SE) and thereby define the dose-response function probabilistically. Although the risk estimates at 1 Gy proposed in [11] were obtained through a log-linear model, the excess relative risk model was preferred in InterCardioRisk tool in order to ensure reasonable risk estimates at the highest doses.

The time between irradiation and the appearance of lens opacities is still uncertain but nevertheless, early work on radiation-induced cataract among the atomic bomb survivors showed an approximate average latency period for development of lens opacities of 2–3 years [42, 43]. As we are quantifying risks of cataracts of a range of severities, starting from stage 1, which are just minor changes in the lens, lower severity than those studied in atomic bomb survivors, we considered a lag of 5 years.

By way of Monte Carlo simulation, the tool uses the dose-response function and the scenario-specific distributions of cumulated absorbed dose to the eye lens to calculate a distribution of RR under each scenario.

The LFR of CNS tumours was estimated using the methods developed by the BEIR VII committee [44] and data from the 1958–98 Life Span Study data [45], as was carried out in developing the NCI RadRAT tool [16]. This is computed as $\text{LFR} = \frac{\text{LAR}}{B}$, where $B = \int_0^{110} m(a)S(a)$ is the baseline risk for a general population ($m(a)$ is the background cancer incidence in the European population) and LAR is the lifetime attributable risk, computed as suggested by the BEIR VII committee:

$$\text{LAR} = \frac{\int_{e+L}^{110} \beta_s D e^{\gamma e^*} \left(\frac{a}{60}\right)^{\nu} \frac{S(a)}{S(e)}}{\text{DDREF}}, \tag{4}$$

where e is the age at exposure, $e^* = \frac{e-30}{10}$ if $e < 30$ or $e^* = 0$ otherwise, a is the attained age and according to the BEIR VII committee and [16], $\beta_s = 0.71, 0.24$ for males and females respectively, $\gamma = -0.3$ and $\nu = -1.4$. L is the latency period, considered to be of 5 years for all solid cancer by BEIR VII committee. $\frac{S(a)}{S(e)}$ is the probability of being alive at age a, given that an individual is alive at age e, and D is the estimated dose. The approach used here for dose and dose-rate effectiveness factor (DDREF) is the same that was used in [16], i.e. described by a lognormal distribution with a geometric mean of 1.5 and a geometric standard deviation of 1.35. LAR can be understood as an approximation to the premature probability of developing a cancer that can be attributed to radiation exposure, while LFR is useful because it is a relative number. Uncertainty in the LAR definition parameters (4) have been taken into account by means of Monte Carlo simulation.

The RR of CNS tumours are calculated according the values reported in [12].

3. Results

The tool provides us with a means to estimate the cumulated absorbed doses to the eye lens and brain (in mGy)—and associated health risks—under the three scenarios, and easily make comparisons between them. As an example, we can estimate the doses and health risks for a 'typical' male interventional cardiologist born in 1960, who worked from 1985 to 2014, carrying out 300 procedures per year between 1985 and 2000, and then 350 per year until 2014. Distributions of cumulated absorbed doses to eye lens and brain under the three RP scenarios ('typical working practices', 'no radiation protection measures used', and 'protective equipment fully employed') are presented as histograms (figure 4).

Median annual absorbed doses for each scenario (figure 5) are also presented by the tool in tabulated form, along with 95% credibility intervals (CI). The figure illustrates an increase in dose of about 15%–20% (depending on the scenario) after 2000 due to increased workload (from 300 annual procedures to 350). It also reflects the impact of the introduction of new radiation protection measures, for instance a large reduction in annual absorbed doses can be seen in 1990,

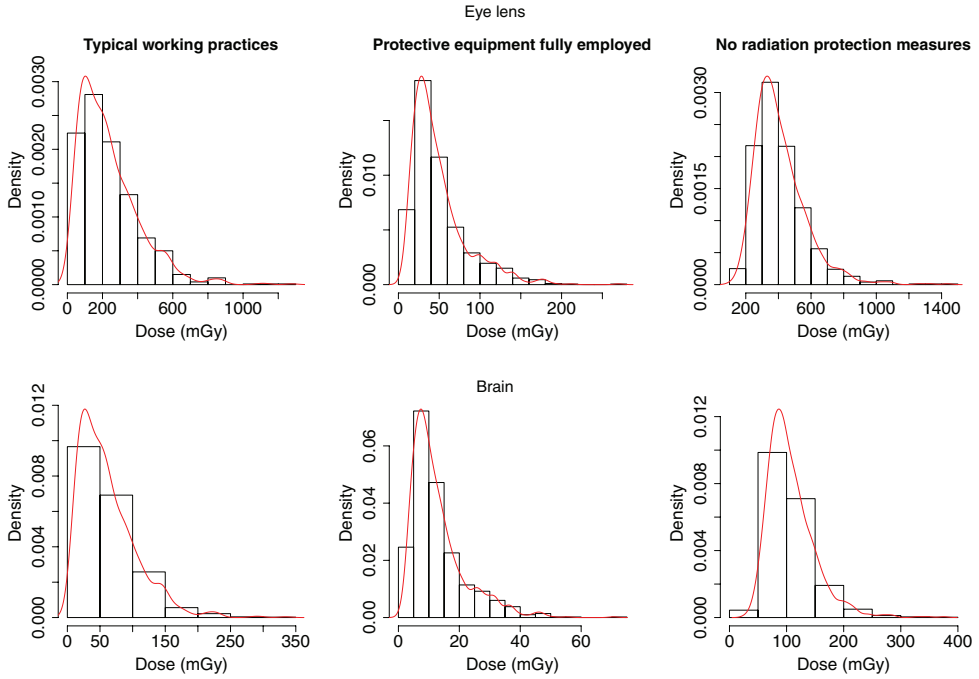

Figure 4. Estimated probability density function of distributions of cumulated absorbed doses (mGy) to the eye lens (upper panel) and brain (lower panel), for a typical cardiologist working between 1985 and 2014.

when an increase of 25% in the usage of lead glasses is assumed. In this example, the estimated total cumulated absorbed lens dose is about 200 mGy (95% CI: 40, 645) under the 'typical working practices' scenario. If no protection methods are used, these values are increased to 380 mGy (95% CI: 200, 800). In the scenario under the usage of all available protection methods, the estimated dose is 40 mGy (95% CI: 10, 140). The R code to generate figure 4 and figure 5 is provided as supplementary material (stacks.iop.org/JRP/36/561/mmedia). All the assumptions on changes in RP measures usage are based on the results of the O'CLOC study (Occupational Cataracts and Lens Opacities in Interventional Cardiology, [21]). The O'CLOC study included about 40 French centers ([46]), with a balanced distribution of the centres across France and a balanced distribution of public and private hospitals ([46, 47]). The resulting differences in estimated health risks calculated for the three scenarios are shown in table 2.

It is clear that the use of protection methods has a great impact on reducing cumulated absorbed doses to the eye lens and, subsequently, on reducing the risk of cataracts. If we compare the doses to the eye lens incurred under a scenario in which no protection methods are used at all, these impacts become all the more apparent. The user can also see the difference between the different protection methods usage scenarios on the cataract risk. For example, figure 6 shows the difference in the distribution of RR and LFR of CNS tumours and RR of stage 1–5 cataracts.

4. Discussion

We developed a novel tool, InterCardioRisk, that allows IC personnel to estimate their annual and cumulated doses to the eye lens and brain, and associated potential health impacts in terms

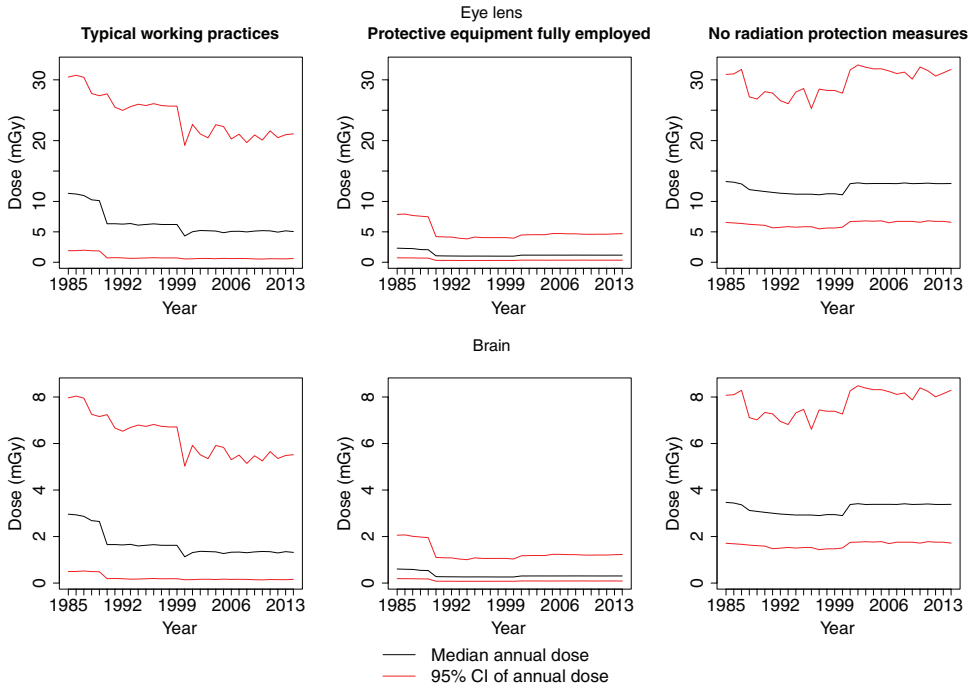

Figure 5. Annual absorbed doses (mGy) to eye lens (upper panel) and brain (lower panel), for a typical cardiologist working between 1985 and 2014.

Table 2. Estimates of potential health risks for the three different RP scenarios, in terms of relative risks of cataracts for doses to the eye lens and RR and lifetime fractional risk (LFR) for CNS tumours, for a typical cardiologist working between 1985 and 2014.

Outcome	Scenario	Measure of risk	Estimate (95% CI)
Stage 1–5 cataracts	Typical working practices	RR	1.11 (1.02, 1.51)
	Protective equipment fully employed		1.02 (1.01, 1.10)
	No radiation protection measures used		1.22 (1.09, 1.58)
CNS tumours	Typical working practices	RR	1.05 (1.01, 1.30)
	Protective equipment fully employed		1.01 (1.00, 1.06)
	No radiation protection measures used		1.10 (1.02, 1.44)
CNS tumours	Typical working practices	LFR	1.00 (1.00, 1.01)
	Protective equipment fully employed		1.00 (1.00, 1.00)
	No radiation protection measures used		1.01 (1.00, 1.02)

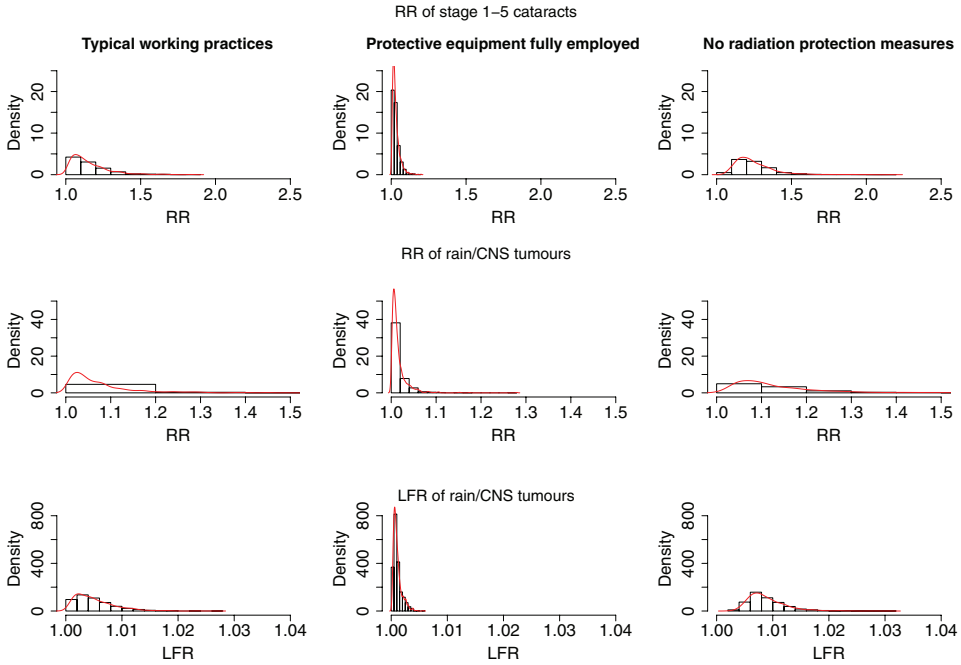

Figure 6. Estimated probability density function of distributions of stage 1–5 cataracts RR (upper panel) and CNS tumours RR and LFR (lower panel) for a typical cardiologist working between 1985 and 2014.

of risk of cataracts and CNS tumours. Specifically, the tool allows the user to compare estimated doses to a worker with a typical career and typical use of RP measures, and the associated estimated risks of cataract and CNS tumour, with the reductions in dose expected where protective equipment is employed to the maximum possible extent. By extension, the output of the tool allows for estimation of the expected health benefits for that population associated with increased use of available RP measures. The InterCardioRisk tool directly supports the aims of RP, and would make a useful addition to the RP training of those working in IC. In particular, the use of LFR as the risk metric facilitates direct comparison with the lifetime cancer risk of a person of the same age and sex in the general population. For those already employing RP practices effectively in their work, the small magnitude of increased risks serves as a reassurance that they are successfully minimising their occupational exposure. By the same token, those not following RP guidelines may be motivated towards employing RP measures to reduce their cumulated doses and attendant health risks.

Cumulative eye lens doses estimated by the InterCardioRisk tool are consistent with the results of the French O'CLOC study [21, 46, 47]. This study presented a retrospective assessment of cumulative eye lens doses for interventional cardiologists and electrophisiologists using dose data from the ORAMED project, as well as information on the workload, radiation protection equipment and dose reduction factors. The authors reported a median cumulative eye lens dose of 309 mSv, ranging from 25 mSv to more than 1600 mSv, for 129 interventional cardiologists at an average age of 51 who had worked for an average period of 22 years, similar to the estimates provided by the InterCardioRisk tool using Jacob's data under the typical working practices scenario (median of 314 mSv, with a credibility interval of (61 mSv–1142 mSv)). In contrast with these dose levels, other studies report cumulative

eye lens doses significantly higher. These studies are based on a different, common methodology [48–51], using experimental data of scattered dose factors per unit DAP measured with electronic dosemeters, corrected by the operator position and the use of protective devices, and reported workload. Cumulative eye lens doses reported in these works are of 6 Sv (100 mSv–27 Sv) (median value, average age of 46, average working period of 14 years) [48], 3.7 Gy (20 mGy–43 Gy) (mean value, average age of 42, average working period of 9.2 years) [50] and 420 mSv (46 mSv–7.3 Sv) (median, average age of 43, average working period of 8 years) [51]. These values lead to average annual doses ranging from 53 mSv to 429 mSv, in contrast with an annual dose of 14 mSv issued from InterCardioRisk and Jacob's paper. The different doses estimated by each methodology fall within the large ranges of dose reported in the literature. The variation in reported doses is associated with the high degree of uncertainty in measurements of lens dose, with different methodologies used, and the assumptions used to extrapolate eye doses from other dose measures [52]. However, we consider that estimates based on ORAMED measurement campaign are likely to provide more realistic outcomes because doses were measured under real conditions.

There have been several reports made regarding radiation-induced cataract in ICs who have performed procedures for a number of years, and of equivalent doses to the lens approaching the annual limit of 150 mSv during angiographic procedures [48, 53–55]. Recent studies have shown that under typical workloads of an IC, the radiation dose to the lens may exceed the current threshold for tissue reactions after several years of work if radiological protection devices are not used and radiological protection principles are not followed [6, 53]. Several surveys of cardiologists and support staff working in catheterisation laboratories, conducted with coordination provided by the International Atomic Energy Agency (IAEA) in Latin America and Asia, have found a high prevalence of lens opacities of the type associated with occupational radiation exposure [50, 53]. These recent data and the mechanistic uncertainties regarding cataract development highlighted the need for a detailed re-appraisal of the radiosensitivity of the lens of the eye. This issue is addressed in Publication 118 of the ICRP and in the Commission's statement on tissue reactions [56, 57]. The previous Commission recommendation [58] of an equivalent dose limit of 150 mSv y^{-1} for occupational exposure in a planned exposure situation (e.g. occupational exposure of interventionalists) has been changed. The Commission now recommends that the lens-equivalent dose limit for chronic occupational exposure should be 20 mSv y^{-1}, averaged over a defined 5-year period, with no single year exceeding 50 mSv (i. e. the same as the annual whole-body limit for workers) [56, 57]. Note that a study performed with data from 1984 through 1988, when both cardiac interventions and fluoroscopic equipment were less sophisticated than they are now, determined that the annual equivalent dose to cardiologists' heads was approximately 20–30 mSv [59]. The Commission considers the threshold for absorbed dose to the lens of the eye to be 0.5 Gy [56]. The Commission judges, based on existing evidence, that an acute dose of up to around 0.1 Gy (100 mGy) produces no functional impairment of tissues, including the lens of the eye with respect to cataract, although the use of a threshold model remains uncertain for this tissue [56].

As the degree of usage of available RP measures determines an operator's absorbed dose to a great extent, our tool provides an invaluable means for an individual to quantify the efficacy of using those measures in their daily practice. Some RP measures like cabins are not generally available or usable.However, very appreciable reductions in absorbed doses can be attained through using the most common protection measures properly, in particular lead glasses and ceiling-suspended screens. The presentation of the estimates of absorbed dose in the various scenarios side by side exemplifies the very real importance of making use of the measures available to reduce dose, further supported by estimation of the associated health risks. The most important sources of uncertainty are taken into account through Monte Carlo

simulation, thereby showing these outputs as ranges. Upon identifying a high rate of radiation lens injuries in a population of Colombian interventional cardiologists [48], the authors highlight the urgent need to take appropriate action to increase the use protective measures and strengthen training programmes in RP. Tools such as the one presented in this work can be useful for this purpose, as the difference in absorbed dose and associated health risks between the distinct scenarios of use of protective measures is easily quantified. Although treatment of cataracts is a relatively straightforward procedure nowadays, this should not encourage interventional cardiologists to take an increased risk of cataracts lightly: not all operations to remove cataracts are successful, and complications may result in irreversible opacities which could diminish a surgeon's ability to continue with their work.

5. Limitations

We consider that the outputs of InterCardioRisk tool are of potentially great usefulness to the IC and RP communities, but with some limitations. Relatively sparse historical data were available on working practices—both in terms of IC procedures and RP measures taken—so estimates of dose made by the tool may be inaccurate when used in those working environments where practices over the past 40 decades have differed greatly to those common in France. Also, it is conceivable that as cardiologists progress through their careers, they may increasingly focus on a particular type of intervention. This may also result in divergence between their true cumulated dose and those estimated by the tool. For example, those working in paediatric IC may be required to work much closer to the x-ray beam due to the size of the patient, and as a result have higher doses. Similarly, those working predominantly in emergency interventional treatment of heart attacks have less time to configure radiation shields prior to catheterisation.

The tool predicts various kind of cataracts at all stages of development from stage 1—defined as discrete posterior subcapsular cataract (PSC) or cortical opacity in a small area of the lens—to stage 5—defined as a mature cataract with complete lens opacification. This is a broad definition, and includes a variety of different kinds of cataract, each of which has a different pathogenesis and prognosis. IR has been found to be most strongly associated with PSC formation [10, 60]. Unlike age-related cortical or nuclear cataracts, which primarily cause a change in visual acuity, a PSC cataract is more likely to result in changes in both visual acuity and contrast sensitivity [61]. The RR of radiation-induced PSC cataracts is somewhat higher than that of other kinds of cataract, hence the tool may be slightly underestimating the risk of cataract specifically related to radiation dose.

Evidently, the validity of our assumption that OR is a good estimate of the RR is dependent on the incidence of the health outcome of interest in the unexposed population (i.e. the baseline rate). Although such an assumption is reasonable for rare outcomes such as cancers, the high incidence of cataracts in the unexposed population results in a slight overestimation of the risk of cataracts when using OR to estimate measures of risk and health impact. It was not possible to adjust the ORs using baseline rates as reliable baseline rates of the specific cataract types of interest were not available for European populations. We simulated the effect of using the OR in place of the RR on our estimates of health impact for a number of baseline rate scenarios. If baseline rates of stage 1–5 cataracts were 25%, we estimated that our risk estimate might be overestimated by less than 10%. The OR reported in [11] are obtained from Chernobyl clean-up workers, and although these are the most comprehensive estimates to date, and are compatible with those obtained from studies of surgically removed cataracts in the atomic bomb survivors study [45], there are issues concerning the adequacy of current dosimetric estimates.

In order to calculate a dose conversion factor between absorbed dose to the eye lens and absorbed dose to the brain, it was necessary to make a number of relatively crude simplifications. TLDs were positioned only in some of the anatomical regions of the brain, and dose was averaged over those regions using their approximate sizes as weights. When combining the brain dose data with dose-response and population data on cancer incidence in the calculation of LFR, it was necessary to assume that the brain and the whole CNS could be considered as 'equivalent', in the sense that dose-response and incidence data were only available for brain/CNS tumours combined. Any dose estimate to the brain is therefore considered to be valid for the CNS; when considering the CNS as a whole, it is therefore possible that dose has been overestimated. Since the majority of CNS tumours occur in the brain, however, and that the brain makes up the greater part of the CNS, we do not imagine that this overestimation has a large impact on the estimates of CNS tumour risk generated by the tool.

6. Recommendations for further work

Following discussions with cardiologists and RP staff, a number of improvements and extensions are planned for the tool. In particular, we would like to include the estimation of absorbed doses for other organs and calculation of risks for other endpoints. Extension of the tool to include other measures of health impact would be merited as a means of maximising the population for which the tool provides useful information. For example, it would be possible to estimate the total disability-adjusted life years (DALYs) for the health outcomes considered. Although not without its drawbacks, the use of DALYs allows for the synthesis and comparison of health impacts due to multiple diseases within a single framework. Currently, it is far from clear which metric might best communicate the gravity of potential health impacts to the target populations of interest i.e. interventional cardiologists, electrophysiologists and RP staff in hospitals. Further work on quantifying the efficacy of the tool to communicate health impacts to IC staff is necessary in order to refine it. A pilot version of the tool was sent to a group of over 100 experts in RP, medical radiation dosimetry and IC together with an online questionnaire designed to gauge their opinions on the user-friendliness of the tool, their perceptions of the magnitude of estimated doses, and the tool's usefulness in terms of improving compliance with RP guidelines and, ultimately, in reducing potential health impacts, and as a perspective to this work, with the aim of keeping the tool updated with the current standard procedures and RP methods usage in IC, a survey will be prepared including questions regarding the protection methods the IC use and their reasons for not following all guidelines.

Acknowledgments

This work was financially supported by funding from the Swiss Federal Office of Public Health. We would like to thank the reviewers for their extremely useful comments, particularly relating to the improvement of the dose estimation methodology. We are also grateful to David Piedra and all the IT team at CREAL for the effort of having the application running.

References

[1] Jones A K, Balter S, Rauch P and Wagner L K 2014 Medical imaging using ionizing radiation: optimization of dose and image quality in fluoroscopy *Med. Phys.* **41** 014301

[2] Thom T *et al* 2006 Heart disease and stroke statistics—2006 update: a report from the american heart association statistics committee and stroke statistics subcommittee *Circulation* **113** e85–151
[3] Togni M, Balmer F, Pfiffner D, Maier W, Zeiher A M, Meier B and Working Group, Interventional Cardiology, Coronary Pathophysiology and European Society of Cardiology 2004 Percutaneous coronary interventions in europe 1992–2001 *Eur. Heart J.* **25** 1208–13
[4] Roguin A, Goldstein J, Bar O and Goldstein J A 2013 Brain and neck tumors among physicians performing interventional procedures *Am. J. Cardiol.* **111** 1368–72
[5] ICRP 2010 *Radiological Protection in Fluoroscopically Guided Procedures Performed Outside the Imaging Department* (*Annals of the ICRP, ICRP Publication* vol 117) (St Louis, MO: Elsevier) pp 1
[6] Kim K P and Miller D L 2009 Minimising radiation exposure to physicians performing fluoroscopically guided cardiac catheterisation procedures: a review *Radiat. Prot. Dosim.* **133** 227–33
[7] Vañó E 2003 Radiation exposure to cardiologists: how it could be reduced *Heart* **89** 1123–4
[8] Cousins C *et al* and International Commission on Radiological Protection 2013 ICRP Publication 120: radiological protection in cardiology *Ann. ICRP* **42** 1–125
[9] Vañó E, Arranz L, Sastre J M, Moro C, Ledo A, Gárate M T and Minguez I 1998 Dosimetric and radiation protection considerations based on some cases of patient skin injuries in interventional cardiology *Br. J. Radiol.* **71** 510–6
[10] Merriam G R and Worgul B V 1983 Experimental radiation cataract—its clinical relevance *Bull. New York Acad. Med.* **59** 372–92 (PMCID: PMC1911644)
[11] Worgul B V *et al* 2007 Cataracts among chernobyl clean-up workers: implications regarding permissible eye exposures *Radiat. Res.* **167** 233–43
[12] UNSCEAR 2006 Report: volume 1. Annex A: epidemiological studies of radiation and cancer *Technical Report* UNSCEAR Vienna, Austria
[13] Braganza M Z, Kitahara C M, Berrington de Gonzlez A, Inskip P D, Johnson K J and Rajaraman P 2012 Ionizing radiation and the risk of brain and central nervous system tumors: a systematic review *Neuro-Oncology* **14** 1316–24
[14] Sadetzki S and Mandelzweig L 2009 Childhood exposure to external ionising radiation and solid cancer risk *Br. J. Cancer* **100** 1021–5
[15] Preston D L, Ron E, Yonehara S, Kobuke T, Fujii H, Kishikawa M, Tokunaga M, Tokuoka S and Mabuchi K 2002 Tumors of the nervous system and pituitary gland associated with atomic bomb radiation exposure *J. Natl Cancer Inst.* **94** 1555–63
[16] de Gonzalez A B, Iulian Apostoaei A, Veiga L H S, Rajaraman P, Thomas B A, Owen Hoffman F, Gilbert E and Land C 2012 RadRAT: a radiation risk assessment tool for lifetime cancer risk projection *J. Radiol. Prot.* **32** 205–22
[17] Buls N, Pagés J, de Mey J and Osteaux M 2003 Evaluation of patient and staff doses during various CT fluoroscopy guided interventions *Health Phys.* **85** 165–73
[18] McKean J W 2004 Robust analysis of linear models *Stat. Sci.* **19** 562–70
[19] R Core Team 2014 *R: A Language, Environment for Statistical Computing* (Vienna: R Foundation for Statistical Computing)
[20] Chang W, Cheng J, Allaire J, Xie Y and McPherson J 2016 Shiny: Web Application Framework for R. R package version 0.13.2. (https://CRAN.R-project.org/package=shiny)
[21] Jacob S, Donadille L, Maccia C, Bar O, Boveda S, Laurier D and Bernier M O 2013 Eye lens radiation exposure to interventional cardiologists: a retrospective assessment of cumulative doses *Radiat. Prot. Dosim.* **153** 282–93
[22] Trianni A, Padovani R, Foti C, Cragnolini E, Chizzola G, Toh H, Bernardi G and Proclemer A 2005 Dose to cardiologists in haemodynamic and electrophysiology cardiac interventional procedures *Radiat. Prot. Dosim.* **117** 111–5
[23] Antic V, Ciraj-Bjelac O, Rehani M, Aleksandric S, Arandjic D and Ostojic M 2013 Eye lens dosimetry in interventional cardiology: results of staff dose measurements and link to patient dose levels *Radiat. Prot. Dosim.* **154** 276–84
[24] Mootha V V, Tesser R and Qualls C 2004 Incidence of and risk factors for residual posterior capsule opacification after cataract surgery *J. Cataract Refractive Surg.* **30** 2354–8
[25] Goni H, Papadopoulou D, Yakoumakis E, Stratigis N, Benos J, Siriopoulou V, Makri T and Georgiou E 2005 Investigation of occupational radiation exposure during interventional cardiac catheterisations performed via radial artery *Radiat. Prot. Dosim.* **117** 107–10

[26] Tsapaki V, Kottou S, Patsilinakos S, Voudris V and Cokkinos D V 2004 Radiation dose measurements to the interventional cardiologist using an electronic personal dosemeter *Radiat. Prot. Dosim.* **112** 245–9
[27] Tsalafoutas I A, Spanodimos S G, Maniatis P N, Fournarakis G M, Koulentianos E D and Tsigas D L 2005 Radiation doses to patients and cardiologists from permanent cardiac pacemaker implantation procedures *Pacing Clin. Electrophysiol.* **28** 910–6
[28] Delichas M, Psarrakos K, Molyvda-Athanassopoulou E, Giannoglou G, Sioundas A, Hatziioannou K and Papanastassiou E 2003 Radiation exposure to cardiologists performing interventional cardiology procedures *Eur. J. Radiol.* **48** 268–73
[29] Lange H W and von Boetticher H 2006 Randomized comparison of operator radiation exposure during coronary angiography and intervention by radial or femoral approach *Catheterization Cardiovasc. Interventions* **67** 12–6
[30] Donadille L *et al* 2011 Staff eye lens and extremity exposure in interventional cardiology: results of the ORAMED project *Radiat. Meas.* **46** 1203–9
[31] Chen W, Yao Y, Zhang S and He D S 2011 Comparison of operator radiation exposure during coronary sinus catheter placement via the femoral or jugular vein approach *Europace* **13** 539–42
[32] Padovani R, Novario R and Bernardi G 1998 Optimisation in coronary angiography and percutaneous transluminal coronary angioplasty *Radiat. Prot. Dosim.* **80** 303–6
[33] Lange H W and von Boetticher H 2012 Reduction of operator radiation dose by a pelvic lead shield during cardiac catheterization by radial access: comparison with femoral access *Cardiovasc. Interventions* **5** 445–9
[34] Properzio W S 1975 The radiological health significance of cardiovascular special procedures *PhD Thesis* University of Florida Gainesville
[35] Vanhavere F *et al* 2011 Measurements of eye lens doses in interventional radiology and cardiology: final results of the ORAMED project *Radiat. Meas.* **46** 1243–7
[36] Schueler B, Sturchio G, Landsworth R, Hindal M and Magnuson D 2009 Does new lightweight leaded eyewear provide adequate radiation protection for fluoroscopists? *Med. Phys.* **36** 2747–8
[37] Vose D 2008 *Risk Analysis—A Quantitative Guide* (New York: Wiley)
[38] Moore W E, Ferguson G and Rohrmann C 1980 Physical factors determining the utility of radiation safety glasses *Med. Phys.* **7** 8–12
[39] Thornton R H, Dauer L T, Altamirano J P, Alvarado K J, Germain J St and Solomon S B 2010 Comparing strategies for operator eye protection in the interventional radiology suite *J. Vascular Interventional Radiol.* **21** 1703–7
[40] Sturchio G M, Newcomb R D, Molella R, Varkey P, Hagen P T and Schueler B A 2013 Protective eyewear selection for interventional fluoroscopy *Health Phys.* **104** S11–6
[41] Kellerer A M, Nekolla E A and Walsh L 2001 On the conversion of solid cancer excess relative risk into lifetime attributable risk *Radiat. Environ. Biophys.* **40** 249–57
[42] Nefzger M D, Miller R J and Fujino T 1969 Eye findings in atomic bomb survivors of Hiroshima and Nagasaki: 1963–1964 *Am. J. Epidemiol.* **89** 129–38
[43] Choshi K, Takaku I, Mishima H, Takase T, Neriishi S, Finch S C and Otake M 1983 Ophthalmologic changes related to radiation exposure and age in adult health study sample, hiroshima and nagasaki *Radiat. Res.* **96** 560–79
[44] National Research Council (U.S.) and Committee to Assess Health Risks from Exposure to Low Level of Ionizing Radiation *Health risks from exposure to low levels of ionizing radiation BEIR VII, Phase 2* (Washington, DC: National Academies Press) ((online). Available: http://site.ebrary.com/id/10120226)
[45] Ozasa K, Shimizu Y, Suyama A, Kasagi F, Soda M, Grant E J, Sakata R, Sugiyama H and Kodama K 2012 Studies of the mortality of atomic bomb survivors, report 14, 1950–2003: an overview of cancer and noncancer diseases *Radiat. Res.* **177** 229–43
[46] Jacob S, Boveda S, Bar O, Brézin A, Maccia C, Laurier D and Bernier M-O 2013 Interventional cardiologists and risk of radiation-induced cataract: results of a French multicenter observational study *Int. J. Cardiol.* **167** 1843–7
[47] Jacob S, Boveda S, Bar O, Brézin A, Maccia C, Laurier D, and Bernier M-O 2010 Occupational cataracts and lens opacities in interventional cardiology (O'CLOC study): are x-rays involved? Radiation-induced cataracts and lens opacities *BMC Public Health* **10** 537
[48] Vañó E, Kleiman N J, Duran A, Rehani M M, Echeverri D and Cabrera M 2010 Radiation cataract risk in interventional cardiology personnel *Radiat. Res.* **174** 490–5

[49] Vañó E, Fernández J M, Sánchez R M and Dauer L T 2013 Realistic approach to estimate lens doses and cataract radiation risk in cardiology when personal dosimeters have not been regularly used *Health Phys.* **105** 330–9
[50] Ciraj-Bjelac O, Rehani M M, Sim K H, Liew H B, Vañó E and Kleiman N J 2010 Risk for radiation-induced cataract for staff in interventional cardiology: is there reason for concern? *Catheterization Cardiovasc. Interventions* **76** 826–34
[51] Ciraj-Bjelac O, Rehani M, Minamoto A, Sim K H, Liew H B and Vano E 2012 Radiation-induced eye lens changes and risk for cataract in interventional cardiology *Cardiology* **123** 168–71
[52] Carinou E, Ferrari P, Bjelac O C, Gingaume M, Merce M S and O'Connor U 2015 Eye lens monitoring for interventional radiology personnel: dosemeters, calibration and practical aspects of H p (3) monitoring. A 2015 review *J. Radiol. Prot.* **35** R17–34
[53] Vañó E, Kleiman N J, Duran A, Romano-Miller M and Rehani M M 2013 Radiation-associated lens opacities in catheterization personnel: results of a survey and direct assessments *J. Vascular Interventional Radiol.* **24** 197–204
[54] Pages J 2000 Effective dose and dose to the crystalline lens during angiographic procedures *JBR-BTR: organe de la Société royale belge de radiologie (SRBR) = orgaan van de Koninklijke Belgische Vereniging voor Radiol. (KBVR)* **83** 108–10
[55] Hidajat N, Wust P, Felix R and Schr R 2006 Radiation dose of the radiologist and the assistant in transarterial hepatic chemoembolization–comparison with the dose limits *RFo: Fortschr. Auf Dem Gebiete Der Rntgenstrahlen Und Der Nuklearmedizin* **178** 185–90
[56] ICRP 2012 *ICRP Statement on Tissue Reactions/Early and Late Effects of Radiation in Normal Tissues and Organs Threshold doses for Tissue Reactions in a Radiation Protection Context* (*ICRP Publication 118, Annals of the ICRP* vol 41) (St Louis, MO: Elsevier)
[57] Authors on behalf of ICRP, Stewart F A *et al* 2012 *ICRP Statement on Tissue Reactions and Early and Late Effects of Radiation in Normal Tissues and Organs—Threshold Doses for Tissue Reactions in a Radiation Protection Context* (*ICRP Publication 118, Annals of the ICRP* vol 41) (Oxford, UK: Elsevier) pp 1
[58] ICRP 1991 *1990 Recommendations of the International Commission on Radiological Protection* (*ICRP publication 60, Annals of the ICRP* vol 21) (St Louis, MO: Elsevier) pp 1
[59] Renaud L 1992 A 5-y follow-up of the radiation exposure to in-room personnel during cardiac catheterization *Health Phys.* **62** 10–5
[60] Little M P 2013 A review of non-cancer effects, especially circulatory and ocular diseases *Radiat. Environ. Biophys.* **52** 435–49
[61] Stifter E, Sacu S, Thaler A and Weghaupt H 2006 Contrast acuity in cataracts of different morphology and association to self-reported visual function *Investigative Ophthalmology Vis. Sci.* **47** 5412–22

Radiation Protection Dosimetry (2016), Vol. 169, No. 1–4, pp. 68–72
Advance Access publication 8 March 2016
doi:10.1093/rpd/ncw019

PATIENT EXPOSURE OPTIMISATION THROUGH TASK-BASED ASSESSMENT OF A NEW MODEL-BASED ITERATIVE RECONSTRUCTION TECHNIQUE

Julien G. Ott[1,*], Alexandre Ba[1], Damien Racine[1], Nick Ryckx[1], François O. Bochud[1], Hatem Alkadhi[2] and Francis R. Verdun[1]
[1]Institute of Radiation Physics, CHUV, Lausanne, Switzerland
[2]Institute of Diagnostic and Interventional Radiology, USZ, Zürich, Switzerland

*Corresponding author: julien.ott@chuv.ch

The goal of the present work was to report and investigate the performances of a new iterative reconstruction algorithm, using a model observer. For that, a dedicated low-contrast phantom containing different targets was scanned at four volume computed tomography dose index ($CTDI_{vol}$) levels on a Siemens SOMATOM Force computed tomography (CT). The acquired images were reconstructed using the ADMIRE algorithm and were then assessed by three human observers who performed alternative forced choice experiments. Next, a channelised hotelling observer model was applied on the same set of images. The comparison between the two was performed using the percentage correct as a figure of merit. The results indicated a strong agreement between human and model observer as well as an improvement in the low-contrast detection when switching from an ADMIRE strength of 1–3. Good results were also observed even in situations where the target was hard to detect, suggesting that patient dose could be further reduced and optimised.

INTRODUCTION

Over the past decade, the radiation dose delivered to patients via diagnostic X-ray imaging has continuously increased until today, where it reaches 25 % of the accumulated man-made and natural radiation contributions. Among that 25 %, computed tomography (CT) raises a particular concern, since this imaging modality represents in Switzerland for example 68 % of the collective dose, yet only 8 % of the number of examinations[1]. In this context, CT manufacturers have developed new strategies like iterative reconstruction (IR) algorithms in order to ensure that the benefits–risk ratio remains in favour of the patient. This new technology certainly improved the clinical practice[2], but it has also led to drastic changes in image perception. Thus, ensuring an adequate level of image quality while keeping patient's exposure as low as reasonably achievable constitutes a new challenge to be addressed. The use of task-based image quality assessment method could represent an efficient way to perform this optimisation scheme[3, 4]. Therefore, the goal of this study was to report and investigate the performances of a new IR technique using a model observer that mimics human detection of low-contrast targets: the channelised Hotelling observer (CHO) model.

MATERIALS AND METHODS

Data acquisition

A dedicated low-contrast phantom (QRM, Moehrendorf, Germany), mimicking the attenuation produced by a patient's chest, was used. The phantom could embed two different custom-made modules in its middle: a homogeneous modulus and another containing low-contrast spherical targets of 6 and 8 mm in diameter with contrast levels of 10 and 20 HU at 120 kVp.

Data acquisition was performed at the University Hospital Zurich on a third-generation dual-source 192-slice CT scanner (SOMATOM Force, Siemens Healthcare, Erlangen, Germany). A tube voltage of 120 kVp, a 300 mm display field of view (DFOV), a 512 × 512 matrix size and 2.0-mm-thick slices, which were reconstructed every 1.0 mm, were used. Acquisitions were performed in the helical mode with a pitch of 0.98. Four dose levels [1.0, 3.5, 8.0 and 15.0 mGy expressed in a volume computed tomography dose index ($CTDI_{vol}$) phantom of 32 cm in diameter] were investigated, using the procedure described in the IEC 60601-2-44[5] to measure the $CTDI_{vol}$. The phantom was scanned 20 times for each condition. Reconstructions were performed using the Siemens advanced model iterative reconstruction (ADMIRE) with strength levels 1 and 3. On the machine, users can choose ADMIRE levels ranging from 1 to 5, with level 1 being closest to the image impression of traditional, filtered back-projection, and level 5 showing the strongest noise reduction. In the end, 32 different categories were obtained (four dose levels, two ADMIRE levels, two contrast levels and two target sizes). From these sets of acquisitions, regions of interest (ROIs) of 41 × 41 pixels (0.59 mm pixel size) containing the centred targets were extracted. For each category, 100 images containing a signal

(20 scans × 5 targets with identical size and contrast in the phantom) and 1000 images with only noise were extracted. The ROIs that contained noise only were extracted from the homogeneous modulus, whereas the ROIs containing the signals came from the low-contrast modulus. This methodology enabled holding the same position on the (x,y) plane for both signal and noise ROIs, in turn enabling solving the noise stationarity problem.

Human observer

In the human observer experiment, three medical physicists took part in four alternative forced choice (4-AFC) experiments in order to yield a percentage of correct responses (PC) indicating how well they managed to detect the signals. The 4-AFC experiment consisted in selecting the signal-present image in a batch of three signal-absent images and one signal-present image, which were presented together in a randomised order. All observers were blinded to the CT acquisition and reconstruction conditions and began their test with a training session that was made of images acquired at high dose level. They were then asked to make decisions for all 32 categories acquired. The previously made acquisitions provided 100 signal-present ROIs and 1000 signal-absent ROIs for each category. ROIs among those data were selected randomly and used for the 4-AFC tests. For each observer and category, every answer to the 100 trials was stored and compared with the correct response, allowing the computation of the PC.

CHO model observer

A model observer enables to predict the detection of low-contrast signals by calculating a scalar response called the decision variable and denoted by λ_i. This parameter is given by

$$\lambda_i = w^T \times g_i, \tag{1}$$

where w is the template of the model observer, and g_i is the analysed ROI ($i = n$ or $i = s$ represents signal-absent or signal-present hypothesis, respectively).

The CHO model used in this study is an anthropomorphic model observer also including preprocessing of the image by a set of channels that enhance some spatial frequencies[6, 7]. The template w_{CHO} of this model is obtained as explained in the following part (extensive details can be found elsewhere[8–11]):

$$w_{\mathrm{CHO}} = \left[\frac{1}{2}(K_{\mathrm{cs}} + K_{\mathrm{cn}})\right]^{-1} (\overline{g_{\mathrm{cs}}} - \overline{g_{\mathrm{cn}}}), \tag{2}$$

where

$$K_{\mathrm{cn}} = U^T K_n U \quad \text{and} \quad K_{\mathrm{cs}} = U^T K_s U. \tag{3}$$

In this equation, K_n and K_s are the covariance matrix calculated, respectively, from the signal-absent and signal-present data, and $\boldsymbol{U}$ is the matrix representation of the channel filters described more extensively below.

In Equation 2, $\overline{g_{\mathrm{cs}}}$ and $\overline{g_{\mathrm{cn}}}$ are the means of the channel outputs under a signal-present and signal-absent hypothesis and can be estimated according to

$$\overline{g_{\mathrm{cs}}} = U^T \overline{g_s} \quad \text{and} \quad \overline{g_{\mathrm{cn}}} = U^T \overline{g_n}. \tag{4}$$

The employed set of channels is called dense difference of Gaussian (DDoG) channels and was described by Abbey and Barrett in 2001[12]. It includes 10 channels for which the radial frequency profile of the jth channel is given by

$$U_j(\rho) = \exp\left[-\frac{1}{2}\left(\frac{\rho}{W\sigma_j}\right)^2\right] - \exp\left[-\frac{1}{2}\left(\frac{\rho}{\sigma_j}\right)^2\right], \tag{5}$$

where ρ is the spatial frequency, $W = 1.67$ defines the bandwidth of the channel, and σ_j is the standard deviation of the jth channel. Each σ_j value is defined by the equation $\sigma_j = \sigma_o \alpha^j$ with $\sigma_o = 0.005$ and $\alpha = 1.4$[12].

The decision variable can then be calculated by injecting the channel output of the ROI (denoted by g_{ci}) and the template w_{CHO} in Equation 1:

$$\lambda_i = w_{\mathrm{CHO}}^T \times g_{\mathrm{ci}}. \tag{6}$$

The PC was obtained using the CHO model to perform 4-AFC tests on the acquired images. The value of the decision variable was used to determine which of the four images contained the signal (the highest value of λ is supposed to be the signal-present image). Then, the results of the model observers were compared with the truth in order to enabling the computation of PCs.

Uncertainty estimation

The uncertainties of the models' results were estimated by performing bootstrap[13]. According to the bootstrap method and the set of 100 signal-present ROIs, the 4-AFC test was performed 150 times for each category, leading to 150 values of PC. Then, the mean and standard deviation of the 150 values obtained were computed in order to determine the final mean PC value as well as its standard deviation for each acquisition condition. This allowed to estimate a 95 % confidence interval. The uncertainties for the human observers were calculated using the results of the three different observers. For each category, the mean PC value of the observers and its

standard error were calculated in order to display a 95 % confidence interval.

RESULTS

In this section, the qualities of the images obtained using the ADMIRE algorithm with strength levels 1 and 3 are assessed through the performances of model (Figure 1) and human observers (Figure 2).

Results of the CHO model with the DDoG channels suggest that both strength levels exhibited PCs in the same range with an increase of a few per cent in the results when switching from strength level 1 to 3. This trend was, however, only observed for certain signals and dose range, namely the lowest contrast (10 HU) associated to low dose levels (1.0 and 3.5 mGy).

Human observers exhibited results very similar to the ones obtained with the CHO model in terms of PC values. The results also suggest that the use of higher ADMIRE strength level is useful to improve the detection of small-size and low-contrast signal under low $CTDI_{vol}$. On top of that, it was observed that the largest signal size (8 mm) with the highest contrast (20 HU) corresponded to a trivially easy task

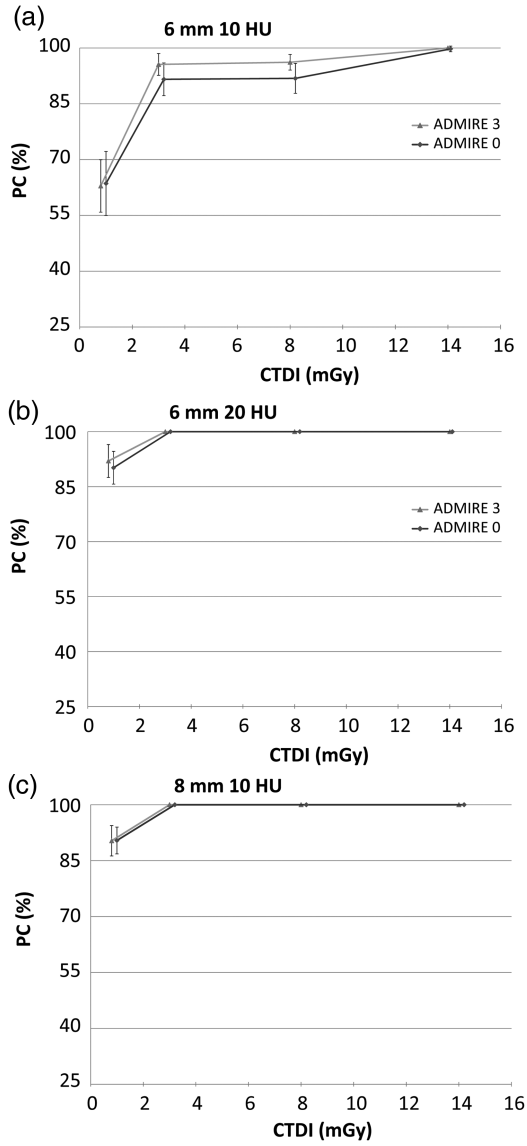

Figure 1. Results of the CHO model observer (in PC, obtained by performing 4-AFC tests).

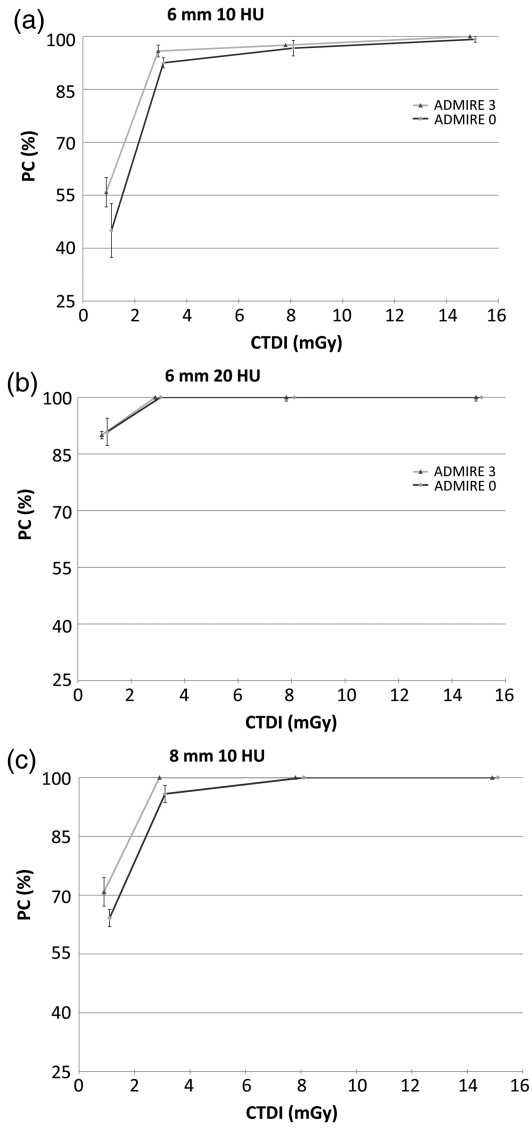

Figure 2. Results of the three human observers (in PC, obtained by performing 4-AFC tests).

with PC always equal to 100 % no matter which dose and ADMIRE level was employed. Those results remained true for both human and model observers and are therefore not presented in Figures 1 and 2.

Model and human observers exhibited a great adequacy in their results, both of them indicating that the use of a higher ADMIRE level enhances the detection when working under conditions where the signal is hard to detect. It was also witnessed that the PC increases with the given dose until it reaches an asymptote and that this asymptote is reached faster when using higher ADMIRE strength level. Furthermore, the results enlighten that no more dose increase is needed once an amount of ~4 mGy is reached because the performance of the human observer is already almost maximal at this point.

DISCUSSION

The goal of the present investigation was to determine if the use of the ADMIRE algorithm at different strength could lead to a high detection performance, therefore allowing a further dose reduction in the clinical practice. The results showed that the CHO model with DDoG channels gave coherent results since it reproduced the behaviour of humans very well and under a wide range of conditions and signal contrasts. The model seems to be very efficient in low-contrast detection and even sometimes overestimates human results for low contrast and low doses. These results are coherent with recent studies from Leng and Yu[14] which showed the efficiency of the CHO model for the low-contrast detection. Also, both model and human observers reported a visible improvement in the low-contrast detection when increasing the ADMIRE strength. This trend was observed when working at low dose levels (<4 mGy) for all signal types. Indeed, when working at higher dose levels, the PCs always reached 100 %, letting no room for improvement. In the end, the use of ADMIRE makes it possible to diminish the dose without losing information in the image. Indeed, the PC results obtained in the study reach very high or perfect values for almost every acquisition condition and signal, indicating that a dose reduction without impacting the detection performance would be possible.

However, some limitations of the present study have to be underlined. First among them, the number of images acquired may be considered as low since not enough ROIs were disposed to separate them in two exploitable data sets. Usually, a first set is used for the computation of the covariance matrix in the determination of the template of the CHO model, while the second data set is used for the computation of the PCs. However, it is worth to underline that Barrett and Myers[15] who studied this problem concluded that using one single set of data remained a reliable way to proceed. Moreover, performing a limited number of acquisitions (20 scans for each acquisition condition in the present case) allowed to reduce the operating time of the device, which is appreciable when working in a clinical environment. The second limitation faced is that the paradigm worked with (when the signal, location and background are exactly known) was simplified and therefore different from real anatomical conditions. The results could nevertheless be used in order to assess the performances of the tested IR algorithms, but it is worth to mention that there is room for a more complex study on the subject.

CONCLUSION

Nowadays, assessing CT image quality cannot be done with image space metrics anymore. Moreover, evidence indicates that frequency metrics should not be used either when working with IR. However, the task-based tool used in this investigation (CHO model observer associated to the DDoG channels) successfully demonstrated its ability to reproduce the human's response in a low-contrast detection task, thus establishing its reliability for image quality assessment.

The results obtained with this tool revealed that the ADMIRE algorithm led to high PCs even in situations where the target was harder to detect (i.e. low $CTDI_{vol}$ and contrast level). Also, using higher ADMIRE strength led to PC improvement, particularly in the low $CTDI_{vol}$ range. Therefore, using those benefits to keep the image quality equivalent to what was previously obtained would enable to spare some delivered dose.

All those elements suggest that the patient dose could be further optimised and reduced thanks to the use of the ADMIRE algorithm and this new CT unit.

FUNDING

This work was partly supported by a grant from the Swiss National Science Foundation (No. 320030-140995). Funding to pay the Open Access publication charges for this article was provided by the institute of radiation physics from Lausanne.

ACKNOWLEDGEMENTS

The authors would like to thank the personal of the USZ for their active participation in the acquisitions, as well as all the readers who took part in the detection studies.

REFERENCES

1. Samara, E. T., Aroua, A., Bochud, F. O., Ott, B., Theiler, T., Treier, R., Trueb, P. R., Vader, J. P. and Verdun, F. R. *Exposure of the Swiss population by medical x-rays: 2008 review.* Health Phys. **102**, 263–270 (2008).

2. Schindera, S. T., Odedra, D., Raza, S. A., Kim, T. K., Jang, H. J., Szucs-Farkas, Z. and Rogalla, P. *Iterative reconstruction algorithm for CT: can radiation dose be decreased while low-contrast detectability is preserved?* Radiology **269**, 511–518 (2013).
3. Brunner, C. C., Abboud, S. F., Hoeschen, C. and Kyprianou, I. S. *Signal detection and location-dependent noise in cone-beam computed tomography using the spatial definition of the hotelling SNR*. Med. Phys. **39**, 3214–3228 (2012).
4. Barrett, H. H., Myers, K. J., Hoeschen, C., Kupinski, M. A. and Little, M. P. *Task-based measures of image quality and their relation to radiation dose and patient risk*. Phys. Med. Biol. **60**, R1–R75 (2015).
5. International Electrotechnical Commission. International Standard IEC 60601-2-44. *Medical Electrical Equipment – Part 2-44: Particular Requirements for the Basic Safety and Essential Performance of X-Ray Equipment for Computed Tomography*, 3rd edn. IEC (2009).
6. Myers, K. J. and Barrett, H. H. *Addition of a channel mechanism to the ideal-observer model*. J. Opt. Soc. Am. **4**, 2447–2457 (1987).
7. Gallas, B. D. and Barrett, H. H. *Validating the use of channels to estimate the linear model observer*. J. Opt. Soc. Am. **20**, 1725–1738 (2003).
8. Beutel, J., Kundel, H. L. and Van Metter, R. L. *Handbook of Medical Imaging. Volume 1. Physics and Psychophysics*. SPIE Press (2000).
9. Castella, C., Abbey, C. K., Eckstein, M. P., Verdun, F. R., Kinkel, K. and Bochud, F. O. *Human linear template with mammographic backgrounds estimated with a genetic algorithm*. J. Opt. Soc. Am. **24**, B1–12 (2007).
10. Yu, L., Leng, S., Chen, L., Kofler, M., Carter, R. E. and McCollough, C. H. *Prediction of human observer performance in a 2-alternative forced choice low-contrast detection task using channelized Hotelling observer: impact of radiation dose and reconstruction algorithms*. Med. Phys. **40**, 041908 (2013).
11. Tseng, H. W., Fan, J., Kupinski, M. A., Sainath, P. and Hsieh, J. *Assessing image quality and dose reduction of a new x-ray computed tomography iterative reconstruction algorithm using model observers*. Med. Phys. **41**, 071910 (2014).
12. Abbey, C. K. and Barrett, H. H. *Human- and model-observer performance in ramp-spectrum noise: effects of* regularization and object variability. J. Opt. Soc. Am. **18**, 473–488 (2001).
13. Efron, B. and Tbishirani, R. J. *An Introduction to the Bootstrap*. CRC Press (1994).
14. Leng, S., Yu, L., Zhang, Y., Carter, R., Toledano, A. Y. and McCollough, C. H. *Correlation between model observer and human observer performance in CT imaging when lesion location is uncertain*. Med. Phys. **40**, 081908 (2013).
15. Barrett, H. H. and Myers, K. J. *Foundation of Image Science*. John Wiley & Sons (2004).

Radiation Protection Dosimetry (2016), Vol. 169, No. 1–4, pp. 78–83
Advance Access publication 2 March 2016
doi:10.1093/rpd/ncw021

BENCHMARKING OF CT FOR PATIENT EXPOSURE OPTIMISATION

Damien Racine*, Nick Ryckx, Alexandre Ba, Julien G. Ott, François O. Bochud and Francis R. Verdun
Institute of Radiation Physics, CHUV, Lausanne, Switzerland

*Corresponding author: damien.racine@chuv.ch

Patient dose optimisation in computed tomography (CT) should be done using clinically relevant tasks when dealing with image quality assessments. In the present work, low-contrast detectability for an average patient morphology was assessed on 56 CT units, using a model observer applied on images acquired with two specific protocols of an anthropomorphic phantom containing spheres. Images were assessed using the channelised Hotelling observer (CHO) with dense difference of Gaussian channels. The results were computed by performing receiver operating characteristics analysis (ROC) and using the area under the ROC curve (AUC) as a figure of merit. The results showed a small disparity at a volume computed tomography dose index ($CTDI_{vol}$) of 15 mGy depending on the CT units for the chosen image quality criterion. For 8-mm targets, AUCs were 0.999 ± 0.018 at 20 Hounsfield units (HU) and 0.927 ± 0.054 at 10 HU. For 5-mm targets, AUCs were 0.947 ± 0.059 and 0.702 ± 0.068 at 20 and 10 HU, respectively. The robustness of the CHO opens the way for CT protocol benchmarking and optimisation processes.

INTRODUCTION

In 1997, the European Council Directive 97/43/EURATOM[1] required that medical physics experts (MPEs) be involved in the optimisation process of radiological diagnostic procedures. That recommendation has been translated into the Swiss Radiological Protection Ordinance and was officially applied in 2008[2]: 'For nuclear medicine applications and for fluoroscopy-guided interventional radiology and computer tomography, the licence holder must periodically enlist the services of a medical physicist'.

The objective is to involve the medical physicist in the optimisation process of medical devices, especially in CT, which is one of the most commonly used tools in the medical imaging field and which is responsible for the highest dose delivered to the population from diagnostic radiology. Evaluating image quality is crucial when optimising or comparing CT devices, reconstruction algorithms and clinical protocols in order to respect the as low as reasonably achievable (ALARA) principle, especially with the introduction of iterative reconstruction into CT because the standard Fourier metrics are no longer applicable[3, 4]. The aim of this study was to provide an objective tool to compare CT protocols and to develop methods to then use the devices at their full potential, i.e. using the minimum dose while maintaining image quality for diagnosis. This optimisation scheme relied on the use of task-based metrics that approximate the clinical task in order to qualify the image quality and facilitate the cooperation between medical physicists, radiographers and radiologists.

Clinical diagnosis is composed of three tasks: the detection task, the localisation task and the characterisation task. In the present case, the detection task performance was evaluated with a mathematical observer model, which is used to substitute the human observer. The use of these tools provides an objective metric to evaluate image quality. The advantage of this approach is that it takes into account the entire imaging chain at the same time as it remains as close as possible to a simplified diagnostic task.

During the authors' visits to the various centres, image acquisitions were performed together with the verification of the indicated volume computed tomography dose index ($CTDI_{vol}$) and the assessment of other parameters such as X-ray beam efficiency and the Hounsfield unit (HU) calibration in water at the available X-ray tube voltages[5]. This contribution will focus on a CT benchmarking based on a model observer. The first aim was the assessment of image quality on several CT units at a given dose level. The second aim was the assessment of image quality while using different acquisition parameters.

MATERIALS AND METHODS

Model observer: channelised Hotelling observer

Anthropomorphic model observers are mathematical models based on the statistical decision theory to estimate the detection performance of human observers. In this study, a linear anthropomorphic model was chosen, namely the channelised Hotelling observer (CHO)[6, 7], which is usually used to evaluate the image quality. As Ott *et al.*[8] demonstrated, the CHO can mimic the human observer performance for a detection task. In this case, the methodology used for the CHO is directly inspired by the methodology used by Ott *et al.*, and extensive details can be found in the chapter on the CHO model observer[8].

Performance measurement of the model observer

All decision variables provide a distribution depending on the presence or absence of a signal. In the receiver operating characteristics (ROC) analysis, if the decision variable calculated using an image containing the signal is above the threshold, then the response is considered true positive. If this variable is calculated with the image containing only noise is above the threshold, then the response is considered false positive. For a given threshold, a true positive fraction (TPF) and a false positive fraction (FPF) are obtained, and the ROC curve is then constructed from pairs of TPF and FPF.

The ROC curve can give a complete description of the performance of an observer. To summarise the performance of an observer, the area under the curve (AUC) can be calculated[9]. It ranges from 0 to 1, with a value of 0.5 meaning that the test is not better than tossing a coin to give a positive or negative answer, and was estimated using the trapezoidal method with 100 points.

Description of phantom and CT units

An abdominal anthropomorphic phantom (Figure 1) (QRM, Moehrendorf, Germany) was scanned in 56 CT units (≈20 % of all CT units in the country). This phantom is composed of an external shell intended to closely mimic the X-ray attenuation of an abdomen during a CT examination, and of two embeddable modules. The materials used represent three densities and anatomical shapes of the human body:

- Liver (55 HU at 120 kV),
- Spleen (55 HU at 120 kV),
- Vertebra (cortical and cancellous bone).

The uniform phantom background is equivalent to the soft tissue of the abdomen (35 HU at 120 kV).

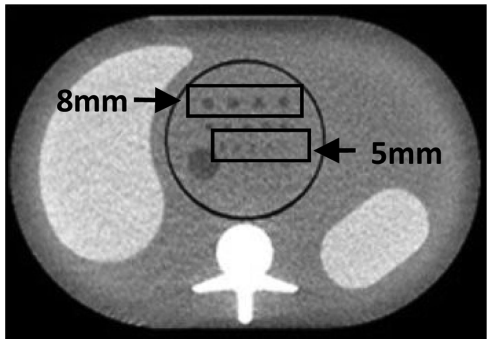

Figure 1. QRM phantom image from an acquisition at a high dose level ($CTDI_{vol}$ 20 mGy). The phantom contains four 8-mm spheres and five 5-mm spheres. The signals represented in this figure have a contrast of 20 HU.

Two modules can be inserted into this external shell: a homogeneous module identical to the background phantom and a module containing low-contrast signals. These signals are spheres of different sizes (8, 6, 5, 4 and 3 mm) with contrasts of −20 and −10 HU at 120 kV with respect to the background.

In 2014, the equipment from four CT manufacturers in Western Switzerland was investigated with the range of the detector coverage represented in Table 1 (in detail 20 devices for Philips, 18 for GE, 12 for Toshiba and 6 for Siemens).

Acquisition protocols

The acquisitions were performed following two protocols:

- One protocol called ‘Reference’ with the same parameters for all radiological services. Acquisitions were performed at 120 kV, and the tube current was adapted to get indicated $CTDI_{vol}$ values of 15 mGy [the diagnostic reference level (DRL) for the abdominal region in Switzerland]. During the visit, the $CTDI_{vol}$ values were measured on each CT unit using a $CTDI_{vol}$ phantom of 32 cm in diameter and a 100 mm pencil ionisation chamber as described in the IEC 60601-2-44[10]. The X-ray tube rotation time was 1 s, and the pitch was close to one. The display field of view (DFOV) was 320 × 320 mm for a 512 × 512 matrix size, in order to have a constant spatial resolution. Slices were reconstructed with a nominal thickness of 2.5 or 2.0 mm associated to an interval of 2.5 or 2.0 mm (depending on the possibilities offered by the different manufacturers), respectively. Images were reconstructed only with the filtered back-projection (FBP) in the axial plane with a standard convolution kernel used locally for abdominal acquisitions.
- The other protocol called ‘Local’ where the acquisition parameters were those usually employed by the centre for the detection of focal liver lesion (i.e. FBP or iterative reconstruction algorithm was used). The DFOV was then adjusted to 320 × 320 mm for all centres in order to obtain comparable pixel sizes. Since the spread in slice thicknesses

Table 1. Number of CT units included in the study for each detector coverage range.

Collimation (number of rows)	Number of CT units
16	10
32	1
40	3
64	36
80	3
128	3

and doses used in the local protocols was large, an alternative metric, called 'volumetric dose', was used. The volumetric dose is defined as the product of the dose and the slice thickness, corresponding to the dose length product of the reconstructed slice.

For the two protocols, the phantom was positioned at the isocentre of the CT unit, and the module containing the low-contrast spheres was scanned 10 times successively. Then, the homogeneous module was scanned without changing the position of the abdomen-like shell.

Generating signal-absent and signal-present images

For practical reasons, only two sphere sizes were investigated, namely the 5 and 8 mm (smaller sizes were not visible enough at the dose levels investigated). For each acquisition, 4 centred regions of interest (ROIs) (22×22 pixels, 1 pixel = 0.625 mm) per sphere size/contrast combination were extracted from the module containing the sphere, and 8 ROIs per slice were extracted from images of the homogeneous module at the same location (x,y) as the ROI containing the signal. Hereafter, for convenience, ROIs will be called signal-present images if the signal is present in the ROIs and signal-absent images if the signal is absent.

RESULTS

'Reference' protocol

Using a $CTDI_{vol}$ of 15 mGy on all systems, the detection performance for a given contrast/diameter combination was globally comparable with a few outliers (Figure 2). Centres 41 and 48 in Figure 2a and Centres 43, 45, 46 and 47 in Figure 2c provided a lower-level image quality when compared with the other centres. For 8-mm targets, the averaged AUCs were 0.999 ± 0.018 at 20 HU and 0.927 ± 0.054 at 10 HU. For 5-mm targets, the averaged AUCs were 0.947 ± 0.059 and 0.702 ± 0.068 at 20 and 10 HU, respectively (the error represents one standard deviation). Thus, the relative standard deviation was in the range of 1–10 %, indicating, for that specific image quality criterion and this specific acquisition protocol, that the CT units in Western Switzerland are relatively homogeneous at the quite high dose level investigated. As expected, the detection was greatly enhanced when the diameter increased (5 vs. 8 mm) as well as when the contrast became higher (10 vs. 20 HU).

'Local' protocol

When using the local protocol instead of the reference protocol, as expected, it was noticed that the detectability still increased with the contrast and the diameter of the spheres. However, it was also discovered that the mean AUC did slightly change depending on the reconstruction algorithms (AUC was lower in iterative than in FBP), but the mean delivered dose was also much lower for the iterative algorithms (no distinction was made between the level of complexity of the iterative algorithms available) compared with FBP. These measurements clearly highlighted the contribution of the iterative algorithm on dose reduction (almost a factor of two) associated to a slight reduction in low-contrast detectability.

Figure 3 illustrates the detection performance for combinations 8 mm/10 HU and 5 mm/20 HU when switching from the reference to the locally implemented protocols. Varying the parameters used [nominal slice thicknesses (ranging from 0.5 to 7 mm), dose levels, algorithm reconstruction and convolution kernels used for standard abdominal protocols] in each centre slightly increased the variability. Moreover, some centres work with unexpected parameters, which deteriorate image quality and increase the image quality variability. In some cases, the $CTDI_{vol}$ was quite low (3.3 mGy) with very thin slice reconstruction thickness (0.5 mm) or the dose was quite high (12.3 mGy) with the reconstruction of thick slices (7 mm), see three red circles in Figure 3. In the first case, even if the image was reconstructed with an iterative algorithm, the low-contrast detectability could not be recovered. In the second case, the partial volume effect was responsible for the poor score obtained.

DISCUSSION

In this study, an objective task-based image quality assessment was performed using a model observer on an anthropomorphic phantom to assess image quality. The CT units in use in the Western part of Switzerland are relatively recent and homogeneous, but the image quality with the 'Reference' protocol was explored at a high dose level. In this case, the discrimination between the CT units is limited, but this benchmark has, however, demonstrated that several units led, for the chosen image quality criterion, to a lower performance. One limit of this 'Reference' protocol is that it investigates the image quality at one dose level and only with the FBP algorithm. The benefits of introducing the iterative algorithm, especially the model-based iterative algorithm, were not explored[11]. In future work, the performance of CT units will be investigated in a range of dose and algorithms in order to be able to qualify image quality including high- and low-contrast performances.

When switching to the 'Local' protocol, the dose and slice thickness varied in a wide range between the centres and noticeable image quality variations were observed. Based on this metric, it will be possible to optimise and standardise the clinical practice to

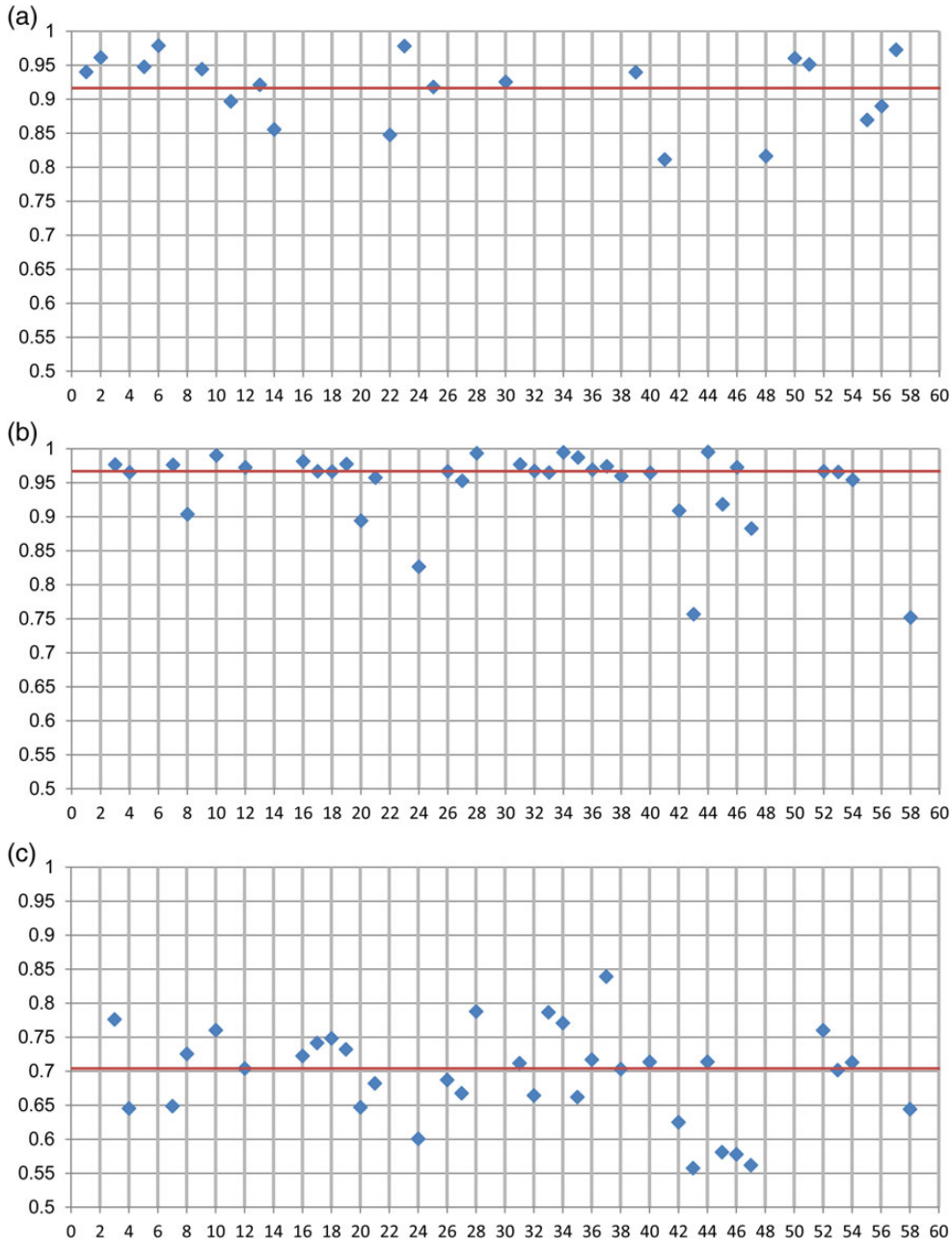

Figure 2. Results of a comparison of the image quality for CT units in Western Switzerland when dealing with the 'Reference' protocol for spheres of 8 mm/10 HU at 2.0 mm slice thickness (**a**), 5 mm/20 HU at 2.5 mm slice thickness (**b**) and 5 mm/10 HU at 2.5 mm slice thickness (**c**). The red line represents the median value.

converge towards a given level of image quality for a particular clinical examination. The main limit of the use of the volumetric dose parameter for that part of the study is the range of slice thickness investigated, since partial volume effects could be very different from one protocol to another. This could be certainly improved by a closer collaboration between the medical physicists and the radiologists when selecting acquisition parameters and the range of reconstructed slice thickness.

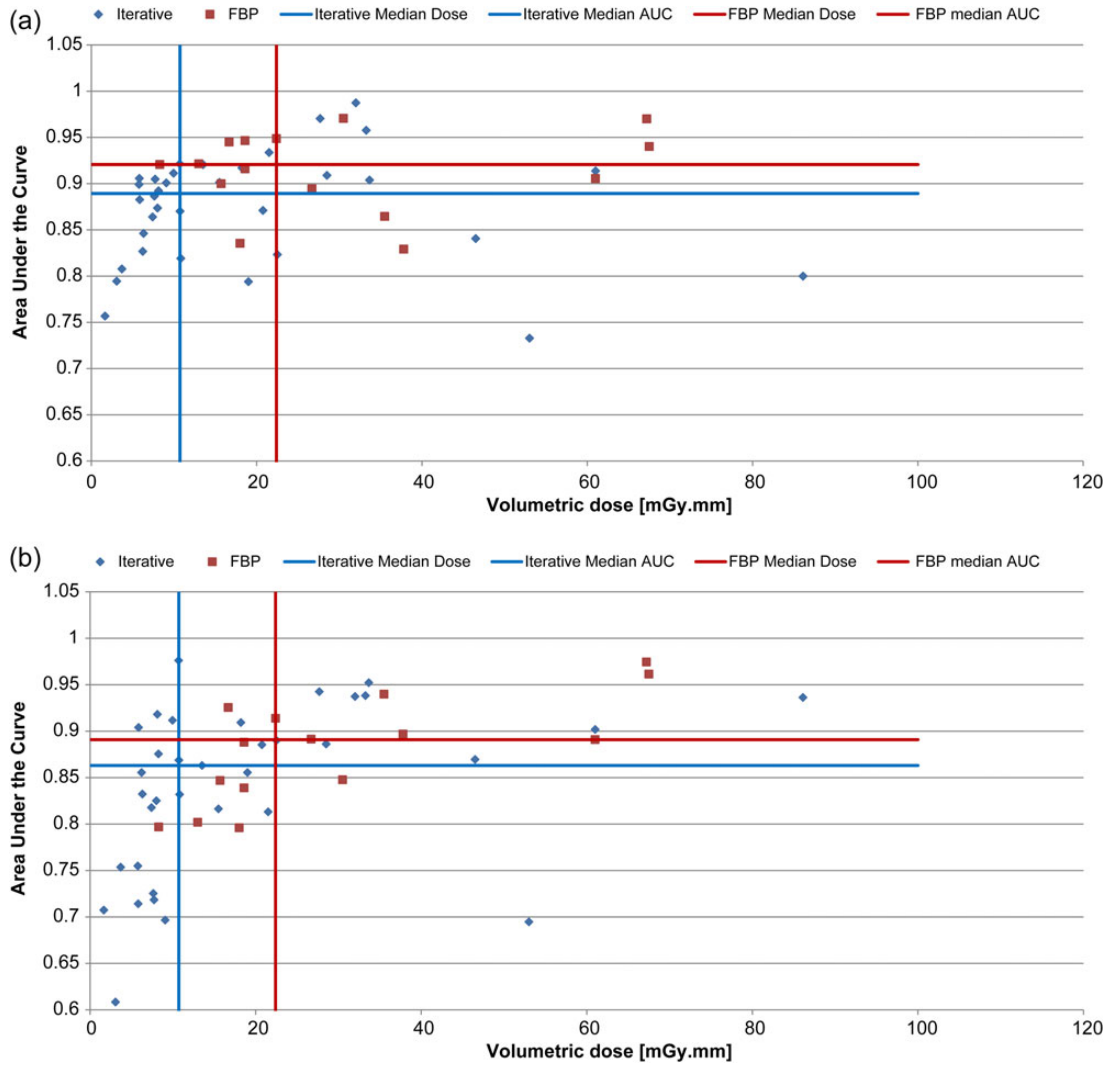

Figure 3. Results of a comparison of image quality for 5 mm/20 HU (**a**) and 8 mm/10 HU (**b**) as a function of the volumetric dose ($CTDI_{vol}$ multiplied by the reconstructed slice thickness for taking into account the various slice thicknesses produced) regarding the practice in Western Switzerland when dealing with the protocol used for the detection of hepatic metastasis. The red circles represent the poor image quality obtained with unexpected parameters (slice thickness inappropriate for the lesion size).

Thus, the proposed method seems suitable for benchmarking the CT unit as well as the clinical protocols. The method could be improved by adding high Z materials targets, making it possible to optimise the choice of X-ray tube high voltage when dealing with injected protocols.

CONCLUSION

A method for benchmarking CT units has been applied to different CT units in Western Switzerland for a specific task (i.e. detection of low-contrast spherical targets); it appears that the image quality was relatively homogeneous. The results also show that the methodology could be used to assess clinically relevant image acquisition protocols to optimise the process of patient exposure. It was observed that the use of iterative reconstruction allowed a significant dose reduction (almost a factor of two) associated, however, with a slight reduction in low-contrast detectability.

REFERENCES

1. EU. *Council Directive 97/43/Euratom of 30 June 1997 on health protection of individuals against the dangers of ionizing radiation in relation to medical exposure, and repealing Directive 84/466/Euratom*. Official Journal of the European Union **L180**(09/07/1997), 22–25 (1997).
2. The Swiss Federal Council. *Radiological Protection Ordinance (RPO) of 22 June 1994, Classified Compilation 814.501*. The Swiss Federal Council (2008).
3. Barrett, H. H., Myers, K. J., Hoeschen, C., Kupinski, M. A. and Little, M. P. *Task-based measures of image quality and their relation to radiation dose and patient risk*. Phys. Med. Biol. **60**, R1–R75 (2015).
4. Brunner, C. C., Abboud, S. F., Hoeschen, C. and Kyprianou, I. S. *Signal detection and location-dependent noise in cone-beam computed tomography using the spatial definition of the Hotelling SNR*. Med. Phys. **39**, 3214–3228 (2012).
5. Ryckx, N., Gnesin, S., Meuli, R., Elandoy, C. and Verdun, F. R. *Medical physicists' implication in radiological diagnostic procedures: results after 1 y of experience*. Radiat. Prot. Dosim. **164**, 120–125 (2015).
6. Barrett, H. H. and Myers, K. J. *Foundation of Image Science*. John Wiley & Sons (2004).
7. Vaishnav, J. Y., Jung, W. C., Popescu, L. M., Zeng, R. and Myers, K. J. *Objective assessment of image quality and dose reduction in CT iterative reconstruction*. Med. Phys. **41**, 071904 (2014).
8. Ott, J. G., Ba, A., Racine, D., Ryckx, N., Bochud, F. O., Alkadhi, H. and Verdun, F. R. *Patient exposure optimisation through task-based assessment of a new model-based iterative reconstruction technique*. Radiat. Prot. Dosim. DOI:10.1093/rpd/ncw019.
9. International Commission on Radiation Units and Measurements. *Receiver operating characteristic analysis in medical imaging*. ICRU Report 79. Journal of the ICRU 8(1) (2008).
10. International Electrotechnical Commission. International Standard IEC 60601-2-44. *Medical Electrical Equipment – Part 2-44: Particular Requirements for the Basic Safety and Essential Performance of X-Ray Equipment for Computed Tomography*. 3rd edn. IEC (2009).
11. Li, K., Garrett, J., Ge, Y. and Chen, G.-H. *Statistical model based iterative reconstruction (MBIR) in clinical CT systems. Part II. Experimental assessment of spatial resolution performance*. Med. Phys. **41**, 071911 (2014).

Radiation Protection Dosimetry (2016), Vol. 169, No. 1–4, pp. 73–77
Advance Access publication 27 February 2016
doi:10.1093/rpd/ncw020

OBJECTIVE TASK-BASED ASSESSMENT OF LOW-CONTRAST DETECTABILITY IN ITERATIVE RECONSTRUCTION

Damien Racine*, Julien G. Ott, Alexandre Ba, Nick Ryckx, François O. Bochud and Francis R. Verdun
Institute of Radiation Physics, CHUV, Lausanne, Switzerland

*Corresponding author: damien.racine@chuv.ch

Evaluating image quality by using receiver operating characteristic studies is time consuming and difficult to implement. This work assesses a new iterative algorithm using a channelised Hotelling observer (CHO). For this purpose, an anthropomorphic abdomen phantom with spheres of various sizes and contrasts was scanned at 3 volume computed tomography dose index ($CTDI_{vol}$) levels on a GE Revolution CT. Images were reconstructed using the iterative reconstruction method adaptive statistical iterative reconstruction-V (ASIR-V) at ASIR-V 0, 50 and 70 % and assessed by applying a CHO with dense difference of Gaussian and internal noise. Both CHO and human observers (HO) were compared based on a four-alternative forced-choice experiment, using the percentage correct as a figure of merit. The results showed accordance between CHO and HO. Moreover, an improvement in the low-contrast detection was observed when switching from ASIR-V 0 to 50 %. The results underpin the finding that ASIR-V allows dose reduction.

INTRODUCTION

Image quality in computed tomography (CT), and hence clinical protocol optimisation, is a challenge because CT delivers the highest dose to the population in Switzerland, as in most Western countries[1]. To overcome this problem, manufacturers developed new technologies (e.g. iterative reconstruction) to minimise the amount of dose delivered. However, those new technologies must be evaluated and optimised[2, 3]. To optimise protocols, it is possible to evaluate simple binary tasks, such as the discrimination between the presence and absence of a pathology, which can be characterised by the use of receiver operating characteristic (ROC) studies[4]. These methods can be used to assess image quality especially when new reconstruction algorithms are implemented[5]. Unfortunately, these studies are time consuming and difficult to implement. Developing a tool based on mathematical model observers like the channelised Hotelling observer (CHO) to optimise clinical protocols and ensure that dose reductions do not affect the detection of low-contrast structures (using a similar paradigm as ROC studies) is an effective way to perform CT image quality—dose optimisation[6]. Nowadays, a new algorithm is often assessed by model observer studies in the image domain because the new iterative algorithms do not respect the shift-invariance and cyclostationarity assumptions necessary to use Fourier-based metrics[7–9]. In this study, the CHO model that mimics the human observer performance was used to assess the dose reduction potential of a new iterative reconstruction algorithm while keeping the image quality constant.

MATERIALS AND METHODS

Data acquisition

An anthropomorphic abdomen phantom (QRM 401, Moehrendorf, Germany) simulating the attenuation produced by a thin patient (equivalent diameter 24 cm) was scanned on a new Revolution CT (GE Healthcare, USA). Two modules can be inserted in the middle: a homogeneous module similar to the phantom's background and a low-contrast module that contains 6 and 8 mm spherical targets with contrast levels of 10 and 20 HU at 120 kV.

The phantom was scanned using the helical mode with a pitch of 0.984 at 120 kVp. The tube current was adapted for three dose levels [5, 10 and 15 mGy, volume computed tomography dose index ($CTDI_{vol}$) values were calculated as described in the IEC 60601-2-44[10] in a 32-cm $CTDI_{vol}$ abdomen phantom]. However, the $CTDI_{vol}$ indicated was overestimated, because it was calculated for a 32-cm CTDI phantom, whereas the phantom measured only 24 cm.

Fifty acquisitions per condition were made, and images were reconstructed using a 320-mm display field of view (DFOV), a 512 × 512 matrix size and a reconstructed slice thickness of 2.5 mm associated to a reconstruction interval of 2 mm. A new iterative algorithm, adaptive statistical iterative reconstruction (ASIR-V) at different levels (0, 50 and 70 %), was used to reconstruct the images[11]. This algorithm is a mixture between ASIR and MBIR, but to decrease the time reconstruction, ASIR-V does not model system optics[12–15]. The ASIR-V level represents the noise reduction rate.

A total of 36 different categories were obtained (three dose levels, two ASIR-V levels, two contrast levels and two target sizes), and 200 regions of interest (ROIs) of 28 × 28 pixels containing centred signals were extracted for each category. The ROIs containing the noise were extracted from the homogeneous modulus at the same (x,y) location as the signals in order to avoid the problem of non-stationary noise.

Model observer: channelised Hotelling observer

In this work, three human observers (medical physicists) and the CHO model performed a four-alternative forced-choice (4-AFC) experiment in which a series of four images were displayed but only one contained a signal. The CHO is a linear and anthropomorphic model that can be used to evaluate the image quality[2, 3]. The methodology used in this paper for the CHO is directly inspired by the methodology used by Ott *et al.*[16]. (The reader interested in all the mathematical details of the process will find extensive details in the chapter on the CHO model observer in Ott *et al.*).

For each trial of four images, the observer had to identify the image that was the most likely to contain the signal. The model observer compared the decision variable of the four displayed images and chose the one with the highest value as a signal-present image. In the end, a percentage correct (PC) was calculated and used as a figure of merit.

The average and standard deviation of the model observer's PC were estimated by performing a bootstrap method[17]. In practice, 1000 4-AFC experiments were performed for each category, and each 4-AFC experiment was created from 100 trials (1 image containing the signal and 3 signal-absent images per trial). Then, the mean and standard deviation of the 1000 PC values were computed. For human observers, the mean value and its standard deviation were calculated using the PC of the three observers. Error bars represent plus or minus one standard deviation.

Internal noise

To adjust the model's response to human observers' responses, it was necessary to reduce the model's performances with an internal noise ϵ because the CHO model with DDoG channels overestimates the performance of human observers in some conditions[18]. First, the decision variable λ was calculated as described in the methodology presented by Ott *et al.*[16], but at the end a random variable was added to obtain a noisy decision variable[8, 16]:

$$\lambda_{noisy} = \lambda + \varepsilon. \quad (1)$$

Internal noise ϵ was added to the decision variable λ with probability proportional to the standard deviation of the distribution of the decision variable amplitude images when the signal was absent:

$$\varepsilon = \alpha \times \sigma_{bg} \times \xi, \quad (2)$$

where α is the weighting factor, ξ is a random number generated between −1 and 1, and σ_{bg} is the standard deviation of the distribution of the decision variable of signal absent.

The α value was obtained by a calibration using images containing the signal 6 mm/20 HU at 10 mGy reconstructed with ASIR-V 50 %. The α value that minimised the difference between the model observers and the human observer was selected.

RESULTS

Figure 1 shows the humans' performances and Figure 2 the model observer's performances using ASIR-V algorithm at different levels. The category 8 mm/20 HU was too trivial (PC always equal to 1 in every conditions), and it was used as a training test for each dose and algorithm level.

For human observers, the results suggest that the detectability slightly increases with the level of ASIR-V (Figure 1). Thus, when the dose increases, PC tends to reach a plateau. This phenomenon was similar when the size or the contrast levels increased. In some conditions, using a higher ASIR-V level slightly improved the detectability, especially at low contrast.

As can be seen in Figure 2, the trends obtained from the CHO with DDoG and without adding internal noise were very similar to those obtained with human observers, even if the model overestimates the human performance and clears the difference between ASIR-V levels. In the high dose range, no significant difference appeared when using ASIR-V 70 % instead of ASIR-V 50 %.

Figure 3 shows the variation of PC as a function of A at a dose level of 10 mGy for the sphere 6 mm/20 HU reconstructed with ASIR-V 0 %. As expected, the higher the A, the lower the PC. The A value that provided the best match between the CHO performance and the human observers' performance for this category was chosen for other categories. The A value that provided the best match was equal to 4.0.

Adding internal noise within the CHO decreased its performance in order to match the human observers. This match was quantified with the root-mean-square error (RMSE). The value of the RMSE for all categories decreased from 0.62 to 0.178 when internal noise was added. Like the human performance, the PC increases with the dose when an internal noise is added. The human's performance is linked with the ASIR-V levels. However, for the model observer, the hierarchy between different ASIR-V levels is not very clear. For example, the PC for the category 8 mm/10 HU became unexpectedly worse at 15 mGy. Thus, the image quality tends to a plateau between 10 and 15 mGy with ASIR-V 70 %

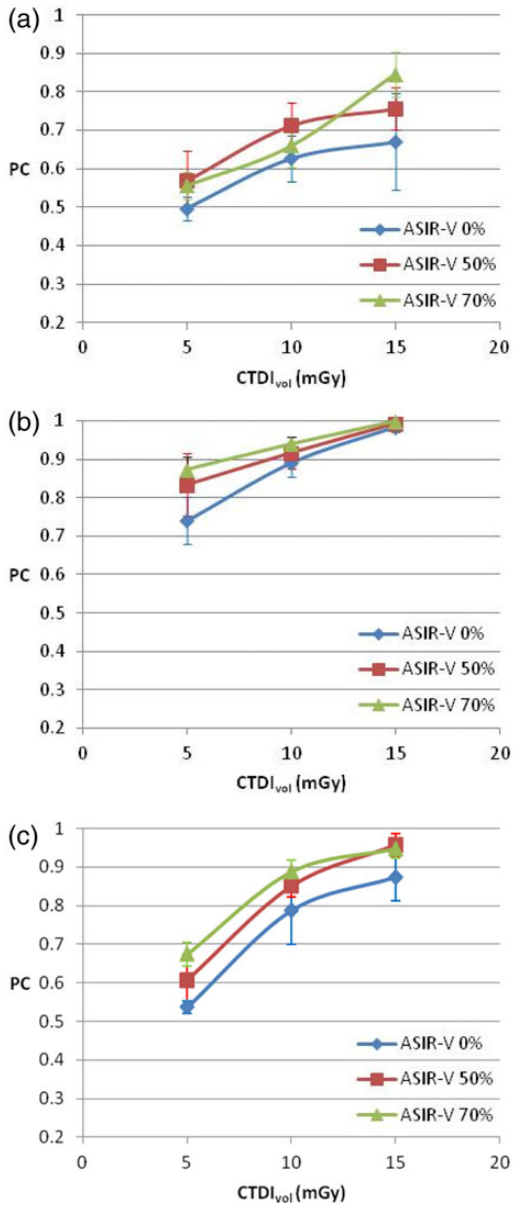

Figure 1. Results of the human observers who performed a 4-AFC test: (**a**) 6 mm/10 HU, (**b**) 6 mm/20 HU and (**c**) 8 mm/10 HU.

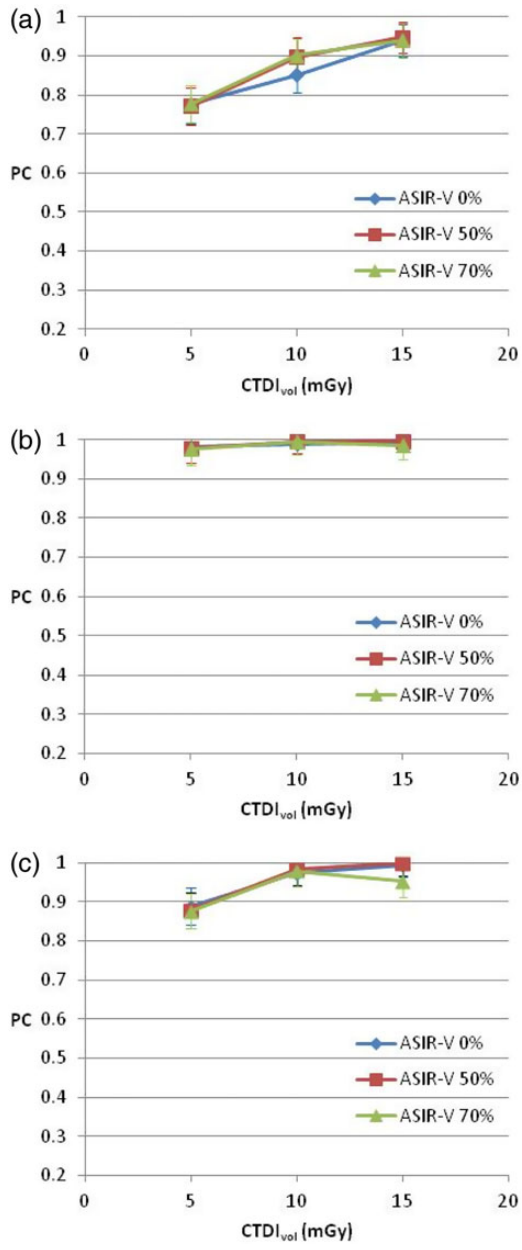

Figure 2. Results of the CHO model observer performing without internal noise and DDoG channel in PC for category: (**a**) 6 mm/10 HU, (**b**) 6 mm/20 HU and (**c**) 8 mm/10 HU.

for the sphere at 6 mm and 10 and 20 HU (Figure 4a and b). For the other levels, the image quality increased by 10 %, whereas the dose was increased by 50 %.

DISCUSSION

In recent years, the introduction of iterative algorithms has led the way to optimising clinical protocols and possibly decreasing the collective effective dose, especially in CT. The aim of this study was to evaluate the impact of the new ASIR-V algorithm on image quality in order to optimise the patient's exposure using a model observer. The results show that the image quality increased with the level of ASIR-V, but

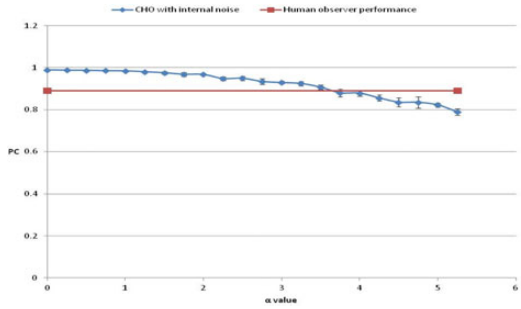

Figure 3. Calibration of the internal noise.

only for the human observer. The human observer seemed more efficient at detecting a signal in a less noisy image, but the results were not statistically significant ($p = 0.26$). The model observer with internal noise function selected allowed to get a better match with human detection performance. Nevertheless, the results could be improved by using more functions since the type of image texture varied in a wide range (new algorithm allowing various strength levels). In spite of this, the authors preferred to use a unique noise function since only one iterative algorithm was used. Thus, the RMSE was just minimised until reaching a plateau, and note that the RMSE was very dependent on an outlier (Figure 4c point at 15 mGy and ASIR-V 70 %). The PC tends to plateau when the dose, the contrast or size increases, and no difference was seen between levels of ASIR-V 50 and 70 %, because this study only focussed on the low-contrast detectability and high-contrast performances were not evaluated. To evaluate the interest of the ASIR-V 70 % or higher, the spatial resolution could be evaluated with the target transfer function[19].

One limitation of this study is the use of a simplistic anthropomorphic phantom. Even if it mimics human body attenuations, it does not contain any texture. Furthermore, only two sizes and two contrasts were investigated. Another limitation is that the paradigm used (signal, location and background are known exactly) was simple and therefore different from actual clinical conditions.

CONCLUSION

Evaluating image quality with frequency metrics is far away from the clinical task. To be close to the concerns of radiologists, task-based tools (e.g. CHO model) must be used to objectively evaluate the image quality. The CHO model with DDoG filter used in this study successfully demonstrated its capacity to mimic the human's performance. Thus, the ASIR-V algorithm evaluated with this tool shows that the image quality on the low-contrast detectability stays high even with the small sphere of low contrast. These findings suggest that patient dose could be reduced

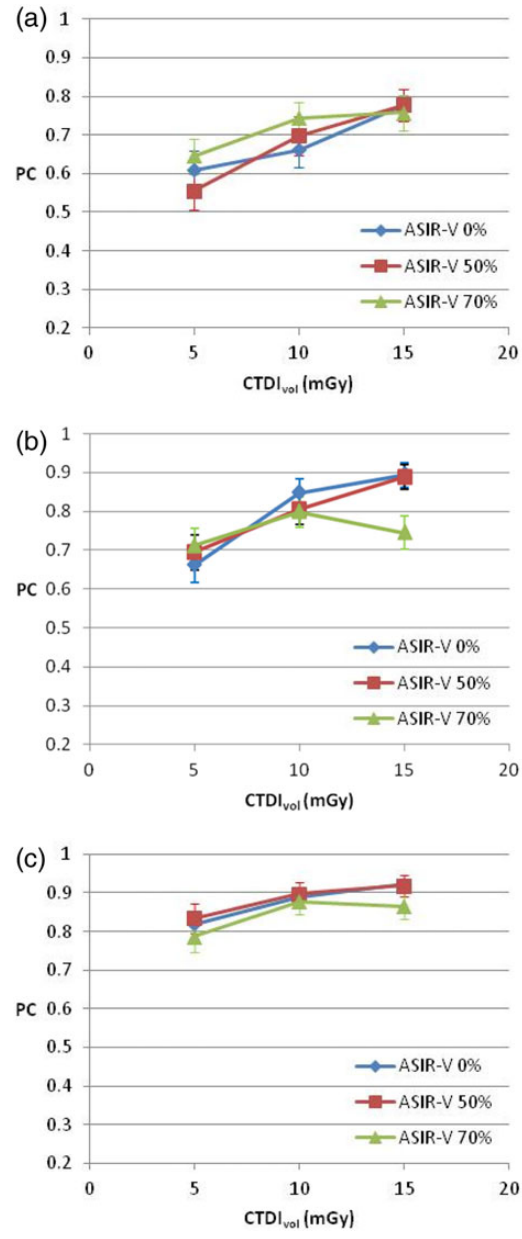

Figure 4. Results of the CHO model observer performing with internal noise and DDoG channel in PC for category: (**a**) 6 mm/10 HU, (**b**) 6 mm/20 HU and (**c**) 8 mm/10 HU.

using the ASIR-V algorithm and the new CT unit evaluated, without decreasing image quality.

REFERENCES

1. Samara, E. T., Aroua, A., Bochud, F. O., Ott, B., Theiler, T., Treier, R., Trueb, P. R., Vader, J. -P. and

Verdun, F. R. *Exposure of the Swiss population by medical x-rays: 2008 review*. Health Phys. **102**, 263–270 (2012).
2. Barrett, H. H. and Myers, K. J. *Foundation of Image Science*. John Wiley & Sons (2004).
3. Vaishnav, J. Y., Jung, W. C., Popescu, L. M., Zeng, R. and Myers, K. J. *Objective assessment of image quality and dose reduction in CT iterative reconstruction*. Med. Phys. **41**, 071904 (2014).
4. International Commission on Radiation Units and Measurements. *Receiver operating characteristic analysis in medical imaging*. ICRU Report 79. Journal of the ICRU 8(1) (2008).
5. Metz, C. E. *ROC methodology in radiologic imaging*. Invest. Radiol. **21**, 720–733 (1986).
6. Barrett, H. H., Myers, K. J., Hoeschen, C., Kupinski, M. A. and Little, M. P. *Task-based measures of image quality and their relation to radiation dose and patient risk*. Phys. Med. Biol. **60**, R1–R75 (2015).
7. Leng, S., Yu, L., Zhang, Y., Carter, R., Toledano, A. Y. and McCollough, C. H. *Correlation between model observer and human observer performance in CT imaging when lesion location is uncertain*. Med. Phys. **40**, 081908 (2013).
8. Yu, L., Leng, S., Chen, L., Kofler, J. M., Carter, R. E. and McCollough, C. H. *Prediction of human observer performance in a 2-alternative forced choice low-contrast detection task using channelized Hotelling observer: impact of radiation dose and reconstruction algorithms*. Med. Phys. **40**, 041908 (2013).
9. Brunner, C. C., Abboud, S. F., Hoeschen, C. and Kyprianou, I. S. *Signal detection and location-dependent noise in cone-beam computed tomography using the spatial definition of the Hotelling SNR*. Med. Phys. **39**, 3214–3228 (2012).
10. International Electrotechnical Commission. International Standard IEC 60601-2-44. *Medical Electrical Equipment – Part 2-44: Particular Requirements for the Basic Safety and Essential Performance of X-Ray Equipment for Computed Tomography*, 3rd edn. IEC (2009).
11. Lim, K., Kwon, H., Cho, J., Oh, J., Yoon, S., Kang, M., Ha, D., Lee, J. and Kang, E. *Initial phantom study comparing image quality in computed tomography using adaptive statistical iterative reconstruction and new adaptive statistical iterative reconstruction v.* J. Comput. Assist. Tomogr. **39**, 443–448 (2015).
12. Singh, S., Kalra, M. K., Hsieh, J., Licato, P. E., Do, S., Pien, H. H. and Blake, M. A. *Abdominal CT: comparison of adaptive statistical iterative and filtered back projection reconstruction techniques*. Radiology **257**, 373–383 (2010).
13. Hara, A. K., Paden, R. G., Silva, A. C., Kujak, J. L., Lawder, H. J. and Pavlicek, W. *Iterative reconstruction technique for reducing body radiation dose at CT: feasibility Study*. AJR Am. J. Roentgenol. **193**, 764–771 (2009).
14. Scheffel, H., Stolzmann, P., Schlett, C. L., Engel, L. -C., Major, G. P., Károlyi, M., Do, S., Maurovich-Horvat, P. and Hoffmann, U. *Coronary artery plaques: cardiac CT with model-based and adaptive-statistical iterative reconstruction technique*. Eur. J. Radiol. **81**, e363–e369 (2012).
15. Patino, M., Fuentes, J. M., Singh, S., Hahn, P. F. and Sahani, D. V. *Iterative reconstruction techniques in abdominopelvic CT: technical concepts and clinical implementation*. AJR Am. J. Roentgenol. **205**, W19–W31 (2015).
16. Ott, J. G., Ba, A., Racine, D., Ryckx, N., Bochud, F. O., Alkadhi, H. and Verdun, F. R. *Patient exposure optimisation through task-based assessment of a new model-based iterative reconstruction technique*. Radiat. Prot. Dosim. DOI:10.1093/rpd/ncw019.
17. Efron, B. and Tbishirani, R. J. *An Introduction to the Bootstrap*. CRC Press (1994).
18. Castella, C., Eckstein, M. P., Abbey, C. K., Kinkel, K., Verdun, F. R., Saunders, R. S., Samei, E. and Bochud, F. O. *Mass detection on mammograms: influence of signal shape uncertainty on human and model observers*. J. Opt. Soc. Am. A **26**, 425–436 (2009).
19. Ott, J. G., Becce, F., Monnin, P., Schmidt, S., Bochud, F. O. and Verdun, F. R. *Update on the non-prewhitening model observer in computed tomography for the assessment of the adaptive statistical and model-based iterative reconstruction algorithms*. Phys. Med. Biol. **59**, 4047–4064 (2014).